Sheffield Hallam University

A Sheffield Hallam University thesis

ProQuest Number: 10701251

ProQuest 10701251

AN INVESTIGATION OF MICROCRACK FORMATION

ON MACHINED SURFACES.

by

Mohamed Gaceb, B. Eng.

A thesis submitted to the COUNCIL FOR NATIONAL ACADEMIC
AWARDS in partial fulfilment for the degree of DOCTOR OF
PHILOSOPHY.

Department of Mechanical and Production Engineering,
Sheffield City Polytechnic. (Sponsoring Estabilshment)

British Steel Corporation. (Collaborating Establishment)

July 1985

بِسْمِ اللهِ الرَّحْمٰنِ الرَّحِيْمِ

اقْرَأْ بِاسْمِ رَبِّكَ الَّذِى خَلَقَ ۝ خَلَقَ الْإِنْسَانَ مِنْ عَلَقٍ ۝ اقْرَأْ وَرَبُّكَ الْأَكْرَمُ ۝ الَّذِى عَلَّمَ بِالْقَلَمِ ۝ عَلَّمَ الْإِنْسَانَ مَا لَمْ يَعْلَمْ ۝

In the name of Allah, the Benefic ent, the Merciful

Read in the name of your Lord who created,

created man from clots of blood.

Read! and your Lord is the most Bounteous,

who has taught the use of the pen,

has taught man that which he knew not.

(Qur'an XCVI: 1-5)

TABLE OF CONTENTS

LIST OF FIGURES

LIST OF PLATES

ACKNOWLEDGEMENTS :

DECLARATION :

    The author declares that no part of this work has been submitted in support of another degree or qualification to this or any other establishement. The author further declares that he has not been a registered candidate or enrolled student for another award of the CNAA or other academic or professional institution during the course of the research programme.

                                     M. Gaceb

ABSTRACT:

AN INVESTIGATION OF MICROCRACK FORMATION

ON MACHINED SURFACES.

M. Gaceb

In recent times a number of workers have pointed out the importance of microcrack formation to the machining process and to surface integrity requirements of machined components. Microcracks have been identified within the shear zone and their presence used to explain some aspects of the chip formation process. It is clear that microcracks represent a major feature in the shear zone in machining, particularily when the workpiece is a two-phase material.

The presence of microcracks in the machined surface was reported some fifteen years ago and confirmed recently. A preliminary study carried out on a number of materials machined under various cutting conditions has indicated that microcracks are produced in machined surfaces as a result of machining.

However, to the present time there has been no systematic study of the formation of microcracks in the machined surface, and their extent, dimensions, and the conditions under which they are produced are completely unknown. In so far as microcracks may affect the fatigue, corrosion and other properties of the machined surface, it is important that a method of quantifying microcrack formation should be found.

A feasibility study has been carried out which has led to the use of the transmission electron microscope as a tool to quantify microcrack formation in the machined surface. A technique based on transmission electron microscopy is described in the present thesis along with its application.

Two new parameters, the microcrack area ratio "Ma" and the microcrack density "Md" are introduced and defined. The extent of microcrack formation in the machined surface is studied as a result of varying:
(i)- cutting speed,
(ii)- undeformed chip thickness,
(iii)- rake angle,
(iv)- workpiece hardness.
The results are discussed and conclusions drawn.

Finally, a number of suggestions for future work are formulated which mark the start of a whole new area of research in surface microcracking.

The quality of the finished surface is an important factor in many machining operations, and is often responsible for the values of cutting speed, tool feed rate, and tool geometry used. Cognizance should be taken of the fact that machining operations often produce a surface with properties which are different from those of the bulk material beneath. Further, the roughness of the finished surface is often different from that expected, or predicted by theory.

Surface integrity is a generic term which is used to describe all aspects of the nature of a surface. It includes the mechanical, physical, and chemical properties of the surface. Surface integrity also includes the geometrical aspects of the surface, in particular its roughness, and any surface features which may be produced as a result of the machining process. Although research has been going on for more than three decades, component surface integrity has not found a widespread use in industry. Its importance, however, is becoming more and more recognized, particularily because serious failures have resulted when integrity was lacking.

The functional behaviour of a machined component can be significantly affected by the nature of its surface. Table 1 illustrates the relationship which exists between surface properties and component failure. At a time when new materials with enhanced strength are being required to carry ever increasing loads, and when surface area to volume ratios are steadily increasing, it becomes important that attention must be given to the nature and integrity of surfaces produced in machining.

Microcracks have been recognized as one component of surface integrity for a number of years and, as shown in table 1, have been considered to play a part in component failure. However, very little is known about the extent of surface microcracking as a result of

machining. Because of this lack of knowledge, examination of the way in which surface integrity affects the functional behaviour of a machined component has in general been carried out without consideration of the role played by surface microcracks. There have, however, been numerous references to the adverse effect that surface microcracking has on fatigue strength and corrosion resistance. On the other hand, surface microcracks could provide a way of "keying-in" surface coatings and could therefore be considered beneficial for electro-plated components, particularily when the component is subjected to compressive in-sevice loading.

It follows from the foregoing discussion that the nature of the machined surface and the microcracks, in particular, should be given more attention which would pave the way towards a better utilization of machined components. With this in mind, and in the light of the current lack of quantitative knowledge relating to the extent of machined surface microcracking, and also because of the uncertainty relating to the functional significance of surface microcracks, a programme of work has been carried out with a view to quantifying the extent of microcrack formation as a result of machining. This programme of work has two main aspects. Firstly, the development of a suitable technique to provide quantitative information concerning surface microcracks. Secondly, to study the variation in surface microcracking with different machining conditions. Correlations between microcracking and cutting speed, undeformed chip thickness, tool rake angle and workpiece material hardness have been established. The results have allowed the drawing up of guidelines for good machining practice when microcrack formation needs to be carefully controlled.

Table 1: Correlation between surface properties and failure causes (after Tonsheff et al [48])

Cause of failure	Physical properties						
	Yield Sress	Hardness	Strength	Fatigue Strength	Residual Stress	Texture	Microcracks
Plastic deformation	*	*					
Scuffing/Adhesion		*					
Fracture/Crack		*					+
Fatigue				*	+	+	*
Cavitation		+					+
Wear		*			+		
Diffusion						x	
Corrosion					+		*

* Strong influence   + Traceable influence
x Supposed influence

CHAPTER 2

FUNDAMENTALS OF THE MACHINING PROCESS

2.1- Description And Terminology Of Machining

2.2- Chip Formation In Machining

2.3- Surface Formation In Machining

2.4- Built-Up-Edge Formation In Machining

2.5- Heat Generation In Machining

2.6- Deformation Zones In Machining

2.7- Stress State Ahead Of The Tool Cutting Edge

2.8- Concluding Remarks

Machining is essentially a simple process in which material is removed from a workpiece using a hard tool moving relative to the surface of the workpiece to produce a machined surface as shown in figure 1. The removed material is in the form of a thin ribbon referred to as the "chip".

Figure 2 shows schematically the relationship between the tool and the workpiece generally known as orthogonal machining. In orthogonal machining the tool cutting edge is perpendicular to the cutting vector. This configuration is usually achieved by feeding the tool into the end of a tube in turning (fig. 2a), or by planing on the top of a strip (fig. 2b). In either case the length of the cutting edge is larger than the width of the machined surface. This is sometimes also referred to as "broad cutting". In orthogonal machining the width "w" is called "the depth of cut".

Figure 3 shows a section through the chip and workpiece, assuming plane strain conditions. As machining proceeds, the chip passes over the rake face of the tool. The angle this face makes with the normal to the machined surface is called the rake angle "α". If this angle is such that the rake face makes less than a 90 degree angle with the machined surface it is known as a positive rake. On the other hand, if the rake face makes an angle greater than 90 degree with the machined surface, the tool is referred to as a negative rake tool. This is illustrated schematically in figure 4.

In order to prevent rubbing between the tool and the machined surface, the tool is provided with a clearance angle "θ". The tool cutting edge is the intersection of two tool faces one of which is the rake face. In orthogonal machining the second face is known as the

flank face and the cutting edge is referred to as a primary cutting edge. The angle contained between the rake face and the flank face is called the wedge angle. In practice, it is not possible to obtain perfectly sharp tools even when the best preparation methods are used. The cutting edge is assumed to be a cylindrical portion meeting the rake face and the flank face tangentially. According to Albrecht [1] the so-called "sharpness" of a tool is defined as the radius of curvature of its cutting edge. The lower the value of the cutting edge radius the sharper the tool and vice-versa for "dull" tools.

Machining takes place (figure 3) when the tool moves with a cutting speed "V" along the surface of the workpiece at a depth "t_1" often referred to as the uncut or undeformed chip thickness (and is abbreviated "UCT"). The thickness of the chip is known as the chip thickness "t_2". In turning the relative motion of the cutting tool with respect to the workpiece is the result of two motions. The rotation of the workpiece determines the cutting speed whereas the undeformed chip thickness is provided by feeding the tool in a direction parallel to the axis of rotation of the workpiece. The feed rate is given in millimeters per revolution of spindle rotation and is equivalent to the undeformed chip thickness in the case of orthogonal machining. The rate at which material is removed from the workpiece is called the material removal rate and is equal to the product of the cutting speed, the undeformed chip thickness and the width of cut (i.e. $MRR = V.t_1.w$).

The ratio of undeformed chip thickness to the chip thickness (i.e. t_1/t_2) is known as the chip thickness ratio and is given the symbol "Rc". The inverse of the cutting ratio is called the compression factor [2].

- 7 -

The regions of contact between the chip and the rake face of the tool, and between the workpiece and the flank face of the tool are known as the chip/tool and work/tool interfaces.

A simple model of the machining process has been introduced by Merchant [3] and is referred to as the shear plane model (figure 5). According to this model the material ahead of the tool is sheared continuously along the shear plane 'AB' which makes an angle "ϕ" with the machined surface. This angle is known as the shear plane angle.

According to a more realistic model as shown in figure 6, in order to produce the chip, shear takes place in a zone of finite thickness. This zone is referred to as the primary shear zone and constitutes the boundary between the unsheared work-material and the body of the chip. Further shear of the chip material occurs in the region near the chip/tool interface which is known as the secondary shear zone or the flow zone of the chip. A third feature which is often observed in machining is the occurrence of the built-up-edge (b-u-e) which is a build-up of material adhering to the rake face of the tool and protruding into the workpiece to a level below that of the lowest point of the tool. The built-up-edge formation will be dealt with in section 2.4.

A comprehensive understanding of the machining process is not possible without the consideration of the mechanical, frictional, and physical aspects of this process. The following sections have been included to give an overview of the main features which are likely to be encountered during a machining operation.

By chip formation it is meant the process of parting off the chip from the workpiece. According to the classification by Ernst [4], there are three types of chip formation. These are shown diagrammatically in figure 7.

The continuous chip (figure 7a) occurs with most ductile materials, for example, mild steel and aluminium and when machining at high cutting speeds. Machining with this type of chip is considered to be a steady state process. Because of the simple geometry of this type of chip formation, it has formed the basis for most of the work on the mechanics of machining.

The continuous chip, in some circumstances, may be accompanied by a built-up-edge of highly deformed material which adheres to the tool tip and periodically builds up and breaks off (figure 7b). This type of chip is important because it occurs for a wide range of materials and under various cutting conditions. Because of its importance the built-up-edge will be discussed in more detail in section 2.4.

The discontinuous chip occurs with brittle workpiece materials (e.g. cast iron and cast brass) and when machining at very low cutting speeds. The tool partly forms the chip before fracture occurs in the primary shear zone and results in a discontinuous chip as shown in figure 7c. The fracture is instigated by the cyclic formation of a crack below the flank face of the tool followed by its propagation right through the primary shear zone.

From a direct observation of the machining process inside a scanning electron microscope, Iwata and Ueda [5] stated that the chip formation transformed occasionally from one type to another, depending on changes in microscopic parameters (e.g., inclusion morphology and

grain boundaries) and in the cutting conditions (e.g., rake angle and cutting temperature).

The merit of each type of chip formation depends on which aspect of machining process needs to be controlled. Continuous chips are usually strong and difficult to break and therefore can cause problems during disposal. The discontinuous chip might solve the problem of disposal but it can lead to chatter and rapid cutting edge wear through fatigue which are undesirable effects. For the design engineer who is concerned with the control of surface quality the continuous with built-up-edge type of chip formation should be avoided as it is detrimental to the surface finish.

2.3- Surface Formation In Machining

The process of producing a new surface in machining is known as surface formation. In the early days of research into the machining process, the emphasis was put onto the improvement of productivity by increasing the material removal rate. This has resulted in considerable work being carried out on the chip formation aspects of machining. Productivity also depends upon long tool life. A great deal of work was, therefore, done on tool wear. Little work, however, has been carried out on the surface formation aspect of machining. This is due to the fact that the concept of surface formation has always been subsumed within that of chip formation. This attitude has been instilled by experimental observations of the machining process which have shown that the surface produced and its features are closely related to the type of chip formation.

Work carried out by Gillibrand [6] has shown that surface formation is in fact worthy of independent investigation. He

described surface formation as a process which takes place when
material which has been initially deformed in shear is subsequently
further deformed by a mechanism peculiar to the vicinity of the tool
cutting edge, and ultimately involves a process of ductile fracture.
According to Gillibrand, the problem of surface formation is also one
of identifying the mechanisms which, while generating the newly
machined surface, invest it with topographical features which are
themselves dependent upon the tool geometry, the cutting conditions,
and the materials being machined. Furthermore the character of the
machined surface is affected by the nature of the contact at the
work/tool interface (i.e. whether sliding or sticking), the presence
or absence of a built-up-edge, and the use of sharp or worn tools.

2.4- Built-Up-Edge Formation In Machining

Built-up-edge formation in machining is peculiar to machining a
material which can adhere to the rake face of the tool under cutting
conditions which promote adhesion. A built-up-edge is formed when the
friction at the tool/chip interface increases to a degree where the
force required to cause sliding is greater than the shear strength of
the chip material. As a result cracks form both below the flank face
and, subsequently, near the tool/chip contact zone. Shearing takes
place at some distance from the tool/chip interface where the weaker
material flows round the hardened built-up-edge. Trent[7] has shown
that the conditions under which the built-up-edge occurs when
machining steel and cast iron may be summarized on a graph of log(V)
versus log(feed). The built-up-edge occurrence is then bounded by a
straight line as shown in figure 8.

As early as 1935, Ernst and Martellotti [8] investigated factors which affect the size of the built-up-edge. They found that the size of the built-up-edge decreased with:

  (i)- a decrease in chip thickness,

  (ii)- an increase in rake angle,

  (iii)- an increase in tool sharpness,

  (iv)- an increase in cutting speed,

and   (v)- the application of a lubricant to the tool rake face.

This work confirmed earlier findings by Schwerd [9] about the influence of cutting speed on built-up-edge formation. Experimental observations by Williams and Rollason [10] have shown that an increase in cutting speed, feed, and workpiece temperature results in a decrease in b-u-e height and sharpness. For low and medium carbon steels, they found that the b-u-e disappears at about 300ft/min (91.4m/min). From the above quoted works it can be concluded that in general the b-u-e disappears at some temperature $T=f(V,a)$ where "V" is the cutting speed and "a" is the feed.

One consequence of the formation of built-up-edge is that the latter partially takes over the work of the tool cutting edge, not only changing the process of chip formation, but also (which is more important) changing the dimensions of the component and character of the machined surface. To be more specific, the built-up-edge may change the effective rake angle and the radius of curvature around which the material flows, hence the friction between flowing and staionary material and the temperatures increase with an increase in the size of the built-up-edge. Figure 9 shows the characteristics of the built-up-edge according to Kaczmarek [11].

Schwerd [9] has explained that at cutting conditions favourable to built-up-edge formation, elements of material adhere to the tool.

The built-up-edge develops in size until it becomes unstable and fractures. The fracture of the built-up-edge results in a fragment of the built-up-edge moving away as part of the surface of the workpiece. A similar fracture occurs on the upper side of the built-up-edge, so that fragments are also carried away by the chip underside. The built-up-edge growth and fracture cycle is shown in figure 10. This instability of the built-up-edge results in a high scatter of surface roughness readings at cutting conditions favourable to built-up-edge formation.

2.5- Heat Generation In Machining

Heat is generated in machining by the work done in the shear zones and by the frictional work where the chip slides over the tool rake face and where the machined surface contacts the flank face of the tool. The temperature distributions in machining are important in that they can influence the properties of the work material being machined and thus play an influential role in the whole of the machining process.

There has been a number of early attempts [12] to calculate the temperatures in machining using the shear plane model of machining. In these attempts the assumption is made that the generation of heat is confined uniformly within the shear plane and at the chip/tool interface rather than being spread over a finite primary and secondary shear zones. This, as shown by Boothroyd [13] will certainly result in the temperatures being overestimated. There has also been attempts by many investigators to measure these temperatures. Investigations in both the theoretical and experimental aspects of temperature

determination have been reviewed in a more detailed manner by Barrow [14].

Recent advances in this topic have been achieved using finite element analysis to calculate the temperature distribution in locations of interest in the tool/chip/workpiece system. The work carried out by Murarka et al [15] is one example and has led to the following conclusions which are in general agreement with data presented by Boothroyd [13] and Barrow [14] :

   (i)- there is a sharp increase in temperature along the rake face for a small distance, then a sharp decrease for a small distance followed by a steady decrease,

  (ii)- there is a sharp increase in temperature along the flank face for a short distance followed by a steady decrease (see figures 11 to 14),

 (iii)- the primary shear zone temperatures increase along a direction parallel to the rake face from the boundary with the unsheared material to the boundary with the body of the chip,

  (iv)- the average shear plane temperature increases with an increase in cutting speed and with a decrease in rake angle,

   (v)- the overall temperatures increase with an increase in cutting speed and/or feed rate (figures 11 and 12),

  (vi)- there exists an optimum rake angle for minimum temperature (figure 13). For example, the maximum temperature is decreased from 585 °C to about 458 °C and is then increased back to 532 °C as the rake angle is increased from 20 to 30degrees and then from 30 to 40degrees, respectively. This was attributed to the increase in the rake angle having two opposing effects: a)- the total energy input to the system and hence the amount of heat generated within the system is decreased calling for an overall

decrease in temperatures and b)- the tool tip area available for heat conduction is decreased promoting the local temperatures to rise. As the rake angle is increased the first factor possibly predominates over the second and as a result the temperatures are decreased, but beyond the balancing point the second factor appears to gain larger importance and the temperatures along tool rake face and tool flank face start rising again.

(vii)- the tool temperatures can be decreased and the workpiece temperatures increased when a small amount of flank wear exists (figure 14). This can be explained by thinking of the wear land as providing a larger area for heat conduction from the tool to the workpiece which is speed-dependent.

(viii)- under similar cutting conditions, lower tempratures are generated with a carbide tool than with a high speed steel tool,

(ix)- the maximum temperature can be reduced by 5 to 10 percent (depending on cutting speed) when using a suitable coolant.

It should be mentioned at this stage that the maximum temperature occurs some way back from the tool tip at the other end of the contact length as figures 11 to 14 show. Although the maximum temperature may go on increasing as the cutting speed is increased, it is not clear that the temperature around the tool tip, which will influence the machined surface, will continue to increase with increase in cutting speed.

While Murarka et al [15] reached some interesting conclusions, they did not, however, provide adequate discussion to conclusions (iv) and (v). While the average shear plane temperature may increase with cutting speed it can, however, be argued that this is only due to

reduced conduction and not due to heat generation. So the temperature will reach a limiting value and will not increase indefinitely. Also the overall temperatures may increase with cutting speed for a different reason, i.e. it includes the additional temperature rise in the secondary shear zone which continues to increase with cutting speed.

2.6- Deformation Zones In Machining

Investigators [16-19] have shown that the shearing process in machining is not restricted to a shear plane but takes place in a zone of finite thickness. Using a cinefilm taken through a microscope, of the side of a workpiece which had been polished and etched, Palmer and Oxley [19] recorded the path followed by individual grains during actual machining operations. They suggested the machining model shown in figure 15.

This model, however, has been criticized on the grounds that the cutting speeds at which the experiments were carried out are very low relative to the usual cutting speed range encountered in machining practice. The rake angles used (i.e. 20 to 50 degrees) were also criticized as being impractical. Another shortcoming of Palmer and Oxley's model is the gap which was shown (figure 15) to exist, between the tool tip, the chip, and the workpiece. This in fact is in conflict with experimental observation that the tool is always in contact with the chip and workpiece, as deduced from the fact that the tool wears on both the flank and rake faces.

The model described above is not complete in the sense that it does not take into consideration the interaction between the chip and tool and the effect of the radius (or bluntness) of the cutting edge

which exists even for "sharp" tools as shown earlier in figure 3. A slip line field which takes this into account has been constructed by Enahoro and Oxley [20] and is shown in figure 16. It was claimed [20] that a stagnation point of the flow occurred on the tool nose and that streamlines above this point flowed into the chip while lower streamlines re-enter the work. It was also assumed [20] that at the stagnation point the material divides and that a very small load-free surface exists adjacent to this point.

On the other hand, Palmer and Yeo [21] considered the possibility of flow round the tool nose and reached the conclusion that the assumed type of flow is impossible, except when there is no friction in the neighbourhood of the stagnation point. This latter is a possibility when the surface of the plastic material is free, rather than flowing round an obstacle which is similar to the model shown in figure 15. The impossibility of this model, however, has already been established. The existence of a dead metal zone immediately ahead of the cutting edge [22], is an acceptable possibility provided it is not confused with any part of the built-up-edge described earlier.

A combination of the slip line fields given in figures 15 and 16 has been constructed by Roth and Oxley [23]. This is shown in figure 17. It is evident from this figure that during machining, plastic deformation occurs in three distinct regions rather than just the two shown in figure 6. These are:

     (i)- the primary shear zone,

     (ii)- the region adjacent to the chip/tool interface or
           secondary shear zone,

and (iii)- the region beneath the cutting edge of the tool adjacent
           to the flank face.

The strong interaction between the friction conditions at the chip/tool interface and material flow in the primary shear zone has been confirmed [24].

One influential feature of the slip-line field shown in figures 15 to 17 is the extension of the primary shear zone below the level of the newly machined surface. This means that material which forms the subsurface layer crosses a deformation zone thus suffering deformation. This suggests that the nature of stresses in the primary shear zone must have a controlling effect on the subsurface layer characteristics.

2.7- Stress State Ahead Of The Tool Cutting Edge

One interesting conclusion from the work by Palmer and Oxley [19] is the variation of the stress within the plastic shear zone from being compressive near the outer free surface to high tensile (i.e. about twice the yield stress of the annealed material) near the tool cutting edge. The change in sense occurs at about one third of the way from the tool point to the free surface of the chip along the shear zone entrance boundary. They concluded that the chip was produced by a combination of bending and shearing actions contrary to the normal assumption of single shear. The existence of this tensile stress is confirmed by photo-elastic work of long standing [25] and by later investigators [26-29] involved in the study of the stress situation in front of the tool cutting edge. This has also been confirmed by the work of Iwata and Ueda [5], Enahoro and Oxley [30], and Ramalingam and Lehn [31].

In an attempt to explain the effect of positive and negative strain hardening rates on the hydrostatic stress distribution, Roth

wrote a paper [27] in which he compared the stress distribution for two materials. The first was a free machining low carbon steel C1114 whose flow stress increased continuously with increasing strain (i.e. positive strain hardening rate). The other was a micro-crystalline wax whose flow stress, with an initial increase at low strains decreased with increasing strain (i.e. negative strain hardening rate). Roth used results from the work by Bitans et al [32] on the wax. The strain hardening characteristics of the two materials were as shown in figure 18. Roth concluded that for the positive strain hardening rate material the hydrostatic stress at the cutting edge was tensile and almost equal to the shear flow stress, whereas for the negative strain hardening rate material, it was highly compressive and approximately 2.5 times the shear flow stress. At the other end of the shear plane, however, it was found that the reverse was true with the hydrostatic stress being compressive for the positive strain hardening rate material and nearly zero for the negative strain hardening rate material.

Similar work was carried out by Oxley et al [26] who considered the effect of using two materials with different strain hardening properties as shown in figure 19. Their results are shown in figure 20. It can be seen from this figure that for the higher strain hardening rate meterial (i.e. the annealed material), the tensile stress at the tool edge is higher. This effect was explained by the suggestion that in passing from A to B (figure 20) the change in slope of the slip line gives a compressive increment while the strain hardening gives a tensile increment. The strain hardening term in the modified Hencky plasticity equations [26] depends on both the strain hardening properties of the material and the width of the shear zone. This explains the finding that the distribution of hydrostatic stress

has been approximately the same for each material. It was considered [26] that if the width of the plastic zone had been the same for each material, the hydrostatic stress would have become tensile far more rapidly for the annealed material than for the cold rolled material. It was also concluded that the difference in strain hardening properties was not reflected in the external parameters of the cutting process (e.g. cutting forces, chip thickness ratio) although the plastic zones were distinctly different. This conclusion is interesting in that it suggests that although the external parameters might be constant, when machining two materials with different stain hardening properties, the deformation to which the subsurface layer is subjected may well be totally different.

As stated before, the above results were based on slow cutting speeds. These were used to minimise strain rate and temperature effects so that the only significant variations in flow stress resulted from strain hardening. At higher cutting speeds, the influence of strain rate and temperature can predominate. While an increase in the strain rate gives rise to a higher flow stress, an increase in temperature results in a lower flow stress as shown in figure 21. It is shown in this figure that the effects of strain rate tend to cancel out the effects of temperature at strain rate values of the order of 10^5 per second. The work carried out by Chakraborti [34] has confirmed the applicability of the analysis by Palmer and Oxley [19] at higher cutting speeds (25 to 50m/min). He found similar results to those of figure 20 [26]. Chakraborti also claimed that as the cutting speed was increased beyond 136m/min up to 213m/min, the penetration of the primary zone entrance boundary into the workmaterial decreased, and a definite contraction of the primary zone entrance boundary occurred. Hence, he concluded, the hydrostatic

stress which was tensile in nature would decrease with increase in the cutting speed.

Rubenstein [35] evolving a theory of orthogonal cutting based on the assumption of an idealized lower boundary of the primary shear zone consisting of two planes, has concluded that the tensile stress in the immediate vicinity of the tool cutting edge is dependent on strain and strain rate. The expression he developed for the tensile stress acting near the tool cutting edge when the influence of strain and strain rate was allowed for, suggest that the tensile stress depends on the following variables :

(i)- the rake angle,

(ii)- the undeformed chip thickness,

(iii)- the cutting speed,

and (iv)- the work hardening characteristics of the work material.

No indication was, however, given [35] as to how the above mentioned parameters affected the tensile stress near the cutting edge. Enahoro and Oxley [30] found that increasing the undeformed chip thickness (from 0.091mm to 0.53mm) or the rake angle (from 35 degree to 50 degree) tends to increase the tensile stress in the vicinity of the tool cutting edge (figure 22). Their results, however, were carried out at very low a cutting speed (i.e. 13.72 mm/min). Bearing in mind the effects of the thickness of the shear zone on the tensile stress ahead of the tool cutting edge, the effects of the cutting parameters may be influential as a consequence of their effects on the thickness of the deformation zone. Refering to the strain hardening term in the modified Hencky equations used by Oxley et al [26], a decrease in the primary shear zone thickness results in an increase in the tensile stress ahead of the cutting edge. From the results obtained by

Kececioglu [36] the average thickness of the primary shear zone is decreased by:

        (i)- increasing rake angle,

and (ii)- decreasing undeformed chip thickness.

Hence the conclusion that increasing rake angle and/or decreasing the undeformed chip thickness both result in an increase in the tensile stress near the tool cutting edge.

2.8- Concluding Remarks:

From the foregoing the complexity in the details of the machining process is manifest. This is reflected by the diversity of ways in which those involved with research in this area have approached and solved the associated problems. There is, however, agreement about the tensile nature of the hydrostatic stress in the immediate vicinity of the tool cutting edge. This is important from the point of view of the topic of the present investigation. The discussion of the consequences of this tensile stress vis-a-vis microcracking will be deferred to chapter9 when it will be considered in the light of the results presented in this thesis. Another interesting feature of the machining process as seen in the above review is the extension of the primary shear zone to a level below that of the nascent surface. The consequence of this is the dependence of the nature of the subsurface layer on the stresses in the primary shear zone. The machined surface becomes, therefore, the result not only of the process of separating the chip from the workpiece but also of the deformation of material to a certain depth below the machined surface.

This deformation is also affected by the temperature distributions present in machining and which will affect the workpiece

material ductility, an important parameter which determines the type of deformation and the mechanisms involved. Also the temperature seems to be the main factor through which cutting variables affect the machining process and hence the state of the machined surface.

As a consequence of the deformation taking place in machining, it becomes important to think of the machined surface not only as a topographical problem (i.e. geometry of the profile), but as a typological problem as well, including all the alterations brought about by the machining process to the subsurface layer. This concept of unifying the geometrical with the typological changes in the machined surface layer is termed "surface integrity" and will be discussed in the next chapter.

CHAPTER THREE

THE NATURE OF MACHINED SURFACES

3.1- Introduction

3.2- Surface Texture

3.2.1- Effect Of Cutting Speed

3.2.2- Effect Of Undeformed Chip Thickness

3.2.3- Effect Of Rake Angle

3.2.4- Effect Of Other Factors

3.3- Change In Surface Hardness

3.4- Residual stresses

3.4.1- Thermal Model

3.4.2- Mechanical Model

3.5- Plastic Deformation

3.6- Phase Transformation

3.7- Other Surface Alterations

3.8- Impact On Functional Behaviour Of Machined Components

3.8.1- Effects Of Surface Roughness

3.8.2- Effects Of Residual Stresses

3.8.3- Effects Of Surface Hardening

3.9- Concluding Remarks

It has been known for a long time that various machining operations produce surface layers of a different nature to that of the base metal. Early work carried out in this field, was primarily directed to the investigation of the effects of grinding hardened tool steels [37,38]. Later investigators [39-50] have considered the effects of different machining processes on various materials.

The nature and characteristics of machined surfaces are receiving more attention, principally for two reasons: The first one is the increasing awareness that the quality of the surface produced in machining can have a significant effect on material properties [51-65]. The second one is the use of components with thinner sections, made possible by the development of stronger materials and prompted by an ever increasing need for lighter components and for conservation of material. This has consequently resulted in higher surface to volume ratios.

The ever increasing demand for product reliability, performance, and longevity cover all engineering components from aerospace applications to automotive and commercial appliances. To satisfy these demands and bearing in mind the ever increasing surface to volume ratios, studies of the nature of the machined surface have been carried out. This in turn resulted in the adoption of a more complete characterization of the machined surface to take into account all the alterations produced in the surface by machining.

In order to implement a complete characterization of the machined surface, it is no longer sufficient to adopt the traditional way of considering the surface profile alone. Rather, both the profile and the state of the subsurface layer are considered.

The general subject of looking at the state of machined surfaces has been developed into a cohesive discipline by J.F. Kahles and M. Field of Metcut Research Associates. The term "Surface Integrity" was coined in 1965 [66] and has received growing acceptance in manufaturing circles, as a generic term which takes into account all the phenomena observed to occur in both the surface and the subsurface layer of a machined component after a machining process.

A number of possible alterations in the subsurface layer produced in machining have been identified and reported [41,67] as being components of surface integrity. These are listed as follows:-

   (i)- surface texture,

  (ii)- change in hardness,

 (iii)- residual stress distribution,

  (iv)- plastic deformation,

   (v)- phase transformation,

  (vi)- tears, laps, and crevice like defects associated with the
        built-up-edge produced in machining,

 (vii)- macrocracking,

and (viii)- microcraking.

Considerable work has been carried out in which individual surface integrity components have been investigated. However, although microcracking is frequently referred to as one component of surface integrity [39-41,63,66-68], it has not to the present day been the subject of in-depth study. The present chapter consists therefore of a brief review of surface integrity research, whilst the consideration of surface microcracking during machining is reserved until chapter 4.

The traditional way of designating the quality of a machined surface is by measuring the surface roughness. The most widely used roughness parameters are the arithmetical mean deviation "Ra" previously known as the (Centre-Line-Average) and the peak to valley height "Rt". An insight into the understanding of the meaning of surface texture and its components is given in the British Standard BSI [69].

A number of quality control type of instruments have been developed in order to study surface finish and its effects on performance in operation. These instruments operate on mechanical, mechanical-electrical, pneumatic, or optical principles. The most versatile of these for workshop use are the mechanical-electrical designs which rely upon the movements of a stylus relative to a datum as it is drawn at constant speed across the machined surface of the specimen. This movement is amplified electronically and the data automatically analysed to give the required surface texture parameters. A graphical readout or computer contour plotting of the surface profile may also be accomplished.

The stylus is a diamond of small tip whose radius of curvature as determined by the razor blade method [70] is of the order of 2 microns. It is worth mentioning that this value is only a minimum value and that the actual value could be as large as 11 microns [70]. This finite value of the tip radius puts a physical limitation on the smallest surface defect recorded by the stylus as fine cracks cannot be penetrated and sharp asperities will be rounded off. This is illustrated in figure 23. In additon some workers [72-74] have claimed that the resolution is reduced by stylus bounce and surface

damage by stylus and skid. The effects of the stylus tip radius and the bounce together with the distortion in the surface profile by the differential magnification scaling should be carefully borne in mind when interpreting stylus instrument traces.

The wide use of the surface roughness parameters as surface finish qualifiers is due to the versatility of the measuring instruments and the speed of measurement in the workshop with the consequence of a considerable amount of work being carried out in this area. More recent developements in this field are high speed [75] and in-process [76] surface roughness measurement techniques.

3.2.1- Effect Of Cutting Speed:

It is reasonably well established that the nature of chip formation with or without built-up-edge formation critically affects the surface roughness [77-81]. The surface roughness variation with cutting speed has been found [81] to follow the trend shown in figure 24. Figure 24a is for a medium carbon steel whereas figure 24b is for a cold-drawn resulphurized steel. This figure shows that increasing the cutting speed will significantly reduce the surface roughness. The reduction in surface roughness with an increase in cutting speed is due to the reduction in the size of the built-up-edge which in turn is due to the higher temperatures. The mechanism by which the built-up-edge affects the surface roughness has been associated with the instability of the built-up-edge [82-83] as described in section 2.4. The same conclusions have been drawn by Williams and Rollason [84] and by Kabaldin [85].

3.2.2- Effect Of Undeformed Chip Thickness:

The undeformed chip thickness has been shown by Shaw et al [86] to have a significant influence on the surface roughness at low cutting speeds as shown in figures 25 and 26. In these figures the surface roughness is shown to increase with an increase in the undeformed chip thickness.

3.2.3- Effect Of The Rake Angle

Rozenberg and Rozenberg [87] found that increasing the tool rake decreased surface roughness when cutting brass. Their results (figure 26) show a decrease in surface roughness with increase in rake angle, this effect being more pronounced at higher values of undeformed chip thickness.

3.2.4- Effect Of Other Factors:

In addition to the above variables, the surface roughness is also affeced by the roughness of the tool cutting edge [88], the use of cutting fluids [87,89], and free machining additives [86].

Sata [77] found that the surface roughness increased with an increase in cutting edge roughness. These results, however, are in conflict with the observation made by Lambert [88] that after the initial period, surface roughness depended primarily on the wear properties of the cutting tool.

Ernst and Merchant [89] have described results which showed that many lubricants reduced surface roughness. On the other hand Rozenberg and Rozenberg [87] found that when machining copper alloys,

the use of lubricants actually increased surface roughness compared to dry cutting.

Finally Shaw et al [86] have shown that free machining additives to the steel tend to decrease the surface roughness.

3.3- Change In Surface Hardness

In any machining operation the surface layer undergoes a change in hardness which can be measured by indentation hardness techniques (e.g. Vickers and Knoop-type indenters). An example of the hardness distribution in the subsurface layer for a low carbon C1018 steel is shown in figure 27. Depending on the cutting conditions and the workpiece material, the subsurface layer undergoes hardening or softening [90]. The hardening of the subsurface layer is associated with the plastic deformation (section 3.5) [90] and/or phase transformation (section 3.6) [40,66]. The softening is associated with overaging [88] and/or phase change [40].

A number of investigators [11,50,91-93] have studied the surface hardness change in machining. Surface hardness has been found [50,91,93] to be a maximum at the surface and to decrease sharply with the depth beneath the surface. Lau and Rubenstein [92] showed that the surface hardening produced in an orthogonally machined surface is increased by :-

(i)- increasing undeformed chip thickness,

(ii)- decreasing rake angle [also ref.93],

(iii)- decreasing clearance angle,

(iv)- increasing flank wear land,

and (v)- decreasing cutting speed.

They added that the influence of the cutting speed is most marked at low speeds. They also anticipated from the observed influence of artificially restricting the length of contact between the chip and the rake face of the tool on the shear plane angle [94] that the surface hardening may be reduced by using restricted rake face contact tools. Their suggestion that an increase in edge sharpness of the tool and the use of an efficient cutting lubricant, will both reduce the surface hardening, is in agreement with results by Kaczmarek [11] and Liu and Barash [93]. It should be mentioned, however, that the cutting speed range used [92] was very low (i.e.0.025 to 3m/min).

Jeelani and Ramakrishnan [50,91] studied the surface hardening at cutting speeds within the range 6 and 49m/min. They found that surface hardness was increased by increasing cutting speed and the tool wear land. This led them to suggest that temperature is an important parameter in surface hardening. Ovseenko et al [95] who looked at the effect of preheating the workpiece prior to turning, confirmed the influential role of temperature on surface hardening (see figure 28). A similar conclusion was reached by Ansell and Taylor [96] who found that ceramic tools produced surfaces with better wearing properties than those produced by carbide tools. They associated this with the hardness of the machined surface and explained it by stating that the thermal properties of ceramic being different from those of carbide tools, higher temperatures were expected when machining with the former.

3.4- Residual Stresses

The machining processes generate residual stresses in the subsurface layer by plastic deformation or metallurgical

transformation. These residual stresses may be deep or shallow, compressive or tensile depending on the machining history. They should be distinguished from the initial stresses existing in the workpiece material prior to machining and the stresses created during machining. The superposition of the initial and machining stresses results in the appearance of the residual stresses. In turning the residual stress distribution in the subsurface layer takes the form shown in figure 29.

The techniques used in the measurment of residual stresses fall into two main categories, namely direct and indirect methods [48,97] using X-ray diffraction technique and the layer removal deflection technique respectively [98].

A number of workers [11,93,99,100] have developed models which would be able to predict the machining residual stresses in the workpiece. Two simple models of residual stress generation in machining have been described by Kaczmarek [11] and Liu and Barash [93] who also provided experimental evidence [99] to support their claims.

3.4.1-Thermal Model:

As a consequence of the heat generation during machining, a temperature field appears in the subsurface layer of the nascent surface. The surface wishes to expand due to its higher temperature. However, the material beneath (which is at a lower temperature), restrains it from expanding as much as its temperature would dictate. It is this restraint due to the underlying material which results in the surface compressive stress. Deeper into the workpiece material the compressive stress decreases finally changing to tensile stress as

shown in figure 30 (position A_1). If the temperature reaches values at which the compressive stress will exceed the yield point, correspondingly reduced at such temperature, then plastic deformation will occur in the surface layer. The value of this temperature for a low carbon steel (C1018) has been calculated by Liu and Barash [99] to be 200 °C which is certainly well below the temperatures expected in machining. As soon as the temperature field shifts, i.e. when point A_1 acquires position A_2, as a result of cooling, the surface layer contracts which temporarily causes a reduction of stress differences. At position A_3 the elastically deformed underlying material will return to its normal state, while the plastically deformed surface layer wishes to contract still further as it is already plastically shortened. After complete cooling (position A_4) a tensile stress will apear in the surface layer, whose further contraction is restrained by the underlying layer, while the latter will be in a state of compression. It is evident from this description that the so-called thermal model of deformation and stress yields tensile stresses in the workpiece surface and its immediate sublayer down to a certain depth.

Henriksen [101] believed that the residual stresses are the function of the mechanical action of the tool rather than the thermal effect of cutting as the residual stress had a maximum value in a direction parallel to the cutting direction. He argued that if the thermal model was true then there was no reason why the residual stress should not be equal in all directions.

3.4.2- Mechanical Model:

The so-called mechanical model or cold model is based on the interaction between the tool point and the workpiece material. As a

result there appears a field of stress creating, if in this layer the yield point is exceeded, plastic deformation at a certain depth. Below the plastically extended layer are layers in a state of elastic extension (figure 31a). As soon as the action of the stress field ceases to act at point A, a contraction of the extended layers will follow. The plastically extended layer will not be able to return to its original state and will be compressed by the deeper layers which will be in a state of tension. Consequently, as a result of mechanical plastic deformation, compressive stresses will appear in the surface layer (figure 31b).

Stresses can also arise from changes in specific volume associated with phase changes. Phase changes associated with an increase in specific volume create a state of compression and those connected with a decrease in specific volume will create a state of tension in the surface layer. An example of this is the transformation of the pearlite and ferrite phases in plain carbon steels to austenite at high temperatures. Back quenching to the temperature of the workpiece which acts as a heat sink can result in the production of untempered martensite whose specific volume is larger than that of austenite. So this will give compressive stresses.

The magnitude of the residual stresses induced in the surface by machining is often considerable (i.e, up to 100,000 psi which is of the order of the real tensile strength at breaking of the material used (a 0.1%C steel) according to Henriksen [101] and in some cases can reach twice the yield stress of the annealed materials [93]. Henriksen found that the residual stresses decreased as the rake angle was increased from 0 to 42 degrees, the extent of this variation being more pronounced at higher values of undeformed chip thickness. This

finding has been reproduced in figure 32 which also shows the residual stress to increase with an increase in the undeformed chip thickness. Increase in cutting speed was also found [101] to cause a reduction in residual stress.

According to the results by Liu and Barash [102] the shape of the cutting edge governs the residual stress near the machined surface while the length of the shear plane governs the bulk distribution of the stress. For example, they found that negative effective clearance angle or large edge radius will modify the stress near the surface to be less tensile. They observed that smaller depth of cut did not necessarily produce low subsurface stresses and speculated that light cuts may give higher tensile residual stresses near the surface. This suggestion, they added, was congruent with experimental results on the effects on residual stresses of grinding in which very small depths of cut are usually taken [41,42,66,103].

The residual stresses have been shown [102] to increase in magnitude with:

(i)- a decrease in the cutting speed from 278m/min to 92m/min.

(ii)- a decrease in depth of cut at a low cutting speed of 92m/min, while the reverse was observed at a cutting speed of 278m/min.

(iii)- an increase in the shear plane length,

and (vi)- an increase in flank wear land.

One phenomenon which can have an effect on the final state of the residual stress in some machined components and which has not been considered by investigators of the residual stress, is the possibility of microcrack appearance. If the conditions of the surface are such that the residual stresses reach the material strength and they are tensile, then microcracks are likely to be produced. This in turn

- 35 -

will allow a relaxation of the residual stresses with the consequence that for surfaces which contain microcracks the residual stresses will be under-estimated. This is the case for brittle materials according to Brinksmeir et al [97], who gave as an example, the spindle of a grinding machine which had been nitrided then ground. Using the magnetic flux test axis parallel cracks could be made visible. They associated these cracks with the high tensile stresses produced by the grinding operation and with the fact that the material, being nitrided, could not deform in a plastic manner which caused it to be cracked. They did not, however, show how the residual stresses were relaxed as a result of these cracks. Another example they gave was the electro-discharge machining which always leads to high tensile stresses. Very often a stress relaxation can be observed when applying high energies [97]. This can be explained by the formation of microcracks in the surface layer.

3.5- Plastic Deformation

Surfaces produced in machining are frequently plastically deformed. The deformed layer on the machined surface can be thought of simply as being that part of the workpiece material which traverses the primary shear zone, is then subjected to stresses resulting from the action of the flank face of the tool, finally passing off with the workpiece. A simplified model of surface formation is shown in figure 33. In this figure, the primary shear zone is such that it extends below the level of the tool point to a depth "z". The tool cutting edge has been magnified to show the radius of curvature which is about 0.0003in (i.e. $\approx 7\mu m$) for a "sharp" tool according to Albrecht [1].

As a result of this tool edge roundness a part of the undeformed chip, plastically strained by the stresses in the primary shear zone, will be pressed down by an amount "x" below the tool adding to the plastic compression of the subsurface layers. After the tool has passed, the surface layer will recover to a height "y".

It follows from the above description that the plastic deformation and the depth of the deformed layer depend on the stresses in the primary shear zone and on the factors affecting them. Jeelani and Ramakrishnan [49,50] found that when machining a titanium alloy and maraging steel, the extent of plastic deformation and its depth of penetration is increased by:

(i)- increasing the cutting speed with no observable deformation at low cutting speed,

(ii)- increasing tool wear land at all cutting speeds,

and (iii)- machining under dry cutting conditions.

These results were explained in terms of the type of friction (i.e. whether sticking or sliding friction) which exists at the interface between the tool flank face and the workpiece surface. Similar observations have been made by a number of other investigators [90,91,104].

The plastic deformation undergone by the surface layer of the workpiece can be measured using a grid technique as described by Jeelani and Ramakrishnan [49]. Turley [105] used taper sections with a slope of 10:1 through the machined surface, to reveal the grain fragmentation caused by plastic deformation [106].

Phase transformations can occur in the subsurface layer of machined surfaces as a result of the heat generation in machining. Examination of phase transformations can be carried out using metallographic techniques followed by microscopic observations. They can also be identified by microhardness studies [98].

When steel, for example, which is a system containing ferrite and pearlite phases is machined, the surface temperature can reach a value high enough to cause a thin layer of the surface to transform to austenite. Back quenching into the workpiece, acting as a thermal sink, will result in the production of untempered martensite in the surface layer. Steels are not unique in this respect as similar transformations occur in many other alloy systems [66]. The layer of untempered martensite is also referred to as the "white layer" because it etches white [40,66].

Liu and Barash [93,99] did not, however, find any evidence of phase transformation either from photographic or microhardness examination when cutting a low carbon steel, although a worn tool (0.254mm flank wear land) was used at a cutting speed of 277m/min and a depth of cut of 0.254mm. Field et al [40] also observed no phase transformation when machining a titanium alloy.

3.7- Other Surface Alterations

In addition to the above surface alterations in machining, the inherent defects within the workpiece material (e.g. inclusions and voids), can be uncovered by the machining process and are then located at the surface in the form of tears or in the surface layer of the

machined component as voids. Some of these defects can be detected by visual examination or by surface penetrant inspection [66]. A number of other defects have been identified by Gillibrand [6] and include:

   (i)- prows,

   (ii)- scales,

   (iii)- dimples,

   (iv)- pits,

   (v)- spines,

   (vi)- grooves,

and (vii)- microcracks.

Although microcracks have been frequently quoted [39-41,63,66-68] as being one important component of surface integrity, they have not been the subject of any systematic studies. There has been, however, a limited amount of research carried out on the microcracking phenomenon in the shear zone of machining. This will be reviewed in the next chapter and preliminary knowledge derived to form the basis of research on the microcracks produced in the machined surface.

3.8- Impact On Functional Behaviour Of Machined Components

Until recent times the production of machined surfaces has been governed by the cost of machining and the surface quality. In specifying surface finish the aesthetics of the surface and tribological requirements of machined components were the factors of concern. The parameter used to quantify surface finish was the surface roughness "Ra" and the lower the value of this parameter the higher the quality level was and vice-versa. The consequence of this, coupled with the versatility of surface roughness measuring

instruments, was the popularity of this approach to surface quality. A recent survey by Devries [63] has established this clearly.

In the previous sections, however, it has been shown that surface roughness is only one of a number of parameters required to describe completely the state of a machined surface. It has also been mentioned that a more comprehensive term which fully describes the nature of the machined surface is surface integrity. To achieve satisfactory in-service functional behaviour of machined components, all the individual components of surface integrity should be considered and controlled. If this is achieved, then the machined components are said to satisfy surface integrity requirements. The effects of some surface integrity components will be reviewed in the following sections.

3.8.1- Effects Of Surface Roughness

The widespread use of surface roughness as a surface finish qualifier has greatly influenced research into the functional behaviour of machined components. Consequently, surface roughness has been related to the functional properties of machined components, for example, fatigue strength, contact fatigue, friction, and wear. This approach, although possibly acceptable, might be in fact ill founded. To carry this argument a stage further, the following examlpe may be given. Although wear can be influenced by surface roughness, it is evident from the work carried out by various investigators on the wear properties of surfaces that the hardness of the surface layer is another influential factor in determining the wear properties of machined components. The survey, quoted earlier [63] also indicated

that considerable research work was needed to provide a better and more complete characterization of machined surfaces.

A review by Moore [107] has shown that the tribology of machined components is affected by their surface roughness. Stress corrosion [108] and fatigue strength [66] have also been claimed to be influenced by surface roughness. The effect of three machining methods on bending and contact fatigue have been investigated by Ovseenko et al [95]. Their results indicated that, for turning, a significant increase in bending fatigue could be obtained by preheating the workpiece prior to machining. They attributed this improvement in bending fatigue to a decrease in surface roughness. They also showed that grinding tended to decrease both bending and contact fatigue as compared to turning. They did not, however, give any surface roughness data for the ground specimens. From their grinding conditions (i.e. gentle), it is reasonable to expect that the surface roughness of the ground specimens will be less than that of the turned specimens (1.3μm to 1.8μm). It can be argued, therefore, that, in this case at least, the machining process is more influential than surface roughness. To support this argument, the work by El-Helieby and Rowe [64] is considered. They showed that variations in surface roughness within the normally encountered range for the grinding process, have no consistent effect on the fatigue behaviour. Their fatigue data, for example, indicated fatigue limits of 461MN/m^2 and 196MN/m^2 for conventional and abusive grinding of En31 steel, respectively, although the surface roughness was practically the same (i.e. 0.56μm and 0.55μm). Also, the fatigue strengths exhibited by gentle and abusive grinding were 883MN/m^2 and 196MN/m^2 , although the surface finishes were in reverse order of quality (i.e. 1.0μm and 0.55μm), respectively. They pointed out, however, that it was

possible for single large scratches to induce fatigue failure, but this extreme, they commented, was outside the normal range of good grinding practice. They added that even so, such scratches could not be detected by the statistical methods characteristic of surface topographic measurements. This led them to conclude that the effect of surface topography had been overemphasized in its connection with the fatigue properties of materials.

3.8.2- Effects Of Residual Stresses

The influence of residual stresses on fatigue strength was stated long ago [38] and has been proved since in a number of investigations. Field and Kahles [66] quoted work on the influence of residual stresses on the fatigue of steels with hardness greater than 250VPN by Morrow and Millan [57] who showed the following:

   (i)- The residual stresses have similar effects on fatigue behaviour of materials as do mechanically imposed static stresses of the same magnitude.

  (ii)- As a conclusion of (i) above, the significant residual stresses are beneficial if compressive and detrimental if tensile, particularily in "hard" materials.

 (iii)- Near the fatigue limit (i.e. long fatigue life) the residual stress remains practically unchanged by the fatigue load.

  (iv)- At stresses above the fatigue limit, residual stresses can relax as an accompaniment of the fatigue process, this effect being greater in "soft" materials and at stresses well above fatigue limit.

   (v)- As a result of (iv), the fatigue life at high applied stresses depends very little on the initial residual stresses.

(vi)- The significant residual stress in bending is the peak value
near the surface whether it is tensile or compressive.

A number of other investigators [53,64,97,103,109,110] have
produced data which supports the above conclusions. Typical examples
are shown in figures 34 and 35. Brinksmeir et al [97], quoting the
work by Polakowski[53], added that the elastic limit in pure tension
and compression loading is lowered by the presence of residual
stresses independent of their distribution.

Fatigue strength is not the only performance consideration with
regard to residual stresses. Stress corrosion, also, can be affected
by the presence of residual stresses [41,66,97]. An example was
quoted [97] in which a stress corrosion problem arose in aluminium
alloy tubes produced in cold extrusion which had been used for
transferring chemical fluids after having been machined by tungsten
carbide tip turning. This stress corrosion was attributed to the high
residual stresses produced in the inner surface by the machining
operation. Table 2 shows the effect of abusive and gentle grinding on
the stress corrosion resistance of two ground hardened steels.
Bearing in mind that abusive grinding results in higher tensile
residual stresses than gentle grinding, it is evident from this table
that the resistance to stress corrosion is impaired by high tensile
residual stresses.

There is evidence that the residual stresses present in the
machined surface can be relieved by suitable techniques and
treatments. Knowing the origins and causes of these residual stresses
is important when undertaking to relieve them. For example, residual
stresses arising from phase change can be relieved by applying a
reversed heat treatment. It has been reported that residual stresses
have been partially relieved by tempering [39] and almost fully

Table 2 : Stress Corrosion Test (Ref. 66)

Specimen	Material	Hardness	Applied Bending Stress on Specimen	Time To Failure in salt spray
1	4340	53 Rc	110,000 psi	435 hours
2	4340	53 Rc	110,000 psi	70 "
3	D6AC	50 Rc	110,000 psi	1,000 " *
4	D6AC	50 Rc	110,000 psi	16 "

* Test discontinued without failure
1 and 3 : gently ground   2 and 4 : abusively ground

relieved by annealing [64] (figure 36). Heat treatment relieving of residual stresses, however, is not too predictable in comparison to tumbling and shot peening whose effects can be accurately predicted [66]. Tumbling and shot peening relieve high tensile residual stresses by superimposing a new compressive stress [66,111,112]. Field and Kahles [66] reported Letner [112] to have shown that the as-ground residual stresses of $827MN/m^2$ on 64Rc steel was reduced to $138MN/m^2$ by tumbling. This represents a reduction in residual stresses of more than 83 percent. Figures 36 and 37 show that stress relief after abusive grinding (i.e. high tensile residual stresses) failed to restore the surface fatigue properties. Bearing this in mind it becomes clear that controlling the process of production of machined components is a positive means of ensuring surface integrity requirements in contrast to uncontrolled machining followed by stress relief operations. Moreover, high residual stresses can result in permanent defects (e.g. surface microcracks) and in stress corrosion neither of which can be cured. The presence of microcracks in the surface could be the reason why heat-treatment stress relief does not restore the fatigue properties of machined surfaces.

3.8.3- Effects Of Surface Hardening:

In addition to the effects of surface topography and residual stresses mentioned above, surface hardening is also considered to have a significant influence on the functional properties of machined components, and more specifically on their contact fatigue and wear properties. The hardened surface layer is characterized by a higher yield point and ultimate tensile strength [11]. Therefore, in the absence of residual stresses, high roughness values, or microcracking, the surface hardening can be thought of as a process of surface strengthening. This statement is supported by the work of Ovseenko et al [95] who showed that hardening has significant effects on both bending and contact fatigue properties. Their work indicated an improvement in the fatigue properties with an increase in the microhardness of the machined surface.

3.9- Concluding Remarks

The foregoing review of the literature available on the subject of the nature of machined surfaces has shown the following:

a)- Surfaces produced by machining processes undergo various changes and alterations which may be detrimental or beneficial depending on the functional operation of the machined component. For example, tensile residual stresses are detrimental to machined components operated in tension. On the other hand compressive residual stresses are advantageous because they close up cracks and raise the tensile threshhold of applied stress to cause propagation.

b)- There is evidence about the influence of the machining parameters on the type and extent of the alterations produced in machining. In addition, all the conditions pertaining to the chip formation influence the characteristics of the machined surface, since both the chip and the machined surface originate in the shear zone.

c)- There is evidence that the surface alterations which result from machining influence the functional properties of the machined product. Research, however, in this topic is lacking for some components of surface integrity. For example, although there is agreement [39,41,48,63,103] that the presence of microcracks in machined surfaces, impairs their fatigue strength characteristics, no work has been carried out to investigate how and to what extent this influence is evident. This is thought to be due to the difficulties involved in the examination of microcracks and the absence of suitable techniques for their measurement.

The importance of measuring techniques for surface microcracks is considerable when it is realized that this will open a whole new area of research involving the effects of the machining variables on microcracking, and the influential role of the latter on the functional properties of machined components. In addition, there has been a growing concern for the problem of short cracks in fatigue during the last decade [113].

The next chapter is aimed at introducing the microcracking phenomenon and the associated up to date knowledge.

CHAPTER FOUR

MICROCRACK FORMATION

4.1- Introduction

4.1.1- Microcrack Nucleation

4.1.2- Microcrack Growth

4.1.3- Microcrack Coalescence

4.2- Shear Deformation Tests

4.3- Microcrack Formation In Machining

4.3.1- Microcracking In The Shear Zone

4.3.2- Microcracks In The Machined Surface

4.4- Discussion And Objectives

4.4.1- Discussion

4.4.2- Objectives

Microcracking is a phenomenon which occurs when a material is subjected to deformation severe enough to cause a concentration of microstresses which are conducive to localized fracture. The formation of microcracks can be thought of as a process including two stages during which different conditions can prevail and different mechanisms can be operative. The first stage consists of the nucleation mechanisms and depends primarily on the presence of potential nucleation sites as well as the action of a critical stress field (i.e. with a magnitude of the order of the cohesive strength of the material). The second stage consists of the growth of the nucleated microcracks and depends on the crack propagation characteristics of the material as well as the persistence of the critical stress field for the growth to be maintained. This stage can take two forms:

a)- the growth of the microcracks,

b)- the coalescence of neighbouring microcracks.

The following sections consider the various mechanisms which can be operative during the formation of microcracks.

4.1.1- Microcrack Nucleation:

A number of investigators [114-121] have proposed and discussed possible microcrack nucleation mechanisms. It should be noted that in trying to suggest such mechanisms the concept of the material as a continuum must be abandoned in favour of the microscopic view of the material as a non-homogeneous matrix containing localized features

(e.g. grain boundaries, voids, solute atoms, particles of the second phase, and dislocations).

Inclusions and second phase particles present in commercial alloys under severe straining, give rise to void formation by decohesion of the particle-matrix interface. Such decohesion can occur even under a predominantly compressive stress field [114]. The mechanism of void formation at inclusions has been observed during rolling by Baker et al [115] who concluded that the strength of the inclusion-matrix interface is relatively low. Once voids have formed they can act as stress raisers and encourage microcrack nucleation by shear linking mechanisms [116].

Microcracks can also be nucleated by:

    (i)- dislocation pile-ups,

    (ii)- intersections of twin bands,

   (iii)- grain boundary fracture,

 and (iv)- cracking in a brittle phase.

A dislocation pile-up occurs when a number of dislocations generated by the deformation process are stopped by a strong obstacle. It has the property of concentrating a tensile stress around the tip of the pile-up of dislocations and this stress concentration can be sufficient to initiate a microcrack. A more comprehensive discussion of this mechanism has been afforded by Mc Clintock and Argon [117] who also discussed microcrack formation by the intersection of twin bands.

Grain boundary fracture can occur either by separation of grains under purely hydrostatic tension [118] or by the motion of dislocations into the grain boundary from one crystal which cannot be accommodated by slip in the other.

The cracking of brittle phases has been frequently observed metallographically [119]. The drag on long cylindrical inclusions

aligned with the direction of maximum tensile strain may result in a normal stress within the inclusion of the order of the flow strength of the matrix times the length to diameter ratio of the inclusion according to studies by Kelly and Davies [120]. Burns and Pickering [121] have suggested that cracking may be initiated in pearlitic structures by any one of three mechanisms:

(i)- the high dislocation density in the pearlite ferrite interface which will increase locally its resistance to plastic deformation,

(ii)- the fracture of cementite lamellae which may lead to a notch effect,

(iii)- the generation of dislocations at a ferrite-cementite interface may lead to the creation of voids and provide nuclei for cracks.

The above described mechanisms are all possible candidates for microcrack nucleation as the various investigations seem to suggest. However, the preponderance of one mechanism over the others for given conditions of the deformation is a strong possibility since the onset of one mechanism can use up the applied energy before it reaches the value for which mechanisms requiring higher energy can be operative.

4.1.2- Microcrack Growth:

The nucleation of a microcrack by plastic deformation does not necessarily result in the formation of an observable microcrack in the machined surface, since the conditions of microcrack nucleation and subsequent development into an observable microcrack can be different. The possibility of rewelding of microcracks in the presence of high compressive stresses can lead to a decrease in the observed number of

- 50 -

microcracks [122]. On the other hand, in the presence of high tensile stresses the microcracks can grow to a size of the order of the mean distance between individual microcracks and thus cause a bridging between neighbouring microcracks. This suggests that the stress state is important for the growth of microcracks, compressive stresses tending to slow or eliminate this growth. Burns and Pickering [121] have discussed the crack propagation in pearlitic structures whereby they suggested that when initiated, a crack can only propagate either by passing round the lamellae, involving some tearing and energy absorption, or by cracking of the lamellae with a similar result. Thus they concluded that pearlite may be considered to be an effective arrester.

In polycrystalline materials, a cleavage microcrack once nucleated, will very likely be stopped by a grain boundary where the cleavage planes will undergo a large and discontinuous change in orientation into the neighbouring grain. Once a microcrack is stopped at a grain boundary, plastic deformation could occur to some extent in the vicinity of the microcrack root and blunt it [117]. This suggests that the grain size also has an important part to play in the microcrack growth stage. For a microcrack to propagate from one grain to another, it is necessary that the energy driving the microcrack growth should provide not only for the surfaces of the microcrack but also the energy necessary to break through the grain boundaries. The smaller the grain size the larger the number of grain boundaries interfering with the microcrack and the slower and more difficult their propagation becomes. A natural consequence of smaller grain size is, therefore, smaller microcracks obtained.

The time during which the stress field acts is also an influential factor in the extent of the microcrack growth. This will be referred to as the "subjection time" in the present thesis.

4.1.3- Microcrack Coalescence:

This can take place when a high tensile stress exists at the tip of the microcracks and when two microcracks are close to each other. Under these conditions, neighbouring microcracks can coalesce to form larger microcracks by part cleavage and part plastic deformation. The result of this coalescence will be a reduced density of relatively larger microcracks.

4.2- Shear Deformation Tests

In an attempt to represent the machining process by a test in which experimental observations and measurements could be more easily made, rigs have been designed [122-124]. These rigs enable the combination of shear and compression to be applied simultaneously.

It has been shown in chapter 2 that when metal is machined, large strains are involved accompanied by significant hydrostatic stress in the shear zones. Bridgeman [125] clearly showed that the greater the hydrostatic compression, the greater the strain at rupture. Similar observations have been made by Walker and Shaw [123], Luong [124], and Luong and Brown [122].

While Bridgeman emphasized the important role of hydrostatic pressure in postponing gross fracture of a specimen, he said little about the mechanism. He also provided little discussion of the shapes

of the stress-strain curves obtained in the presence of large hydrostatic pressures.

It is well known that materials subjected to an applied stress behave according to two classes of deformation. The first class is the elastic deformation which is reversible and as soon as the applied stress is removed, the material returns to its original state. The second class is the homogeneous plastic deformation which is permanent even when the applied stress is released. Walker and Shaw [123] have proposed that a third class of deformation must be added that is predominant when large shearing strains occur accompanied by a large normal compressive stress on the shear plane. This new class of solid behaviour, they suggested, involves deformation due to the motion of microcracks much as the deformation of a liquid occurs as a result of the motion of the structural holes that characterizes the liquid state. Thus it was suggested [123] that large strains are possible in metal cutting according to the mechanism of formation and rewelding of microcracks. Typical shear stress-strain curves at different values of compressive stress obtained by Walker and Shaw are shown in figure 38. This figure shows that as the shear strain increases up to a critical value (marked "Ecr" in the figure for subsequent reference), the shear stress also increases up to a maximum. With further increase in strain above "Ecr", the shear stress starts dropping. Walker and Shaw propose that at any given large strain (i.e greater than the critical strain), an equilibrium exists between microcrack appearance and disappearance. The equilibrium shifts to induce a preponderance of microcracks, as the strain approaches its value of gross fracture. Experimentally they showed that at low strain rate, there was a decrease in shear stress at large strains (i.e Ecr.) when steels with different sulfur content were sheared under a superimposed

compressive stress. They attributed this negative work hardening phenomenon to the reduction in the real area available to resist shear due to the presence of microcracks. They advanced as evidence that they recorded acoustic measurements indicating noise sources associated with microcrack formation . This was, however, only stated and the details of how they did this were not presented.

It is also shown in figure 38 that as the compressive stress is increased the onset of negative work hardening is delayed to a higher value of the shear strain. It was also found [123] that the presence of sulfur which appeared to have an embrittling effect when the hydrostatic pressure was zero, tends to promote the rewelding of the microcracks, when a large compressive hydrostatic stress is acting on the shear plane. This action of sulfur is consistent with the fact that an increased sulfur content promotes the formation of a stable built-up-edge in machining.

These observations by Walker and Shaw have been confirmed by Luong [124] who examined polished sections of shear test specimens for microcracks. His work confirmed the dependence of the negative work hardening on the microcrack formation. However, he suggested that in addition to the reduction of the real area to resist shear, microcracks may decrease the flow stress by acting as stress raisers. He proceeded then to check this suggestion by analysing test results obtained from shearing resulphurized steel at low strain rate. Taking an arbitrary average size of the microcracks (he gave no indication of how this was determined), he calculated the actual area resisting shear by substracting the total area of microcracks from the instantaneous cross-sectional area. From this, he then went on to calculate the reduction in stress due to the microcracks. He found that the reduction in area contributes only a small percentage to the

reduction in shear stress. For example, at a strain of 5.5 the reduction in area due to microcracks contributes only 10 percent of the total reduction in shear stress, this percentage decreasing with increasing strain. This indicates that, although the reduction in area due to microcracks is in part responsible for the reduction in flow stress, it is not the major mechanism. This led Luong [124] to suggest that the local stress concentration around inclusions must play an important role in decreasing the bulk shear stress. In other words, the tip of the microcrack acts as a stress raiser which facilitates dislocation flow in the region near the inclusions. This suggestion is in line with Iwata's findings [126] that the strain around a manganese sulphide (MnS) inclusion is much higher than the bulk strain and that local strain increases rapidly as a microcrack grows.

The above proposal has also been adopted by Luong and Brown in a recent investigation [122]. Typical results from their investigation are presented in figures 39 and 40. The densitiesof microcracks at a given strain are indicated adjacent to the stress-strain curves. It can be seen from these figures that the density of microcracks increases with increasing strain and complete fracture occurs at a strain in excess of that for the onset of microcrack formation. The difference between the onset of microcrack formation and fracture being enhanced by superimposed compressive stress.

A comparison between figures 39 and 40 shows that the main features of the shear at large strains are not dependent on strain rate. However, the maximum stress values at high strain rate are higher than the corresponding values at low strain rate which may be attributed to the strain rate sensitivity of the material. Also the density of microcracks was higher at higher strain rates.

The effect of the material composition was also part of the investigation by Luong and Brown [122] who tested resulphurized and mild steels as well as a high purity copper which is a single phase material. The resulphurized steel was found to have a significantly higher number of microcracks in the defomation zone than the mild steel. The high purity copper, on the other hand, did not exhibit any microcrack formation. This led Luong and Brown to suggest that a second phase is necessary for microcrack formation. In addition, the stress strain curve for the copper obtained in the presence of a compressive stress, did not show any negative work hardening. Moreover, it was noted [122] that the resulphurized steel had a steeper negative work hardening slope than the mild steel and it was concluded that this was associated with the higher number of microcracks found.

Based upon the above observations, Luong and Brown [122] have put forward a number of proposals one of which is of particular interest to the present investigation. They suggested that the increase in ductility with increase in compressive stress can be attributed to the influence of compressive stress on the dynamic behaviour of microcracks. More precisely, the superimposed compressive stress tends to delay the formation of microcracks at low strains and inhibits their growth and coalescence at large values of strain.

The above reported investigations, alt hough incorporating superimposed stress and strain rates of the order of those typically found in machining, fail to represent the machining process in a faithful manner. This is because the temperature inherent in machining and the tensile stress ahead of the tool cutting edge have not been considered. It is, however, expected that the density of microcracks will be significantly inreased in the presence of a

superimposed tensile hydrostatic stress as compared to a superimposed compressive stress. This can readily be derived from the comparison of figures 39a and 39b or 40a and 40b. It is seen from these figures that, for a given strain, the microcrack density for zero compressive stress is greater than when a compressive stress is applied. Consequently, a superimposed tensile stress is expected to result in an even higher microcrack density, provided coalescence does not occur. Also the temperature can affect the microcrack formation by changing the ductility of the material. Hence, it can be concluded that while the shear deformation tests can give a simplified picture of what goes on in the shear zone at locations where compressive hydrostatic stresses prevail, it cannot be used to describe the shearing process at the vicinity of the tool cutting edge for the reasons just mentioned above. Consequently, the use of these shear test results must be treated carefully when seeking explanations for the microcracks found in the machined surfaces.

Bearing this in mind, the next section is a review of the research on the microcracking in the shear zone during actual machining.

4.3- Microcracking In Machining

In machining the microcracking phenomenon has been established to occur with a number of different materials machined over a wide range of cutting condititons.The two major areas of importance from the machining standpoint regarding the microcracking, are the shear zone and the machined surface.

4.3.1- Microcracking In The Shear Zone:

Microcracks have been observed in the deformation zones when machining two phase materials by a number of investigators [127-135] using various techniques. For example, quick stop device [128,129], fractographic technique [130], and machining inside a scanning electron microscope [131,132], are some of the methods used.

One of the earliest works on the microcracking in machining was carried out by Komanduri and Brown [133] in an investigation as part of a basic study of the types of chip formation in machining. When machining with a continuous chip formation, they observed voids alongside and within the pearlite islands near the center of the shear zone. For the cutting conditions used there was no void coalescence to form microcracks.

In the other hand, when machining in the presence of a built-up-edge, they observed large microcracks in the secondary shear region between the stationary built-up-edge and the flowing chip. These were aligned generally parallel to the tool rake face. In the workpiece, below the tool they found a region of large strain with microcracks parallel to the cutting direction. At the tip of the built-up-edge the chip was claimed to separate from the work material by coalescence of the microcracks formed to generate a gross crack. It was also brought to notice [133] that the microcracks formed in the tip of the built-up-edge tend to close as the chip slides up the face of the adhered material. Examinations of the latter at higher magnifications revealed this to be heavily worked ferrite, separated by layers of pearlite with some very small scattered voids present. It was thus suggested [133] that larger microcracks which existed as

the built-up-edge was deposited had been rewelded as proposed by Walker and Shaw [123].

As regards the segmental chip formation, Komanduri and Brown proposed that this involves an instability which may arise from the negative stress-strain material characteristic which had been noted at large strains [122-124], i.e. at the onset of microcrack formation. To verify this proposal, the deformation zone was therefore, observed at different stages of the segmentation. In segmental chip formation, the plastic zone was observed to cycle backwards and forwards relative to the cutting tool. At the instant when the plastic zone is closest to the tool, examination of the deformation zone revealed very small voids, similar to those observed in the continuous chip formation. As the plastic zone moved forward, away from the tool, the shear strain increased and the voids coalesced to form microcracks. Microcracks of considerable size were observed [133] all along the shear zone from the tool nose out to the free surface and they could be seen to represent a significant proportion of the material area which was resisting the plastic shear stress. Near the free surface of the chip and workpiece, the microcracks tended to run together to give gross cracking. This gross cracking, initiating at the free surface, seemed to be instrumental in the rapid return of the plastic zone towards the tool rake face [133].

As for the discontinuous chip formation, Komanduri and Brown [133] stated that this is an extreme case of the segmental chip formation which involves complete fracture of the chip once coalescence of the microcracks has started. While this explanation may be valid for the segmental chip formed in machining steel, it appears that it is not the only mechanism of segmental chip formation by virtue of the fact that segmental chips are also produced in

machining pure iron [6] which is thought to be less prone to microcrack formation as will be seen shortly.

Doyle [130], using fractographic techniques, has found evidence of microcracking within the shear zone in the form of serpentine glide markings when machining impure iron and plain carbon steel with continuous chip formation. This led him to suggest that this type of chip formation is governed by the formation and linking of microcracks, and that the critical condition for shear is that high strains be generated within small volumes. He also found that the cutting forces increase with increase in the carbon content. He explained this trend in the cutting forces on the basis that microcracks only initiate and propagate in the ferrite phase and that the amount of this phase continually decreases with increase in the carbon content. Therefore, he added, it becomes increasingly difficult to shear due to the limited microcrack growth and hence the cutting forces increase. He did not, however, comment on the fact that increasing cutting forces with increase in carbon content could be simply explained by the associated increase in hardness, i.e. increase in resistance to gross plastic deformation.

Brown and Luong [128,129] carried out an investigation to study the influence of the cutting conditions on the microcrack formation in the deformation zones when machining a mild steel. They observed microcracks in all types of chip formation in machining as shown in table 3. In all cases, they found that the microcrack density was greatest around the tool cutting edge radius with a decreased number of microcracks in the primary shear region. They also observed that under several cutting conditions, microcracks formed in the work material below the tool and in the chip near the free surface. The microcrack density was found [128,129] to increase as the cutting

Table 3 : Microcracks observed when machining mild steel SAE 1015;
clearance angle 7°; UCT=0.25mm; orthogonal cutting at end
of tube of outer diameter=100mm and wall thickness=5.6mm.
(Refs. 128 and 129)

Test	Rake Angle (deg)	Cutting Speed (m/min)	Type of chip Produced	Observation of microcracks
A	15	18	Partially discontinuous	Microcracks along the "shear-plane" particularily near the tool edge.
B	15	25	Continuous with b-u-e.	Considerable density of microcracks near the tool edge. Some microcracks near the middle of the "shear-plane" but less than in test A.
C	15	137	Continuous and curly	Very few voids in the middle of the shear region.
D	0	25	Continuous	Approximately the same microcrack distribution as in test A.
E	0	58	Segmental	Significant void formation in the middle of the shear zone and at the tool edge.
F	0	137	Continuous	Approximately as for test C.

speed was increased up to 25m/min and thereafter further increase in cutting speed yielded less microcrack formation.

Alterations of the rake angle between 0 and 15degrees appeared to have little effect on the microcrack density, although there was a slight increase in microcrack formation with decrease in rake angle at low cutting speeds [128,129]. The microcracks were found to follow the general direction of the shear plane and the long axis of each microcrack lay roughly parallel to this direction. In all cases, the density of microcracks close to the cutting edge of the tool, was greater than in the middle region of the deformation zone.

Some microcracks were also observed [128] below the tool cutting edge and specific patterns of microcracks were associated with the fine undulations on the free surface of the chip.

On the question of the microcracks not being a real cutting phenomenon, Brown and Luong [128,129] discounted the possibility of them arising from thermal stresses induced after rapid stopping of the cutting process and the consequent cooling. They justified the above by the fact that as the cutting speed was increased beyond the 25m/min value, the microcrack density decreased with increase in the cutting speed. In other words, there were less microcracks in the presence of higher thermal gradients.

From the above observations , Brown and Luong [129] hypothesized that the variation in microcrack density with the change in the cutting speed is associated with the change in the type of chip formation. At low cutting speeds the temperatures are low so that the coefficient of friction on the rake face is high and the work material tends to have a high flow stress. High friction on the rake face and high material flow stress are both conducive to high values of the strain in the primary deformation zone. Since microcrack formation is associated with large strain situations [122-124], one would expect the microcrack density to increase with decrease in cutting speed. This is the case for speeds above the 25m/min as observed by Brown and Luong [128,129]. At speeds below this value, the observed reverse in trend was exlpained by the assertion that microcracks run together to form gross cracks or a semi-discontinuous chip (as in test A, table 3), or at still lower speeds, a completely discontinuous chip [129].

The increase in microcrack density which was observed when the rake angle was decreased, was explained by noting that the strain in the primary shear zone must increase as the rake angle decreases. The rake angle decrease causes the primary deformation zone to rotate forward ahead of the tool. This means that the chip thickness increases relative to the undeformed chip thickness and, in fact, the

- 62 -

strain of plastic deformation is greater, a situation which increases the likelihood of microcrack formation.

An important conclusion by Brown and Luong [128,129] is the observation that the microcacking phenomenon is apparently associated with the two-phase nature of the material leading to the belief that there is a strong possibility of microcracks not forming when machining a single phase material. This conclusion is congruent with the results [122] in large strain deformation of high purity copper which is a single phase material.

Resulphurized steels have been investigated at very low cutting speeds [126,131,132]. Under these conditions, extensive microvoid formation has been observed in association with the manganese sulphide inclusions which appear to act as non-deforming particles. At the higher cutting speeds used in practical machining operations, it is expected that the higher workpiece temperature may cause softening of the manganese sulfide and hence under these conditions microvoid formation may be eliminated. To examine the validity of this speculation, Brown and Luong [134] machined a free machining steel in the form of a circular disk to approximate orthogonal machining. From the examination of chip roots in the scanning electron microscope, they found evidence of inclusions which were considerably deformed during machining at high speeds. They observed apparent "crack like" features extending out from the manganese sulfide inclusions. X-Ray mapping with probe facility on the scanning electron microscope, enabled them to confirm that the crack-like features were not rich in manganese which led them to suggest that these were indeed microvoids. They thus concluded that, although at higher cutting speeds manganese sulfide inclusions do not behave as non-deforming particles, there is

sufficient difference in their mechanical properties from that of the ferrite matrix for microvoids to be initiated in the latter.

Iwata and Ueda [5] directly observed the chip formation of pure aluminium, low carbon, resulphurized and leaded steels using a technique which enabled them to perform orthogonal "micro-machining" inside the scanning electron microscope [127]. In particular, they were interested in the study of the dynamic crack formation in a machining process. Although the test temperature could be controlled up to 800°C, the effect of strain rate was not represented by virtue of the very low cutting speeds used in these tests (i.e. 0.15-0.2m/min). However, Iwata and Ueda were able to observe the machining process in the microscale, remembering that the method they used involved observation at the outside of the cut (i.e. conditions are plane stress not plane strain). They found that in the primary shear zone, voids form and grow at the interface between the ferrite matrix and non-deformable inclusions (MnS) and they play an essential part in crack formation. On the other hand, in the vicinity of the tool cutting edge, the crack nucleation was observed to be frequently generated by the collision of inclusions with the tool cutting edge.

From the above observations Iwata and Ueda [5] classified the types of crack formation into two major groups; one being generated in the vicinity of the cutting edge, the other in the primary shear zone. The former includes:

- the cracks nucleated below the flank face of the tool,

- the crack formed near the chip/tool interface,

- the crack induced by inclusions just near the cutting edge.

The latter includes:

- internal cracks such as the crack resulting from void formation around non-deformable inclusions, and

- the crack associated with fracture of inclusions in the primary

shear zone.

No microcracks were observed when machining pure aluminium.

The first attempt to quantify microcracks in machining is due to Luong [124,135] who reported that the width of microcracks, at a value in the range 0.7 to 2 microns, was not significantly influenced by the variation in cutting conditions. In comparison, he found [135] that the length and number of microcracks did depend on their location in the deformation zone. For example, the average length was 5microns in the middle of the deformation zone and up to 25microns near the tool rake face. In particular, Luong used the scanning electron microscope to count the number of microcracks for a given area ($0.015mm^2$) within the primary shear zone. The variation of the microcrack density with the cutting speed is reproduced in table 4 which also gives the cutting and thrust forces as well as the type of chip formation.

Table 4 : Variation of microcrack density and cutting forces with workpiece material and cutting speed (after Luong [135]).

Material	Cutting speed (m/min)	Chip formation	Average microcrack density per $0.015mm^2$	Fc (N)	Ft (N)
Mild Steel	3	Quasi-continuous	3	3634	1364
	10	b-u-e.	2	3821	1650
	25	b-u-e.	3	3634	1760
	45	b-u-e.	1	3728	1870
	80	Continuous	0	3728	2013
Resulphurized Steel	3	Continuous	7	3215	660
	10	"	5	3168	704
	25	"	6	2436	748
	45	"	2	3122	968
	80	"	1	3308	1254

Tool : 15° Rake; 7° Clearance; 0.25mm Undeformed chip thickness and thickness 8mm width of cut.

It can be seen from the above table that the microcrack density generally decreases with increase in cutting speed. Also, the cutting forces tend to increase with decrease in the microcrack density.

Luong [135] also found that the distribution of micrcracks and their behaviour are not uniform throughout the deformation zone. The microcrack density decreased from the region in the immediate vicinity of the tool cutting edge to the free surface of the chip. In conclusion, he stated that the number of microcracks formed in the deformation zone generally decreases with an increase in the tool rake angle or a decrease in the undeformed chip thickness.

4.3.2- Microcracks In The Machined Surface:

Prior to the generation of a machined surface, the work-material is subjected to a high level of deformation. It is possible that within the workpiece material traversing the primary deformation zone, microcracks are formed prior to their appearance in the machined surface. This possibilty is supported by the frequent mention of microcracks in surface integrity considerations as discussed in chapter 3.

It is evident from the previous section that most of the observations on the microcracking in machining have been made in the shear deformation zone and in the chip formation. However, a number of investigators [5,124,128,129,135] did in fact indicate the presence of microcracks below the tool flank and around the tool cutting edge. Luong [135] even speculated that some of the microcracks formed below the tool flank face may also be left in the newly machined surface.

Up to date there has been no systematic study carried out on the microcracks produced during machining in the machined surface,

although a few investigators [6,136-138] have observed the existence of these microcracks on machined surfaces. These observations were only made as part of a general study on the formation of machined surfaces and their fine features.

Black and Ramalingam [136] while looking at the fine structure of the machined surface, observed the microcrack distribution on surfaces generated by a number of machining processes. According to their studies, the microcrack ditribution in machined surfaces is a function of process variables, and to a minor extent, of material. They claimed that higher cutting forces, associated with low rake angle cutting and the presence of hard second phase particles in a reduced mobility dislocation matrix, accentuate the microcrack formation problem in high strength materials, leading to a higher density of defects at and close to the newly generated surface. This finding seems to suggest that there is some sort of relationship between the microcracks in the machined surface and those in the shear zone since the microcrack density has been claimed [128,129] to increase with a decrease in rake angle at low cutting speeds and with the presence of hard particles as discussed in the previous section.

According to Black and Ramalingam, there seemed to be no obvious origin of the microcracks observed in the machined surface. However, these authors believed that microcracks originate when the severely strain hardened material experiences a radial tensile stress field after passing the tool tip. Basing their argument on the assertion that inclusions and second-phase particles present in commercial alloys under severe straining during chip formation give rise to void formation by decohesion of the particle-matrix interface, they propose that this is likely to lead to microcrack formation behind the tool tip.

While investigating the micro-features of the machined surfaces of steel and pure iron, Gillibrand [6] confirmed the existence of surface microcracks in the steel surface at different cutting speeds in the range 76 to 229m/min. He estimated the depth of the microcracks to vary between a maximum of 5microns and a minimum of 0.2microns, at the low end of the speed range. He also observed long thin microcracks projecting into the workpiece in association with pits, machined surface features which he described as being the result of microvoids lying slightly beneath the plane of separation between the chip and the machined surface, but during growth intersect the latter at one side.This is illustrated in figure 41.

At the higher cutting speeds, a large area which was relatively smooth was observed. This smooth area was found [6,137] to stand slightly proud of the surrounding material on the original surface. Interestingly, this change in surface elevation was observed to occur in each case at a microcrack. On the other hand Gillibrand did not observe any microcracks on surfaces machined in pure iron and concluded that the microcracks were associated with the existence of a second metallurgical phase in steel. He commented that in general pure materials are more ductile than alloys which suggests a possible correlation between ductility and microcrack formation in machining. The formation of microcracks was also found [137] to increase when machining cast iron which was attributed to the reduction in ductility as anticipated.

A further observation made by Gillbrand [137] was that microcracks were associated with groove formation in the machined surface of steel and a 60/40 brass but not when machining cast iron. Groove formation was associated with the high inherent ductility of the workpiece material. From this it seems that microcracks form a

boundary between a high ductile area of material and a lower ductility phase. This could be the basis for a proposal that microcracks in the machined surface form at the boundary between the soft and hard phases of the material (e.g. ferrite and pearlite in steel).

4.4- Discussion And Objectives

4.4.1- Discussion:

From the foregoing literature review on the microcracking in machining, it is evident that the shear zone microcracking has received much more attention than the microcracks produced in the machined surface. This situation follows a similar trend to that of the machining process in general where the chip formation has been the subject of the major part of the research.

The proposal that microcracks are present in the machined surface is supported by the finding that the density of microcracks in the shear zone is greatest at the immediate vicinity of the tool cutting edge [128,129]. Their presence in the machined surface has been confirmed by direct observation [6,136-138] using transmission electron microscopy.

The work reviewed in this chapter indicates the following:

1. The microcracking in the shear zone can explain the type of chip formation [133]. Note should be taken, however, that segmental chip formation occurs when machining pure iron, but is not due to microcrack formation. Obviously other mechanisms exist.

2. The microcracking both in the shear zone [122,128,129] and in the machined surface [136-138] has been associated with the two-phase

nature of the workpiece material. It has in fact been shown that it does not occur when machining pure materials [122,136-138].

3. The density of microcracks depends on their location in the shear zone. It is greatest at the vicinity of the cutting edge and decreases towards the free surface of the chip.

4. The microcrack density increases with a decrease in cutting speed [128,129] down to a critical value of the cuttng speed. The reverse in trend at lower cutting speeds was explained by the mechanism of coalescence of microcracks to give a lower density of relatively larger microcracks.

5. No significant effect was observed [128,129] on the microcracking in the shear zone when changing the rake angle between 0 and 15 degrees. But a slight increase in the microcrack density was claimed to occur with a decrease in rake angle at low cutting speeds.

6. The effects of the cutting speed and the rake angle on the density of microcracks in the shear zone were explained in terms of the influence of these two variables on the strain of deformation [128,129]. As the strain is increased, the microcrack density is expected to increase as suggested by the results from shear deformation tests [122]. If the density of microcracks reaches a point where coalescence of neighbouring microcracks is initiated, it will then start to decrease causing a reversal in the trends. Consequently, larger microcracks are produced.

7. The cutting forces have been observed to decrease with increase in the microcrack density [135].

Having shown that the microcracks exist in the machined surface as the various reports indicate, and having established the lack of any systematic studies in this area, it is proposed that a

consideration should be given to an in-depth study of the microcracks produced in the machined surface during machining. Having said this, it now remains to specify the nature of such consideration. A look through the literature presented in this chapter indicates beyond doubt, that a suitable technique has not been devised, as yet, to enable the measurement of the surface microcracks. Moreover, no parameters have been introduced which represent the surface microcracks in a quantitative manner. Bearing the above state of affairs regarding the surface microcracks, a number of objectives have been set out for the present investigation in order to fill the void in this area and carry out a systematic study of the microcracks obtained in machined surfaces.

4.4.2- Objectives:

1. Development of suitable techniques to enable the examination and measurement of the microcracks produced in machined surfaces.

2. Introduction and definition of appropriate parameters which quantitatively represent the microcracking in the machined surface.

3. Application of the microcrack measurement techniques to investigate the effect on the microcracking parameters of a number of variables associated with the machining process. The variables considered can be subdivided into three groups:

   (i)- Process variables which include the cutting speed and the undeformed chip thickness,

   (ii)- A cutting tool variable, i.e. the rake angle,

   and (iii)- Material variables which include the microstucture and the material hardness.

In addition to the above which are the primary objectives of the present investigation, a secondary objective is the classification of the microcracks observed during the present investigation and the use of this classification to explore the possibility of correlating the type of microcracks with the sources and mechanisms causing their formation.

Finally judging by the exploratory nature of the present investigation, suggestions for future work and improvements will be formulated upon the completion of this thesis.

CHAPTER FIVE

PRINCIPLES AND TECHNIQUES OF ELECTRON MICROSCOPY

5.1- Introduction

Until recently, the most widely used method of investigating the nature and character of machined surfaces has been the use of surface profile measuring instruments known as stylus instruments. To provide a visual examination of the machined surface, optical microscopes have also been used. Attempts to correlate the surface features observed by optical microscopy and the traces of the surface profile obtained by stylus instrument measurements have, however, proved difficult. This is thought to be due to the ability of the stylus to pick up details smaller than those resolved by the optical microscope and to the fact that the vertical and horizontal magnifications on the trace are dissimilar. In order to obtain supplementary information from a visual examination the resolution of the visual instrument should be better than or at least approach that of the stylus instrument.

In the past few years, a number of techniques have been introduced within the subject of eletron microscopy to provide high powers of resolution and magnification. Work by Black and Ramalingam [136] and Gillibrand [6,137,138] have shown that these techniques can be used to provide additional information about the fine details of machined surfaces through a visual examination. One drawback of electron microscopy, however, is the fact that electron microscopes are expensive laboratory instruments and often necessitate laborious time consuming preparatory work prior to examination of the machined surface. Despite these drawbacks this technique remains the only alternative when very fine details which cannot be resolved by stylus instruments are to be examined visually.

The techniques of electron microscopy fall into two broad categories:

(i)- Scanning electron microscopy (SEM),

and (ii)- Transmission electron microscopy (TEM).

Preliminary examination of machined surfaces using both the SEM and the TEM revealed that the latter constitutes a powerful tool for the study of microcracks which also offered possibilities of quantitative studies. One problem of using the TEM lies in the difficulties involved in the preparation of specimens coupled with interpretational problems of the image obtained using this instrument. This could, however, be overcome by a working knowledge of both the principles and techniques associated with electron microscopy.

In carrying out studies using electron microscopy, the intending user is faced with two possible solutions to the above problems. He either undertakes to go through a long process of learning and understanding the principles of electron micrscopy and mastering the techniques involved therein, or he relies upon laboratory technician staff for the preparation of specimens for the TEM. The decision on which course to follow depends upon the purpose of the use of this technique. If the nature of the studies undertaken necessitates extensive use of electron microscopy, then a lot of time can be saved if the user gains knowledge and expertise in the use of the TEM and the associated techniques. Otherwise, the second alternative is preferable to save the user the time required for learning the techniques.

In the present investigation it was realized, after the preliminary studies, that a regular and extensive use of the TEM was to be made. Therefore, the author apprenticed himself to the techniques associated with the TEM and applied his mind to modify the available techniques to suit best the requirements of the present

investigation. An added bonus other than gaining the expertise, was the help it provided with the interpretational problems.

Bearing the above discussion in mind, this chapter has been included to provide a firm understanding of both the principles and the techniques of transmission electron microscopy.

5.2- Comparison Between Light And Electron Microscope

A microscope is an optical system which transforms an "object" into an "image" while making the latter larger than the former (i.e. magnifying the object). The concepts of magnification, resolution, depth of field, and lens aberration are very important in electron microscopy. To provide a basic understanding of electron microscopy, these terms are defined in the following sections within the more familiar context of the light microscope.

5.2.1- Magnification:

The simplest optical microscope, which has been in use since the early seventeenth century, is a single lens or "magnifying glass" as shown schematically in figure 42. From this figure it can be shown that the magnification is given by:

$$M = L/f \text{ --------------(1)}$$

The image is viewed on a screen or recorded on a photographic plate. Magnification of an object without severe distortion of the image is very limited using a single lens and for higher magnifications, combinations of lenses are used so that the total magnification is achieved in two or more stages. A simple two stage microscope is shown schematically in figure 43. The first lens, the "objective

lens", provides an inverted image at B with a magnification L_1/f_1 and the second lens, the "projector lens", gives a final upright image at a further magnification L_2/f_2. The image at C has a total magnification:

$$M = (L_1/f_1).(L_2/f_2) \text{------------------}(2)$$

In principle, it is possible to increase the magnification by :

(i)- adding a number of projector lenses,

(ii)- increasing L_1 and L_2 in equation (2),

or (iii)- decreasing f_1 and f_2.

However, for convenience, a compact instrument is needed so that rather than increasing the length L_1 and L_2 or adding magnification stages, it has become the practice in light microscopy to change f_1 and f_2 so that a choice of set magnifications can be selected by just interchanging lenses of different focal lengths. There is, however, a magnification above which no more detail is revealed and this is known as "empty magnification". The reason for this limitation is discussed in the next section.

5.2.2- Resolution:

In order to compare the electron microscope with the light microscope the factors controlling resolution have to be known. The resolution is defined as the closest spacing of two points which can clearly be seen through the microscope to be separate entities. This should be differentiated from the smallest point which can be seen with the microscope, which will often be smaller than the resolution limit.

Even if all the lenses of the microscope were perfect and introduced no distortions in the image, the resolution would

nevertheless be limited by a diffraction effect. Diffraction occurs wherever light passes through an aperture or the lenses so that a parallel beam of light, which would be seen as a spot, is transformed into a series of cones which are seen as circles known as Airy's rings. If the intensity of light is plotted across the series of rings, the resulting distribution will be as shown in figure 44 which also shows the Airy's disc. The central spot of the Airy disc contains 84 percent of all the light intensity and, for light of a given wavelength, has a diameter inversely proportional to the diameter of the aperture from which the diffraction is occurring.

The resolution defined earlier is the minimum distance between two central spots for which they can be distinguished. Based on Rayleigh's criterion, the two points can just be distinguished when the maximum intensity of an Airy disc coincides with the first minimum of the second. Spots cease to be distinguishable when the sum of curves ceases to have two maxima. This is illustrated in figure 45 from which it can be seen that the resolution limit is $d_1/2$. The sum of curves is shown dotted. From diffraction theory d_1 is related to the wavelength "λ" of the light used by:

$$d_1 = 1.22 \lambda / \mu \sin \alpha \text{ ----------------(3)}$$

where "μ" is the refractive index of the medium between the object and the objetive lens, and "α" the semi-angle subtended by the microscope aperture (figure 46). From the above equation it is obvious that the resolution can be improved by either a decrease in "λ" or an increase in $\mu \sin \alpha$. However, it is not practically possible to make $\mu \sin \alpha$ much greater than 1.6 since $\sin \alpha$ must be less than unity and the highest refractive index is about 1.7. Therefore, the factor controlling the resolution limit is the wavelength of the light used.

5.2.3- Depth of Field:

In any microscope the image is only accurately in-focus when the object lies in the appropriate plane (strictly the surface of a sphere). If part of the object being viewed lies above or below this plane, then the equivalent part of the image will be out of focus by some amount. The distance above and below the plane of focus for which the eye can detect no change in sharpness of the image is known as the depth of field. In most microscopes this distance is rather small and, therefore, in order to produce sharp images the object must be very flat. An approximate expression for the depth of field Δ (in millimeters) of a microscope is given by:

$$\Delta = (\lambda/\mu\sin^2\alpha)(1/7M\sin\alpha) \quad mm. \text{ -------(4)}$$

where "M" is the magnification.

It is clear from the above expression that as the resolution is improved (equation 3) and the magnification increased, the depth of field becomes smaller.

5.2.4- Aberrations In Optical Systems:

In the discussion so far, it has been assumed that all the components of the microscope are perfect and will focus the light from a point on the object to a similar point in the image. This is very difficult to achieve in practice because of lens aberrations, namely:

- chromatic aberrations which depend on the wavelength content of the light, and

- monochromatic aberration which affect even light of a single wavelength.

Monochromatic aberrations arise because of the different path lengths of different rays from an object point to the image point. The simplest of these is spherical aberration which is illustrated in figure 47. The portion of the lens farthest from the optical axis brings rays to a focus nearer to the lens than the central portion of the lens. Another way of expressing this concept is to say that the optical ray path length from object point to focussed image point should always be the same. This implies that the focus for marginal rays is nearer to the lens than the focus for axial rays. A disc of least confusion exists at the best compromise position of focus.

A related effect is that of astigmatism which arises when the lens has slightly different optical properties in the horizontal and vertical directions. The result is the existence of focus for horizontal direction at a different position from the focus for vertical direction. A similar effect arises if the lens does not have identical optical properties across the whole of its area. All the monochromatic aberrations are improved if only the central portion of the lens is used (i.e. if the size of the lens aperture is reduced). Unfortunately, as discussed in section 5.2.2, this impairs the resolution of the microscope.

5.2.5- The Effect Of Using Electrons Instead Of Light:

In a number of ways, electron optics are just the same as light optics and all the terminology used above applies in electron microscopy. However, there are two important differences each of which has led to the development of a particular type of electron microscope.

While light may be described in terms of photons or as radiation of wavelength 400-700nm ($1nm=10^{-9}$m), electrons can also be considered as radiation with wavelengths between 0.001 and 0.01nm. The first difference between electrons and light is that their wavelengths differ by a factor of the order of 10^5. The implications of this for microscopy are enormous but in most cases lead to a simplification.

The most important difference arising from the shorter wavelength of an electron beam is that electrons are very much more easily absorbed by many materials than light. This is so severe an effect that in order to use electrons in a microscope, the optical paths should be evacuated to a vacuum of better than 0.0001 Torr (1 Torr=1mm Hg).

Since, as will be seen later, the lenses in an electron microscope are merely magnetic fields, then there are only small changes of refractive index as the electrons pass through each lens. Hence the value of μ in equation (3) and (4) can be approximated to unity. Furthermore the angles through which the electrons need to be deflected are very small so that the approximation $\sin\alpha = \alpha$ (α in radians) can be made to a very high degree of accuracy. These simplifications mean that the theoretical resolution of the electron microscope can be written as:

$$d_1 / 2 = d_0 = 0.61\lambda / \alpha \text{------------(5)}$$

which would mean that with typical values of $\lambda=0.0037$nm and $\alpha=0.1$ radians, a resolution of about 0.02nm is expected. Unfortunately, however, this sort of resolution cannot be achieved in the transmission electron microscope because of lens aberrations. Whereas in a light microscope it is possible to correct both chromatic and monochromatic aberrations by using subtle combinations of lenses, there is no such possibility with an electron lens since its

refractive index cannot be changed. Consequently, although chromatic aberrations can be virtually eliminated by using electrons of a very small range of wavelengths, it is not possible to eliminate the monochromatic aberrations, especially the spherical aberration.

The only way of minimizing this, is to restrict the electrons to paths very near the optical axis (i.e. near the centre of the lens) by using a small objective aperture. This reduces α and therefore makes the resolution worse. There is an optimum size of aperture (i.e value of α) for which the resolution is smallest. Using this aperture it is possible with a good transmission electron microscope to resolve two points about 0.3nm apart. This is approximately the separation of atoms in a solid.

One benefit, however, from having to keep α small in order to reduce the effect of spherical aberration, is that of a larger depth of field when using electrons. Using the electron approximation, equation (4) can be re-written as:

$$\Delta = (\lambda / \alpha^2) + (1/7M\alpha) \quad mm. \quad \text{---------(6)}$$

It can be seen that as α is reduced the depth of field increases very rapidly. This is one of the major advantages of electron microscopes.

The second difference between electrons and light is that electrons carry a charge. Not only does this mean that electromagnetic fields can be used as lenses for electrons but it opens up the possibility of scanning a beam of electrons back and forth across the specimen. The application of this approach has led to the development of the scanning electron microscope.

In conclusion of the above discussion, it can be stated that electron microscopes offer higher resolution, higher magnification, greater depth of field, and greater versatility than the light micrscopes, although involving a considerable increase in cost.

5.3- Interaction Between Electron Beam And Specimen

One further difference between light microscopy and electron microscopy is that in the former there is a tendency to ignore most of the interactions beween the light and the specimen. This is not the case for electron microscopy where the interaction of electrons with the material through which they pass may have more serious consequences. For example, it has already been seen that because of the scattering of electrons by gas molecules in the air, the electron microscope must be operated in vacuum.

It is therefore important that the nature of the possible interactions between the electron beam and the other parts of the microscope (e.g. lenses) and between the electrons and the specimen, should be understood in order to appreciate the way in which an electron microscope works and the meaning of the information which is obtained using this instrument. To achieve this understanding, the nature of the electron and the possible interactions with an atom are considered in details in the folowing sections.

5.3.1- Properties Of Electrons:

An atom is usually thought of as a nucleus carrying a large positive charge and is surrounded by a cloud of negatively charged electrons which exactly neutralize this charge. The electrons are considered to occupy particular orbits or "shells", which are labelled K,L,M and so on. The electrons in the outermost shells can be removed if they are given only a very little extra energy compared to those in the shells nearest to the nucleus. Therefore electrons are fairly

readily detached from their atoms since the necessary energy can be easily supplied. It is this easy availability and their low mass which make the electrons so useful.

An electron, considered as a particle, carries a single negative charge $e=1.6 \times 10^{-19}$ C and has a rest mass $m_e = 9 \times 10^{-31}$ Kg. If a single electron is accelerated by a large potential difference V, then its velocity v can approach the velocity of light c, and relativistic effects become important. One of these is that its mass will increase compared with its rest-mass m_e, according to the equation:

$$m = m_e / \sqrt{[1-(v/c)^2]} \text{------------(7)}$$

If the electron is thought of as a wave, then its wavelength and its momentum must be connected by de Broglie's relationship:

$$\lambda = h/mv \text{------------------(8)}$$

where h is the Planck constant. In addition, the energy given to the electron is equal to the energy represented by the relativistic change in mass i.e.,

$$eV = (m-m_e)c^2 \text{--------------(9)}$$

If equations (7),(8), and (9) are combined the wavelength of the electron is found to depend on the potential difference, or accelerating voltage in the following way:

$$\lambda^2 = h^2/(2eVm_e + (e^2)(v^2)/c^2) \text{----(10)}$$

which, when the values of h, e, m_e, and c are substituted, becomes :

$$\lambda = \sqrt{[1.5/(V + 0.978 \times 10^{-6} V^2)]} \text{ nm.------(11)}$$

For an accelerating voltage of 80kV the wavelength of the electron is found from equation (11) to be equal to 0.0042nm.

5.3.2- Electron Beam Generation:

The electrons are generated in two ways by a device known as the "electron gun". The most widespread system uses thermionic emission from a heated tungsten filament. At temperatures in excess of 2700 °K a tungsten wire emits an abundance of both light and electrons. In a light bulb only the light is used but in an electron gun the electrons are also accelerated across a potential difference between 20 to 1,000 kilovolts to generate a monochromatic beam of electrons. The general features of a thermionic triode electron gun are shown in figure 48. The elctron gun consists of tungsten wire bent into a hairpin (the cathode) held at a high negative potential with respect to the anode and the rest of the microscope column. Electrons emitted from the filament are accelerated rapidly towards the anode and a beam of high energy electrons is emitted through the circular hole at its centre into the microscope column. A Wehnelt cap which is held at a voltage slightly more negative than the filament, enables the diameter of the area at the end of the filament which emits electrons to be controlled. The most important feature of the gun is that the paths of the electrons leaving the anode usually cross over at one point in space and hence the gun is acting as a lens. The diameter of the electron beam at the cross over is dependent on the area of the filament which is emitting electrons and hence can be controlled by the difference in potential between the filament and the Wehnelt cap. This cross over diameter is effectively the size of the electron source and is of great importance in calculation concerning the resolution of electron microscopes. One limitation of thermionic emission is the brightness of the beam it can emit.

An alternative method of generating the electron beam is known as field emission and can provide higher brightness than thermionic emission by a factor of about one million. This is based on the fact that if a metal surface is subjected to a very high electric field (greater than 10^9 V/m) it is possible for electrons to leave the surface without needing to be given the amount of energy represented by the work function. The result is that many more electrons can be drawn from a piece of tungsten than it is possible using thermionic emission. Unfortunately in order to make such a field emission gun work several rather stringent experimental conditions must be met. The only possible way of creating an electric field greater than 10^9 V/m is to make the tip of the tungsten filament extremely sharp (i.e. the diameter of the tip must be about 0.1micron), which makes the filament exremely fragile. The other main difficulty is that the vacuum in the gun must be better than 10^{-9} Torr compared with 10^{-5} for a thermionic gun. On the positive side, however, the field emission is hardly dependent at all on the temperature of the filament and so the tungsten point can be used at room temperature.

5.3.3- Deflection Of The Electrons/Electron Lenses:

The developments of electron lenses stems from the realization in the 1920's that a beam of electrons could be focussed by either an electrostatic field or a magnetic field. Both types of field have been used in electron lenses but the electromagnetic lens is by now virtually universal.

The key to an understanding of what is essentially a very simple lens is the direction of the force on a moving electron in a magnetic field. If an electron moving with velocity "v" experiences a magnetic

field of strength "B", then it suffers a force F=B.e.v in a direction perpendicular to both the direction of motion and the magnetic field. Expressed more concisely in vector form, this force is given by:

$$\bar{F} = e(\bar{B} \wedge \bar{v}) \text{-----------(11)}$$

A typical electromagnetic lens is designed to provide a magnetic field almost parallel to the direction of travel of the electrons. An electron entering the lens (figure 49) experiences a magnetic field "B" which can conveniently resolve into components "B_{ax}" along the axis of the microscope and "B_{rad}" in a radial direction. Initially the electron is unaffected by "B_{ax}" which is parallel to its direction of travel, but experiences a small force B_{rad}.e.v from the small radial component. This force causes the electron to travel in a helix along the lens. As soon as it starts to spiral, however, it has a component "$v_{\perp}$" perpendicular to the plane of paper and experiences a force B_{ax}.e.$v_{\perp}$ in a radial direction. Thus the helical path follows a tighter and tighter radius and the effect is that a parallel beam of electrons entering the lens is caused to converge to a point exactly as light is focussed by a glass lens.

Figure 49 is a diagrammatic representation of a typical electron lens arrangement. The basic components include a coil consisting of a large number of turns of wire which is wound on a soft iron core (C) which has only a very small accurately machined air gap (G), across which the field is produced. By varying the current passing through the coil, typically from 0 to 1Ampere, the magnetic field strength and hence the focal length of the lens can be varied at will. Although the several lenses in any one microscope may differ in shape and size, they will conform to the general pattern laid out in figure 49. An important feature, for which there is no analogy in the light microscope, is the spiralling of the electrons as they travel through

- 87 -

an electromagnetic lens. Since it is very rare for the electron to travel an integral number of turns of the spiral as it passes through the lens, in general there is a rotation of the image caused by the lens. This is not a distortion since the image is otherwise unaffected.

5.3.4- Scattering Of Electrons By The Atoms Of The Specimen:

In electron microscopy , electrons enter the specimen and the same or different electrons leave it again to form the image. Consequently, it is vitally important to understand the interactions which are possible between electrons and atoms in a solid specimen so that the image can be interpreted. The response of a "thin" specimen to an electron beam which strikes its surface takes a number of forms as shown in figure 50 where the size of the atoms is greatly exagerated to enable a clear understanding of what goes on within the specimen. The transmitted electrons are those which pass through the specimen without being deflected or losing energy and form "pure" electron beams. This will only occur if the specimen is very thin (less than 1micron) for most materials. In this case the large majority of electrons will follow path "0" on the basis that the specimen is composed of atoms which are themselves free space.

A number of electrons, however, will pass very close to the strongly positively charged nucleus of an atom and are deflected from their path by the attraction of the opposite charges. Depending on how close an electron approaches to the nucleus and how fast it is travelling (i.e, energy), it may be deflected only slightly from its path (path 1) or at the other extreme may be deflected through an angle approaching 180 degree (path 4) and travel back in the opposite

direction. The significant point about this type of scattering is that the electron loses virtually no energy in the process and changes its direction without slowing down. This type of scattering is called "elastic" scattering. The proportion of elastically scattered electrons increases with specimen thickness as this increases the probability of passing a nucleus. The angle at which electrons are scattered decreases with increase in the accelerating voltage. The higher the atomic number of the element encountered the higher the scattering angle.

Interactions with one of the orbital electrons of an atom involve two bodies of the same mass. In this case the two identically charged particles repel one another and some of the energy of the incident electrons is transferred to the orbital electron, the beam of electrons subsequently travelling on at lower energy, but in a direction altered only slightly (path 2) from its incident path. This type of scattering is known as "inelastic" scattering. If an electron suffers a succession of inelastic collisions, it will eventually lose all its energy and will be stopped in the specimen, the probability of this happening increasing with the thickness of the specimen. This is why, in specimens thicker than 1μm, very few electrons are transmitted right through the specimen. The secondary effects generated by the incident electron beam illustrated in figure 50 are not discussed here but have been included for completeness. The influence of the scattering mechanisms on the final contrast in the image will be discussed in section 5.5.

The transmission electron microscope (TEM) is a high resolution instrument which operates on the basis of the ability of electrons to be transmitted across thin film specimens as discussed in the previous section. The geometrical optics of the transmission electron microscope bears a strong theoretical resemblance to the light microscope optics. The general layout of the basic components of both types of microscopes is shown in figure 51. In what follows, a modern six lens transmission electron microscope, shown schematically in figure 51b, will be described.

The light source of the light microscope is replaced in the electron microscope by an electron gun whose function is to provide a stable source of electrons which form the monochromatic electron beam. The most common types of TEM have guns capable of accelerating the electrons to voltages between 20kV and 100kV although the latest developments have shown electrons accelerated to voltages of over 1,000kV. Below the electron gun the diameter of the electron beam is controlled by the condenser system which consists of two lenses, an aperture, and a stigmator coil. Condenser lens 1 presents to condenser lens 2 an image of the electron cross-over in the electron gun which is of reduced size. Condenser lens 2 focusses this image on to the specimen plane. The use of a two lens system gives greater flexibility of operation over a single lens system. The size of the beam may be further limited by insertion of the condenser lens aperture into the beam path. Limitation of the beam size so that only the required area of a sample is illuminated prevents damage to other sample areas and reduces angular width of the beam and associated spherical aberrations. Also in good electron microscopy practice, the

final image must be as bright as possible. For example, it is not
sensible to "waste" electrons by illuminating an area of say 1mm
diameter when the area viewed is only 10μm across. Therefore, the
illuminating electron beam is "condensed" until it is only a little
larger than the field of view.

Below the condenser lens system lies the specimen chamber, which
is one of the most crucial parts of the microscope, since so many
delicate mechanisms must be built into a small place. The essential
requirement is that the specimen, which is likely to be about 2mm
square or less and less than one micron thick, must be held in exactly
the correct position in relation to the objective lens. Since it is
not very useful to be able to study only one area of the specimen, a
mechanism is included which will move the specimen in a horizontal
plane to enable the operator to look around the specimen and select
the most interesting parts to photograph. Not only must this
mechanism be so fine that it can move the specimen smoothly over
distances as small as 1μm, but when the appropriate area for high
magnification photography has been selected, the specimen must not
move as much as 1nm per second (1mm in 12 days) or the resulting
micrograph, taken with a photographic exposure of several seconds,
will be blurred. Moreover,the necessity to be able to remove the
specimen from the microscope and replace it with another one in a
matter of minutes without losing the vacuum under which the microscope
is operating makes this part of the microscope very sophisticated
indeed. This is achieved by the use of a specimen carrier which can
accommodate up to 6 specimen holders and an airlock so that only a
small volume needs to be evacuated by the vacuum pump each time the
specimens are introduced, instead of the whole microscope.
Immediately below the specimen is the objective lens which has an

aperture holder which carries three or four circular pinholes of different sizes. In practice, holes of diameter between 20 and 100μm in platinum or molybdenum sheets are used. The choice of aperture defines the numerical aperture of the objective lens and hence the angular aperture α and the ultimate resolution of the microscope (equation 5). The objective aperture has another role, as will be discussed in section 5.5, in that it improves the contrast in the final image. Without an aperture in place, the image of almost any specimen appears uniformly grey rather than black and white. The objective lens gives a focussed and magnified intermediate image of the specimen. This lens is a critical component of the TEM as it limits the resolving power of the instrument. The objective lens also contains the stigmator coils which compensate for any astigmatism caused by the lens or aperture contamination.

Below the objective lens there are two other lenses:i.e., the intermediate and projector lenses which play an important role in the final magnification of the image. They may be excited to give a highly magnified image of the intermediate image formed by the objective lens. Here, the excitation of lenses depends on whether high or low magnifications are required. At low magnification the intermediate lens operates at constant current while the current in the projector lens is changed to magnify. At high magnifications the projector lens operates at constant current while the current in the intermediate lens is changed to magnify. The total magnification of the image is equal to the product of the magnifications at different stages. i.e.

$$M = Mo \times Mi \times Mp$$

In the plane of focus between the intermediate lens and the projector lens is another set of apertures by which different sized areas of the

- 92 -

field of view can be observed. These apertures are very similar to the objective apertures but are known as field limiting or diffraction apertures.

The information impressed on the electron beam during its travel down the microscope column and through the specimen is extracted by impinging the electron beam onto a fluorescent screen and, whenever required, allow it to fall onto a photographic plate to obtain a permanent record of the features of interest using standard photographic techniques. The records obtained in this way are referred to as "electron micrographs".

5.5- Image Formation

The image formation process in any electron microscope is the result of impinging on a fluorescent screen an electron beam which has lost a number of its electrons while passing through the specimen. The interaction between the electron beam and the specimen has been discussed in section 5.3.4. The image on the fluorescent screen is made up of spots whose brightness depends on the number of electrons falling on the spot and hence depends on the type of interaction that the electrons at the spot have had with the atoms in the specimen. This dependence of the brightness on the number of electrons transmitted through the specimen is responsible for the contrast in the final image.

There are two ways in which electrons can be removed from the electron beam:

(i)- by introducing a barrier into the path of the electrons,

(ii)- by increasing the thickness of the specimen so that more electrons are absorbed into the specimen.

The elastically scattered electrons can be extracted from the main beam to produce the necessary contrast in the final image. If an aperture is placed into the objective lens some of the elastically scattered electrons are prevented from contributing to the image. In this way contrast is produced. The smaller the aperture the greater the number of lost electrons and the better the resulting contrast in the final image. A number of limitations of this contrast system are, however, imposed. Smaller apertures require more accurate centring and are more susceptible, nearer to the beam axis, to heating and thermal drift, so that alignment stability becomes a problem.

The number of lost electrons can also be increased by increasing the objective focal length (i.e. the distance between the specimen and the objective lens) as shown in figure 52. This is usually done by using a different specimen holder which holds the specimen at a larger distance from the objective lens. The holder is usually referred to as the high contrast specimen holder (see figure 53). The effect of this on the elastically scattered electrons is illustrated in figure 52 where the dotted lines indicate the lost electrons.

The variation of the accelerating voltage is yet another method of improving contrast. The angles at which eletrons are scattered decrease with increase in accelerating voltage. Hence lower values of accelerating voltage should be used when high contrast is required.

Also heavy metals usually give better contrast when combined with the shadow casting techniques discussed in section 7.4.3. It is sufficient for the time being, to say that shadow casting produces a film of metal whose thickness varies with the topography of the shadowed specimen surface. As the thickness of the specimen is increased the probability of electrons being scattered also increases. Consequently, the number of electrons transmitted through the specimen

decreases. Parts of the specimen where the thickness is very small so that the specimen is "transparent" to the electron beam, will produce bright spots on the fluorescent screen. Those parts where the thickness is greater than a critical value (about $1\mu m$ for most materials) will produce dark areas on the final image. The contribution of both dark and bright areas will constitute the contrast of the final image which will be representative of the topography of the shadowed surface. In the present investigation this type of contrast has been used to advantage for the production of the image contrast as well as the interpretation of the micrographs of machined surfaces and the identification of the microcracks present in these surfaces. A discussion of the micrograph interpretation and ways of identifying various features of machined surfaces is included in section 5.7. when a firm understanding will be based on a working knowledge of the procedures and techniques of the preparation of specimens for TEM examination.

5.6- Specimen Preparation For The TEM

As electrons are readily scattered by metals, the materials and components used industrially cannot in general be examined directly in the TEM so that special preparation techniques are required. This is one of the most difficult, yet essential, aspects of transmission electron microscopy. The requirements are very stringent indeed. In order that electrons can be transmitted through, the specimen must be only 100nm thick or less, which is about one five-hundredth of the thickness of aluminium foil used in the kitchen. In addition, the preparation method should not introduce any artefacts (i.e. alterations in features to be examined) to the specimens.

There are two major types of specimen preparation procedures, namely, the replica technique and the thin foil technique. This section will be dealing specifically with the replica technique as the present investigation was concerned with the topographical features of the machined surface.

Briefly, however, the thin foil technique involves reducing the thickness of the metal until it can be penetrated by the electron beam of the TEM. The limiting thickness depends on the atomic number of the metal and the electron accelerating voltage at wich the TEM is operated. This technique is used when studying, in detail, the microstructure of materials.

The replica technique enables the reproduction of surface topography of the specimen in a thin film of material which is not easily decomposed by the electron beam. Carbon is a usual material for thin film specimens. The topography can be reproduced by using either a single-stage direct replica or a two-stage plastic/carbon replica. In the single stage replica technique a carbon is evaporated directly on to the prepared surface. Then because the carbon layer is somewhat porous, it may be removed by etching the surface to dissolve the metal away from the carbon film. The two stage plastic-carbon replica involves replicating the surface topography on a thin plastic strip followed by evaporating a carbon layer onto the plastic replica and then dissolving the plastic away to leave a thin carbon film which is a reproduction of the topography of the replicated surface.

For the examination of machined surfaces two-stage replication techniques are found to be satisfactory provided the standard procedures are modified to suit the need. A detailed description of the procedures used in the present investigation is presented in section 7.4.

To explain how the TEM micrographs are interpreted a schematic section through a surface is shown in figure 54a. When the specimen is exposed to the electron beam a sequence of shades (i.e. contrast) is obtained in the final image, which results from the interactions between the electrons in the impinging beam and the atoms in the specimen. Figure 54b shows the thin film specimen obtained by replication of the topography of the machined surface. The dark layer is the gold/paladium shadowing layer and the brighter layer reperesents the backing carbon layer which presents a uniform thickness to the electron beam. Detailed description of how the TEM specimens were prepared is presented in section 7.4. The shadowing layer film presents a thickness which varies from zero to a maximum associated with deep features of the machined surface. The resulting contrast depends on the shadowing layer and varies from white (i.e. bright) to black (i.e. dark) shades.

The contrast of the final image will consist of three shades, namely white, grey, and black. The grey which is the dominant shade forms the background of the image and corresponds to areas of the surface which are near to perpendicular with respect to the electron beam axis. The white shades correspond to areas where no shadowing material has been deposited and so all the incident electrons on these areas are transmitted through with no interference and contribute to the brightness of the white areas. The dark shades represent areas where the shadowing layer is so thick that no electrons are transmitted through. These areas correspond to features departing from the nominal surface profile (i.e. steps and microcracks). The shades resulting from the examination of a specimen representing the

surface profile shown in figure 54a are indicated in figure 54c. The letters "G", "B", and "W" refer to grey, black, and white shades respectively. It can be seen that it is possible to identify the various features of the machined surface by the shade sequence across them in the in-plane-shadowing-direction.

The shade sequence for a microcrack which is the feature of importance in the present investigation, is grey-black-white-grey as shown in figure 55. The existence of another grey of very small width between the black and white shades observed in some micrographs gives an indication that the microcrack produced on the surface replica was a blunt one. The significance of this middle grey is discussed in section 6.6 in terms of the penetration of the replicating material inside the microcracks and the collapse of slender features during the handling of the specimen.

On the micrographs the reverse shade sequence to that of a microcrack (i.e. sequence G-W-B-G) looks the same. From this it follows that features having the reverse sequence might be misinterpreted for microcracks. For example, a sharp peak on the machined surface will correspond on the TEM micrographs to the same shade sequence as that of a microcrack. There are, fortunately, two ways in which this confusion can be avoided. First of all it can be shown (cf. figure 56) that the extent (i.e. the width) of the white shade is far larger for a microcrack than for a peak. Secondly, the in-plane shadowing directions can be used to standardize the direction for viewing the micrographs when interpreting them.

MEASUREMENT OF MICROCRACKS

6.1- Introduction

6.2- Choice Of Electron Microscope Technique

6.3- Choice Of Magnification

6.4- Quantitative Representation Of Microcracks

6.4.1- Measurement Of Microcrack Surface Area

6.4.2- Counting The Number Of Microcracks

6.4.3- Depth Of Microcracks

6.4.4- Length Of Microcracks

6.5- Microcracking Parameters

6.5.1- The Microcrack Area Ratio "Ma"

6.5.2- The Microcrack Density "Md"

6.6- Limitations And Improvements Of The Measurement Technique

6.6.1- Shadowing Direction

6.6.2- Penetration Of Replicating Material Into Microcracks

6.6.3- Collapse Of Slender Features Of TEM Specimens

6.6.4- Assessment Of The Technique

6.7- Classification Of The Microcracks

6.1- Introduction

It was concluded in chapter three that a need was felt by people concerned with surface integrity for a more complete characterization of the machined surface by considering all the components of surface integrity. Such a consideration will not be complete unless the surface microcracks which are an integral component of surface integrity are included. While practically all the other components, as discussed in chapter three, have been the subject of quantitative investigation , the microcracks in the machined surface have not.

It has been shown in chapter four that the microcracking in machining is a phenomenon not very well understood up to now. It has also been shown that virtually all the work which has been carried out in this field has been concerned with the occurrence of this phenomenon in the shear zone of machining while no quantitative work is reported to have been carried out on the microcracks present in the machined surface. This is probably due, as discussed in chapter four, principally to two reasons:

a)- the absence of an appropriate technique for the measurement and of suitable parameters to quantify the microcracks,

b)- the microcracking phenomenon within the shear zone has been used to explain other aspects of machining, viz., type of chip formation, built-up-edge, and cutting force variation.

The objective of the present investigation, as mentioned earlier, is to carry out a systematic study on the microcracks present in the machined surface. Before this can be done, however, it is necessary to find ways of measuring and quantifying microcracks. A suitable technique for the measurement of microcracks is introduced and used in

the present investigation. The stages involved in its developement are described in the following sections.

6.2- Choice Of Electron Microscope Technique

Extensive work on both scanning and transmission electron microscopy, led to the suggestion of using micrographs obtained from transmission electron microscopy for the microcrack measurement. The scanning electron microscope could not be used because microcracks on the machined surface (which is rough by electron microscopy standards) could not always be seen. The superiority of the TEM in this respect is due to the different depth of field. The larger the depth of field the smaller the resolution as shown in section 5.2.3. For machined surfaces observed in the scanning electron microscope a large depth of field enables the examination of the roughness of the surface. This reduces the resolution and consequently excludes fine features from the final image.

Another possible reason for microcracks not being resolved by the SEM is the geometry of microcracks. In a scanning electron microscope, only objects which lie in planes perpendicular to the optic axis will be reconstructed with minimum distortion. For a highly tilted surface (i.e. profile with large slopes), the magnification perpendicular to the tilt axis will be less than the magnification parallel to the tilt axis by a factor equal to $\cos\theta$, where "θ" is the angle of tilt. Figure 57 illustrates the effect of the tilt of a surface irradiated by the electron beam, on the magnification of the image. The magnification in the SEM image is given by:

$$M = L/1$$

where "L" is the cathode ray tube (CRT) scan length which is fixed and "1" is the length of the side of the area scanned on the specimen. Figure 57a shows how "1" changes with the slope of the surface. Using the above equation for the different angles of tilt, it can be shown that as the tilt angle increases, the magnification decreases (i.e. with reference to figure 57, $M_0 > M_1 > M_2 > M_3$). In the extreme case when the surface becomes parallel to the electron beam axis (i.e. angle of tilt approaching a value of 90degrees) the magnification tends to zero and the surface element scanned is lost. Figure 57c shows a section perpendicular to a surface microcrack. The new surfaces "$\overline{x}$", generated as a result of microcrack formation, are shown to have a large tilt. Consequently, the microcrack which is already a very small surface feature is largely reduced in size on the CRT and subsequently lost. The edges of the microcrack opening "y" will, however, generate a limited number of signals but these will be confused with the background "noise" produced as a result of the roughness of the surface. It would be possible to see these microcracks as lines provided the surface is polished to get rid of the background noise. This is not a practical solution since the polishing will remove a layer of surface material and with it the microcracks, these being shallow compared to other surface features.

In the case of transmission electron microscopy the microcracks are not directly examined on the machined surface. Owing to the fact that microcracks are reproduced by replication, the results of any TEM examination depend considerably on how good the replication of the microcracks was. Moreover the methods of TEM specimens preparation can be used to enhance the strength of the TEM. For example, the techniques of shadow casting with a heavy metal, as described in

section 7.4.3. have been used in the present investigation to expose the microcracks and improve contrast. Therefore utmost care must be taken during the preparation stages of TEM specimens.

6.3- Choice Of Magnification

Preliminary work was undertaken to determine the extent of microcracking on surfaces machined under different conditions. This indicated that a console magnification of 3,000 times (i.e. 900 times when corrected for the high contrast specimen holders used) would cater for the range of microcracking susceptibilty of the materials used. A statistical means was used to find the smallest number of micrographs necessary for the measurement of microcracks as described in appendix 1.

6.4- Quantitative Representation Of Microcracks

The first step towards microcrack measurement after carefull examination of the microcracks in the TEM was to think about possible parameters for quantitative representation of surface microcracks. A number of possibilities were considered:

      (i)- the microcrack area per unit specimen area,

     (ii)- the number of microcracks for a chosen (standard) specimen

          area determined by the number of micrographs used,

    (iii)- the depth of the microcracks,

and (iv)- the length of the microcracks.

Finding simple ways of measuring the above, meant taking photomicrographs of the microcracks within a given specimen area and measuring either on prints or on negatives exposed to a light source.

Bearing in mind the cost involved, the number of micrographs was kept to the minimum possible and measurements were restricted to the negatives to cut down on printing time and expense.

6.4.1- Measurement Of Microcrack Surface Area:

The measurement of the microcrack area is made possible by the shadow casting technique which is responsible for the white area (shade) obtained in the micrographs and related to the microcrack surface as explained in section 5.7. Past experience has shown the benefits from shadowing at 45 degrees to the machined surface and 45 degrees into the lay to the final micrograph contrast. One added benefit from the point of view of microcrack measurement, is illustrated diagrammatically in figure 58. It can be seen that the depth "h" of a microcrack is equal to the width "d" of the white area in the micrograph. Therefore, the measurement of the surface area of the white band in micrographs is a direct measure of the microcrack area.

A micrograph showing the effect of shadowing on the microcrack appearance is shown in plate 1. The contrast sequence from A to B in this micrograph is in fact that of a microcrack (see section 5.7). The white area represents the microcrack area whose measurement is sought. To do this, it was decided to use a transparent grid pattern which is shown in plate 2. The grid pattern was drawn on an A3 polydraw (polyester drafting film) sheet and its photograph taken. Then, it was reduced to the size of the TEM micrograph negatives and printed on a transparency. Two copies were obtained which were used as standard measuring grids for the measurement of microcracks throughout the present investigation.

The measurements were made by superimposing the standard measuring grid onto the micrograph negative as shown in plate 3. The number of unit squares which fell within the white area of the micrograph associated with microcracks was then determined by counting. Light was shone through a glass painted in mat white for convenience and sharpness of contrast. Portions of unit squares falling within the measured area were estimated and added up as the counting was carried out. The set up for microcrack measurement is shown schematically in figure 59.

6.4.2- Counting The Number Of Microcracks:

The counting of the microcracks on an electron micrograph proved to be difficult and tedious. The microcracks were observed to have a wide variation in size, shape, orientation, and distribution. Furthermore, many microcracks overlapped and prolonged each other which made it sometimes difficult to draw a separating line between different microcracks. However, one consolation was the fact that microcracks could easily be recognized owing to the contrast sequence technique outlined in section 5.7.

The necessity to draw some kind of criteria was felt before any counting could be undertaken. Two conditions were imposed to facilitate the task. The first one was that only microcracks which were distinct from each other (i.e. not overlapping) were to be counted as different microcracks. In other words, if two or more microcracks had run into each other, they were counted as one microcrack only. This is a sensible assumption in that one way in which microcracks grow, is by the coalescence of smaller microcracks to form bigger ones. Once they have coalesced the microcracks are

only counted as one microcrack. The second criterion was that only microcracks were counted which had a "size" (i.e. the microcrack area measured by the method described in the previous section) equal to, or greater than, one unit square of the standard measuring grid.

6.4.3- Depth Of Microcracks:

Technically speaking the depth of each microcrack could be measured at any point along the length of the microcrack. This has been shown in figure 58. The depth of a microcrack is measured by drawing a line normal to the microcrack direction and measuring the width along this line of the white area representing the surface of the microcrack. This method, however, presented some difficulties and an alternative way of determining the average depth of microcracks was sought. The difficulties involved were associated with the shadowing direction, the point along the microcrack at which to measure, and the number of measurements necessary. An attempt was made to calculate the average depth of microcracks using the measured microcrack area as described in section 6.4.1 and the total length of the microcracks the details of which will be explained in the next section. The details of the calculation procedures are included in appendix 2. An attempt to measure the maximum microcrack depth, although technically possible, did not result in any consistent trend with the variables considered in the present investigation.

6.4.4- Length Of Microcracks:

The measurement of the length of microcracks proved to be difficult given the shape of the microcracks and their orientation

with respect to the in-plane shadowing directions. However, the approximate length of a microcrack may be measured directly from the micrograph. This was done using the same measuring grid used to measure the microcrack area. But there are some problems associated with such measurements. First of all the length of the microcracks which will be shadowed will not necessarily be equal to the actual length of the microcracks. In other words, lengths of microcracks which are parallel to the in-plane shadowing directions will not exhibit any shadowing effect. Therefore, the contrast sequence technique cannot be used successfully to identify the microcracks to be measured which lie along the in-plane shadowing direction. The second difficulty associated with the measurement of the microcrack length is that measurements will be repeated for the two in-plane shadowing directions "S_1" and "S_2". An example illustrating how this repetition occurs is shown in figure 60. There will also be few microcracks whose length will be only measured once. A reasonable suggestion, though, would seem to be to add both lengths and divide by two. This would give a conservative estimate of the total length of microcracks which can be used as a quantifying parameter on its own or replaced in equation (A10) to give the average depth of microcracks.

6.5- Microcracking Parameters

Having considered the above possibilities for microcrack measurement, two parameters have been introduced and are defined in the next two sections.

6.5.1- Microcrack Area Ratio "Ma":

This parameter has been given the symbol "Ma" and is defined as the percentage ratio of the counted number of unit squares falling within the white area of the micrographs (cf. section 6.4.1) over the total number of unit squares of the standard measuring grid. The choice of this parameter to quantify the microcracks has been dictated by the difficulties associated with the determination of the depth and length of the microcracks as discussed earlier on. The above parameter incorporates both of these dimensions as shown in figure 61. In this diagram it is seen that the area of the white band is in effect equal to the product of the elemental width and the elemental height integrated over the length of the microcrack.

Rather than measuring both the depth and length of microcracks, the area was determined directly using the standard measuring grid. The measuring grid was 84mm long by 57mm wide giving a standard number of unit squares of 4788. Taking into account a linear magnification of 900 times, the surface area of the grid is equivalent to a machined surface area of:

$$A = 4788/900 \times 900 = 0.0059 \text{ mm}^2$$

i.e. about 0.006mm^2 to within 1.7% precision.

For measurements based upon 10 micrographs, the microcrack area ratio is given by :

$$Ma = 100 \times \sum_{i=1}^{10} A_i / 47880 = (478.8)^{-1} [\sum_{i=1}^{10} A_i]$$

where A_i is the total microcrack area (i.e. number of unit squares counted) for each micrograph used. The approximation of the above equation to:

$$Ma = (480)^{-1} \sum_{i=1}^{10} A_i$$

can be made and only an error of 0.25% is introduced.

6.5.2- The Microcrack density "Md":

This is defined as the number of microcracks counted (see section 6.4.2) for a given area represented by 20 micrographs at a magnification of 900 times and is given the symbol "Md". The choice of the area was only arbitrary and is based upon the minimum number of micrographs used for the measurements and to the fact that two complementary shadowing directions were used (cf. section6.6.1). The area represented by 20 micrographs is about 0.12 mm^2 therefore the density of microcracks per mm^2 can be obtained by dividing the microcrack density by 0.12.

6.6- Limitations And Improvements Of The Measurement Technique

6.6.1- Shadowing Direction:

One major source of error results from the shadowing of the replica. During the preparation of the specimen for TEM examination, it was decided to do the shadowing of the plastic replica at angles of 45 degrees to the machined surface and 45 degrees into the cutting direction. It is the shadowing process which enables the microcracks to be recognized by virtue of the sequence of shades in the contrast of the micrographs, the carbon coating being just a backing layer to hold the specimen together after the plastic replica is dissolved.

It can be shown that any microcrack which lies in the in-plane shadowing direction will not be affected by the shadowing process thus not being recognized from the micrograph obtained. A remedy would be to choose a shadowing angle which does not correspond to any microcrack direction. Previous experience, gained while observing

microcracks on the machined surface of a free machining steel, showed that at least for this material, the direction of the microcracks did not have a definite trend. Microcracks due to inclusions were of the closed type (cf. section 6.7) each having either the whole or partial shape of the contours of the inclusions. For this type of microcracks there is no appropriate shadowing angle to produce the microcrack shade sequence on the whole of the length of the microcracks.

As an alternative solution, the idea arose of using two complementary shadowing directions, which would complement each other in the measurement of microcracks. Two sets of micrographs had to be produced for each machined surface, one for each shadowing direction. The microcrack area ratios obtained from each set were then combined to give an average microcrack area ratio of the machined surface under consideration. The microcrack area ratio determined in this way gives a conservative estimate of the real value as those microcracks which lay parallel to any in-plane shadowing direction will only be measured once in the complementary shadowing direction. The underestimate depends on the number and size of microcracks laying in any shadowing direction. Figure 62 shows how a simply shaped microcrack will be measured in the two complementary shadowing directions.

6.6.2- Penetration Of Replicating Material Into Microcracks:

One inherent error which can arise in the microcrack measurement technique is associated with the replication process. Doubt has always been expressed by those introduced to the technique for the first time, about whether the replicating material does in fact reach the bottom of the microcracks. It is reasonable to suggest that unless the microcracks are open and shallow as shown in figure 63a,

the replicating material will not reach the bottom of the microcracks. This phenomenon is shown in figure 63b, in which the distance not covered by the replicating material is indicated by "ϵ". Errors imparted to the measurement by poor penetration of the replicating material into the microcracks, can be estimated conveniently from the micrograph. Figure 64 shows schematically the micrograph preparation procedures and the effect of poor penetration. It has been assumed in the present investigation that microcracks have a sharp bottom as shown in figure 64a. The sharpness of the peak of the replica corresponding to the bottom of the microcrack should give an indication about how deep in the microcrack the replcating material has penetrated. This is shown clearly in figure 64b. The shadowing effect on the three replicas is shown in figure 64c. The contrast sequence is written under each diagram. It is interesting to note from this figure that the contrast sequence obtained in the micrographs due to shadowing, not only enables the identification of the microcracks (cf. section 5.7), but gives a clear indication about the extent of penetration of the replicating material inside the microcracks. Thus the sequence G-B-W-G (i.e. Grey-Black-White-Grey) means good penetration whereas the sequence G-B-G-W-G means incomplete penetration. The extent of penetration is proportional to the width of the middle grey band of the microcrack contrast sequence. In other words, the wider the middle grey band is, the poorer the penetration of the replicating material inside the microcracks will be and vice versa. Micrographs at higher magnification can be used to show the middle grey band clearly as in plate 4.

The error incurred by poor penetration to the microcrack area ratio "Ma", expressed as a percentage error, can be estimated from the geometry of the shadowing of microcracks. Figure 65 shows the

- 111 -

influence of poor penetration of the replicating material on the shadowing effect. The poor penetration has been exaggerated for clarity of the geometrical analysis.

It can be shown (see appendix 3) that the percentage error in the microcrack area ratio due to poor penetration of the replicating material is given by:

$$dMa/Ma = 50a [(1/b)+(1/w)]$$

where "a" represents the width of the middle grey band,

"b" the width of the black band,

and "w" the width of the white band in the contrast sequence of the measured microcracks.

6.6.3- Collapse of Slender Features Of TEM Specimens:

During specimen preparation, the replica is subjected to stresses which may cause the collapse of slender features like the peaks corresponding to microcracks. Actions such as stripping the plastic replica from the machined surfaces, shadowing, coating, cutting up of specimens to put on the support grids, or the dissolving of the plastic can set up these stresses. Furthermore, the action of the electron beam can cause thermal stresses when the specimen is in the electron microscope.

The resulting micrograph will have a middle grey area which can also be darker depending on how far the slender features have collapsed. Figures 66 and 67 show a schematic representation of how this collapse occurs and its effect on the contrast sequence of the microcracks. Figure 66 shows the collapse of the plastic replica after being stripped off from the replicated machined surface. Figure 67 shows the collapse of the microcrack features to occur after

- 112 -

shadowing and carbon coating have been applied. The difference between the two types of collapse is associated with the intensity of the middle grey band. The collapse of the plastic relica is indicated by a lighter grey colour.

To illustrate this collapse phenomenon the same micrograph as that shown in plate 4 is selected. Equation (6.1) still applies and both sources of error (i.e. poor penetration and collapse) contribute to the errors. Apart from the darkness of the middle grey band, however, the two sources of errors can be distinguished by the variability in the width of the middle grey band along the microcrack length. The extent to which the replicating material goes down into the microcracks can be assumed to be roughly constant given the same materials and the same solvent. The micrograph in plate 4 shows that the width of the middle grey band is not constant. Therefore, the bigger contribution to the middle grey band shown in plate 4 is due to the collapse of the slender feature representing the microcrack.

6.6.4- Assessment of the technique:

Like any newly developed technique, the microcrack measurement technique has its own limitations as discussed above. Improvements are possible some of which have already been achieved and will be discussed in the next chapter. The cost incurred by the use of micrographs can reach very high proportions if care is not taken to restrict the number of micrographs taken to a strict minimum according to some accuracy criteria. Statistical analysis was used to find the minimum number of micrographs needed to give consistent and repeatable results at the 5 percent significance level as described in appendix 1. Also the time spent when taking the measurements was considerable

and this is due to the manual counting of small unit squares on the standard measuring grid.

To assess the microcrack measurement technique preliminary tests were carried out on three materials (i.e. EN1A, EN8, and EN57) and statistical analysis performed to verify the reproducibility of the measurements as described in appendix 1.

6.7- Classification Of The Microcracks

The possibility of classification of the microcracks observed in machined surfaces was also explored. Plate 5 shows some examples of the types of microcracks found on the machined surface of a resulphurized steel. An attempt to classify these microcracks is shown in table 5 below. Although not being within the scope of the present investigation, the feasibilty of correlating the types of microcracks to their originating sources and causes looks promising and is an open area for future work.

Table 5 : Classification of microcracks

Micrograph (Plate 5)	Type of microcrack	Description
-	A	Microcrack normal to lay.
-	B	Microcrack at angle less than 90° to lay.
1 and 8	C	Closed-pattern microcrack.
2	D	Compound microcrack.
3	E	Microcrack parallel to lay.
4	F	Smoothly curved microcracks.
5	G	Irregular (ragged) microcrack.
6	H	Deep microcrack (i.e d>2xl).
7	I	Ordered pattern microcracks (e.g a group of 4 B-type microcracks).

CHAPTER SEVEN

EXPERIMENTAL PROCEDURES

7.1-   Cutting Tests

7.1.1- Cutting Tools

7.1.2- Workpiece Material

7.1.3- Preparation Of The Workpiece

7.1.4- Cutting Conditions

7.1.5- Quick-Stop Device

7.1.6- Force Measurement During Machining

7.2-   Hardness Measurement

7.3-   Surface Roughness Measurement

7.4-   Transmission Electron Microscopy

7.4.1- Preparation Of The Machined Surface

7.4.2- Replication Of The Machined Surface

7.4.3- Shadowing Of The Plastic Replica

7.4.4- Carbon Coating Of The Shadowed Replica

7.4.5- Dissolving Of The Plastic Replica

7.5-   TEM Examination Of The Specimens

The lathe used for the cutting tests was a Churchill Denhams model Sriov 22" swing centre lathe with infinitely variable speed control (i.e. 0-2,000 rev/min), a 30kW power, and a choice of 54 feed rates in the range 0.057-3.175mm/rev (cf. plate 6). All the cutting tests were carried out under orthogonal cutting conditions (i.e. plane strain was assumed). This was achieved by feeding the tool axially into the end of a tube rotating in the spindle of a lathe as shown schematically in figure 68. The actual experimental set up is shown in plate 7. The tool cutting edge lay in a plane which was perpendicular to the direction of cutting.

7.1.1- Cutting Tools:

The cutting tools used were steel cutting grade P20 brazed carbide tips. To make sure that the same starting conditions of the tool cutting edge existed, the tool was freshly ground before each cutting test. This was ensured by:

(i)- measuring the roughness along the cutting edge of the tool,

(ii)- measuring the radius of the tool cutting edge to keep a check on its sharpness.

The roughness of the cutting edge of the tool was controlled to a value better than 0.7 microns.

Measurements of the cutting edge radius were carried out in two stages. The first stage involved traversing the stylus of a roughness measuring instrument (with the skid removed, i.e use of external datum) across the cutting edge as shown in figure 69 and obtaining a trace of the cutting edge radius. A typical trace obtained in this

way is shown in plate 8. Note that the magnification of the trace is equal in both the vertical and horizontal directions. The second stage was to measure the radius of the tip of the stylus trace. This was done using a desk top optical microscope incorporating a lens inscribed with a series of circles of differing radii in the range 0.02-0.5mm. The procedure was to fit one of these circles to the tip of the stylus trace. This was carried out while viewing the trace of the cutting edge radius through the microscope at a magnification of X30. Using the above procedure the radius of the tip of the trace was measured to be approximately equal to 7microns. Making allowance for a stylus tip radius of about 2microns the tool cutting edge radius was determined to be equal to 5microns for a 5 degree positive rake angle.

The tools were designed to fit in the tool holder of a quick stop device and had a flat at the top of their body for positioning and clamping in the tool holder. The carbide tips were brazed on tools as shown in figure 70.

7.1.2- Workpiece material:

Metallography was used to examine the chip roots, the microstructure, and the inclusion content of the materials used in the present investigation. Standard metallographic procedures were followed which consisted basically of:

(i)- cutting out of the specimen so that its size was at least one centimeter smaller than the size of the mount (1 inch diameter) in the transverse direction to avoid breaking of the mount during polishing,

(ii)- cleaning the surfaces of the specimen thoroughly from oil and dirt to provide good adherence between the specimen and the mount,

(iii)- mounting the specimen in bakelite ensuring that the thickness of the mount was ideally half its diameter. Conductive bakelite was used for specimens destined for scanning electron microscopy,

(iv)- polishing the specimen gradually using silicon carbide paper of decreasing coarseness and finishing on diamond wheels of 6 and 1 micron,

(v)- etching the specimen to reveal structural details by the preferential attack of reagents on metal surfaces. The etchant used in the present investigation was a solution of 2% nital which is commonly used for etching plain carbon steels.

The surfaces of the metallographic specimens were examined using either optical microscopy or scanning electron microscopy. The optical microscope was used to examine the microstructure and the inclusion content of the materials as well as the built-up-edge on the chip roots. The scanning electron microscope was used to examine the chip roots obtained by the quick-stop technique and, in conjunction with electron probe micro-analysis (EPMA), to identify the phases and the inclusions within the material.

The optical microscope used was a Zeiss Ultraphot compound microscope incorporating a camera which enabled records to be kept of the microstructure and inclusion content of the materials.

The workpiece material used to carry out the cutting tests in the present investigation was a medium carbon steel "EN8" in the normalized condition.The composition of this material is shown in table 6. Typical micrographs showing the microstucture of this steel

in the transverse and longitudinal directions of the bar are shown in plates 9 and 10.

Table 6 : Composition of En8 steel used (wt %)

C	Mn	Si	S	P	Ni	Cr	Mo	Al
.395	.85	.35	.036	.009	.14	.19	.04	.03

7.1.3- Preparation Of the Workpiece:

The test workpieces were prepared from rolled bar.   The bar was bored out and machined to give a tube of wall thickness 5mm as shown in figure 68. This preparation procedure was used for bars which had small diameters. For larger diameters of the bar this method is wasteful and an alternative method was employed. The alternative preparation procedure was to machine a recess at the end of the bar using a special tool as shown schematically in figure 71a.   The thickness of the wall was then reduced to the required value by machining on the outside of the bar.   The length of the recess, and thus the number of tests which could be conducted after each workpiece preparation, was greatly reduced. One test only could be carried out after each preparation and this was found to be time consuming. This problem was overcome by using an alternative tool as shown in figure 71b, whose main body was designed in a way so as to allow longer recesses to be cut out off the end of the bar and this resulted in a set of tests for each preparation of the workpiece. An added bonus from using the second method of workpiece preparation was that the central portion of the workpiece could be used as a centre to mount the workpiece between the chuck and the tail stock centre as shown in

plate 7. This resulted in extra rigidity to the workpiece during machining tests. Also the central portion could be used for subsequent sets of tests thus giving substantial saving in material.

7.1.4- Cutting Conditions:

Four sets of cutting tests were carried out under dry cutting conditions to investigate the effects of machining variables on the microcracking produced in the machined surface.

The first set of cutting tests were conducted to investigate the effects of the cutting speed which was varied between 3 and 400m/min. These tests were carried out using a tool with a 5 degree positive rake angle while the undeformed chip thickness was kept constant at a value of 0.244mm.

The second set of cutting tests were carried out at a cutting speed of 200m/min using a tool with a 5 degree positive rake angle. These tests were conducted to investigate the effects of the undeformed chip thickness which was varied in the range 0.057mm to 0.396mm.

The third set of cutting tests was carried out to investigate the effect of varying the rake angle while the undeformed chip thickness was kept constant at a value of 0.244mm. Tests varying the rake angle were conducted for two cutting speeds. For a cutting speed of 200m/min, the rake angle was varied between 5 degree negative and 30 degree positive. For a cutting speed of 50m/min, the rake angle was varied through the range 10 degree negative to 30 degree positive.

The fourth set of cutting tests was carried out to investigate the effect of subjecting the workpiece material to various heat treatments. The hardness of the material was measured for each heat

treatment and was found to vary in the range 180 to 350 VPN (Vickers hardness). These cutting tests were carried out at a cutting speed of 200m/min with an undeformed chip thickness of 0.244mm and using a tool having a 10 degree positive rake angle.

7.1.5- Quick-Stop Device:

The quick-stop device is an instrument used to quickly disengage the tool from the workpiece during machining. The efficiency of this device depends on the acceleration with which the tool is moved away from the workpiece. The device enables the machined surface and chip root to be preserved for subsequent electron microscope examination. The machined surfaces in the present investigation were obtained using the quick-stop device shown in plate 11.

Plate 12 shows the quick-stop device and the associated accessories. A humane killer gun is used to provide the high acceleration required. The tool is held in place by a tool holder resting on a shear pin strong enough to withstand the cutting forces. The tool holder can rotate around a pivot situated at the back of the shear pin. When the humane killer gun is fired, the pressure build-up in the firing chamber accelerates the hammer which hits the top of the tool holder. Under the action of the impact of the hammer the shear pin breaks and releases the tool holder which rotates around the pivot thus disengaging the tool from the workpiece. The tool holder is then brought to a halt by plasticine. In order to allow for the feeding action of the tool a cant angle is provided so that the tool retraction from the workpiece takes place at an angle to the machined surface, hence avoiding contact between the latter and the tool flank after the quick-stop has been operated. Plate 13 shows the quick-stop

device used in the pesent investigation mounted on the cross-slide of the lathe and ready for a machining operation. Plate 14 is a close up showing the tool holder, the machined surface, and the hole through which the hammer hits the tool holder.

Immediately after the quick-stop device had been operated, the spindle rotation was stopped and a squirt of oil was put on to the machined surface to preserve it (i.e. reduce oxidation and corrosion to a minimum) for subsequent examination and measurements. It was then parted off and numbered using an etching pen for identification later on. Machined surfaces parted off are shown in plates 12 and 17.

7.1.6- Force Measurements:

The cutting force "Fc" and the feed force "Ft" acting on the tool during machining were measured using a dynamometer in conjunction with an ultra-violet (U-V) recorder. The dynamometer used was a Kistler quartz multicomponent dynamometer type 9257A which could measure vertical forces in the range 0-10 kN and horizontal forces in the range -5 to +5 kN with a resolution of 0.01 N. The experimental set-up for force measurement is shown in plate 15. The compound slide had been removed and the dynamometer is shown bolted on the cross-slide of the lathe. The cutting tool was held in a tool holder which was clamped on top of the dynamometer. Plate 16 shows the ultra-violet recorder and the amplifier used.

7.2- Hardness Measurements

A Vickers hardness machine was used to measure the hardness of the material used at different heat treatments. The measurements were

based on the average of five readings taken at the middle of a ground area of the workpiece and at random locations around the workpiece surface. It was ensured that measurements were carried out at a diameter corresponding to that of the tube used for the cutting tests to allow for any microstructural variation with radius of the bar. The hardness measured for the different heat treatments of the medium carbon steel used in the present investigation are tabulated in table 7.

Table 7 : Hardness measurements results
for heat treated En8 steel.

Heat treatement	Hardness (VPN)
As-received (Normalized)	208
Fully-annealed	180
Quenched in oil	350
Quenched and tempered 1	260
" " " 2	285
" " " 3	320

7.3- Surface Roughness Measurements

The surface roughness was measured using a Taylor-Hobson Talysurf type 5-120(M) stylus instrument. The measurements were taken both parallel and normal to the cutting direction. The value of surface roughness in each direction was determined from the average of five readings taken at random locations around the machined surface.

7.4- Transmission Electron Microscopy

The success of transmission electron microscopy work depends on the quality of the specimens prepared and the fidelity with which they

reproduce the machined surface under investigation. In the present investigation a considerable amount of time and effort was spent obtaining the necessary expertise for successful specimen preparation. The complete specimen preparation procedures followed is illustrated by figure 72 and the details explained in the following sections.

7.4.1- Selection And Preparation Of The Machined Surface:

The first problem at this stage was how to select an area which was representative of the machined surface. The following factors had to be considered:

a)- the variability within the machined surface,

b)- contamination by impurities (i.e. dirt from the atmosphere), finger prints, spots, specks, or isolated non-representative portions present on the surface and which may be transferred to the replica,

and c)- changes associated with poor replication of the surface.

To cater for the variations in the surface, preliminary work was carried out which involved taking a number of replicas at randomly selected locations of a machined surface. The microcracking parameters were then determined using the microcrack measurement technique described in chapter 6 and the results compared. It was found that the area equivalent to the minimum number of micrographs as determined in appendix 1, was representative of the machined surface.

To avoid replicating contamination particles, a good wash of the machined surface is recommended prior to any replication. For best results, the surfaces to be replicated were washed with liquid soap and water twice, rinsed with alcohol until no water was left on them, then dried in a hot air stream from a hair drier and put into a clean

closed container filled with acetone so that the specimen was completely submerged by acetone.

Soaking in acetone was carried out for two reasons. The first one was for further cleaning of the machined surface as some of the oil applied onto the latter upon completion of the cutting test, could have been left in small cavities and microcracks even after cleaning with soap and water. To ensure that the acetone entered all the microcracks and small cavities thus expelling the oil present therein, soaking was continued overnight before replication was finally done. The second reason for soaking in acetone, was to allow the acetone (which was used as the softening agent of the replicating material) to wet all the small cavities and microcracks so that to improve the penetration of the replicating material into the microcracks by surface tension.

7.4.2- Replication Of The Machined Surface:

This is defined as the technique which enables the reproduction of the surface topography on the surface of a suitable replicating material. TEM examination of machined surfaces depends greatly on the exactness with which the surfaces to be looked at are reproduced by the replication method. Three factors influence the success of surface replication:

(i)- the replicating material,

(ii)- the softening agent,

and (iii)- the operator's expertise.

Preliminary work with methyl acetate sheets and with cellulose acetate sheets indicated that best results were obtained using the

latter as the replicating material with acetone as the softening agent (i.e. solvent).

The basic procedure was to cut a piece of acetate sheet (about 20mm by 3mm), soften the underside in acetone, lay it on the surface, and strip off when completely dried. Utmost care was taken to avoid dust from the atmosphere to be deposited on the machined surface by keeping the latter covered except for when the replicating material was being applied. The replicating sheet was also wiped with a clean tissue before use, so as not to waste the considerable care taken in preparing the surface by using a dirty or contaminated (e.g. due to finger prints) replicating sheet. During the softening process of the acetate sheet, air bubbles could form and adhere to the underside of the replicating sheet. It was realized that this occurred when the acetone used for softening the acetate sheet had been used for a number of replications. Changing the acetone at regular intervals was found to suppress bubble formation. Also, gentle dipping of the acetate sheet into the acetone resulted in a reduction of bubble formation and their adherence to the replicating material. In addition, during the laying of the replicating sheet onto the surface, it was found that by carefully laying the softened acetate sheet in the manner shown by figure 73, it was possible to avoid entrapping these air bubbles between the surface and the acetate sheet.

As soon as the replicating sheet is laid onto the surface and the acetone starts to evaporate, the plastic hardens and contracts into the surface features. It should be emphasized at this stage that a fast evaporation rate of the acetone will result in a rushed and incomplete marriage of the surface and the underside of the plastic replicating sheet. Therefore, a slow evaporation is desired to allow the replcating material time to take the shape of the surface

features. This was achieved by keeping the surface to be replicated in an acetone atmosphere prior to and after replication. A small drop of acetone at the bottom of the container was found to be enough to provide the necessary atmosphere which would slow down the acetone evaporation process thus allowing the softened plastic sheet time to sink into the surface depressions. A quick check on how well the replication had been carried out, was the ease with which the replica could be stripped off the surface when dry.

During the stripping of the replica from the surface, damage to some slender features can take place. This phenomenon is referred to as the "collapse of slender features" and its effects on the TEM observations have been explained in section(6.6.3). One way of preventing this damage from happening was to refrain from stripping off the replica which was left on the surface after replication until it flaked off by itself. For rougher surfaces the stripping was extremely difficult and the replica never flaked off on its own. For these replicas only, stripping off was assumed to give acceptable results when the replica was left on the surface for more than a full day as it was then found to strip off more readily. This was found to produce some errors due to the collapse of slender features.

Once the replica had been stripped off the machined surface, it was turned over and stuck with sellotape onto a glass slide and labelled for subsequent identification. Due care was taken to avoid dirt depositing onto the replica surface by ensuring a clean working environment. The procedures described above are shown in plate 17.

Emphasis must be put on the fact that, although the replica cannot be produced identical to the replicated surface, this method is recognised as giving accurate copies of the machined surface and has

become a standard technique in transmission electron microscopy [139,140].

7.4.3- Shadowing Of The Plastic Replica:

Shadowing was carried out to improve contrast on the final TEM image and to allow quantitative studies of the microcracks present on the machined surface as discussed in chapter 6. Shadowing is a process which involves evaporating an appropriate material onto the surface replica at a chosen angle. This was carried out in high vacuum inside an Edwards E306 vacuum coating unit which is shown in plate 18. The controls are shown in plate 19. The shadowing material was evaporated in the tungsten basket located in the bottom part of the vacuum chamber as shown in plate 20, and across which a high voltage was applied. The glass slide carrying the replicas was stuck with double sided sellotape to a disc at the top of the vacuum chamber. To allow adjustment of the shadowing direction, the glass slide holder could be rotated in two orthogonal planes defining angles to the surface of the replica and to a reference axis in the plane of the replica face (i.e. axis corresponding to the cutting direction on the machined surface). The procedure was to:

  (i)- place the glass slide so as to give a shadowing direction at 45 degree angle to the replica face and 45 degree angle into the cutting direction,

 (ii)- place the shadowing material in the tungsten basket,

(iii)- take the coating chamber down to a vacuum better than about 0.00004 Torr (1Torr=1mm Hg),

 (iv)- apply a steadily increasing voltage across the tungsten basket while observing the shadowing material through the glass wall

of the vacuum chamber. As soon as melting of the shadowing material starts taking place, the voltage should be held constant until complete evaporation is achieved. This process is illustrated in figure 74.

It is the shadowing process which is responsible for the contrast obtained in the transmission electron microscope images. Bearing in mind that interpretation of TEM micrographs is only possible with a good understanding of the final contrast produced in the image, a sound knowledge of the shadowing process is called for. A number of parameters must be considered when shadowing the surface replica, viz.,

- the atomic number of the shadowing material,
- the distance from the evaporation source to the replica face,
- the shadowing angles,
- the quality of the vacuum under which shadowing is carried out,
- the severity of the voltage applied across the tungsten basket,
- the cleanliness of the shadowing medium,

and - the amount of shadowing material evaporated.

As stated in section 5.3.4, the atomic number of the material of a specimen impinged upon by the electron beam, influences the scattering of the electrons. The higher the atomic number of the material the higher the scattering angle and hence the larger the proportion of lost electrons and the better the contrast produced. Gold-Paladium (Au/Pd) has been used as the shadowing material throughout the present investigation. Also the density of the shadowing material affects the thickness of the coating produced. A laboratory expression relating the thickness of the coating obtained by evaporation to the mass of shadowing material is given by:

$$m = 16 . \pi . r^2 . \rho . t / 3 \sin \alpha$$

where "m" is the mass of shadowing material used,

"r" the distance of the replica face from the shadowing source,

"ρ" the density of the shadowing material,

"α" the angle made by the shadowing direction with the replica face,

and "t" the thickness of the shadowing film produced.

It can be seen from the above equation that the thickness of the film obtained by shadowing depends on the mass of material evaporated, the shadowing angle, and the distance from the evaporation source. This equation is based upon the assumption that given a point source, uniformly distributed spherical evaporation takes place. In other words, if the evaporation source was enveloped by a spherical surface, a film with constant thickness will be deposited on to the surface. In the present investigation a shadowing film thickness of 25 Å was obtained by evaporating 46.16 mg of gold-paladium, given a shadowing angle of 45 degree, a distance from the evaporating source of 0.22m (standard value for the coating unit used), and a density of 16,100 kg/m^3 for the gold-paladium.

The choice of the shadowing angle was so as to facilitate measurements and standardization of the microcrack measurement technique as discussed in section 6.4.1. Two complementary directions in the plane of the machined surface were required to be translated into shadowing directions. The angles corresponding to these directions will be referred to as the "in-plane shadowing angles" (ipsa) so as to be distinguished from the shadowing angle mentioned above. The in-plane shadowing directions (ipsd's) were determined in a manner so as to be at right angles (i.e. complementary) to each other and oriented into the cutting direction as shown in figure 75a

where they are termed directions "a" and "b". With respect to the replica face (replica turned over), the in-plane geometry of shadowing is as shown in figure 75b.

Contamination of the replica can originate from dirty evaporating baskets (i.e. oxide films on unused baskets or dust deposited from the atmosphere). To eliminate this occurrence, new baskets were always flashed. This consisted of performing the evaporation procedure with an empty basket prior to shadowing. It was also noticed that some shadowing material was always left at the bottom of the basket making the first shadowing film thinner than subsequent ones. To allow for this a small amount of shadowing material was put into the tungsten basket prior to the latter being flashed.

7.4.4- Carbon Coating Of The Shadowed Replica:

The shadowed replica contains discontinuities in the shadowing film especially when the shadowing material meets up with peaks and protruding features on the replica face. In addition, the specimen film "transparency" criteria (i.e. capability to transmit electrons) sets a limit on the thickness of the film, a thicker specimen resulting in higher scatter and very minute proportions of electrons passing through as discussed in section 5.3.4. These two characteristics make the shadowing film thin, weak, and easy to break, hence the need for strengthening to allow subsequent handling. The strengthening of shadowed replicas was provided by evaporating a backing film onto the surface of the shadowed replica. This backing film should be of a light material (i.e. small atomic number) so as to give the thickness required to hold the shadowing film together without impairing the transparency of the specimen to electrons. In

the present investigation carbon which is the most commonly used has been selected as the backing film material. The carbon coating should not contribute to nor affect the contrast produced by the shadowing process. This was achieved by evaporating the carbon in a direction normal to the replica face, resulting in a carbon film of uniform thickness. Evaporation was carried out in the Edwards E306 vacuum coating unit shown in plate 18. The set-up for carbon coating is shown in plate 21.

The carbon was evaporated from two carbon rods located in the top part of the vacuum chamber and through which a high electrical current was passed. The rods were shaped in the manner shown schematically in figure 76. The procedure was to:

- place the glass slide with the shadowed replicas flat on the bottom of the vacuum chamber,

- pump down to a vacuum better than 0.00004Torr,

- increase the voltage between the carbon rods at a moderate rate until blue sparkles are emitted by the rods indicating the start of the evaporation process.

- This voltage was then held for a time corresponding to the required thickness of the carbon coating.

When the temperature of the carbon rods became too high a safety thermal cut-out device was provided which would open the circuit supplying the voltage. To resume the evaporation process, the unit had to be allowed to cool down for at least ten minutes before the reset button was depressed and evaporation resumed again. A filter paper was placed on the bottom of the vacuum chamber underneath the glass slide to give a rough guide on the thickness of the carbon coating.

The thickness of the carbon film is an important parameter especially for subsequent processing and during the TEM examination of the specimens. Thin carbon films were found to break easily whereas too thick carbon films tended to curl away from the copper support grids during handling and examination in the TEM. The optimum thickness of the carbon film was estimated from the shade obtained on the filter paper after carbon had been evaporated. It was found that a silver grey shade on the filter paper gave the necessary thickness to provide adequate strength for the carbon coating. A slightly darker shade was required for rougher surfaces. The shades determined above were used to standardize on the thickness range of the carbon film.

7.4.5- Dissolving Of The Plastic Replica:

After shadowing and carbon coating, the plastic replica had to be dissolved. This was done using acetone as the solvent. During soaking in acetone the replica with the shadowing and carbon coatings had to be supported to avoid distortions which would result in the breakage of the film and the introduction of artefacts from the changes incurred to the topography by such distortions. Adequate support was provided by three millimeter diameter support grids. The grids are usually made of copper and vary in their number of squares per given area (usually one square inch). Grids with different mesh size (c200 and c300) were used prior to the selection of the grid for use in the present investigation. Grids c300 (c refers to copper and 300 to the number of squares per square inch) were found to reduce the breaking of the specimen film by providing a better support. An added

benefit with the finer mesh was the fact that it added a larger conducting area of contact with the specimen, hence assisting in preventing the specimen from charging up and overheating. Specimens that are prone to charge up should be mounted in a manner such that the charge or heat can be conducted away so as to prevent a build-up which eventually destroys the specimen either chemically or by overheating.

The procedure used in the present investigation for mounting the specimens onto the support grids and dissolving the plastic away, was as follows:

(i)- using a surgical knife, the specimen was cut into small squares suitable in size for mounting onto the three millimeter diameter copper support grids,

(ii)- the support grids were put onto a copper gauze partly soaked in acetone,

(iii)- the specimen cut squares were then mounted onto the mat face of the support grids.

Preliminary experimental work indicated that best results could be achieved by mounting the cut squares onto the support grids with the carbon coating facing downwards. The common practice of mounting the specimens with the carbon film facing upwards was found to result in extensive breakage.

The soaking process is shown diagrammatically in figure 77. Past experience showed that complete dissolving of the plastic could be achieved only after a number of soaks in acetone. The first soak always took longer (about one and a half hours). Subsequent soaks were of half an hour each. The acetone was changed afresh after each soak until the plastic was completely dissolved. Any plastic remaining on the specimen would have adverse effects both on the

- 134 -

specimen itself and during TEM examination depending on the amount of
plastic left. A large amount of remaining plastic will cause the
specimen and grid to curl up on themselves and destroy the specimen
film. A small amount will not cause the curling up effect but will
obliterate the specimen surface in the TEM thus resulting in poor
illumination. Charging up also can take place due to the insulation
provided by the plastic.

Bearing the above in mind, it can now be stated that some means
of checking whether all the plastic had been dissolved or not, was of
utmost importance. A straight forward way of doing so was to follow
the standard practice of carrying out three soaks, mounting on the
TEM, observing whether any plastic was left, and re-soaking if
necessary. This method was found to be time consuming and there was
always the risk of destroying the specimen during mounting into and
dismounting from the TEM specimen holder.   In addition, there was the
risk of breaking the specimen film during the hardening and softening
of the remaining plastic by the stresses set up in the specimen. An
alternative to the above method is described below.

Two containers were provided for the soaking.   The copper gauze
with the specimens was soaked in one of them for the required time.
At the end of the soak the required amount of fresh acetone was put
into the second container. The copper gauze was then transferred to
the second container from the first which was left open on a window
sill for the acetone to evaporate.   When the acetone had evaporated a
white deposit was left at the bottom of the container.   This white
deposit is the plastic which had been dissolved from the specimen by
the acetone during the first soak. The above process was repeated
until no trace of the white deposit was observed upon evaporation of
the acetone, indicating that the plastic had been thoroughly dissolved

from the specimens. Plate 22 shows the traces of white deposit after successive soaks until no trace is observed.

The above described checking technique was found to be both effective and invaluable in that it provided a simple way of ensuring complete dissolving of the plastic prior to TEM examination of the specimens. The time involved in the soaking had been considerable and since the early stages of the present investigation, its reduction remained a target. Experience gained from using this soaking technique showed that the solution (i.e. acetone and dissolved plastic) retained by the copper gauze during transfer from the saturated to the fresh acetone, was of a significant amount. This retained saturated solution contributed to the saturation of the fresh acetone in the new container hence reducing its dissolving power. A paper tissue was used to drain the retained solution from the copper gauze before transferring the latter into the fresh acetone. This resulted in a large reduction of the numbers of soaks necessary for complete dissolving of the plastic.

A further improvement was to move the acetone around the copper gauze to speed up the dissolving process by allowing the specimen direct contact with the acetone. This was found to reduce the time for each soak. An exception, however, was the first soak which was done slowly and without agitation of the container.

Finally one factor which influenced the soaking times was the number of specimens put onto the copper gauze at a time. Upon completion of the dissolving of the plastic from the specimens, the latter were picked up with tweezers and stored in a special storage box with identification facility until TEM examination. The storage box and the dissolving process are shown in plate 23.

Selected specimens were mounted and examined in the JEOL JEM 100B transmission eclectron microscope shown in plate 24. Plates 25 to 27 show the details of the TEM column, the left hand and the right hand side controls respectively. Prior to examination, the specimens on copper grids were mounted in the high contrast holders (plate 28), which were then located in the specimen holder magazine shown in plate 29. The specimens were examined at a magnification of 900 times using an accelerating voltage of 80 kV. After a preliminary scan around the specimen to gain acquaintance with the surface features and to build an appreciation of how representative individual micrographs could be, twelve micrographs were obtained randomly for each specimen making a total of 24 micrographs for each machined surface. The number needed was 20 the extra four micrographs were taken to be used in case of damage during photography and development of the negatives.

Photomicrography was made possible by the existence of camera facilities incorporated wihin the TEM. In the present investigation, ILFORD plates type EM4 with a sensitivity of 3.5 suitable for use with the dispensing and receiving magazines (figure 78) have been used. The photographic plates were mounted in cassettes which were located in the dispensing magazine onto a spring loaded bottom as shown in figure 79.

Information or measurements can be extracted either from the micrograph prints or negatives. The negatives were used in the present studies to measure the microcracks using the technique described in chapter 6. Interpretation of the TEM micrographs has been discussed in section 5.7. The micrographs were taken in a random manner to provide some statistically significant means of measurement.

Extra information that could be obtained from the TEM micrographs is the characterization of the microcracks observed according to the classification proposed in section 6.7. This information is qualitative and will only be complete when accompanied by a catalogue of micrographs (e.g Plate 5).

CHAPTER EIGHT

RESULTS

8.1- Variation Of Microcracking Parameters With Cutting Speed

8.2- Variation Of Microcracking Pararmeters With Undeformed Chip
Thickness

8.3- Variation Of Microcracking Parameters With Rake Angle

8.4- Variation Of Microcracking Parameters With Workpiece Hardness

8.5- Results Of Surface Roughness Measurements

8.6- Results Of Metallography Studies On Heat Treated Steel

8.7- Results Of The Force Measurement Tests

8.1- Variation Of Microcracking Parameters With Cutting Speed

The variation of the microcracking parameters with a change in the cutting speed is shown in figures 80 and 81. These results can be found in tabulated form in appendix 5. Typical micrographs showing the microcracking in surfaces machined at a low and high cutting speeds are presented in plates 30 and 31.

8.2- Variation Of Microcracking Parameters With Undeformed Chip Thickness

The microcracking parameters were determined for surfaces machined with undeformed chip thicknesses in the range 0.057mm to 0.396mm and are tabulated in appendix 5. The variation of the microcracking parameters with increase in undeformed chip thickness is shown in figures 82 and 83. Typical micrographs showing the microcracks on surfaces machined with a small and large undeformed chip thickness are presented in plates 32 and 33.

8.3- Variation Of Microcracking Parameters With Rake Angle

The microcracking parameters of surfaces machined using tools with rake angles in the range 5 degree negative to 30 degree positive, are tabulated in appendix 5. The variation of the microcracking parameters with a change in the tool rake angle at a cutting speed of 200m/min is shown in figures 84 and 85. Typical micrographs for a negative rake angle, a small positive rake angle, and a large positive rake angle are shown in plates 34 to 36 respectively.

The variation of the microcracking parameters with the rake angle for a cutting speed of 50m/min is shown in figures 86 and 87.

8.4- Variation Of Microcracking Parameters With Workpiece Hardness

The results for the microcracking parameters obtained when machining a medium carbon steel which had undergone different heat treatments, are tabulated in appendix 5. The variation of the microcracking parameters with an increase in the material hardness is shown in figures 88 and 89. Typical micrographs of machined surfaces of a fully annealed, as-received (normalized), quenched-tempered and quenched medium carbon steel are presented in plates 37 to 42 respectively.

8.5- Results Of Surface Roughness Measurements

The results of surface roughness measurements are tabulated in appendix 5. The variation of surface roughness measured both parallel and normal to the cutting direction, with change in cutting speed, undeformed chip thickness, and rake angle is shown in figures 90 to 95 respectively.

8.6- Results Of Metallography Studies On Heat Treated Steel

The micrographs obtained from the metallographic studies on the medium carbon steel subjected to a number of heat treatments are presented in plates 43 to 48.

In the normalized (as received) condition (plate 43), the microstructure is made up essentially of pearlite (dark areas) with a

distribution of large areas of polygonal ferrite. Plate 43a also shows the inclusion content in the normalized medium carbon steel to have a clustered distribution. Electron probe micro-analysis (EPMA) in the scanning electron microscope was used to identify these inclusions and the results showed that they were mainly manganese sulphides (MnS) with other constituents of complex nature (i.e a mixture of silicates, chromates, and nickel). The inclusions have an elongated shape in a direction parallel to the axis of the bar. In other words, they are normal to the machined surface. The preferential site of the inclusions was observed to be the relatively softer micro-constituent of the material (i.e. ferrite phase).

In the fully annealed condition, the grain size is smaller than that for the normalized (as received) steel, as shown in plate 44b. This is not what is expected (i.e normally full-annealing gives rise to coarser microstructure than normalizing). One explanation for the coarser grain of the normalized material is that in the as received state the material is not truly normalized. For example hot-rolling could have been carried out at a much higher temperature than that of the full-annealing (around 830°C) which would be responsible for the bigger grain size. In the fully annealed state, the ferrite assumes a banded structure which plays host for the elongated inclusions in the material (plate 44a).

In the quenched and tempered condition the structure is mainly martensitic with a fine distribution of retained austenite (white areas) as shown in plate 47. In the extreme case for severe quenching the structure would be fully martensitic (i.e single-phase). On tempering at low temperatures, optical metallography only reveals a darkening of the etched martensite. This darkening of the etched martensite is associated with the precipitation of carbide plates at

grain boundaries. At the higher tempering temperatures the globular stucture of the lower hardness tempered martensites appears (plates 45 and 46) with the appearance of a ferrite phase (white areas).

A fully martensitic microstructure was aimed at when the medium carbon was quenched but as the micrographs in plate 48 show, this was not achieved. It can be seen that a significant amount of ferrite (white areas) is still present.

8.7- Results Of The Force Measurement Tests

The results of the force measurements are tabulated in appendix 5. The variation of the specific cutting energy (cutting force per unit area of uncut chip) with change in cutting speed, undeformed chip thickness, and rake angle is shown in figures 96 to 98.

CHAPTER NINE

DISCUSSION

9.1- Introduction

9.2- Effect Of Cutting Speed On The Microcracking In The Machined
     Surface

9.2.1- Temperature Effects

9.2.2- Time Effects

9.2.3- Stress Effects

9.3- Effect Of Undeformed Chip Thickness On The Microcracking In
     The Machined Surface

9.4- Effect Of Rake Angle On The Microcracking In The Machined
     Surface

9.5- Effect Of Workpiece Hardness On The Microcracking In The
     Machined Surface

9.6- Role Of Built-Up-Edge In Microcrack Formation And In Variability
     Of The Results

9.6.1- Role Of Built-Up-Edge In Microcrack Formation

9.6.2- Role Of Built-Up-edge In Variability Of The Results

9.7- Microcrack Coalescence

9.8- Comparison Between Microcracking In The Machined Surface And
     Microcracking In The Shear Zone

9.9- Treatment Of The Results

9.10- Recommended Machining Code Of Practice For Component Strength

9.1- Introduction

The microcracking phenomenon, as observed in the present investigation, occurs in the machining process for a wide range of workpiece material and cutting conditions. The results presented in the previous chapter show that the occurrence and extent of the microcracks in the machined surface vary with workpiece material, cutting tool variables, and cutting conditions. The present studies were, however, limited to the orthogonal machining in turning because it is the geometrically simplest machining process.

The results obtained in this investigation are unique and their significance is discussed in the light of the various aspects of the machining process. Some of the reported work on the microcracking in the shear zone, although qualitative in nature, will be scrutinized in the light of the present investigation. Also, the exploratory nature of the present investigation opens the doors for a number of speculations which will lead to the proposal of possible areas for future work. As it stands, the completion of the research programme which has culminated in the present thesis, is by no means the end of the microcracking problem. It is rather the start of a whole new area of research on the nature of machined surfaces and a lot of work remains to be done in this area yet.

9.2- Effect Of Cutting Speed On The Microcracking In The Machined Surface

The variation in the microcracking parameters with a change in the cutting speed is shown in figures 80 and 81. In these figures, the microcracking parameters are shown to decrease with increase in

the cutting speed. The trends, however, are not so straight forward at the low end of the cutting speed range. They show a high variability in the microcrack area ratio "Ma" for a cutting speed range below 100m/min. This variability of "Ma" at low cutting speeds can be explained by the occurrence of the built-up-edge in machining.

The cutting speed range in which the cutting tests were carried out can be divided into two main ranges. One for which machining takes place in the presence of a built-up-edge and the other for which the built-up-edge has disappeared. A number of ways are reported to have been used to determine the cutting conditions for built-up-edge occurrence. The empirical charts by Trent [7] are but one example. Oxley [141] has considered the question of how machining theory might be used to predict the built-up-edge range. His approach was based on the reasoning first suggested by Shaw [86] using the temperature as a criterion for built-up-edge occurrence.

Using the Scanning Electron Microscope, chip roots obtained by the quick stop technique can be examined to determine the built-up-edge formation range. The presence of the built-up-edge can also be indicated by built-up-edge debris being present both on the machined surface and on the chip underside. Using the above technique, it was found that the built-up-edge, although reduced in size, was still present at a cutting speed of 75m/min. At a cutting speed of 100m/min., there was no trace of the built-up-edge, the feed for these tests being 0.244mm.

An alternative way of finding out at what cutting speed the built-up-edge disappears, is to consider the surface roughness. The surface roughess, as discussed in section 3.2, is strongly affected by built-up-edge formation. The variation of the Centre-Line-Average (CLA) roughness "Ra", measured both parallel and normal to the cutting

direction, with the cutting speed is shown in figures 90 and 91 respectively. The highest value of parallel surface roughness is shown in figure 90 to occur at a cutting speed of about 10m/min. Assuming that at low cutting speeds the surface roughness is due mainly to built-up-edge effects, then this curve can be used to predict the cutting speed range at which the built-up-edge disappears. In figure 90 the surface roughness decreases considerably between a cutting speed of 10m/min. and 50m/min. A steadier decrease is observed thereafter up to a cutting speed of about 200m/min. at which a constant value of surface roughness is reached. Although the cutting speed for built-up-edge disappearance cannot be pinpointed exactly, it can be deduced from the above observations that the built-up-edge disappears at a cutting speed between 50m/min. and 200m/min. A close look at figure 91 shows that the surface roughness measured in a direction normal to the cutting direction, decreases with increase in the cutting speed above the maximum roughness range up to a value of about 100m/min. With further increase in the cutting speed there is no significant change in the normal surface roughness. This is explained by the effect of the built-up-edge interference with the tool cutting edge/machined surface interaction. The occurrence of the built-up-edge results in the machined surface being generated at a distance away from the tool cutting edge and flank face. As the cutting speed is increased, the size of the built-up-edge decreases resulting in a more and more stable built-up-edge until it finally disappears. This has two effects:

- The first one is that the size of the built-ip-edge debris left on the machined surface become smaller and less frequent.
- The second effect is that contact between the tool cutting edge and the workpiece is restored thus allowing the machined surface to be

generated at the tool flank face which leaves its roughness (which is constant) on the machined surface. It can be seen from figure 91 that the surface roughness reaches a constant value of about 0.5μm, which is incidentally of the order of the roughness of the tool cutting edge (i.e. 0.45-0.65μm), at a cutting speed of 100m/min.

Basing the argument on the above discussion and on the Scanning Electron Microscope examination of the chip roots, it can be concluded that the built-up-edge completely disappears at a cutting speed of 100m/min. This agrees with experimental work by Williams and Rollason [10] on low and medium carbon steel (see section 2.4).

It is proposed that the generally high levels of microcrack area ratio and microcrack density at low cutting speeds is associated with the presence of a large built-up-edge.

Looking at the variation of the microcrack area ratio with cutting speed (figure 80), the variability of the results is seen to increase considerably for values of the cutting speed below 100m/min. which is the estimated value for built-up-edge disappearance. This strongly supports the suggestion formulated earlier that the built-up-edge has a significant part to play in the variability of the results obtained. The discussion of how built-up-edge presence causes the high level of microcracking parameters and its effects on the variability of the results observed in figure 80 is deferred to section 9.6 when its effects on the machining process and on the replication technique will be considered.

Above a cutting speed of 100m/min., the microcrack area ratio is shown to decrease with increase in the cutting speed. The results shown in figure 80 are characterized by a rapid decrease between a cutting speed value of 100m/min. and a value of 200m/min. followed by

a steady slow decrease and approaching assymptotically the zero value at very high cutting speeds.

The variability in the results of the microcrack density is less evident as shown in figure 81. From this figure it can be seen that the general trend is a decrease in the microcrack density with increase in the cutting speed. The curve can be approximated to a straight line with a good correlation (i.e. r=-0.928).

Bearing in mind the effects of the cutting speed on various aspects of the machining process, a number of explanations of the trends obtained in figures 80 and 81 above the built-up-edge range are proposed.

9.2.1- Temperature Effects:

The generation of higher temperatures as the cutting speed is increased affects the flow properties of both the matrix and the second phase particles of the workpiece material. The association of microcrack formation with the inclusion content and the two-phase nature of the material has been discussed at length in section 4.3. The influential factor is the difference in elastic/plastic properties between the matrix and the inclusions or second phase particles. The material used in the present investigation as shown in plate 43, was a medium carbon steel which consisted of almost equal quantities of ferrite and pearlite with a distribution of manganese sulphide (MnS) inclusions confined to the ferrite phase. The difference in elastic/plastic properties between the matrix and second phase can be represented by the relative plasticity index which is the ratio of the true deformation of the second phase over the true deformation of the matrix. This parameter has been shown by Gove and Charles [142] to be

approximately inversely proportional to the hardness ratio (i.e. Hardness of inclusion over Hardness of matrix). In other words as the hardness ratio increases the relative plasticity index decreases and vice-versa. The variation in the hardness of the various phases of 0.2%C and 0.13%C steels with increase in the working temperature has been investigated by Gove and Charles [143]. Their results show a decrease in the hardness of both ferrite and pearlite phases with increase in temperature as shown in figure 99. From this figure it can be seen that the hardness ratio between pearlite and ferrite decreases from a value of about 2.0 at 20 °C to a value of about 1.36 at a temperature of 700 °C. This means that as the temperature increases, the relative plasticity index approaches unity and so the difference in elastic/plastic properties between ferrite and pearlite becomes smaller. As the difference in the deformation charcteristics between the two phases decreases, so does the susceptibility of microcrack formation. This can be one explanation which justifies the general trends in the results plotted in figures 80 and 81 which show a decrease in the microcracking parameters with increase in the cutting speed. Another temperature effect is the change in the ductility of the material. As discussed in section 4.1.1, microcracks can be nucleated by dislocation pile-ups at grain boundaries provided no slip occurs in adjacent grains to accommodate the dislocations. High ductility of the material provides such slip planes and so decreases the likelihood of microcrack nucleation at grain boundaries. Also, it has been shown in section 4.1.2 that once nucleated, microcracks meeting a grain boundary can be blunted by plastic flow occurring ahead of the tip of the microcrack, this plastic flow being enhanced by higher material ductility.

9.2.2- Time Effect:

If the formation of microcracks is thought of as the generation of two new surfaces, then the controlling factor will be the energy available for the creation of such surfaces and the time during which this energy is applied. Considering microcrack formation to occur in two stages, namely the nucleation stage and the growth stage, the latter stage can take place at a lower applied energy than the former because once a microcrack has been nucleated, it acts as a stress raiser and hence any subsequently applied stress will be "magnified". While the nucleation of microcracks depends mainly on the presence of weak sites coupled with the stress situation, as discussed in section 4.1, the growth depends both on the applied stress and the time during which this stress is allowed to act. Obviously, as the cutting speed is increased, the time taken by an element of material to traverse the shear zone, referred to as the "subjection time" from now on, will decrease accordingly. This will consequently decrease the extent of microcrack growth. In addition, as the cutting speed is increased, the thickness of the shear zone also decreases [36]. This has the added effect of shortening the subjection time and so reduces the microcrack growth stage still further.

Basing the argument on the above philosophy, an explanation of the decrease in the microcracking parameters with an increase in the cutting speed is associated with the subjection time. Once a microvoid has been nucleated at a weak site in the material, the stress situation proceeds to the formation of a microcrack either by coalescence of a group of microvoids or under the action of the applied stress whose effect is magnified by the stress raising nature of the microvoids. Microcrack growth starts to occur and will

continue taking place for as long as the critical stress situation is maintained. In consequence, the microcracks grow for a length of time equal to the subjection time defined earlier. From the foregoing, the following can be stated:

- The higher the cutting speed the lower the subjection time, the smaller the size of the microcracks obtained in the machined surface, and the smaller the microcrack area ratio.

In the extreme case the subjection time may become too small to even allow the formation of microcracks resulting in a smaller number of microcracks. This also explains the trends obtained in figure 81 showing the microcrack density to decrease as the cutting speed is increased reaching a minimum value of 15 microcracks per $0.12mm^2$ (or 125 per mm^2) at a cutting speed of 400m/min.

9.2.3- Stress Effects:

A number of stress situations may arise during machining as discussed in section 2.7. Two of these are considered for the explanation of the trends obtained in figures 80 and 81. The first one is the stress ahead of the cutting edge acting at the onset of plastic deformation on elements of material as they approach the tool cutting edge. The second is the residual stress remaining in the machined surface after the tool cutting edge has left the machined surface. The subjection time of the first type of stress depends on the cutting speed as explained in the previous section. The subjection time of the residual stresses is not affected by the cutting speed in that they remain in the machined surface after the machining operation has been terminated.

The tensile stress in the immediate vicinity of the tool cutting edge has been reported [34] to decrease with increase in the cutting speed. This would suggest that less microcrack formation would take place in the material while traversing the primary shear zone resulting in less microcracks being obtained in the machined surface as the cutting speed is increased. This agrees with the results presented in figures 80 and 81. Hence the tensile stress near the tool cutting edge seems to be related to the microcrack formation in the machined surface and can be used to explain the trends obtained for the variation of the microcracking parameters with the cutting speed.

In addition the residual stress in the machined surface can reach values twice the yield stress of the annealed material [93]. The relaxation of residual stresses by the formation of microcracks [97] or growth of the microcracks formed in the subsurface layer as it traverses the primary shear zone has been discussed in section 3.8.2. Work by Liu and Barash [102] has shown that the residual stresses in the machined surface decrease as the cutting speed is increased from 92m/min to 278m/min. This trend is similar to that observed for the microcracking parameters as shown in figures 80 and 81. It is therefore suggested that the residual stress generated in the machined surface as influenced by the cutting speed, also can contribute to the formation of surface microcracks.

9.3- Effect Of Undeformed Chip Thickness On The Microcracking In
       The Machined Surface

The variation of the microcrack area ratio "Ma" and the microcrack density "Md" with change in the undeformed chip thickness

is shown in figures 82 and 83. The trends show a decrease in the microcrack area ratio "Ma" with an increase in the undeformed chip thickness. Similar trends are observed for the microcrack density "Md" at values of undeformed chip thickness above 0.138mm. The reversing of the trends at lower values of undeformed chip thickness will be discussed in terms of the microcrack coalescence phenomenon (cf. section 9.7). The variation of "Ma" with undeformed chip thickness consists of a sharp decrease up to a value of "UCT" of about 0.1mm followed by a steady decrease as the "UCT" is increased still further with a departure from this trend at an "UCT" value of about 0.2mm where a sharp jump in "Ma" is observed. The general trend is of the same character as the variation of the specific cutting energy with increase in the "UCT" shown in figure 97 which does not however, explain the sudden increase in the value of "Ma" at t=0.2mm. In a similar fashion to the discussion of the previous section, the trends are examined in the light of the effect of the undeformed chip thickness on the built-up-edge occurrence and the stresses present in the machined surface during and after machining. Trent [7], Ernst and Martellotti [8], and Williams and Rollason [10] have shown that starting with conditions of machining with no built-up-edge, a decrease in the undeformed chip thickness can result in built-up-edge occurrence. The undeformed chip thickness influences the formation of built-up-edge mainly as a result of changes in the amount of heat which is generated. The smaller the undeformed chip thickness, the higher the cutting speed for which the built-up-edge disappears. Using surface roughness as a means of estimating built-up-edge occurrence range, figure 92 is considered. It can be seen from this figure that the parallel surface roughness increases rapidly at values of undeformed chip thickness below 0.1mm and could be an indication of

the presence of a built-up-edge. In figure 82 the microcrack area ratio is observed to decrease sharply when the undeformed chip thickness is increased between 0.057 and 0.099mm. The high level of microcrack area ratio and microcrack density at low values of undeformed chip thickness, can therefore, be explained by built-up-edge occurrence during machining.

In section 2.7 it was shown that the tensile stress in the immediate vicinity of the tool cutting edge increases as the undeformed chip thickness is decreased. This can be offered as a possible explanation of the trends in the variation of "Ma" and "Md" as the undeformed chip thickness is increased above the built-up-edge formation range. In addition, the residual stresses can also be used to explain these trends. The tensile residual stress obtained in the machined surface has been shown by Liu and Barash [102] to decrease as the depth of cut is increased, when machining at a cutting speed of 92m/min. At a cutting speed of 278m/min. they found that this trend was reversed. Their cutting tests were carried out under orthogonal cutting conditions, so that their depth of cut is equivalent to the undeformed chip thickness considered here. Henriksen [101] for his part found that the residual stress increased as the undeformed chip thickness was increased. He observed this trend for plain carbon steels with different carbon contents. But the cutting speed at which he carried out his cutting tests (i.e. 4.8m/min.) was within the built-up-edge formation range and cannot be used to explain the results of the present investigation which is based on cutting tests at 200m/min. The results by Liu and Barash [102] do not give a clearcut indication as to how the residual stresses are affected by the undeformed chip thickness at a cutting speed of 200m/min. However, this cutting speed lies in the middle of the range between

the two cutting speeds used by Liu and Barash. Therefore, it can be assumed that the cutting speed used in the present investigation is near to the value for which a reverse in trends occurs and hence that at this cutting speed there is no significant effect of the undeformed chip thickness on the residual stresses. It should be noted that this only applies to the range of undeformed chip thickness considered by Liu and Barash (i.e. 0.127 to 0.254mm).

Based on the above discussion it is suggested that the variation in the microcracking parameters with increase in undeformed chip thickness above the built-up-edge formation range, can be explained in terms of the combined effect of the tensile stress acting during machining in the immediate vicinity of the tool cutting edge and the residual stress remaining in the machined surface after the tool cutting edge has left the workpiece.

9.4- Effect Of Rake Angle On The Microcracking In The Machined Surface

The variation of the microcracking parameters with the rake angle of the cutting tool, when machining at a cutting speed of 200m/min is shown in figures 84 and 85. The microcrack area ratio "Ma" is shown to increase as the rake angle is increased. The rate of this increase also is shown to increase with an increase in the rake angle. Considering the experimental points plotted in figure 85, it can be seen that the microcrack density "Md" is approximately constant up to a rake angle of about 15 degrees, a value above which a sharp increase is observed followed by a decrease at rake angles above 25 degrees.

The above observed trends are explained in terms of the stresses acting on the machined surface sublayer during and after a machining

operation. It is well known [35] that a narrow wedge promotes high tensile stresses in a material into which the wedge is indented (e.g. crack propagation proceeds more readily the smaller the angle of the crack and this results in the splitting action of an axe or chisel). As the rake angle is increased, the tool approaches a narrow wedge more closely so that the tensile stress also increases. This is supported by the discussion in section 2.7 of the work by Kececioglu [36] in which it was concluded that the tensile stress in the immediate vicinity of the tool cutting edge increases with increase in the rake angle.

Henriksen [101] has found that the tensile residual stresses in the machined surface after a machining operation decrease with an increase in the rake angle of the tool for a number of plain carbon steels having different carbon contents (0.1% to 0.7%). Their tests, however, were carried out at a cutting speed of 4.8m/min which is small compared to the cutting speed used in the present investigation. The author did not find any data relating the tensile residual stress to the rake angle of the tool for cutting condiions similar to those used in the present work.

The discussion can be based, alternatively, on the so-called mechanical model of residual stress generation proposed by Kaczmarek [11] (section 3.4.2). This model is based on the interaction between the tool cutting edge and the workpiece material. It predicts the appearance of compressive stress components in the subsurface layer as a result of mechanical plastic deformation.

As the rake angle is increased, the component of the cutting force normal to the cutting direction (usually referred to as the feed force) decreases as shown in figure 100. Similar results have been obtained by Connolly and Rubenstein [28] who also observed that the

largest decrease was for the range in rake angle between 10 and 20 degrees. A decrease in the feed force means that the material flowing past the flank of the tool is subjected to smaller normal stresses when machining with higher rake angles. It follows from this that if the rake angle is increased, the surface layer is subjected to a reduced mechanical plastic deformation. Consequently, according to the mechanical model of residual stress generation (cf. section 3.4.2), this will result in a decrease of the compressive residual stress component in the machined surface. By superimposition of this decreasing compressive stress component on the tensile stress resulting from the machining temperature according to the so-called thermal model (section 3.4.1) an overall increase in the resultant residual stress is obtained. This suggests that the tensile residual stress also contributes to the microcrack formation in the machined surface. From the above discussion, it seems that both the tensile stress in the vicinity of the tool cutting edge and the tensile residual stress are instrumental in the surface microcrack formation, in that their variation with the change in rake angle follows the same trends as that of the microcracking parameters "Ma" and "Md".

The decrease in the microcrack density, observed at rake angle values above 25 degrees (figure 85) can be explained by the microcrack coalescence phenomenon which will be discussed in section 9.7.

The variation of the microcracking parameters with a change in the rake angle, when machining at a cutting speed of 50m/min. is plotted in figures 86 and 87. As discussed in section 9.2, machining at this cutting speed took place in the presence of a built-up-edge. Under these circumstances, the nominal rake angle is irrelevant and the results can have some variability as discussed in section 9.6. This is shown by the trendless features of the results in figure 86.

The range of variation in the microcrack area ratio "Ma" is smaller than the variability range shown in figure 80 which was suggested to be due to built-up-edge formation. The results presented in figures 80 and 86 both seem to support the suggestion about the effect of the built-up-edge on the variability of the results.

Again the variability is less evident in the case of the microcrack density which, after an initial decrease, shows an increasing trend with increase in the nominal rake angle (figure 87). This trend should be compared with that in results by Ernst and Martellotti [8] who showed that the size of the built-up-edge decreases with increase in the rake angle.

9.5- Effect Of Workpiece Hardness On The Microcracking In The
      Machined Surface

The variation of the microcracking parameters with the material hardness is shown in figures 88 and 89. These figures show the microcracking parameters to decrease when the material hardness is increased up to a value of 320 VPN. With further increase in the material hardness, the microcracking parameters are seen to increase. A number of factors related to the microstructure which may have an influential effect on the trends observed are considered in the following, and possible explanations proposed.

The concept of microcrack formation as a result of the difference in the elastic/plastic properties of the two phases in the material has already been discussed in section 9.2.1 of this chapter. The heat treatments to which the medium carbon steel used in the present investigation has been subjected, affect the material in a number of ways;

a)- The ferrite (i.e. softer phase) content in the material decreases from the full-annealed to the quenched (fully martensitic) state.

b)- The grain size decreases between the full-annealed and the quenched state.

c)- The hardness increases from the full-annealed to the quenched state.

a) and b) being well known effects and their measurement outside the scope of the present investigation, only c) has been measured. Bearing in mind the difference in elastic/plastic properties of the phases in the material, less microcrack formation is expected to take place for the fully martensitic microstructure (one phase) material. This is congruent with the present experimental results which show a decrease in the microcracking parameters as the microstructure of the material is changed from a ferrite-pearlite structure (two-phase) to a fully martensitic (one-phase) structure (see figures 88 and 89).

The dependence of the microcrack growth on the grain size has been discussed in section 4.2.2. The smaller grain size reduces the microcracking by a process of grain boundary interference with the growth of the microcracks. A comparison between plates 43 and 44 shows that the grain size for the as-received (normalized) material is greater than the fully-annealed material whereas in figures 88 and 89 the amount of microcracking is greater for the fully-annealed structure. The banding of ferrite around the MnS inclusions is very much in evidence in the fully-annealed material and can explain the higher values in microcracking parameters.

An additional factor which may explain the decrease in microcracking parameters with an increase in workpiece hardness for the quenched and tempered specimen is associated with the effect of tempering on the microstructure. It has been known for some time

[144] that as-quenched martensite when reheated, is allowed to decompose producing ferrite and carbide. At the start of tempering, extremely thin plates of unidentified carbide appear, visible only by high resolution electron microscopy. As the tempering temperature is increased the carbide plates thicken, and in the case of plain carbon steel at a tempering temperature of around 100°C, can be identified as a hexagonal carbide with an approximate composition of $Fe_{2.4}C$. From this point, the hardness gradually decreases, but the steel becomes more ductile. Further increase in tempering temperature results in the transformation of any retained austenite and conversion of the carbide to Fe_3C. As the tempering temperature is increased, the carbide particles grow in size. The precipitation of these carbides result in grain boundary weakening and so this explains the increase in microcracking parameters as the tempering temperature is increased.

The slight increase in the microcrack area ratio and microcrack density at a hardness value of about 350 VPN (so-called quenched state) was thought to be unexplained and the test was repeated. Similar results were obtained which confirmed the experimental points plotted in figures 88 and 89. An attempt to conduct a cutting test at a higher workpiece hardness (520 VPN) to provide further evidence resulted in the disintegration of the cutting tool. In the process of seeking an explanation for the change in trends it was finally realized, while examining the microstructures of the material in the optical microscope, that the severity of the quenching was not high enough to give a fully-martensitic structure and that retained austenite was present. This can be seen from a comparison of the microstructures shown in plate 47 (quenched and tempered) with that shown in plate 48 (quenched). Bearing in mind that the quenched and tempered microstructures proceeded from a material which had been

subjected to a different quenching treatment, the above comparison shows that the latter took place in a more severe environment. The tempering, although softening the material to a hardness less than 350 VPN, resulted in a microstructure which was nearer to the fully martensitic structure than the so-called "quenched" material. This would suggest that the hardness is not the only influential factor affecting the microcracking in the machined surface without reckoning the effect of the microstructure.

Additional support to the above statement can be provided by considering the effect of tempering on hardness. The formation of carbide plates during tempering sets-up coherency strains resulting in an increase in hardness which more than offsets the softening due to the depletion of carbon in the martensite [144] and there is an overall increase in hardness. In other words, tempering at low temperatures results in an increase in hardness as well as a weakening of grain boundaries by carbide precipitation and so the material would be more prone to microcracking.

An interesting consequence of the results presented in figures 88 and 89, is that it is in contradiction to the suggestion that a possible correlation between material ductility and microcrack formation exists (see section 4.3.2). While this may be true for pure materials which are relatively more ductile than alloys, it cannot, however, be generalized to include multi-phase materials. The fact that pure materials do not form microcracks is probably due to the absence of microcrack nucleation sites (e.g. impurities, inclusions, hard particles, second phase ...etc.).

9.6- Role Of Built-Up-Edge In Microcrack Formation And In Variability
     Of The Results

9.6.1- Role Of Built-Up-Edge In Microcrack Formation:

The formation of a large built-up-edge during machining leads to
an increase of the length over which shearing of the surface layer
takes place as illustrated in figure 101a. An analogy can be drawn
between this situation and the situation where two surfaces slide
against each other. As shearing takes place, tensile stresses are
set-up in the machined surface behind the built-up-edge. These
tensile stresses can be large enough to bring about the formation of
microcracks in the machined surface as the latter leaves the
built-up-edge. The tensile stress analysis is illustrated in figure
101b. As the cutting speed (or undeformed chip thickness) is
increased, the built-up-edge decreases in size and so does the length
over which shearing takes place resulting in a decrease of the tensile
stress set-up in the nascent surface. This consequently, decreases
the likelihood of microcrack formation. This explains the high levels
of microcrack area ratio and density obtained at low values of cutting
speed or undeformed chip thickness and supports the suggestion
formulated in sections 9.2 and 9.3 about the influential part played
by the built-up-edge in microcrack formation.

The built-up-edge can also have an indirect influence on the
microcracking in the machined surface. Starting with the presumption
that the built-up-edge which occurs in machining replaces the tool
cutting edge in its cutting action, it is proposed that the
built-up-edge can affect the machining process by increasing the
effective rake angle. Considering the variation of the microcracking

parameters with increase in rake angle (figures 84 and 85), it can be seen that increasing the rake angle used in the tests carried out results in an increase in "Ma" and only a slight decrease in "Md" up to a rake angle of 15 degrees followed by an increase thereon for higher values of rake angle.

In conclusion to the above discussion it can be stated that the built-up-edge affects the microcrack formation in the machined surface by:

a)- creating tensile stresses in the machined surface as the latter ceases to contact the built-up-edge,

b)- increasing the effective rake angle of the cutting tool.

9.6.2- Role Of Built-Up-Edge In Variability Of The Results:

When discussing the variability in "Ma" at the low end of the cutting speed range (i.e. V < 100m/min.), it was suggested that this was caused by the presence of an unstable built-up-edge. In this section the above suggestion is examined and discussed further in the light of the results obtained for the effects of the rake angle on "Ma" and in terms of the effects of the built-up-edge on the replication of the machined surface.

From figure 80 (dotted curve) it can be seen that the variability range of the results is below the level of microcrack area ratio reached at onset of built-up-edge formation (i.e. as the cutting speed is decreased). A drop in the microcrack area ratio appears to have taken place as the cutting speed is decreased below the value for built-up-edge disappearance. A number of factors are believed to have caused the drop in microcrack area ratio and the variability in the results when machining with a built-up-edge.

It is thought that the drop in "Ma" is not real but is mainly due to the difficulty in measurement associated with the application of the microcrack measurement technique to rough surfaces. It is well established that the built-up-edge plays an important part in the roughness of machined surfaces. The higher surface roughness associated with built-up-edge affects the exactness with which the machined surface is replicated. This occurs because the replicas have to be stripped off rough machined surfaces and so there is always the possibility of the collapse of slender features taking place as discussed in section 6.6.3. Under these circumstances it is expected that "Ma" will be underestimated which is congruent with the direction of the variability shown in figure 80. The collapse phenomenon explains the drop in the level of microcrack area ratio and can account for more than 50% drop in the microcrack area measured for large microcracks.

The variability which accompanies the drop in microcrack area ratio can be accounted for by the unstable nature of the built-up-edge. This unstability of the built-up-edge causes the variabilty in the results both directly and indirectly. The direct effect is through the tensile stress set up in the machined surface due to shearing at the built-up-edge/surface interface and its variation with the size of the built-up-edge. The indirect effect is through the variation of the effective rake angle with the size of the built-up-edge and the influence of the latter on the surface replication process.

9.7- Microcrack Coalescence

The phenomenon of microcrack coalescence has been discussed in section 4.1.3. It occurs either in the presence of a high tensile stress or when the microcrack density reaches a critical value so that the distance between indivividual microcracks becomes so small that bridging of neighbouring microcracks is encouraged. In the present investigation the microcrack density represents the number of microcracks counted in a given standard area of the machined surface (section 6.5.2). A sudden reversal in the trends of increasing microcrack density at high values can be explained by the microcrack coalescence phenomenon provided that the microcrack area ratio does not experience the same reverse in the trends. This explanation is even more viable if the tensile stress causing the microcrack formation can be determined and reaches high values at the onset of trend reversal in the microcrack density. A model of microcrack coalescence based on the variation of both the microcracking parameters "Ma" and "Md" is illustrated in figure 102 which incorporates the condition for the onset of microcrack coalescence. It is suggested that a critical value of the microcrack density "Md,crit." will be reached before onset of microcrack coalescence. This critical value depends on the stress level present and the size of the microcracks. While the stress level is governed by the energy available, the size of the microcracks is represented by the microcrack area ratio "Ma". In other words, the higher the energy available and the higher the value of "Ma", the lower the critical value of the microcrack density will be.

Basing the argument on the above philosophy, figures 82, 83 and 84, 85 are redrawn in figures 103 and 104, respectively to enable a

comparison with the microcrack coalescence model presented in figure 102. It can be seen that, according to this model, figures 103 and 104 suggest that microcrack coalescence occured for values of undeformed chip thickness smaller than about 0.138mm (figure 103) and for rake angles greater than about 25 degrees (figure 104).

An interesting feature of figures 103 and 104 is the value of the microcrack density at the onset of presumed microcrack coalescence. Whereas this value is equal to about 92 in figure 103, it is about 128 in figure 104. The respective values of "Ma" are 0.345 and 0.51. These values suggest that "Md-crit" for larger microcracks is higher than for smaller microcracks contrary to what was anticipated above. Without considering the stress causing the microcrack formation, however, it is not appropriate to draw any conclusions from the values of "Ma" alone. There is unfortunately no data available yet on the tensile stress values in machining under various cutting conditions. Alternatively, assuming that the specific cutting energy "Esp." is somewhat an indication of the stress situation in machining, the product of "Ma" by "Esp" is considered instead. If this product is calculated for the critical conditions (i.e. onset of microcrack coalescence), and the ratio for the two situations is determined, it is found that this ratio is approximately equal to unity (more precisely 1.04). This finding suggests that there is a maximum value of the product "Ma.Esp" above which microcrack coalescence takes place resulting in an increase in "Ma" and a decrease in"Md".

It is also interesting to note that the ratio of average microcrack size for the two situations of microcrack coalescence is also close to unity (i.e. 1.06).

9.8- Comparison Between Microcracking In The Machined Surface And

Microcracking In The Shear Zone

A comparison between the microcracking which occurs during
machining in the shear zone and the microcracking obtained in the
machined surface, is inspired by the fact that prior to its formation,
the machined surface and its sublayer originate in the shear zone as
discussed in section 2.6. Review of the literature (section 4.3.1)
has shown that a limited amount of work has been carried out on the
microcracking in the shear zone and results have been obtained
relating the latter to the cutting speed, the undeformed chip
thickness, and the rake angle when machining two-phase materials.
Work which has been carried out by Luong and Brown [124,128,129] has
shown that the microcrack density in the shear zone increases with
increase in the cutting speed up to a certain value (25m/min) and then
decreases with further increase in the cutting speed up to a value of
137m/min. which was the maximum cutting speed they considered.
Comparing these results with those obtained in the present
investigation (figure 81) leads to the suggestion that the cutting
speed has similar effects both on the microcracking in the shear zone
and on the microcracks in the machined surface. Luong's tabulated
results [124] have been plotted in figure 105 which also includes the
results from the present investigation for the cutting speed range
considered by Luong. The curves plotted in figure 105 show similar
trends, i.e, a decrease in both machined surface and shear zone
microcracking with increase in cutting speed. Luong also claimed that
the microcracking in the shear zone increased with increase in
undeformed chip thickness but did not mention either the cutting speed
used or the range of undeformed chip thickness considered. Their

results, however, in combination with the results in the present investigation suggest that the undeformed chip thickness has opposite effects on the microcrack density in the shear zone and in the machined surface.

In addition, Luong and Brown found that alterations in the tool rake angle between 0 and 15 degrees appeared to have little effect on the microcrack density in the shear zone when machining a low carbon steel at a cutting speed of 137m/min. They also claimed that there was a slight increase in the microcrack density in the shear zone with a decrease in the rake angle at low cutting speed (25m/min.). Looking at figure 85, the microcrack density in the machined surface appears to be unaffected by the change in rake angle from 0 to 15 degrees when machining at a cutting speed of 200m/min. At low cutting speed of 50m/min., however, it can be seen from figure 87 that a change in rake angle from 0 to 15 degrees has a significant effect on the microcrack density in the machined surface. The trends observed in figure 87 are the reverse of those observed by Luong and Brown. This may be explained either by the built-up-edge having different effects on the deformation in the shear zone and the subsurface layer, or simply by the variability due to machining in the presence of a built-up-edge.

From the foregoing discussion, it can be proposed that, although the cutting speed seems to have similar effects on the microcrack density in the shear zone and in the machined surface, no definite relationship exists between the microcracking in the shear zone and the microcrack formation in the machined surface.

Regression analysis based on the least square method, has been performed on the results obtained in the present investigation to establish the degree of correlation which exists between the microcracking parameters and the machining variables as well as the material hardness. This was done using a computer statistical package (STATPK) available on the mainframe computer at the Sheffield City Polytechnic.

The data obtained for the variation of the microcracking parameters with increase in the cutting speed followed the exponential law equation in the form:

$$Ma = K_1.\exp(N_1.V)$$
$$Md = K_2.\exp(N_2.V) \qquad \Big\} \text{------(9.1)}$$

where "Ma" is the microcrack area ratio,

"Md" is the microcrack density,

"V" is the cutting speed,

K_1, K_2, N_1 and N_2 are arbitrary constants which depend on the material and the cutting conditions.

In order to ensure that the microcracking parameters will fit satisfactorily the above equation, graphs of Log(Ma)-V and Log(Md)-V were plotted when straight lines were obtained. N_1 and N_2 are the slopes of the regression lines. Log K_1 and Log K_2 are the intercepts.

To find N_1, N_2, K_1 and K_2 the "REGRESSION" and "TRANSFORMATION" analyses available in the computer statistical package were used. The "TRANSFORMATION" analysis was used to transform the data into a Log base. The "REGRESSION" analysis was then applied to the transformed data in the following way. Equations (9.1) can be re-written in the form:

$$\left.\begin{array}{l} \text{Log Ma} = \text{Log } K_1 + N_1 \cdot V \\[2mm] \text{Log Md} = \text{Log } K_2 + N_2 \cdot V \end{array}\right\}\text{------(9.2)}$$

The application of the regression analysis resulted in the following equations:

$$\left.\begin{array}{l} \text{Ma} = 1.76491 \, \exp(0.00863V) \\[2mm] \text{Md} = 136.5335 \, \exp(0.00498V) \end{array}\right\}\text{--------(9.3)}$$

In order to find the degree of correctness of the assumption that the data on the Log (Ma)-V and Log (Md)-V graphs represented straight lines, the correlation coefficient "r" was also determined. It was found to be equal to -0.940 for the data on "Ma" and -0.938 for the data on "Md". The values of intercepts K_1, K_2 and slopes N_1, N_2 were rounded up using the statistical techniques described in appendix 4. The curves fitted using the equations obtained by the regression anlysis have been drawn in figures 80 and 81. Adjacent to these curves the above equations together with the values of the correlation coefficients are also included.

The following is a summary of the results of the regression analysis applied to the experimental data. The values of slopes and intercepts have been rounded up using the statistical technique in appendix 4.

a)- Cutting Speed "V" :

$$\text{Ma} = 1.82 \, \exp(-0.009V) \qquad r = -0.940$$

$$\text{Md} = 140 \, \exp(-0.005V) \qquad r = -0.938$$

b)- Undeformed chip thickness "t" :

$$Ma = \frac{Log(t)}{42 - 4.8(Log\ t)} \qquad r = 0.962$$

$$Md = \frac{Log(t)}{-0.017 + 0.0054Log(t)} \qquad r = -0.835$$

c)- Rake angle "α" :

$$Ma = 0.152exp(0.06\alpha) \qquad r = 0.961$$

$$Md = 55exp(0.024\alpha) \qquad r = 0.793$$

d)- Material hardness "H" :

$$Ma = 484.07H^{-1} - 1.4 \qquad r = 0.932$$

$$Md = 29,479H^{-1} - 61 \qquad r = 0.943$$

It can be seen from the above results that for the majority of cases there is good correlation (i.e. $|r| > 0.9$) between the microcracking parameters and the variables investigated. The above expressions along with the correlation coefficients are shown in figures 80 to 89 which also include the curves represented by these expressions.

The ranges in the machining variables for which very good correlation could be achieved were those for which machining was carried out without built-up-edge formation and for which there was no reverse in trends associated with the microcrack coalescence phenomenon discussed in section 9.7 of this chapter. For these ranges of the variables considered, regression analysis was performed on the data (original or transformed) and the results are summarized in the

following subsections. Analysis of variance and T-test were also performed by the regression analysis and results for T and F values are also included. The T and F values give an indication of whether two sets of data are significantly different at the significance level considered. The T value is the ratio of the mean difference of the two sets of data over the standard error of the mean. The F value is the ratio of two independant estimates of the variance of a single normal universe of experimental data.

The correlation coefficient could be improved for regression equation of Ma versus V if the range in cutting speed is considered for which there is no built-up-edge formation (in our case, when V is in the range 100m/min to 400m/min).

The resulting equation is:

$$Ma = 232,624V^{-2.55} \qquad r = -0.988$$

$$T = -12.687 \qquad F = 160.959$$

Also, it can be seen that the correlation factors for Md versus t and Md versus α are comparatively small. This is due to the microcrack coalescence and therefore an improvement can be obtained by considering the range in t and α for which there is no microcrack coalescence (i.e. 0.138mm<t<0.396mm and -5deg.<α<25deg.).

The resulting regression equations are:

$$Md = 18.75.t^{-0.81} \qquad r = -0.998$$

$$T = -25.628 \qquad F = 656.773$$

and

$$Md = 0.005.\alpha^{3} \qquad r = 0.945$$

$$T = 4.988 \qquad F = 24.881$$

Using the above results figures 80, 83 and 85 can be redrawn as shown in figures 106 to 108 to illustrate fitted curves for conditions of no built-up-edge occurrence and no microcrack coalescence.

9.10- Recommended Machining Code Of Practice For Component Strength

Examination of the machined surface using transmission electron microscopy in the course of the present research programme has shown that the microcracks present in the machined surface assume a random orientation throughout the range of cutting conditions used. They are, therefore, believed to affect the fatigue properties of machined components subjected to a tensile stress situation regardless of the orientaion of the applied stresses.

Component strength as discussed in section 3.8, has been related to the surface integrity of the component. More specifically, the surface roughness has been claimed to affect the stress corrosion [108] and the fatigue strength [66] of machined components. Results by Ovseenko et al [95] have shown that the bending fatigue strength could be improved by a decrease in the surface roughness. Bearing in mind that in the above studies the microcracking of the machined surface had not been considered by the above quoted workers, it is suggested that the influence of the surface roughness on the fatigue properties of machined components could have been overemphasized. This suggestion is in line with the conclusion arrived at by El-Helieby and Rowe [64] whose studies led them to confirm that the effect of surface roughness had been overemphasized in its general relationship with fatigue properties of materials, which they suggested could be dominated by residual stress patterns.

The above suggestion is examined in the light of the results obtained in the present investigation. Figure 90 shows the surface roughness to decrease as the cutting speed is increased. A similar variation trend is observed for the surface roughness measured in a direction normal to the cutting direction (fig.91). These trends are of the same character as those observed for the variation of the microcracking parameters with increase in cutting speed (see figures 80 and 81). It is suggested that when microcracking and surface roughness go hand-in-hand, the reduced fatigue strength is primarily due to the microcracking and not to the surface roughness as generally believed. A discriminating experiment should be carried out.

On the other hand, if the variation of surface roughness with change in undeformed chip thickness and rake angle were considered, it is found that there is no significant trend as shown in figures 92 to 95. Comparing these results with those for the variation of the microcracking parameters shown in figures 82 to 85, it can be seen that conditions giving no significant change in surface roughness also give a wide variation in the microcracking parameters. This would suggest that there is no consistent connection between surface topography as measured by stylus instruments and the fatigue properties of materials.

A parallel situation has been considered by El-Helieby and Rowe [64] who carried out tests on ground surfaces. They measured the fatigue strength as well as the surface roughness of specimens prepared under both gentle and abusive grinding conditions. They found that the fatigue strength of the material varied when the surface roughness either remained constant or changed in reverse to the trend in fatigue strength variation. This finding led El-Helieby

and Rowe to conclude that the surface roughness had been overemphasized in its relation to fatigue properties of materials.

From the above observations, it can be concluded that there would appear to be some connection between surface roughness and fatigue properties when the cutting speed is considered as the controlled variable affecting the surface roughness. The same is not true when considering the undeformed chip thickness and the rake angle since these variables do not affect significantly the surface roughness while playing an influential part in the variation of the microcracking parameters. It is therefore concluded that, in the light of the present study, the emphasis put on the surface roughness connection with the fatigue strength of components should be re-evaluated taking into account the microcracks which may be present in the surface. This would help in suppressing the wide disagreement amongst those who carried out work relating fatigue properties to the surface roughness. To reconcile both views, it is proposed that the cutting conditions should be stated whenever data on the fatigue strength variation with the surface roughness is stated. It is also proposed that surface roughness is not the only, if at all, influential factor as far as the material strength is concerned and that other factors should also be considered. El-Helieby and Rowe [64] have proposed the residual stress to be another influential factor. While accepting this proposal, it is further suggested that the microcracks present in the machined surface may play a major role in this respect. This is because while the residual stress acts as an additional stress to the applied stress, the microcracks present in the machined surface act as stress raisers and their effect is to magnify the applied stress many times over. The possibility of

relaxation of the residual stresses as a result of microcrack formation in the surface (cf. section 3.4) should be born in mind.

It follows from the foregoing discussion that component strength requirements can be achieved by a close control of the machining process so that only those cutting conditions which give low values of the microcracking parameters are used. From the results obtained in the present investigation it is possible to propose a code of good machining practice for component strength. This code of practice is the one which results in a low value of the microcracking parameters and can be summarized as follows :

1)- As high a cutting speed as practically possible:

When machining with an undeformed chip thickness of 0.244mm and 5 degree positive rake angle, an increase in the cutting speed from 100m/min. to 400m/min. resulted in a reduction of 96% of the microcrack area ratio "Ma" and 83% of the microcrack density "Md".

2)- The undeformed chip thickness should be as high as possible:

When machining at a cutting speed of 200m/min. with a cutting tool rake angle of 5 degree positive, "Ma" can be reduced by 90% when the undeformed chip thickness is increased from 0.057mm to 0.396mm and "Md" can be reduced by 57.6% for an increase in the undeformed chip thickness from 0.138mm to 0.396mm.

3)- Use cutting tools with low rake angles (less than 15 degrees for the cutting conditions of the present investigation):

At a cutting speed of 200m/min. and an undeformed chip thickness of 0.244mm, "Ma" can be reduced by 87.7% when the rake angle is decreased from 30 degrees to 5 degree negative and "Md" can be reduced by 57.4% when the rake angle is decreased from 25degree to 15 degree positive. The biggest improvement in "Ma" and "Md" is obtained by decreasing the rake angle down to a value of 15 degree positive.

In conclusion it can be seen from the above that a good machining practice in terms of microcrack formation in the machined surface is the one carried out at high cutting speeds, high undeformed chip thickness, and low rake angles. It should be borne in mind that this proposed code of good machining practice has been established in terms of the extent of surface microcracking and that it is in no way the optimum machining practice. The latter can only be established provided that all the surface integrity requirements are accounted for. It is also interesting to note that in general, the above recommendations tend to produce low residual stresses in the machined surface, low surface roughness values and high metal removal rates.

CONCLUSIONS AND RECOMMENDATIONS FOR FUTURE WORK

10.1- Conclusions

10.2- Recommendations For Future Work

1. A transmission electron microscope technique has been developed and used to examine the extent of surface microcrack formation following a machining process.

2. Two microcracking parameters have been defined and used to provide quantitative information about the extent of surface microcracking. The parameters are the microcrack area ratio, "Ma" expressed as a percentage and the microcrack density, "Md" expressed as a number of microcracks per given area.

3. A systematic study has been carried out to determine the way in which surface microcracking is affected by:

     (i)- cutting speed;

    (ii)- undeformed chip thickness;

   (iii)- tool rake angle;

    (iv)- workpiece material hardness.

4. Both "Ma" and "Md" were found to decrease in magnitude as the cutting speed was increased from 100m/min to 400m/min, approaching constant value at high speed. At cutting speeds below 100m/min, measurements of both "Ma" and "Md" showed considerable variability which was attributed to the occurrence of built-up-edge.

5. Both "Ma" and "Md" were found to decrease in magnitude as the undeformed chip thickness was increased from 0.057mm to 0.396mm, approaching a constant value at the higher values of undeformed chip thickness.

6. When machining was carried out at a cutting speed of 200m/min, "Ma" was found to increase as the tool rake angle was increased from -5 to +30 degrees. The microcrack density "Md" was found to increase as the rake angle was changed from +15 to +25 degrees. Increasing the rake angle from -5 to +15 degrees was not found to produce any significant change in "Md". A change in rake angle between +25 and +30 degrees was found to produce a decrease in "Md".

7. Both "Ma" and "Md" were found to decrease in magnitude as the workpiece material hardness was increased from 180 VPN (fully-annealed condition) to 350 VPN (oil-quenched condition).

8. The changes in "Ma" and "Md" produced by cutting speed, undeformed chip thickness and tool rake angle have been discussed and explained in terms of:
   (i)- built-up-edge occurrence;
   (ii)- machining temperatures;
   (iii)- the subjection time (i.e. the time taken to traverse the shear zone);
   (iv)- the tensile stress in the vicinity of the cutting edge;
   (v)- the residual stress produced in the machined surface.

9. The changes in "Ma" and "Md" produced by the workpiece hardness have been discussed and explained in terms of:
   (i)- the microstructure change from two-phase (ferrite-pearlite) towards single-phase (fully-martensitic),
   (ii)- the grain size and banding of ferrite,
   (iii)- the weakening of the grain boundary by carbide precipitation.

10. The variability in the results which was observed at low cutting speeds (i.e. below 100m/min) has been discussed and explained in terms of built-up-edge formation. The influence of the built-up-edge was associated with the following factors:

- its effect on the tensile stresses set-up in the machined surface by sliding action;

- its replacing the tool in its cutting action, i.e. by altering both the effective rake angle and increasing the bluntness of the tool;

- its unstable nature, i.e. tensile stresses set-up in the machined surface, effective rake angle and bluntness of the tool continuously change during its cyclic build-up and fracture;

- its effects on the replication of the machined surface (i.e. it worsened the difficulties experienced in surface replication).

11. The change in trends of "Md" at values of undeformed chip thickness below 0.138 mm (figure 83) and rake angle above 25 degrees (figure 85) was discussed and explained in terms of the coalescence of microcracks. A model of the microcrack coalescence phenomenon based on "Ma" and "Md" being plotted on the same graph has therefore been suggested. According to this model, microcrack coalescence occurs when "Md" suddenly changes from an increasing trend to a decreasing trend while the "Ma" keeps its increasing trend (see figure 102).

12. The existence of a critical value of "Md" corresponding to the onset of microcrack coalescence has been posited which depended on a critical value of the product of the specific energy and "Ma". The values of this product for the two instances where microcrack

coalescence was suspected were calculated and their ratio was found to be close to unity with a value of 1.04. It was further noted that the ratio of average microcrack size for the two situations of microcrack coalescence was also close to unity (i.e 1.06).

13. Comparison between the present work and work by Luong [124] has shown that the cutting speed has similar effects both on the microcracking in the shear zone and in the machined surface. No connection was however found when undeformed chip thickness and rake angle were considered. It was concluded that there was no consistent relationship between microcrack formation in the shear zone and in the machined surface.

14. It has been proposed that, besides residual stresses, microcracks present in the machined surface play the most influential part in the fatigue strength of materials.

15. The surface roughness Ra has been found to be unaffected by changes in undeformed chip thickness and in rake angle. It was thus confirmed that the effect surface roughness had on the fatigue properties of materials had been overemphasized and should be re-evaluated.

16. A machining code of practice has been proposed. The object of this code is to control the extent of surface microcracking as a result of machining, and thus to enhance component surface integrity.

17. The correlation between microcracking and machining variables has been examined using statistical methods. Regression analysis has provided the following relationships:

a)- Cutting speed "V":

(i)- $M_a = 1.8 \exp(-0.009\ V)$ $r = -0.940$

(ii)- $M_d = 140 \exp(-0.005\ V)$ $r = -0.938$

b)- Undeformed chip thickness "t":

(iii)- $M_a = \dfrac{\text{Log}(t)}{42 - 4.8(\text{Log}\,t)}$ $r = 0.962$

(iv)- $M_d = \dfrac{\text{Log}(t)}{-0.017 + 0.0054\text{Log}(t)}$ $r = -0.835$

c)- Rake angle "α":

(v)- $M_a = 0.152 \exp(0.06\,\alpha)$ $r = 0.961$

(vi)- $M_d = 55 \exp(0.024\,\alpha)$ $r = 0.793$

d)- Workpiece hardness "H":

(vii)- $M_a = 484.07\ H^{-1} - 1.4$ $r = 0.932$

(viii)- $M_d = 29{,}479\ H^{-1} - 61$ $r = 0.943$

Correlation factors for regression equations (i), (iv) and (vi) can be improved if conditions of no built-up-edge formation and no microcrack coalescence are considered.

1. The present work has been limited to orthogonal machining in turning and to machining medium carbon steel. A possible area for future work is to extend the present investigation to include a wider range of materials machined with a secondary cutting edge and by other conventional and non-conventional machining processes.

2. The cutting tests were carried out using "sharp" tools. It would be interesting to investigate the effect of using tools with large cutting edge radii or flank wear lands. A particular ly important aspect of this proposed future work is to compare this situation with that for which machining is carried out in the presence of a built-up-edge. This will throw some light into the suggestion made in the present thesis as to the effect of the built-up-edge in causing the high levels of microcracking parameters observed.

3. Bearing in mind that the technique for the measurement of microcracking in machined surfaces is new, a number of improvements may be considered. Suggestions are put forward here which are the result of a long experience with the technique.

    a)- The length of time spent and the strenuous efforts required when measuring the microcrack area, call for the design of an instrument which will enable these measurements to be carried out quickly and automatically. Moreover, the need for a large number of micrographs was found to be costly. One major improvement which will enhance the credibility of the technique as an effectively cheap, simple and easily reached

tool for measurement of microcracks is to suppress the need for micrographs. There are two ways in which this could be achieved: (i)- by using a fluorescent screen in the TEM, with a grid pattern inscribed in it which will enable the measurement of the microcrack area; or (ii)- by introducing a grid into the path of the electrons transmitted through the specimen. In this way electrons hitting the grid will be removed from the electron beam whereby only electrons passing through the inside of the grid squares will impinge on the fluorescent screen. The final image on the screen will consist of a grid similar to the one introduced into the path of the beam and the image corresponding to the specimen.

b)- A further improvement is to incorporate a microprocessor to enable the calculation of the microcracking parameters. This will reduce the time and efforts involved in the calculation and enable a greater area of the machined surface to be used for the calculation which will in turn improve the statistical power of the measurements.

4. Another direction which can be followed in future work and which will be of benefit for design engimeers will be to investigate the effects of the microcracking on the effective operational behaviour of machined components. Now that a technique for the measurement of microcracks has been successfully developed, the effect of microcracking parameters can be tested against the various functional properties of interest. Some areas which offer great scope for research are the effect on fatigue strength, corrosion resistance, electro-plating and coatings. It is thought by the author that this will throw some light into the

controversial question of how disadvantageous or "advantageous" microcracks are for the satisfactory working operation of machined components.

5. A repeat of the present experiments under a more tightly controlled set of conditions and a greater number of points will be beneficial and will give more evidence to the observations and the conclusions drawn from the results in the present investigation. It should be noted that the nature of the present work was exploratory and further work is needed as suggested above to derive final observations on the surface microcrack formation phenomenon.

6. The material hardness which has been taken as representing the material properties is thought to give no description of the elastic/plastic properties of the various phases of the material and of the microstructure. Therefore, more representative parameters like grain size, relative plasticity index and second phase content would be more appropriate.

7. A further area which might give some important results is to use the SEM to count the microcracks per unit length on polished cross-sections perpendicular to the machined surface and compare the present results with the linear distribution of microcracks determined from the microcrack density "Md" (i.e $\sqrt{Md}$ assuming regular distibution of microcracks).

8. It would also be of interest to re-assess or confirm some of the suggestions put forward in this thesis as to the role of the stresses, temperature and microstructure on the microcracking in the machined surface. This can be done by carrying out tests in

which the above are measured and correlated to the microcracking parameters obtained.

9. An alternative and direct way of correlating the microcracking in the shear zone and the microcracks in the machined surface would be to apply the microcrack measurement technique to the shear zone of polished chip roots.

10. Finally, the possibility of classification of the microcracks as suggested in the present investigation can be considered in more detail and used to correlate the microcracks and their extent to material microstructure (e.g second phase, inclusions, grain size...etc.).

1. ALBRECHT, P.
   "New Developments In The Theory Of The Metal Cutting Process:
   I- The Ploughing Process In Metal Cutting", Trans. A.S.M.E.,
   Vol.82(B), Nov.1960, pp.348-358.

2. KRONENBERG, M.
   "Machining Science And Applications -Theory And Practice For
   Operation And Development Of Machining Processes", Pergamon Press
   (1966).

3. MERCHANT, M.E.
   "Mechanics Of The Cutting Process", J. Appl. Phys., Vol.16
   (1945), pp.267-318.

4. ERNST, H.
   "Physics Of Metal Cutting", Trans. A.S.Metals, 'Symposium On
   Machining Of Metals', 1958, pp.1-34.

5. IWATA, K. and UEDA, K.
   "The Significance Of Dynamic Crack Behaviour In Chip Formation",
   Annals Of The CIRP, Vol.25/1 1976, pp.65-70.

6. GILLIBRAND, D.
   "Surface Formation During Machining", Ph.D. Thesis, University Of
   Nottingham, May 1975.

7. TRENT, E.M.
   "Metal Cutting", Butterworths (1977).

8. ERNST, H. & MARTELLOTTI, M.
   "Metal Cutting - TheFormation And Function Of The Built-Up-Edge",
   Mech. Eng., Aug. 1935, pp.487-498.

9. SCHWERD, F.
   "Neue Untersuchungen Zur Schnittheorie Und Bearbeit Barkeit",
   Stahl Und Eisen, April 1931, Vol.16, pp.481-491.

10. WILLIAMS, J.E. and ROLLASON, E.R.
    "Metallurgical And Practical Machining Parameters Affecting
    Built-Up-Edge Formation In Metal Cutting", J. of the Institute of
    Metals, Vol.98, 1970, pp.144-153.

11. KACZMAREK, J.
    "Principles Of Machining By Cutting, Abrasion, And Erosion", Pub.
    Peter Peregrinus Ltd., Stevenage, 1976.

12. TAY, A.O. STEVENSON, DE VAHL, DAVIS, and OXLEY, P.L.B.
    "A Numerical Method For Calculating Temperature Distributions In
    Machining From Force And Shear Angle Measurements", Int. J. Mach.
    Tool Des. Res., Vol. 16, Pergamon Press 1976, pp.335-349.

13. BOOTHROYD, G.
    "Temperatures In Orthogonal Metal Cutting", Proc. Inst. Mech.
    Engrs. Vol.177 1963, pp. 789-810.

14. BARROW, G.
"A Review Of Experimental And Theoretical Techniques For Assessing Cutting Temperatures", Annals Of The CIRP, Vol.22/2 1973, pp.203-211.

15. MURARKA, P.D. BARROW, G. and HINDUJA, S.
"Influence Of The Process Variables On The Temperature Distribution In Orthogonal Machining Using The Finite Element Method", Int. J. Mech. Engng. Sci., Vol.21, Pergamon Press 1979, pp.445-456.

16. OXLEY, P.L.B.
"Mechanics Of Metal Cutting", Int. Res. in Prod. Engng., Proc. Int. Production Engng. Res. Conf., Pittsburgh, Am. Soc. Mech. Engrs. 1963, p.50.

17. ZOREV, N.N.
"Results Of Work In The Field Of The Mechanics Of The Metal Cutting Process", Proc. Instn. Mech. Engrs. Conf. On Technology Of Engng. Manufacture, London 1958, p.255.

18. HITOME, K.
"Fundamental Machinability Research In Japan", Trans. Am. Soc. Mech. Engrs. (Series B) Vol.83, 1961, pp.531-544.

19. PALMER, W.B. and OXLEY, P.L.B.
"Mechanics Of Orthogonal Machining", Proc. Instn. Mech. Engrs. London 1959, Vol.173, pp.623-654.

20. ENAHORO, H.E. and OXLEY,P.L.B.
"Flow Along Tool-Chip Interface In Orthogonal Metal Cutting", J. Mech. Engng. Sci., Vol.8(No.1) 1966, pp.36-41.

21. PALMER, W.B. and YEO, R.C.K.
"Metal Flow Near The Tool Point During Orthogonal Cutting With A Blunt Tool", Proc. 4th Int. mach. Tool Des. Res. Conf. 1964, Pergamon Press, Oxford.

22. FORM, G.W. and BEGLINGER, H.
"Fundamental Considerations In Mechanical Chip Formation", Annals of the CIRP, Vol.XVII 1970, pp.153-167.

23. ROTH, R.N. and OXLEY, P.L.B.
"Slip-Line Field Analysis For Orthogonal Machining Based Upon Experimental Flow Fields", J. Mech. Engng. Sci., Vol.14 No.2, 1972, pp.85-97.

24. ZOREV, N.N.
"Interelation Between Shear Processes Occurring Along Tool Face And On Shear Plane In Metal Cutting", Int. Res. Prod. Engng., Int. Production Engng. Research Conf., Pittsburgh 1963. Also ASME 1964, p.42.

25. COKER, E.G. and FILTON, L.N.G.
"A Treatise On Photo-Elasticity", Cambridge University Press, 1931.

26. OXLEY, P.L.B. HUMPHREYS, A.G. and LARIZADEH, A.
    "The Influence Of Rate Of Strain Hardening In Machining", Proc.
    Instn. Mech. Engrs., Vol.175 No.18, 1961, pp.881-891.

27. ROTH, R.N.
    "The Effect Of Positive And Negative Strain Hardening Rates On
    Stress Distributions In Orthogonal Machining", Int. J. Mach. Tool
    Des. Res.,Vol.17, Pergamon Press 1977, pp.39-46.

28. CONNOLLY, R. and RUBENSTEIN, C.
    "The Mechanics Of Continuous Chip Formation In Orthogonal
    Cutting", Int. J. Mach. Tool Des. Res., Vol.8, Pergamon Press
    1968, pp.159-187.

29. KITA, Y. IDO, M. and KAWASAKI, N.
    "A Study Of Metal Flow Ahead Of Tool Face With Large Negative
    Rake Angle", J. Engng. Ind., August 1982, Vol.104, pp.319-325.

30. ENAHORO, H.E. and OXLEY, P.L.B.
    "An Investigation Of The Transition From Continuous To
    Discontinuous Chip In Orthogonal Machining", Int. J. Mech. Sci.,
    Vol.3 1961, p.145-156.

31. RAMALINGAM, S. and LEHN, L.L.
    "A Photo-Elastic Study Of Stress Distribution During Orthogonal
    Cutting. Part 1: Workpiece Stress Distribution", J. Engng. Ind.,
    Trans. ASME (B), Vol.93, 1971, pp.527-537.

32. BATINS, K. and BROWN, R.H.
    "An Investigation Of The Deformation In Orthogonal Cutting", Int.
    J. Mach. Tool Des. Res., Vol.5 1965, pp.155-165.

33. BAILEY, J.A. and SINGER, A.R.E.
    "Effect Of Strain Rate And Temperature On The Resistance To
    Deformation Of Aluminium, Two Aluminium Alloys And Lead", J.
    Inst. Metals, Vol.92, 1963-64, pp.404-408.

34. CHAKRABORTI, S.K.
    "A Study Of The Effects Of Manganese Sulfide Inclusions On
    Plastic Deformation And Fracture In A Metal Cutting Process With
    Particular Reference To Machinability", Ph.D. Thesis 1974,
    University Of Salford, Dept. of Mechanical Engng.

35. RUBENSTEIN, C.
    "The Influence Of Strain-Rate In Orthogonal Cutting", Int. J.
    Mach. Tool Des. Res., Vol.12 1972, pp.105-120.

36. KECECIOGLU, D.
    "Shear-Strain Rate In Metal Cutting And Its Effects On Shear Flow
    Stress", Trans. ASME, Vol.80 (Part 1) 1958, pp.158-168.

37. TARASOV, L.P. and LUNDBERG, C.O.
    "Nature And Detection Of Grinding Burn In Steel", ASM Trans.,
    Vol.41 1949, pp.893-939.

38. TARASOV, L.P. HYLER, W.S. and LETNER, H.R.
   "Effect Of Grinding Conditions And Resultant Residual Stresses On The Fatigue Strength Of Hardened Steel", Proc. Am. Soc. Test. Mat., Vol.57 (1957), pp.601-622.

39. PHILIPS, J.L.
   "Effect Of Machining On High-Strength Low-Alloy Steels", Machinability Conference (1965), Iron and Steel Institute, London, pp.93-101.

40. FIELD, M. KAHLES, J.F. and KOSTER, W.P.
   "The Surface Effects Produced In Non-Conventional Metal Removal -Comparison With Conventional Machining Techniques", ASM Metals Engineering Quarterly, Vol.6 No.3, August 1966, pp.32-45.

41. FIELD,M. KOSTER, W.P. and KAHLES, J.F.
   "Effect Of Machining Practice On The Surface Integrity Of Modern Alloys", Procs. Int. Conf. on Manufacturing Technol. ASTM, Sept. 1967, pp.1319-1336.

42. BELLOWS, G.
   "Surface Integrity Of Electro-Chemical Machining", ASME Paper No.70-GT-111, May 1970.

43. KOSTER, W.P. FRITZ, L.J. and KOHLS, J.B.
   "Surface Integrity In Machining Of 4340 Steel And Ti-6Al-4V", SME Technical Report No.IQ71-237, April 1971.

44. PREVEY, P.S. and FIELD, M.
   "Variation In Surface Stress Due To The Metal Removal", Annals of the CIRP, Vol.24/1 1975, pp.497-501.

45. BAILEY, J.A. JEELANI, S. and BECKER, S.E.
   "Surface Integrity In Machining AISI 4340 Steel", J. Eng. Ind., Vol.98 (Series B) No.2 (1976), pp.999-1007.

46. BAILEY, J.A.
   "Surface Damage During Machining Of Annealed 18% Nickel Maraging Steel: Pt.I- Unlubricated Conditions; Pt.II- Lubricated Conditions", Wear, Vol.42 (1977), pp.277-303.

47. SNOEYS, R. MARIS, M. and PETERS, J.
   "Thermally Induced Damage In Grinding", Annals of the CIRP, Vol.27/2 (1978), pp.571-581.

48. TONSHOFF, H.K. and BRINKSMEIR, E.
   "Determination Of The Mechanical And Thermal Influences On Machined Surfaces By Microhardness And Residual Stress Analysis", Annals of the CIRP, Vol.29/2 (1980), pp.519-530.

49. JEELANI, S. and RAMAKRISHNAN, K.
   "Subsurface Plastic Deformation In Machining Annealed 18% Ni Maraging Steel", Wear, Vol.81 (1982), p.263.

50. JEELANI, S. and RAMAKRISHNAN, K.
   "Subsurface Plastic Deformation In Machining 6Al-2Sn-4Zr-2Mo Titanium Alloy", Wear, Vol.85 (1983), pp.121-130.

51. HANKINS, G. BECKER, M.L. and MILLS,
    "Further Experiments In The Effect Of Surface Conditions On The
    Fatigue Resistance Of Steels", J. Iron and Steel Inst., Vol.28
    No.1 (1936), p.399.

52. FLUCK, P.G.
    "The Influence Of Surface Roughness On The Fatigue Life Scatter
    Of Test Results Of Steel", Proc. A.S.T.M., Vol.51 (1951),
    pp.584-592.

53. POLAKOWSKI, N.H.
    "Effect Of Residual Stress On The Yielding And Strain-Ageing Of
    Carbon Steel", J. Iron and Steel Inst., 1952, pp.369-376.

54. VITOVEC, F.H. and BINDER, H.F.
    "Effect Of Specimen Preparation On Fatigue", WADC Technical
    Report 56-289, August 1956.

55. TARASOV, L.P. HYLER, W.S. and LETNER, H.P.
    "Effects Of Grinding Direction And Abrasive Tumbling On The
    Endurance Limit Of Hardened Steel", A.S.T.M. Preprint 71 (1958).

56. REED, E.C. and VIENS, J.A.
    "The Influence Of Surface Residual Stress On Fatigue Limit Of
    Titanium", Trans. A.S.M.E., J. Eng. Ind., Feb.1960, pp.76-78.

57. MORROW, J.D. and MILLAN, J.F. (Editors).
    "Influence Of Residual Stress On The Fatigue Of Steel", SAE
    Handbook Supplement J 783 (1961).

58. LESCOP, P. and LEYDIER, G.
    "Influence Of Grinding Wheel Grades And Of Coolants On The
    Endurance Limit Of Titanium Alloy TA-4M(Ti-8Al-4Mn)", SNECMA
    (Paris) Report No.3443 (1964).

59. GURKLIS, J.A.
    "Metal Removal By Electro-Chemical Methods And Its Effects On
    Mechanical Properties Of Metals", DMIC Report 213, Jan.7 (1965).

60. GLAESER, W.A.
    "Surface Effects In Metal Deformation", SME Technical Paper
    No.MF69-101 (1969).

61. MATALIN, A.A.
    "Effect Of Machining Methods On The Service Properties Of
    Components", Russian Engineering Journal, Vol.XLVIII, No.11,
    pp.62-66.

62. FIELD, M.
    "Surface Integrity - A New Requirement For Improving Reliability
    Of Aerospace Hardware", 18th. SAMPE National Symposium, April
    1973.

63. DEVRIES, M.F. FIELD, M. and KAHLES, J.F.
    "Relationship Of Surface Roughness And Surface Integrity To
    Functional Properties", Annals of the CIRP, Vol.25/2 1976,
    pp.569-573.

64. EL-HELIEBY, S.O.A. and ROWE, G.W.
   "Influences Of Surface Roughness And Residual Stress On Fatigue
   Life Of Ground Steel Components", Metals Technology, June 1980,
   pp.221-225.

65. EL-HELIEBY, S.O.A. and ROWE, G.W.
   "A Quantitative Comparison Between Residual Stresses And Fatigue
   Properties Of Surface Ground Bearing Steel", Wear, Vol.58 (1980),
   pp.155-172.

66. FIELD, M. and KAHLES, J.F.
   "The Surface Integrity Of Machined And Ground High Strength
   Steels", DMIC Report 210, October 1964,pp.54-77.

67. FIELD, M. and KAHLES, J.
   "Review Of Surface Integrity Of Machined Components", Annals of
   the CIRP, Vol.20/2 1971, pp.153-163.

68. LESKOVAR, P. and PEKLENIK, J.
   "Influences Affecting Surface Integrity In The Cutting Process",
   Annals Of The CIRP, Vol.31/1 1982, pp.447-450.

69. BRITISH STANDARDS.
   "Method For The Assessment Of Surface Texture", British standard
   BS 1134: Part 1 (1972).

70. VORBURGER, T.V., TEAGUE, E.C., SCRIRE, F.E. and ROSBERRY, F.W.
   Wear, Vol.57 (1979), p.39.

71. RADHAKRISHNAN, V.
   "Effect Of Stylus Radius On The Surface Roughness Values Measured
   With Tracing Stylus Instruments", Wear, Vol.16 (1970),
   pp.325-335.

72. QUINEY, R.G., AUSTIN, F.R. and SARGENT, L.B., Jr.
   "Measurement Of Surface Roughness And Profiles On Metals", Trans.
   A.S.L.E., Vol.10 No.2, 1967, p.193.

73. TUCKER R.C, Jr. and MEYERHOFF, R.W.
   "An SEM Study Of Surface Roughness Measurement", Proc. 2nd Annual
   Scanning Electron Microscope Symposium, Chicago,1969.

74. GUERRERO, J.L. and BLACK, J.T.
   "Stylus Tracer Resolution And Surface Damage As Determined By
   Scanning Electron Microscopy", Trans. A.S.M.E. J. Engng. Ind.,
   November 1972, pp.1087-1093.

75. JANSSON, D.G. ROURKE,J.M. and BELL, A.C.
   "High Speed Surface Roughness Measurements", Trans. A.S.M.E, J.
   Engng. Ind.,Vol.106, February 1984, pp.34-39.

76. SHIRAISHI, M.
   "In-Process Measurement Of Surface Roughness In Turning By Laser
   Beams", J. Engng. Ind., Vol.103, May 1981, pp.203-209.

77. SATA, T.
   "Surface Finish In Metal Cutting", Annals of the CIRP, Vol.12/4
   1963, p.190.

78. OLSEN, K.V.
   "Surface Roughness As A Function Of Cutting Data When Fine Turning Steel", Europaischer Maschinen, Markt No.4 1964, p.43.

79. TAKEYAMA, H. and ONO, H.J.
   "Study On Roughness Of Turned Surface", Bull. Jap. Soc. Prec. Eng., Vol.4 1966, p.274.

80. BOOTHROYD, G.
   "Fundamentals Of Metal Machining And Machine Tools", Mac-Graw Hill Book Company, 1975.

81. CHANDIRAMANI, K. and COOK, N.H.
   "Investigations On The Nature Of Surface Finish And Its Variation With Cuuting Speed", Trans. A.S.M.E., J. Engng. Ind., Vol.86 No.2 (Series B), May 1964, pp.134-144.

82. FIELD, M.
   "Plastically Deformed Debris And Built-up-Edge Produced On Surfaces By Chip Removal And Abrasive Machining Processes", Annals of the CIRP, Vol.23/1 1974 pp.191-192.

83. TURLEY, D.M. and DOYLE, E.D.
   "The Importance Of Surface Characterization In Surface Treatment Processes", Wear, Vol.81 (1982), pp.145-158.

84. WILLIAMS, J.E. SMART, E.F. and MILNER,
   "The Metallurgy Of Machining", Metallurgia, Vols.1;2;3 1970, pp.3, 51, 89.

85. KABALDIN, Y.U.G.
   "Temperature And Adhesion In Continuous And Interrupted Machining", Machines and Tooling, Vol.51 No.4, 1980, pp.27-29.

86. SHAW, M.C. USUI, E. and SMITH, P.A.
   "Free-Machining Steel: III- Cutting Forces, Surface Finish And Chip Formation", Trans. A.S.M.E., Vol.83 (Series B) 1961, pp.181-193.

87. ROZENBERG, A.M. and ROZENBERG, O.A.
   "Surface Finish In The Broaching Of Non-Ferrous Metals", Russian Engng. J., No.6 1965, p.66.

88. LAMBERT, H.T.
   "Relation Between Grinding Methods (Including Electrolytic Grinding) and Tool Performance", Annals of the CIRP, Vol.12/1 1963, p.45.

89. ERNST, H. and MERCHANT, M.E.
   "Chip Formation, Friction And Finish", Trans. Amer. Soc. Metals, 1941 Machining Of Metals, p.368.

90. BAILEY, J.A. and JEELANI, S.
   "State Of Subsurface Region In Machining Solution Treated And Aged 18% Nickel Maraging Steel", Wear, Vol.72 (1981), pp.237-243.

91. JEELANI, S. and RAMAKRISHNAN, K.
    "Subsurface Plastic Deformation In Machining Annealed Red Brass",
    Wear, Vol.82 (1982), pp.67-

92. LAU, W.S. and RUBENSTEIN, C.
    "The Influence Of Flank Wear, Cutting Speed, and Cutting Fluid On
    The Surface And Sub-Surface Work-hardening Produced In An
    Orthogonal Planing Operation", Int. J. Mach. Tool Des. Res.,
    Vol.12 (1972), Pergamon Press, pp.311-323.

93. LIU, C.R. and BARASH, M.M.
    "The Mechanical State Of The Sublayer Of A Surface Generated By
    Chip Removal Process: Part 1- Cutting With A Sharp Tool",
    A.S.M.E. J. Engng. Ind., Vol. No.4, Nov.1976, pp.1192-1201.

94. SATA, T.
    Int. Research In Prod. Engng., A.S.M.E., New-York (1963), p.18.

95. OVSEENKO et al
    "The Effect Of Machining Methods On The Fatigue Strength Of
    Rolling Mill Rolls", Russian Engng. J., Vol.60 No.9, pp.47-48.

96. ANSELL, C.T. and TAYLOR, J.
    "The Surface Finishing Properties Of A Carbide And Ceramic
    Cutting Tool", Advances in Mach. Tool Des. Res., 1962, Oxford
    Pergamon Press Ltd, pp.225-243.

97. BRINKSMEIER, E., CAMMETT, J.T., KONIG, W., LESKOVAR, P., PETERS,
    J. and TONSHOFF, H.K.
    "Residual Stresses- Measurement And Causes In Machining
    Processes", Annals of the CIRP, Vol.31/2 (1982), pp.491-510.

98. FIELD, M. KAHLES, J.F. and CAMMETT,J.T.
    "A Review Of Measuring Methods For Surface Integrity Annals of
    the CIRP, Vol.21/2 (1972),pp.219-238.

99. LIU, C.R. and BARASH, M.M.
    "The Mechanical State Of The Sublayer Of A Surface Generated By
    Chip Removal Process: Part2- Cutting With A Tool With Flank
    Wear", A.S.M.E. J. Engng. Ind., Vol. No.4, Nov.1976,
    pp.1202-1208.

100. SYREN, B.
    "Der Einfluß Spanender Berbeitung Auf Das Biegewechselverk-
    formungsverhalten Von Dr.-Ing. Diss. Univ. Karlsruhe, 1975
    (Quoted in ref.93).

101. HENRIKSEN, E.K.
    "Residual Stresses In Machined Surfaces", Trans. A.S.M.E.,
    Vol.73, Jan.1951, pp.69-76.

102. LIU, C.R. and BARASH, M.M.
    "Variables Governing Patterns Of Mechanical Residual stress In A
    Machined Surface", Trans. A.S.M.E., J. Engng. Ind., Vol.104,
    Aug.1982, pp.257-264.

103. Von TURKOVICH, B.F. and FIELD, M.
     "Survey Of Material Behaviour In Machining", Annals of the CIRP,
     Vol.30/2 (1981), pp.533-540.

104. BAILEY, J.A. and JEELANI, S.
     "Surface Integrity In Machining 18% Nickel Maraging Steel",
     S.M.E. Paper IQ 74-185 (1974).

105. TURLEY, D.M.
     "Deformed Layers Produced By Machining 70/30 Brass", J. Int.
     Metals, Vol.96 Pt.3 1968, pp.82-86.

106. TRENT, E.M.
     "Conditions Of Seizure At The Tool-Work Interface", Iron and
     Steel Inst. Special Report 94 'Machinability' 1967, pp.11-18.

107. MOORE, D.F.
     "A History Of Research On Surface Texture Effects", Wear, Vol.13
     (1969), pp.381-412.

108. HOWARD, R.T.
     "The Marine Corrosion Handbook", Mc Graw-Hill Company Of Canada
     Ltd (1960), pp.236-250.

109. FIELD, M. and KOSTER,W.
     "Optimizing Grinding Parameters To Combine High Productivity With
     High Surface Integrity", Annals of the CIRP, Vol.27/1 (1978),
     pp.523-526.

110. KOSTER, W.
     "Surface Integrity Of Machined Materials", Metcut Research
     Associates Inc., Cincinnati, Ohio, Report AFML-TR-74-60, April
     1974.

111. KAHLES,J.F. and FIELD, M.
     "Surface Integrity- A New Requirement For Surfaces Generated By
     Material-Removal Methods", Proc. Instn. Mech. Engrs. (Properties
     and Metrology Of Surfaces), Vol.182 Pt.3K, Nov.1967-68, pp.31-45.

112. LETNER, H.R.
     "Stress Effects Of Abrasive Tumbling", Trans. A.S.M.E., Vol.51
     (1958), pp.402-420.

113. DE LOS RIOS, E.R. TANG, Z. and MILLER, K.J.
     "Short Crack Fatigue Behaviour In A Mediun Carbon steel", Fatigue
     Engng. Mater. Struct., Vol.7, No.2, 1984, pp.97-108.

114. ASHBY, M.F.
     Philos. Mag., Vol.4 1966, p.1156.

115. BAKER, T.J. GOVE, K.B. and CHARLES, J.A.
     "Inclusion Deformation And Toughness Anisotropy In Hot-Rolled
     Steels", Metals Technology, April 1976, pp.183-193.

116. BURGARD, H.C., Jr.
     Physics and Non-Destructive Testing, New York 1967, pp.55-82.

117. Mc CLINTOCK, F.A. and ARGON, A.S.
"Mechanical Behaviour Of Materials", Addison-Wesley Publishing
Company Inc. 1966.

118. Mc CLINTOCK, F.A. and O'DAY, W.R. Jr.
Proc. 1st. Int. Conf. Fracture, Sendai 1 1965, pp.75-98.

119. Mc CLINTOCK, F.A.
"Local Criteria For Ductile Fracture", Int. J. of Fracture
Mechanics, Vol.4 No.2, June 1968, pp.101-130.

120. KELLY, A. and DAVIES, G.J.
"The Principles Of The Fibre Reinforcement Of Metals",
Metallurgical Reviews, Vol.10 1965, pp.1-78.

121. BURNS, K.W. and PICKERING, F.B.
"Deformation And Fracture Of Ferrite-Pearlite Structures", J.
Iron and Steel Institute, November 1964, pp.899-906.

122. LUONG, L.H.S. and BROWN, R.H.
"The Role Of Microcracks In Large Plastic Deformations", J.
Engng. Ind., Vol.103, Nov.1981,pp.431-436.

123. WALKER, T.J. and SHAW, M.C.
"On The Deformation At Large Strains", Adv. Mach. Tool Des. Res.
Conf. 1969, pp.241-252.

124. LUONG, H.S.
"Discontinuities And Their Effects On Work Materials In Chip
Formation", Proc. Australian Conf. on Manufacturing Engng., Inst.
of Engrs. (Australia), Adeleide 1977, pp.122-126.

125. BRIDGMAN, P.W.
"Studies In Large Plastic Flow And Fracture", Mac Graw-Hill Book
Company, 1952.

126. IWATA, K.
"The Effect On Machinability Of Infinitesimal Amounts Of Elements
In Steel", Proc. Int. Conf. on Production Technology, Instn. of
Engrs. (Australia), Melbourne 1974, p.183.

127. IWATA, K. UEDA, K. and SHIBASAKA, T.
"Analysis Of Cutting Mechanics By Direct SEM Observation (1st.
Report: Dynamic Behaviour Of Manganese Sulfide Inclusions During
Machining)", J.S.P.E. No.111 1973, p.21.

128. BROWN, R.H. and LUONG, H.S.
"Some New Observations Of The Deformation Zone In Orthogonal
Cutting Of Mild Steel", Annals of the CIRP, Vol.23/1 1974,
pp.7-8.

129. BROWN, R.H. and LUONG, H.S.
"Observations Of Deformation In The Orthogonal Machining Of A
Mild Steel", Metals Technology, Vol.2, Jan.1975, pp.2-7.

130. DOYLE, E.D.
"Mechanisms Of Plastic Instability In The Machining Of Metals",
Proc. Int. Conf. on Prod. Technology, Inst. of Engrs.
(Australia), Melbourne 1974, pp.161-166.

131. IWATA, K. and UEDA, K.
"Dynamic Behaviour Of Manganese Sulphide Inclusions In Machining
Under Scanning Electron Microscope Observation", Proc. Int. Conf.
on Production Engng., Japan Soc. of Precision Engrs., Tokyo 1971,
p.516.

132. HAZRA, J. RAMALINGAM, S. and CAFFARELLI, D.
"A Study Of Chip Formation In Free Machining Steels Carried Out
Within A Scanning Electron Microscope", Proc. Int. Conf. on Prod.
Engng., Japan Soc. Precision Engrs., Tokyo 1974, pp.509-515.

133. KOMANDURI, R. and BROWN, R.H.
"The Formation Of Microcracks In Machining A Low Carbon Steel",
Metals and Materials, Vol.6, December 1972, pp.531-533.

134. BROWN, R.H. and LUONG, H.S.
"The Influence Of Microstructure Discontinuities On Chip
Formation", Annals of the CIRP, Vol.25/1 1976, pp.49-52.

135. LUONG, L.H.S.
"Influence Of Microcracks On Machinability Of Metals", Proc.
Australian Conf. On Manufacturing Engng., Inst. of Engrs.
(Australia), Adelaide 1977, pp.122-126.

136. TEMPLE BLACK, J.T. and RAMALINGAM, S.
"Fine Structure Of Machined Surfaces", Int. J. Mach. Tool Des.
Res., Vol.10 No.4, Pergamon Press 1970, pp.439-463.

137. GILLIBRAND, D.
"A Visual Examination Of Surface Roughness", The Production
Engineer, May 1980, pp.31-34.

138. GILLIBRAND, D.
"The Inherent Roughness Of A Machined Surface", S.M.E. (Society
of Manufacturing Engrs.) Technical Paper No. MF80-905.

139. KAY, D.H.
"Techniques Of Electron Microscopy", Blackwell Scientific
Publications, Oxford 1965.

140. GLAUERT, M.
"Practical Methods In Electron Microscopy", Vol.1 (1979) and
Vol.8 (1980), Elsevier North Holland Publishing Company.

141. OXLEY, P.L.B.
"A Mechanics Of Machining Approach To Assessing Machinability",
Proc. 22nd Int. MTDR Conf. Manchester England, Sept. 16th-18th
1981, pp.279-287.

142. GOVE, K.B. and CHARLES, J.A.
"Further Aspects Of Inclusion Deformation", Metals Technology,
September 1974, pp.425-437.

143. GOVE, K.B. and CHARLES, J.A.
"The High-Temperature Hardness Of Various Phases In Steel",
Metals Technology, June 1974, pp.279-283.

144. WILSON, R.
"Metallurgy And Heat Treatment Of Tool Steels", Mac-Graw Hill
Book Company, (1975).
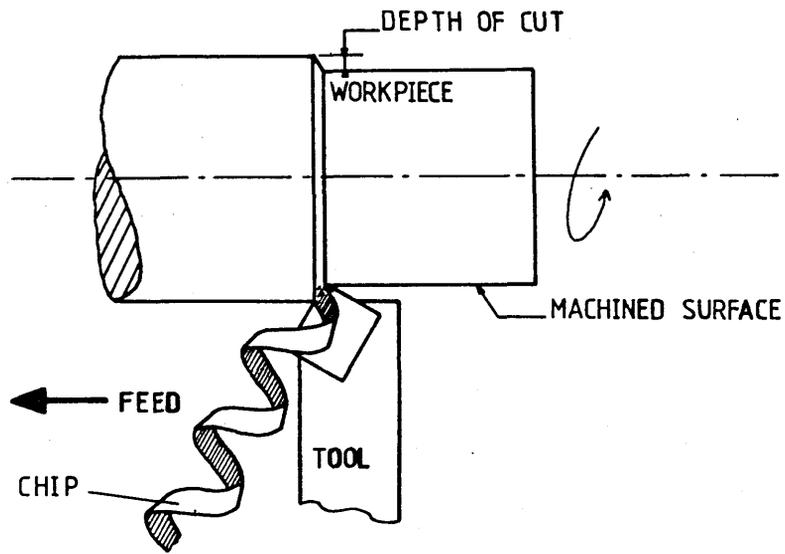
FIG. 1   MACHINING PROCESS (TURNING)
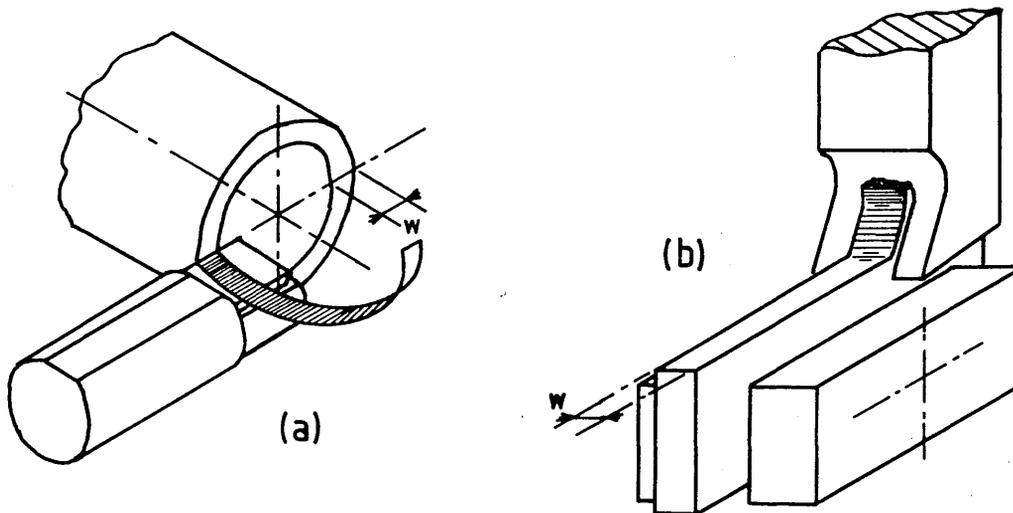
FIG. 2   ORTHOGONAL MACHINING IN
a) Turning   b) Planing
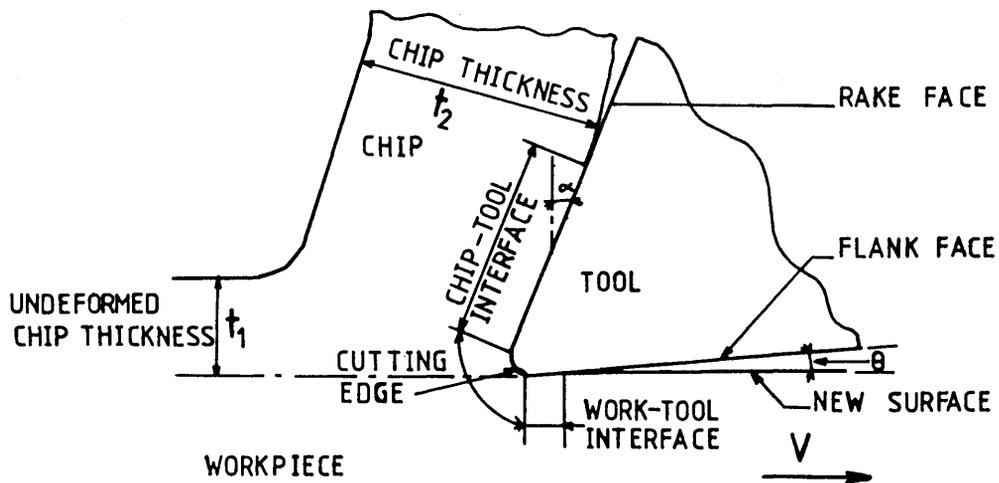
FIG. 3   SCHEMATIC REPRESENTATION OF
ORTHOGONAL MACHINING
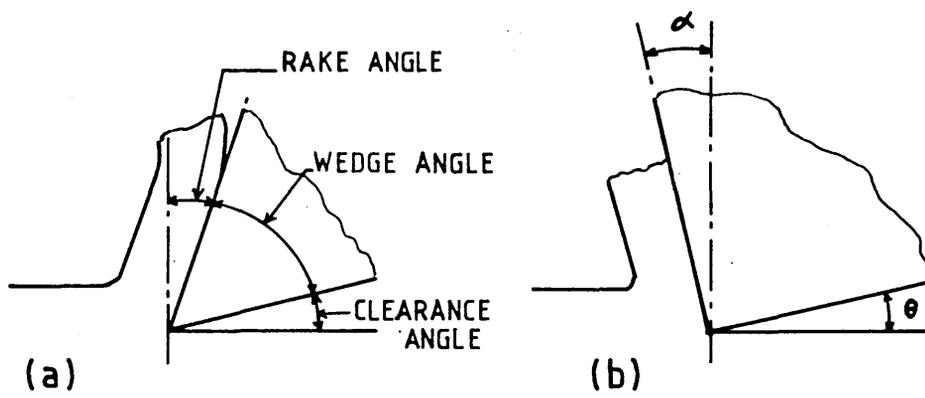
FIG. 4   CUTTING TOOL ANGLES
a) Positive rake   b) Negative rake
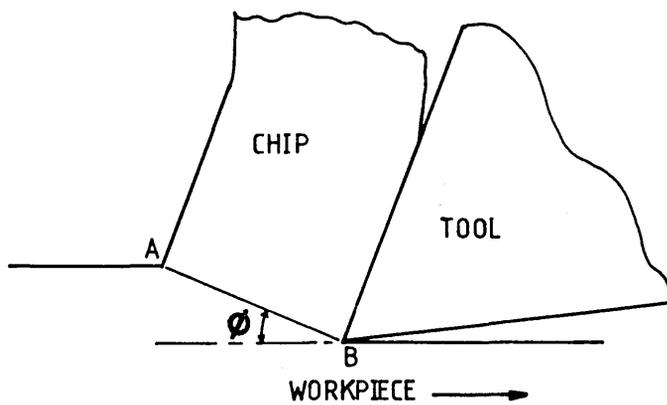
FIG. 5   SHEAR PLANE MODEL OF MACHINING
(Ref. 3)
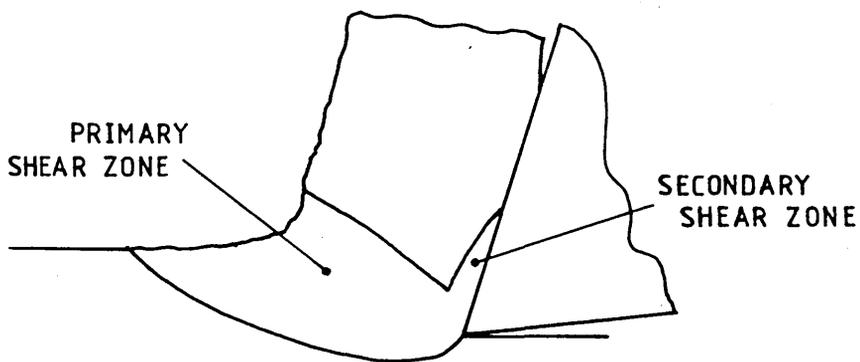
FIG. 6   SHEAR ZONE MODEL OF MACHINING

FIG.7: TYPES OF CHIP FORMATION
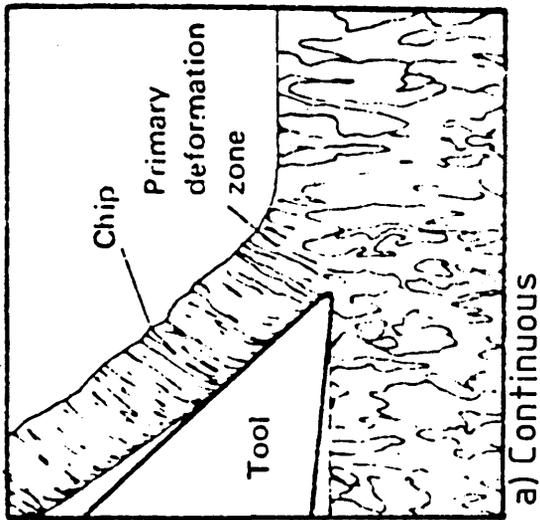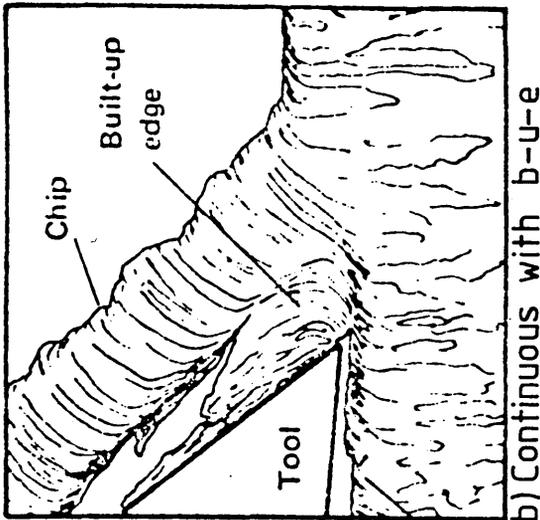
a) Continuous

b) Continuous with b-u-e

c) Discontinuous

-205-
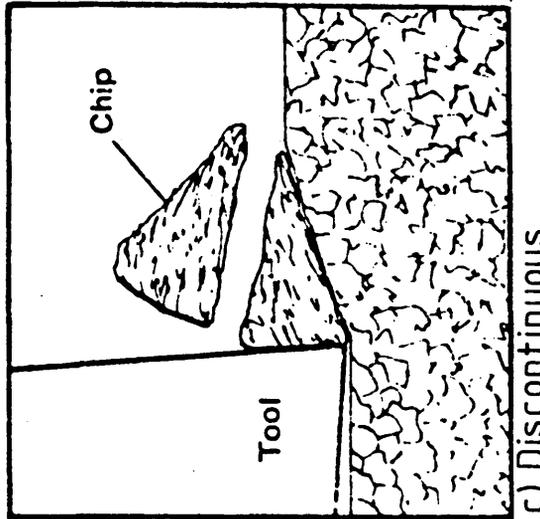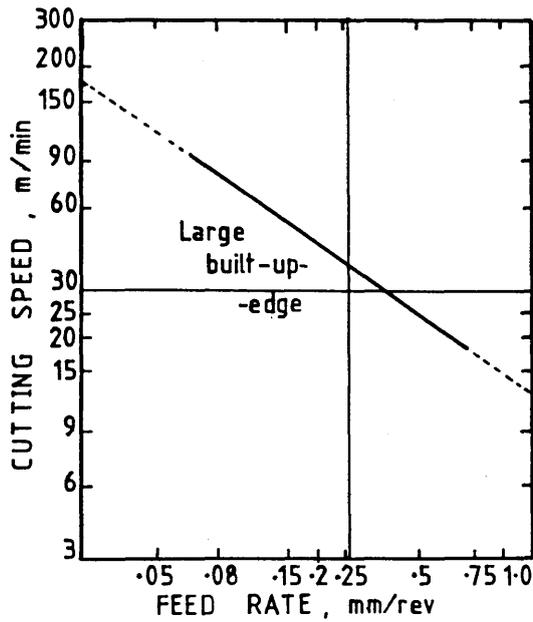
FIG. 8   **BUILT-UP-EDGE OCCURRENCE FOR 0.4% C STEEL** (Ref. 7)
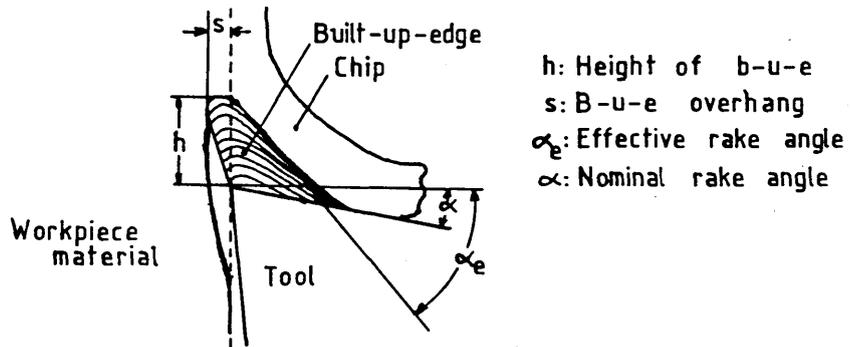
FIG. 9   **GEOMETRICAL CHARACTERISTICS OF THE BUILT-UP-EDGE** (Ref. 11)

h: Height of b-u-e
s: B-u-e overhang
α_e: Effective rake angle
α: Nominal rake angle
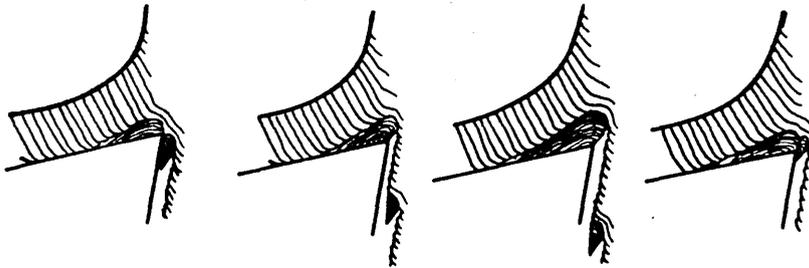
FIG. 10   **BUILT-UP-EDGE GROWTH AND FRACTURE CYCLE** (Ref. 9)
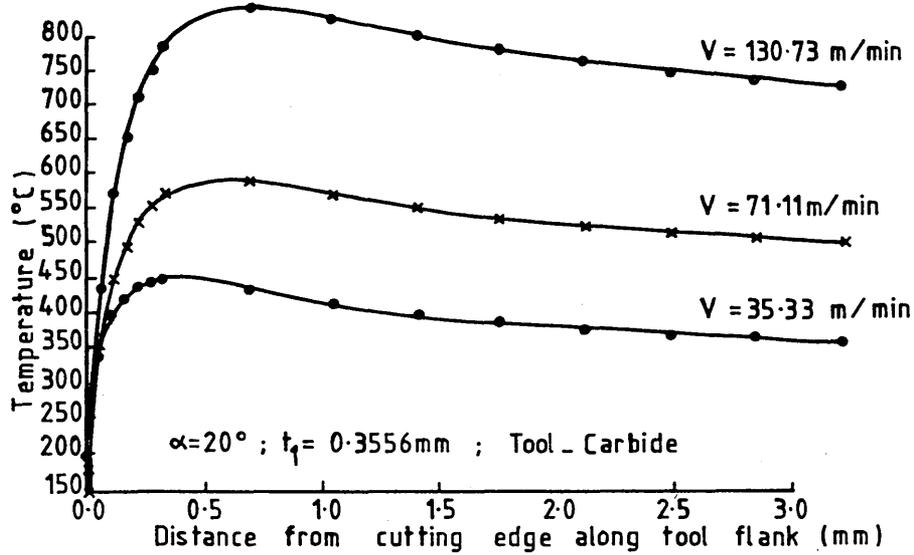
FIG.11   EFFECT OF CUTTING SPEED ON FLANK
FACE TEMPERATURES   (Ref. 15)
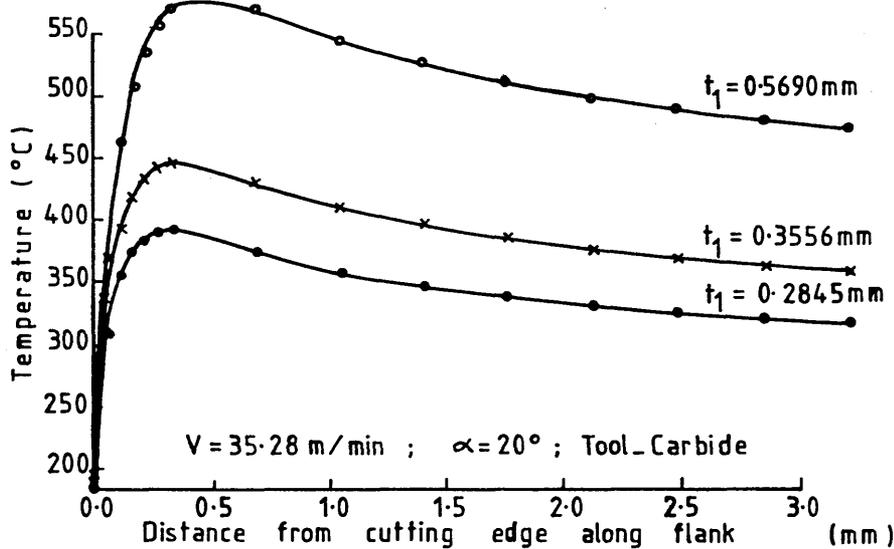
FIG.12   EFFECT OF FEED ON FLANK FACE
TEMPERATURES   (Ref. 15)
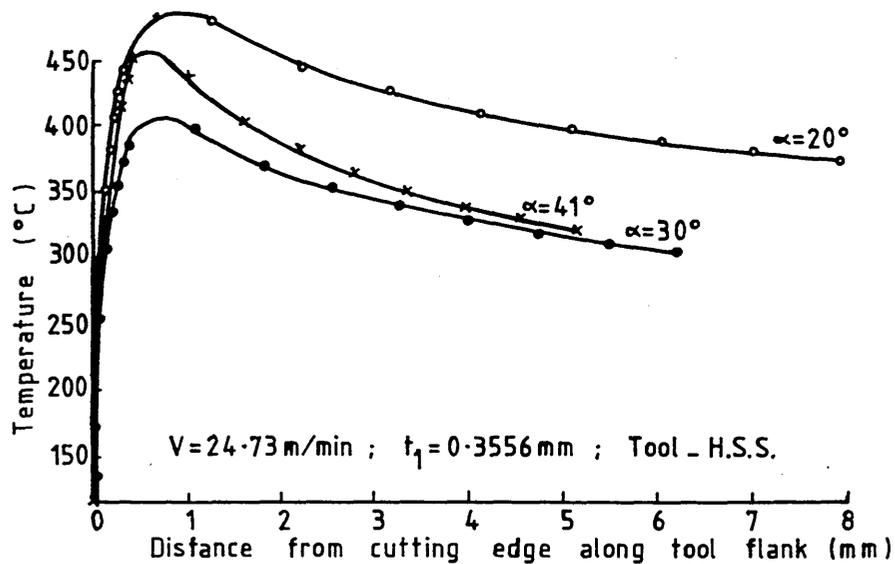
FIG. 13   EFFECT OF RAKE ANGLE ON FLANK
FACE TEMPERATURES   (Ref. 15)
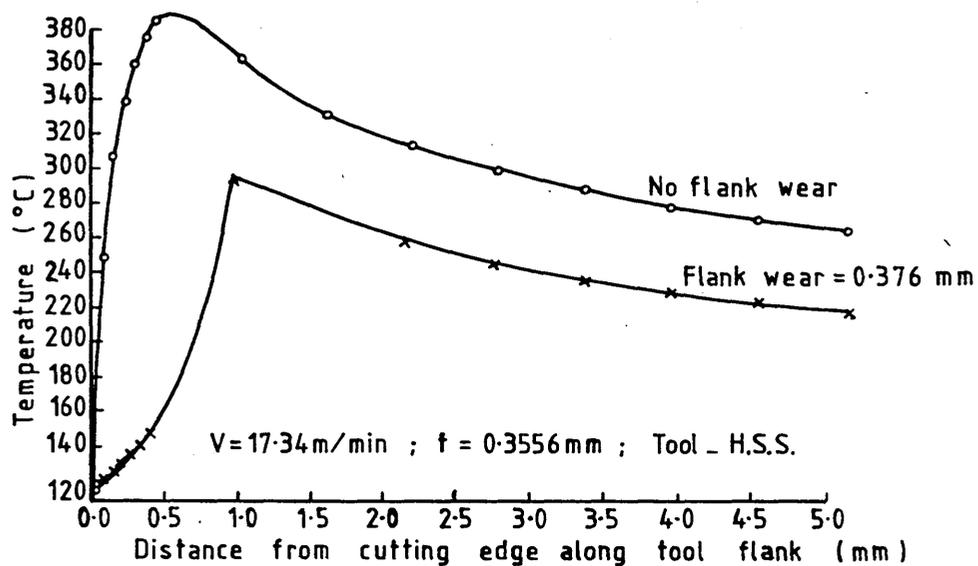
FIG. 14   EFFECT OF TOOL FLANK WEAR ON
FLANK FACE TEMPERATURES (Ref. 15)
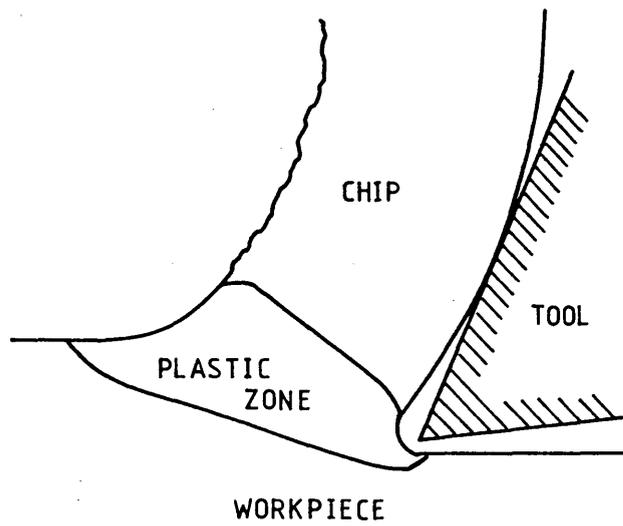
FIG. 15   MACHINING MODEL PROPOSED BY
          PALMER AND OXLEY   (Ref. 19)
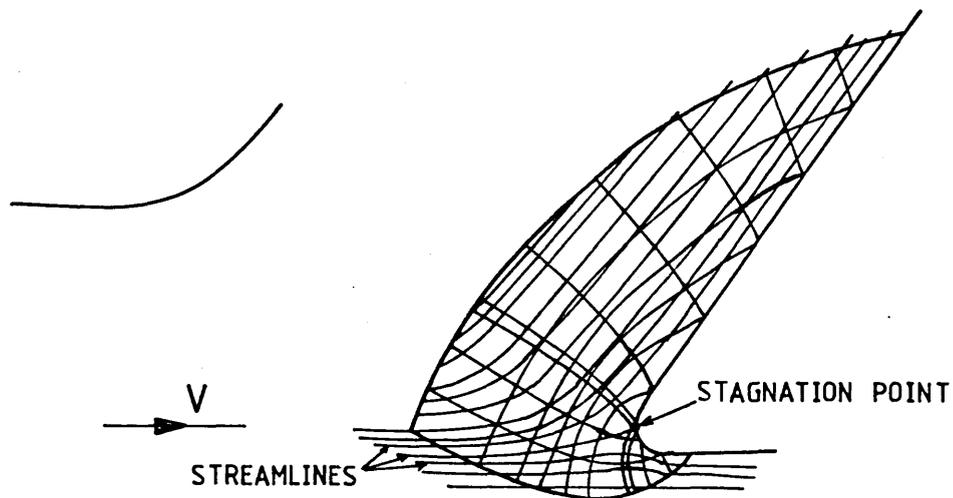
FIG. 16   SLIP-LINE FIELD FOR FLOW ALONG
          CHIP/TOOL INTERFACE AND AROUND
          CUTTING EDGE   (Ref. 20)

STREAMLINES
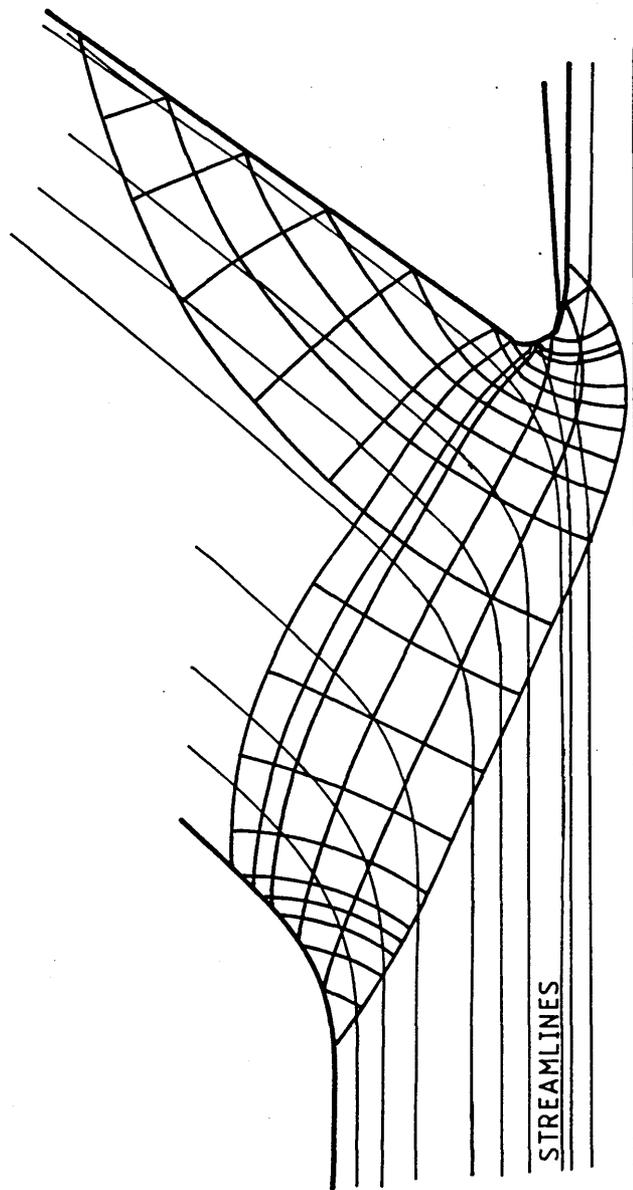
FIG.17 SLIP-LINE FIELD ANALYSIS OF SHEAR ZONES IN MACHINING (Ref. 23)
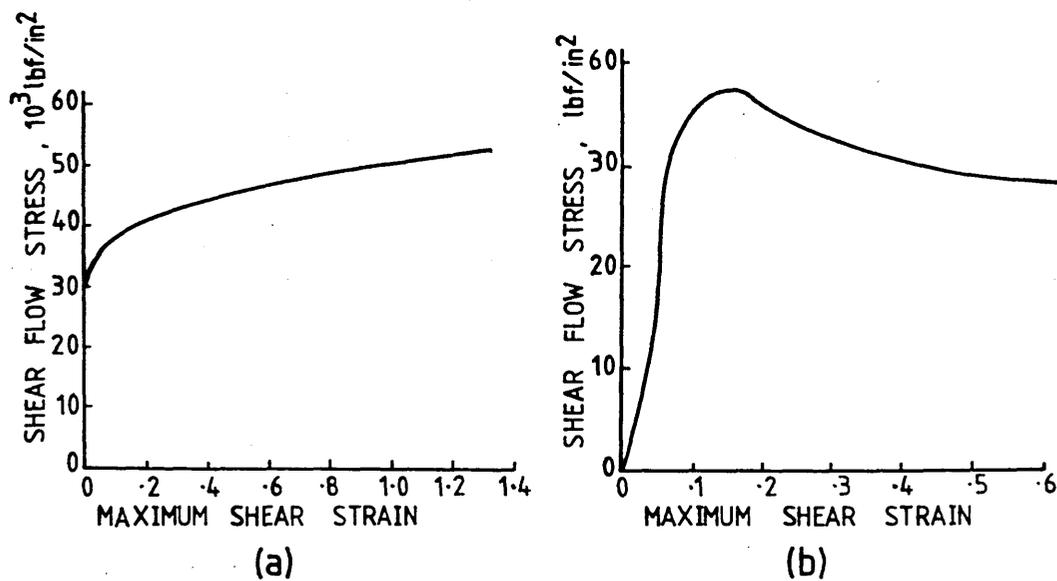
FIG. 18   STRAIN-HARDENING CHARACTERISTICS   OF

a) free machining steel   b) wax   (Ref. 27)
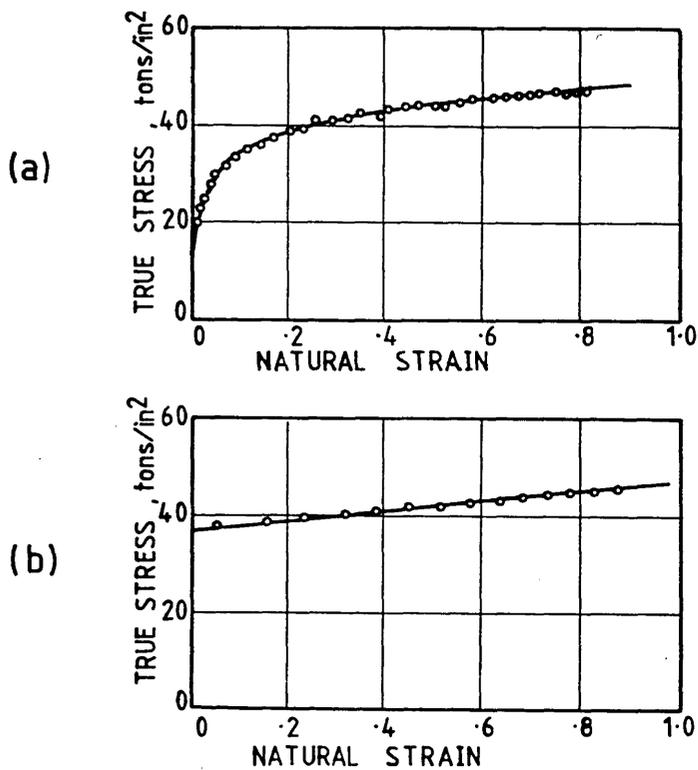
FIG. 19   STRAIN-HARDENING   CHARACTERISTICS

a) Annealed material   (Ref. 26)
b) Cold-worked material

COMPRESSIVE TENSILE B A

COMPRESSIVE TENSILE B A

A B

A B
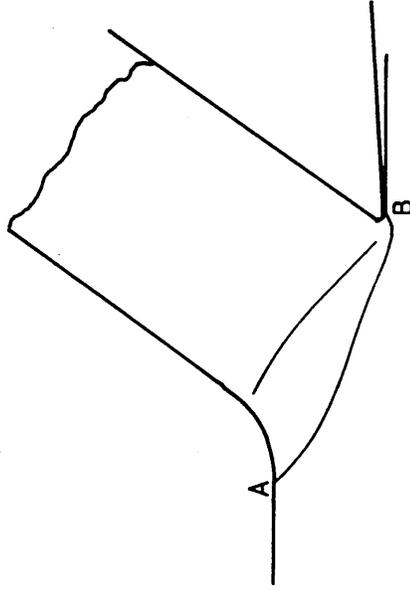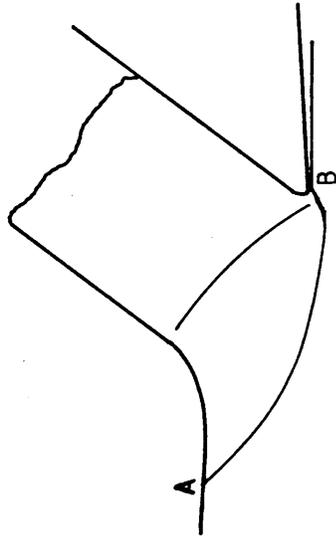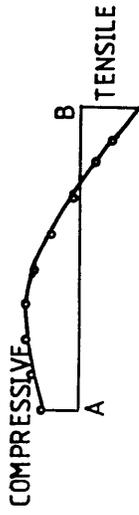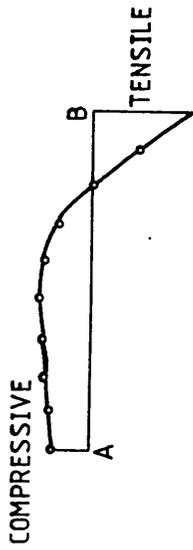
a) ANNEALED MATERIAL

b) COLD-WORKED MATERIAL

FIG. 20 HYDROSTATIC STRESS DISTRIBUTION AND PLASTIC ZONE

(Ref. 26)
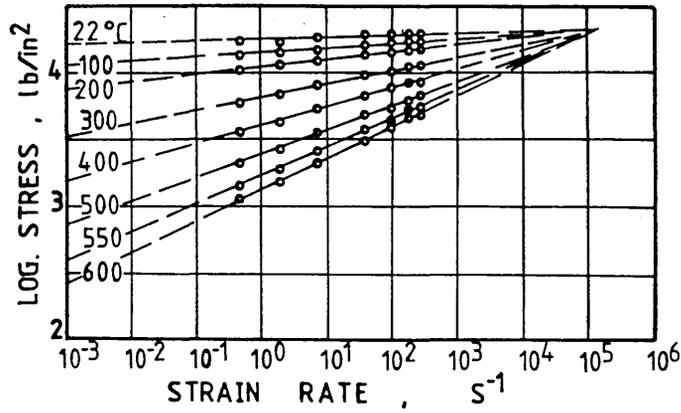
FIG. 21   EFFECT OF STRAIN RATE AND
TEMPERATURE ON FLOW STRESS IN
ALUMINIUM   (Ref. 33)
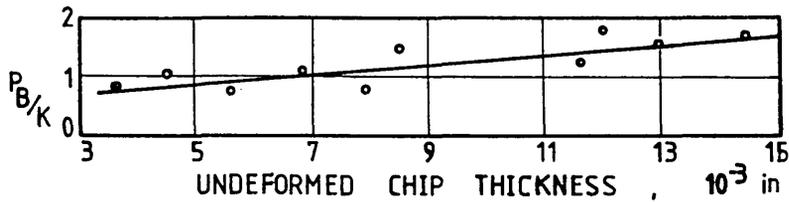
FIG. 22   EFFECT OF UNDEFORMED CHIP THICKNESS
ON THE TENSILE STRESS NEAR THE TOOL
CUTTING EDGE   (Ref. 30)
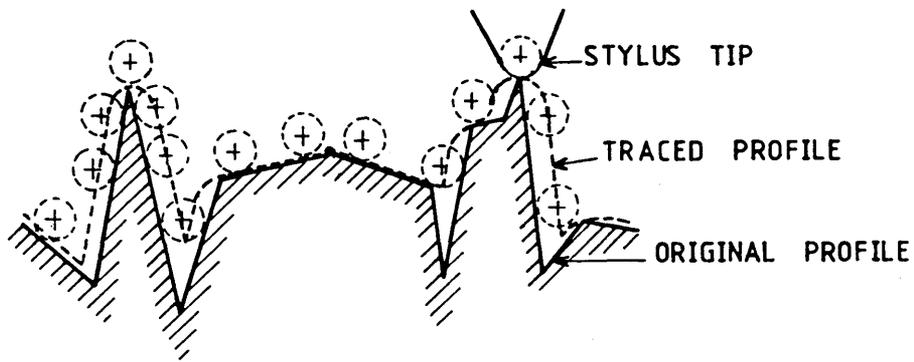
FIG. 23 EFFECT OF STYLUS RADIUS ON THE
PROFILE TRACED

a) Material 4340

Rake: 6°

Clearance: 4°

t = 0.008"/rev

b) Material MXC

Rake: 0°

Clearance: 10°

t = 0.008"/rev
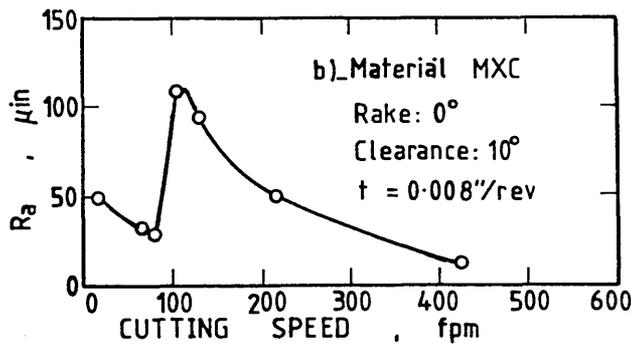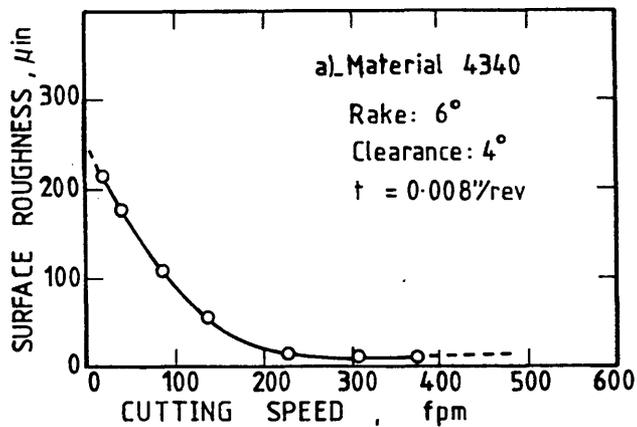
FIG. 24 EFFECT OF CUTTING SPEED ON THE
SURFACE ROUGHNESS FOR TWO MATERIALS

(Ref. 81)
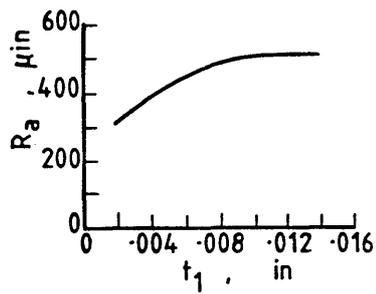
(a) Cutting Speed: 50fpm   (b) Cutting   Speed: 200fpm
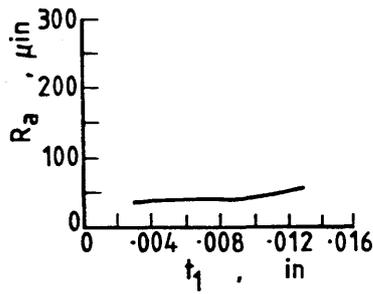
FIG. 25   EFFECT OF UNDEFORMED CHIP THICKNESS
ON THE SURFACE ROUGHNESS   (Ref. 86)
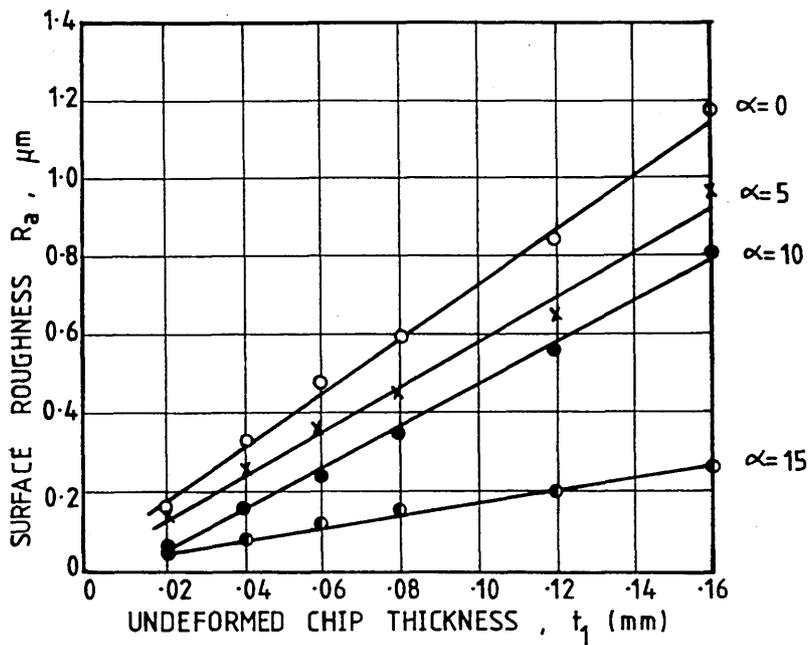
FIG. 26   EFFECT OF RAKE ANGLE AND UNDEFORMED
CHIP THICKNESS ON SURFACE ROUGHNESS

(Ref. 87)
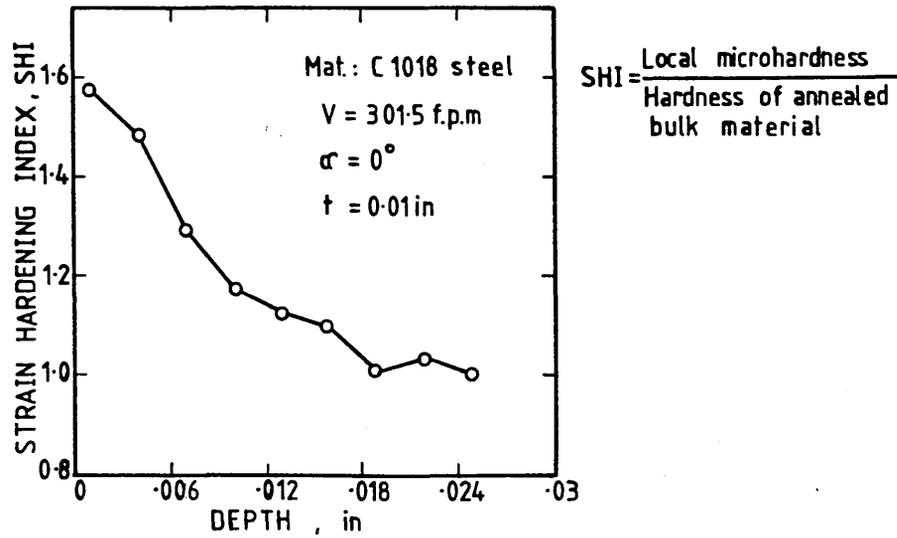
FIG. 27 <u>HARDNESS CHANGE DISTRIBUTION IN SUBSURFACE LAYER</u>   (Ref. 93)
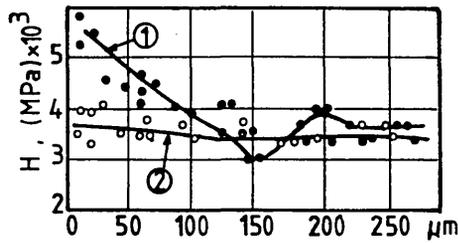
FIG. 28 <u>MICROHARDNESS DISTRIBUTION IN TURNING</u>
① Preheating temperature = 250 °C   (Ref. 95)
② NO preheating
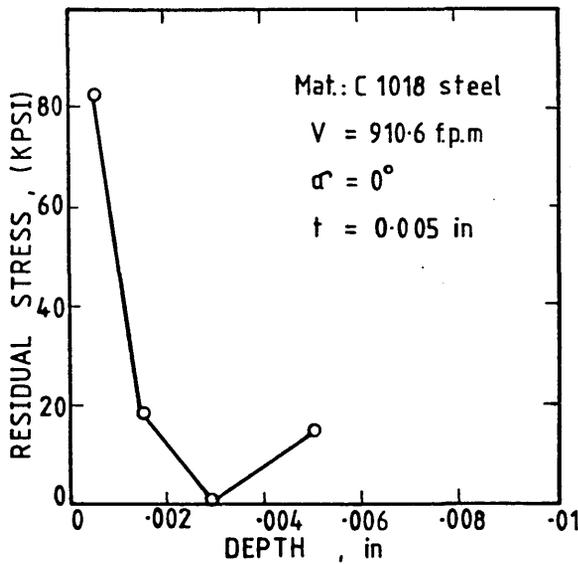
FIG. 29 <u>RESIDUAL STRESS DISTRIBUTION IN SUBSURFACE LAYER</u>   (Ref. 93)
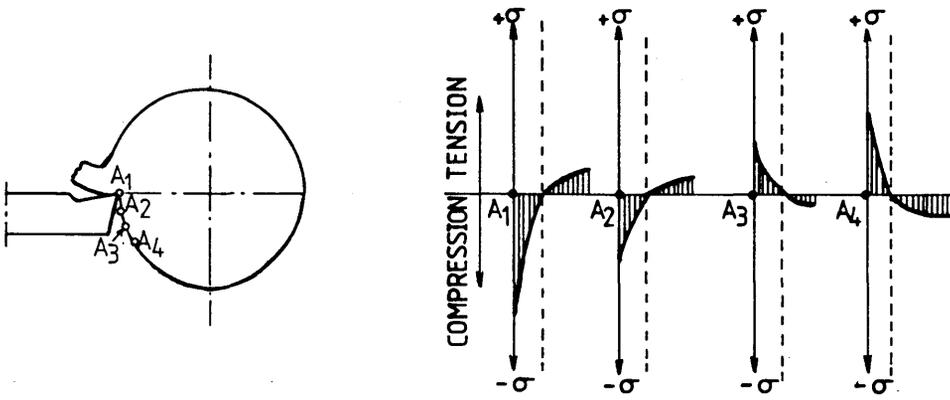
FIG. 30 RESIDUAL STRESS GENERATION BY THE
SO-CALLED THERMAL MODEL   (Ref. 11)

(a)

(b)
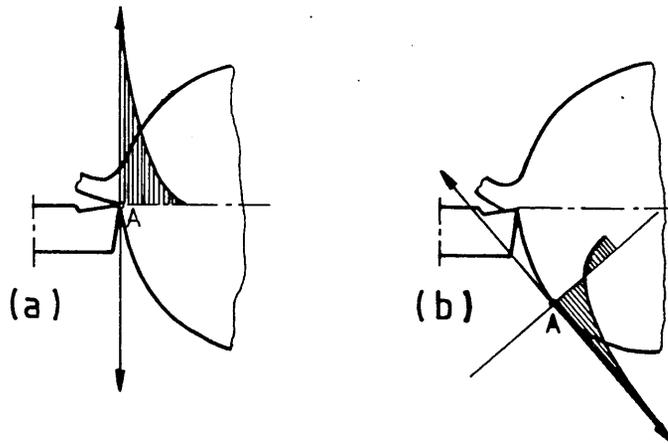
FIG. 31 RESIDUAL STRESS GENERATION BY THE
SO-CALLED MECHANICAL MODEL (Ref. 11)
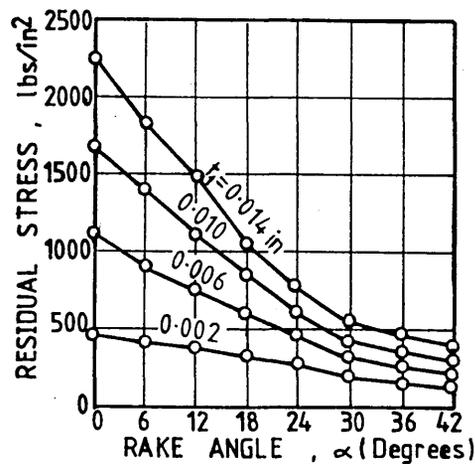
FIG. 32 EFFECT OF RAKE ANGLE AND UNDEFORMED
CHIP THICKNESS ON RESIDUAL STRESS (Ref. 101)
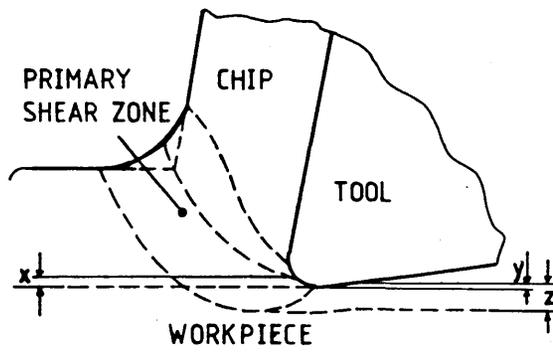
FIG. 33 MODEL OF SURFACE FORMATION
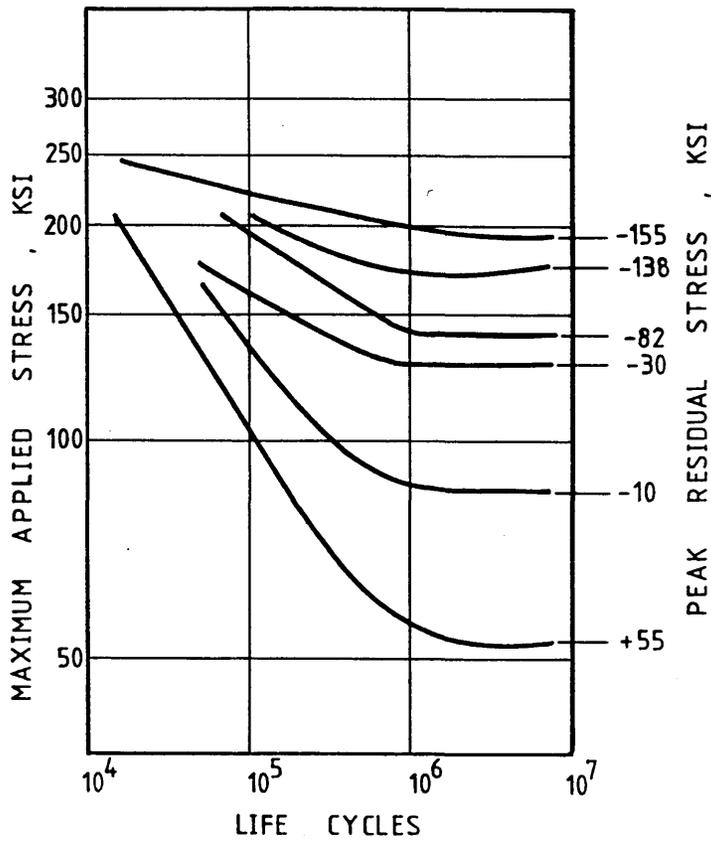
FIG. 34 EFFECT OF RESIDUAL STRESS ON
FATIGUE LIFE OF SAE: 5160 STEEL
(Ref. 66)
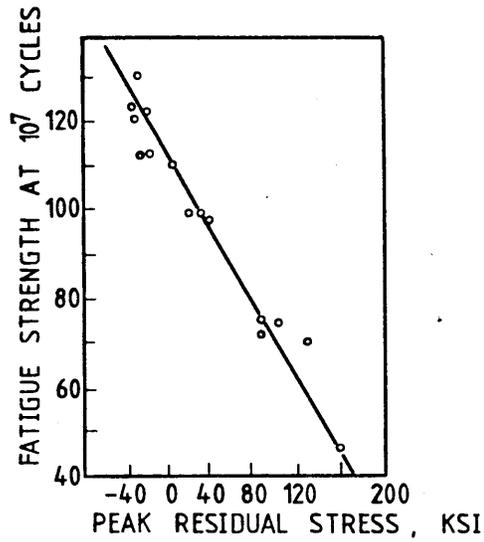
FIG. 35 EFFECT OF RESIDUAL STRESS ON THE
FATIGUE STRENGTH IN 4340 STEEL
(Ref. 103)
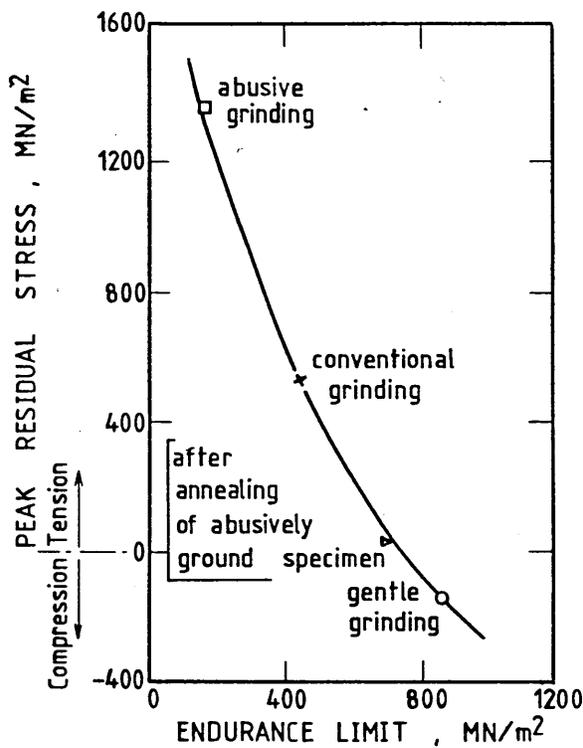
FIG. 36 EFFECT OF RESIDUAL STRESS ON THE
ENDURANCE LIMIT IN En 31 STEEL
(Ref. 64)
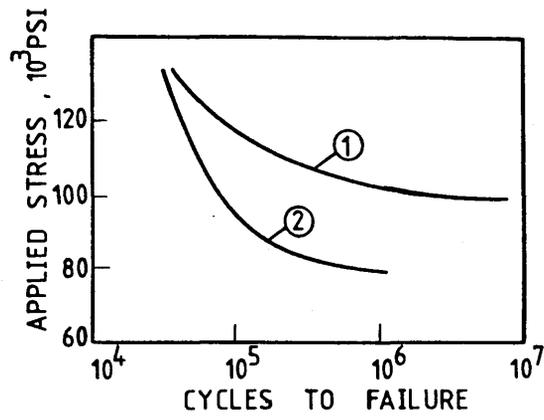
FIG. 37 <u>RESULTS OF FATIGUE TESTS ON GROUND</u>
<u>4330 M HIGH TENSILE STEEL</u> (Ref. 39)

① LOW STRESS GRIND _ STRESS RELIEVED
② ABUSIVE GRIND _ STRESS RELIEVED
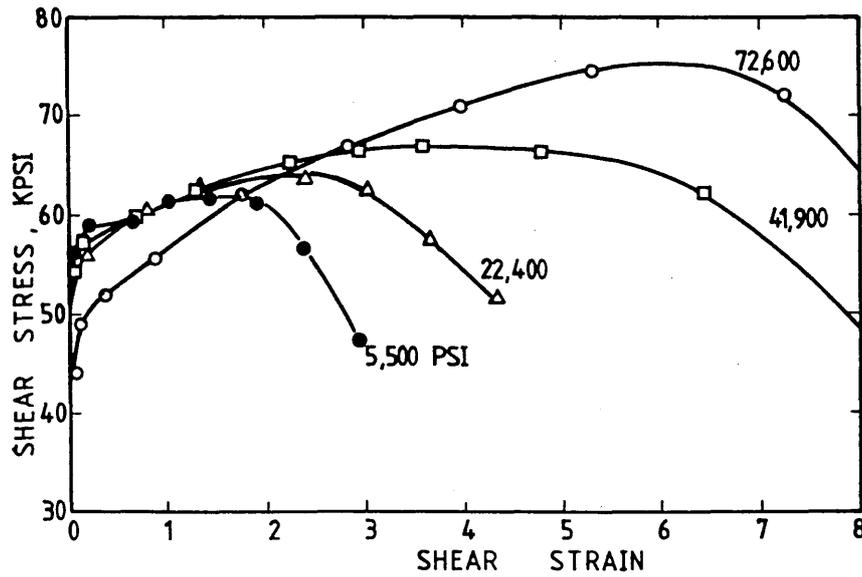
FIG. 38 SHEAR STRESS-STRAIN CURVES AT DIFFERENT
LEVELS OF AXIAL COMPRESSIVE STRESS
(Ref. 123)

(a)

(b)
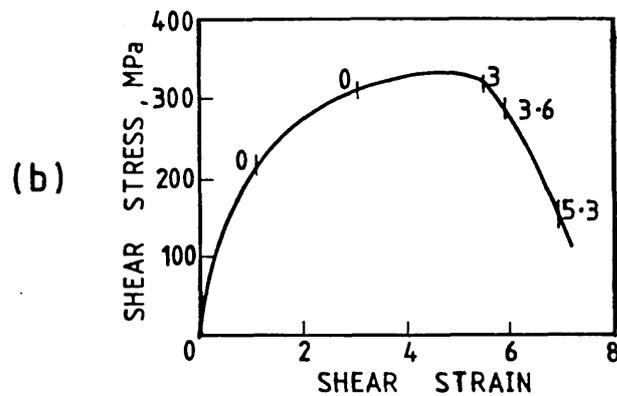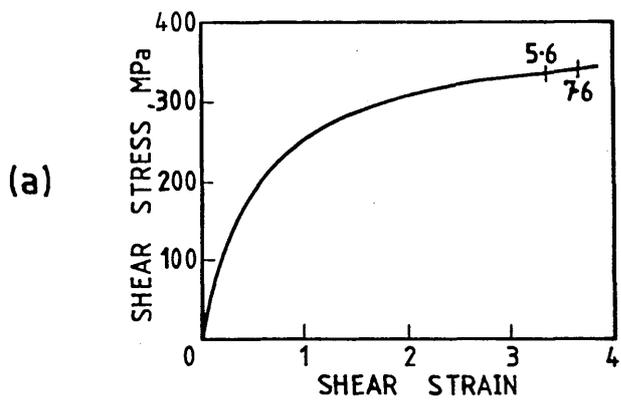
FIG. 39 STRESS-STRAIN CURVES OF CS:1114 STEEL
TESTED AT A STRAIN RATE OF 0·7 s⁻¹ (Ref. 122)
Compressive stress: zero for (a) & 340MPa for (b)

(a)

(b)
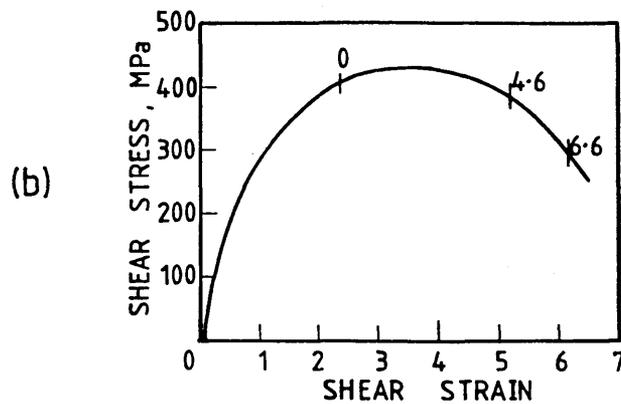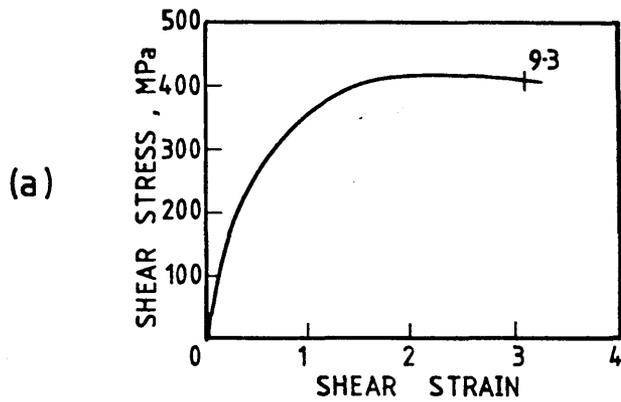
FIG. 40 STRESS-STRAIN CURVES OF CS:1114 STEEL
TESTED AT A STRAIN RATE OF 5,000 s⁻¹

Compressive stress: zero for (a) & 340MPa for(b)
(Ref. 122)
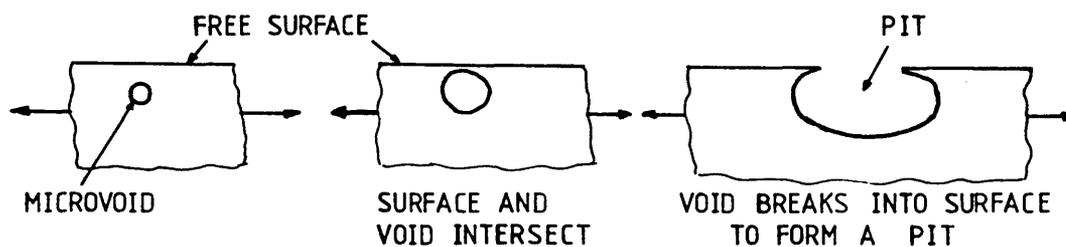
FIG. 41 PIT FORMATION (Ref. 6)
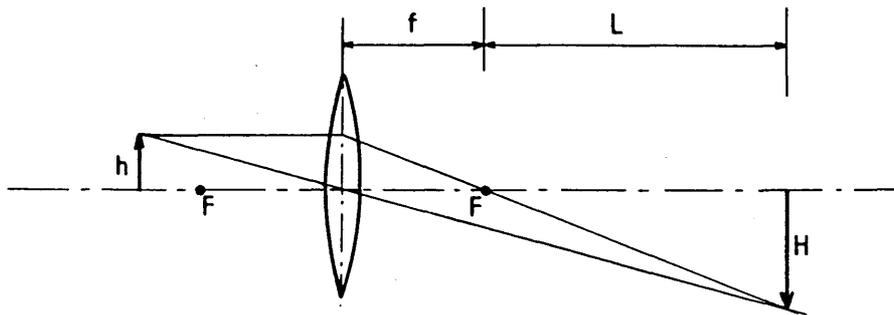
FIG. 42 FORMATION OF A MAGNIFIED IMAGE BY
A SINGLE LENS
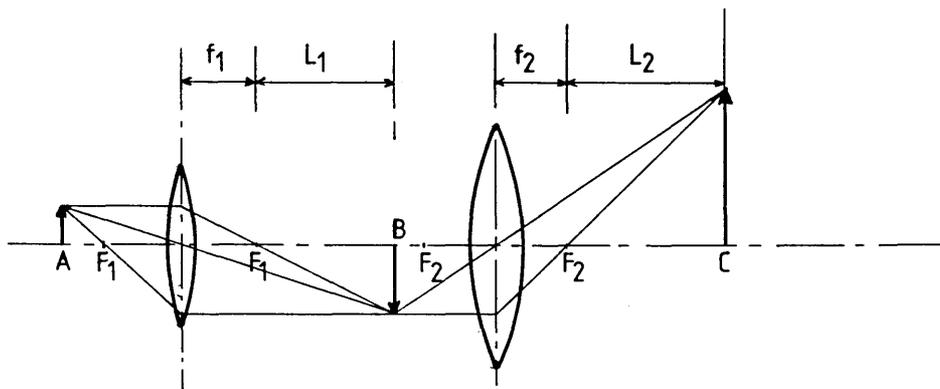
FIG. 43 DIAGRAM OF A SIMPLE TWO-STAGE
PROJECTION MICROSCOPE
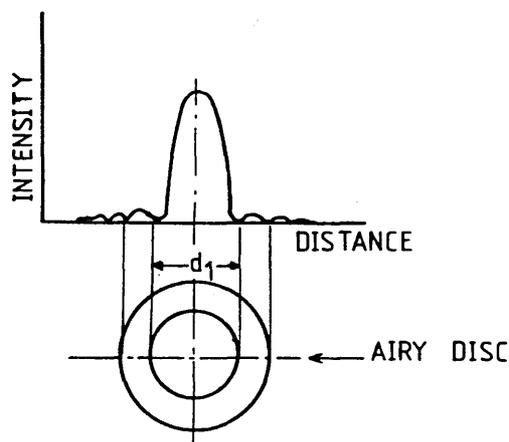
FIG 44 DISTRIBUTION ACROSS AIRY DISC OF
THE INTENSITY OF LIGHT
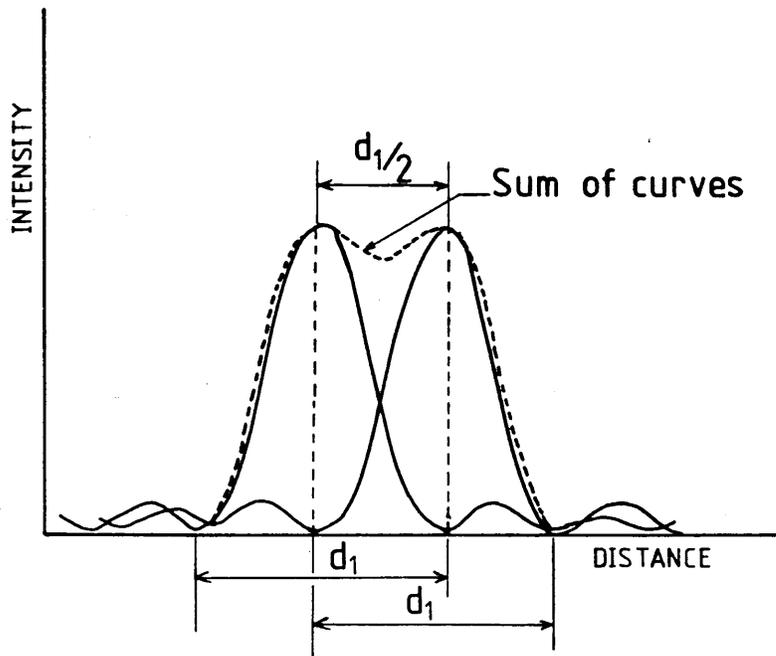
FIG. 45 INTENSITY OF THE AIRY RINGS FROM TWO
NEIGHBOURING PINHOLES
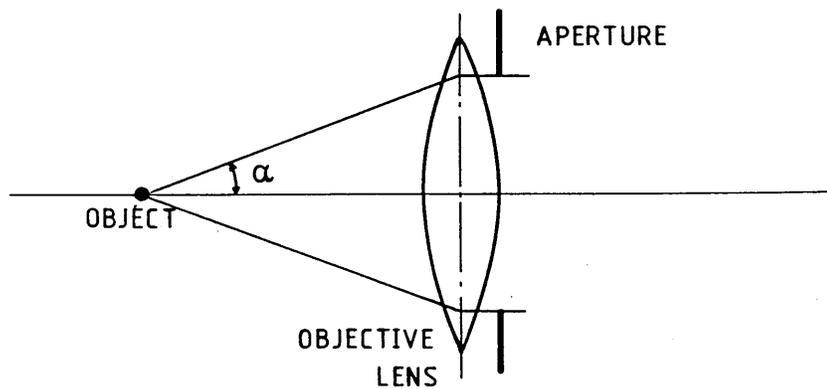
FIG. 46 DEFINITION OF THE SEMI-ANGLE "α"
SUBTENDED BY AN APERTURE

FIG. 47 SPHERICAL ABERRATION

marginal focus   disc of least confusion   axial focus

FILAMENT

WEHNELT CYLINDER

ANODE
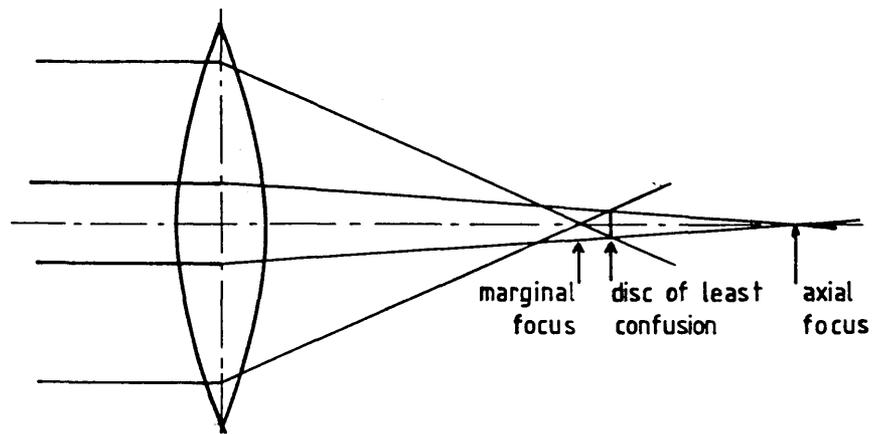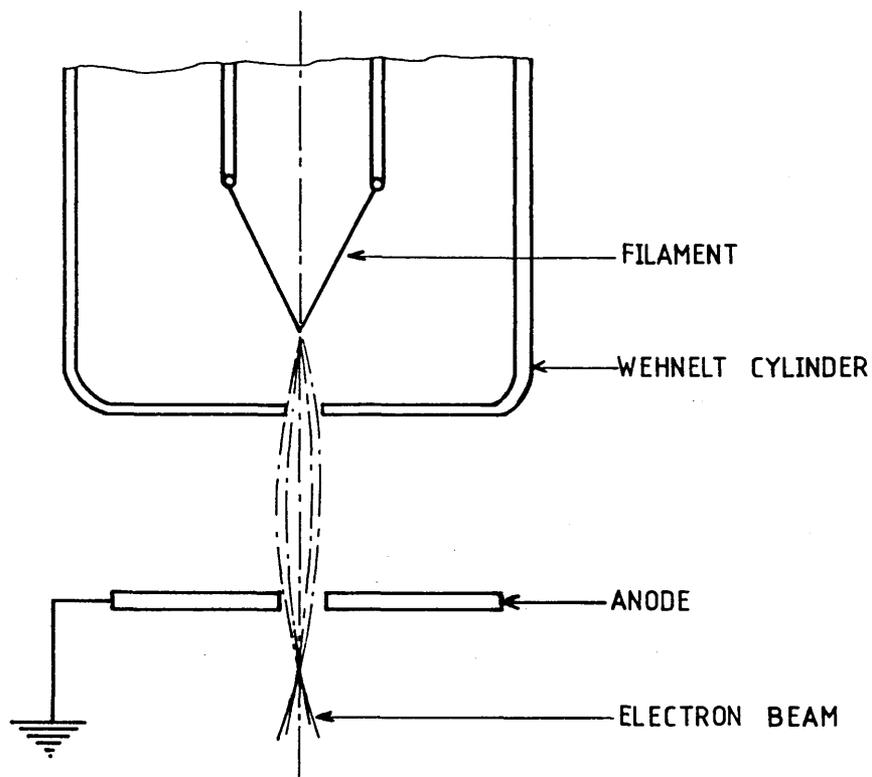
ELECTRON BEAM

FIG. 48 ELECTRON GUN ASSEMBLY
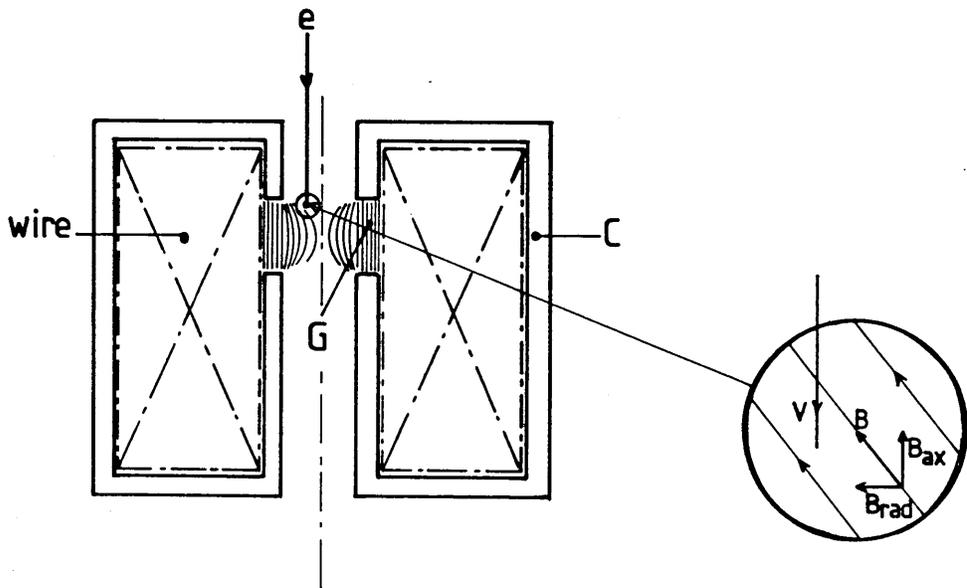
FIG. 49 TYPICAL ELECTRON LENS ARRANGEMENT AND ACTION ON ELECTRONS
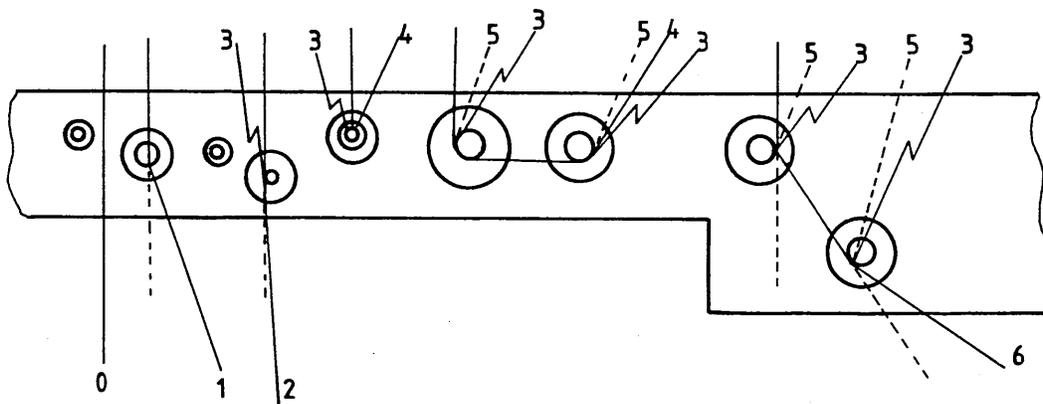
FIG. 50 ELECTRON-BEAM/SPECIMEN INTERACTION

"0" TRANSMITTED ELECTRONS
"1" ELASTICALLY SCATTERED ELECTRONS
"2" INELASTICALLY SCATTERED ELECTRONS
"3" X-RAYS
"4" REFLECTED ELECTRONS
"5" SECONDARY ELECTRONS
"6" HIGH ANGLE SCATTERING FROM THICKER SPECIMENS

Light Source

Aperture

CONDENSER LENS
(One or two lenses)

SPECIMEN (or REPLICA)

OBJECTIVE LENS

PROJECTOR LENS

FINAL IMAGE

(a)

High Voltage Cable

ELECTRON
GUN
ASSEMBLY

Filament

Anode

Earth

Aperture

Aperture

INTERMEDIATE LENS
(One or two lenses)

Aperture

TRANSMITTED SIGNAL IMAGE

(b)
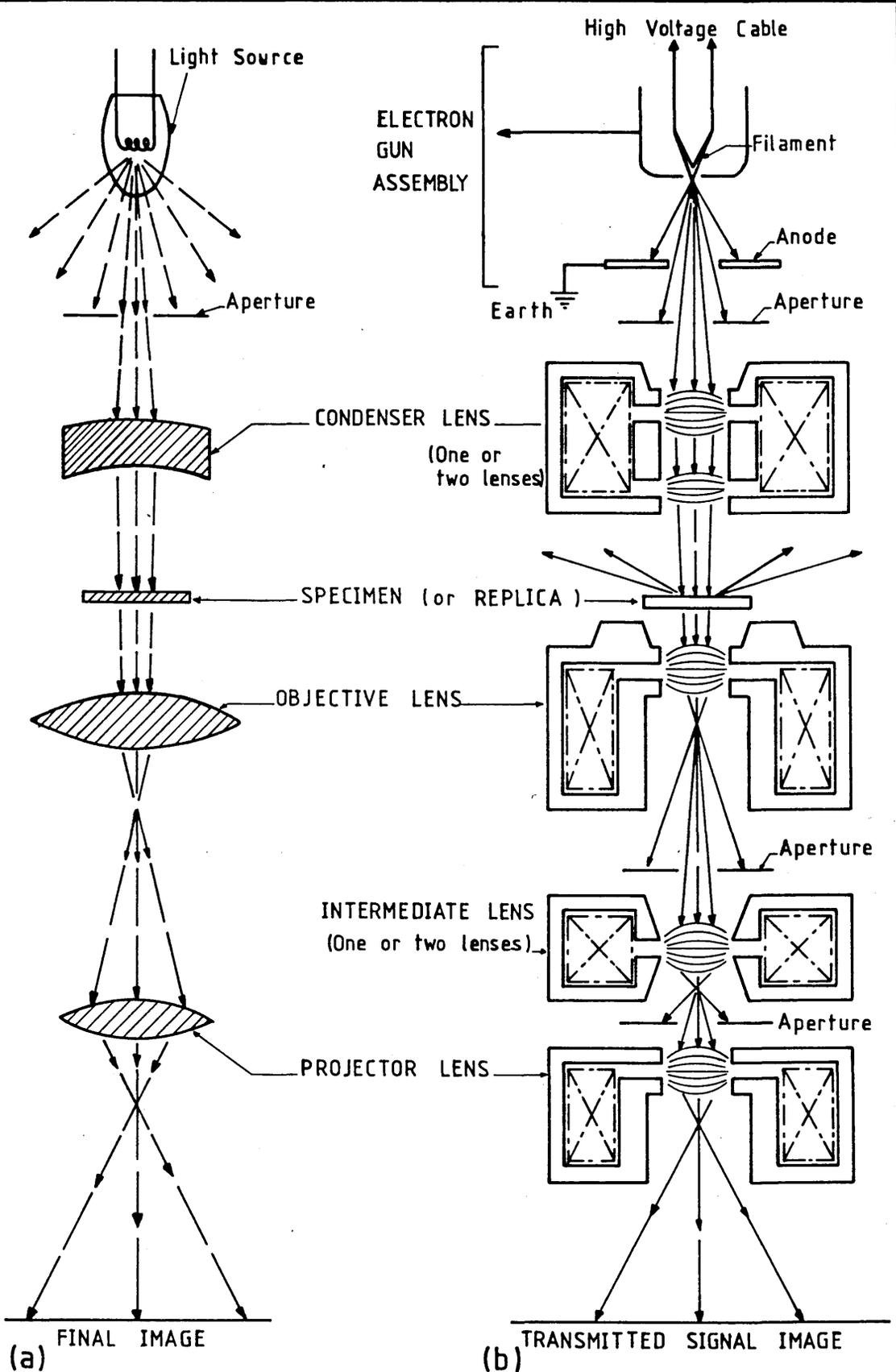
FIG. 51   COMPARISON BETWEEN LIGHT AND ELECTRON
MICROSCOPES

(a) Light   (b) Electron
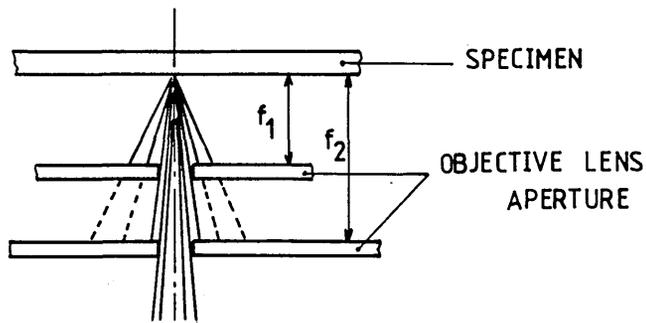
FIG.52 EFFECT OF FOCAL LENGTH ON EXTRACTION OF ELASTICALLY SCATTERED ELECTRONS

f_1 small focal length _ lower contrast

f_1 larger focal length _ higher contrast

(a)

(b)
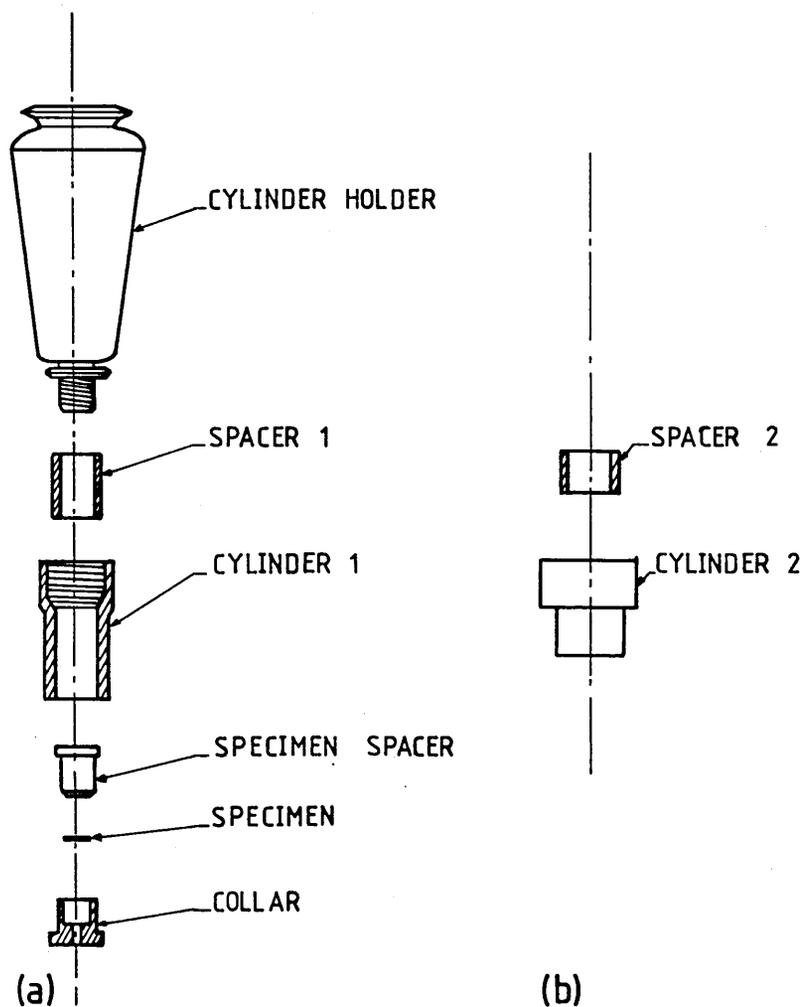
FIG. 53 SPECIMEN HOLDER COMBINATIONS

(a) Standard

(b) High contrast

(a)

MACHINED SURFACE

(b)

SHADOWING METAL

CARBON

(c)   G   W GB   G B   G   W   G   B W   G
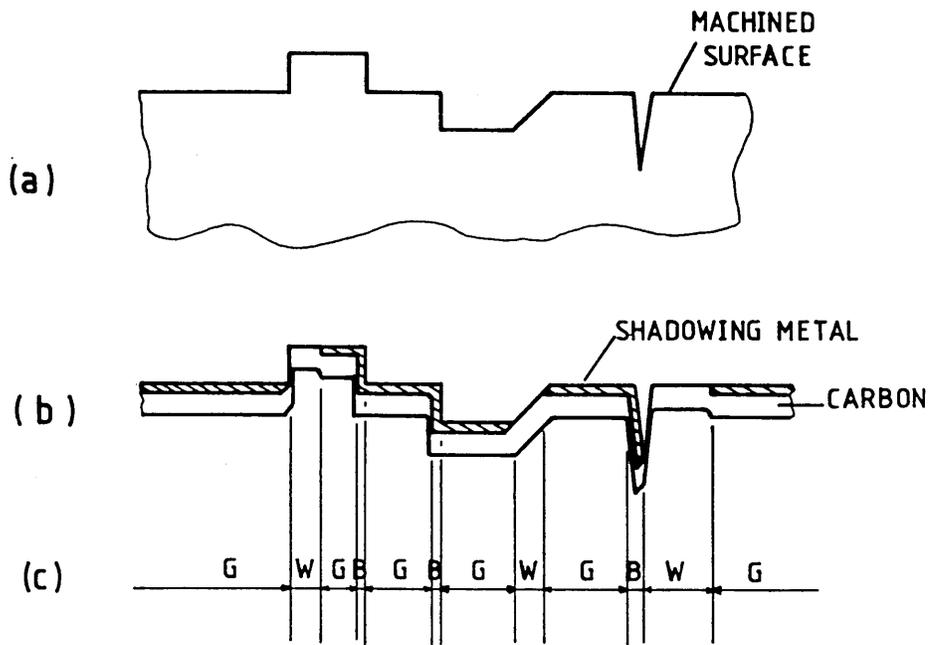
FIG. 54 CONTRAST PRODUCED BY SHADOWING

(a) Surface to be replicated
(b) TEM specimen
(c) Contrast shade sequence

ELECTRON BEAM

GOLD PALADIUM

CARBON

G   W   B   G

G: GREY   W: WHITE   B: BLACK
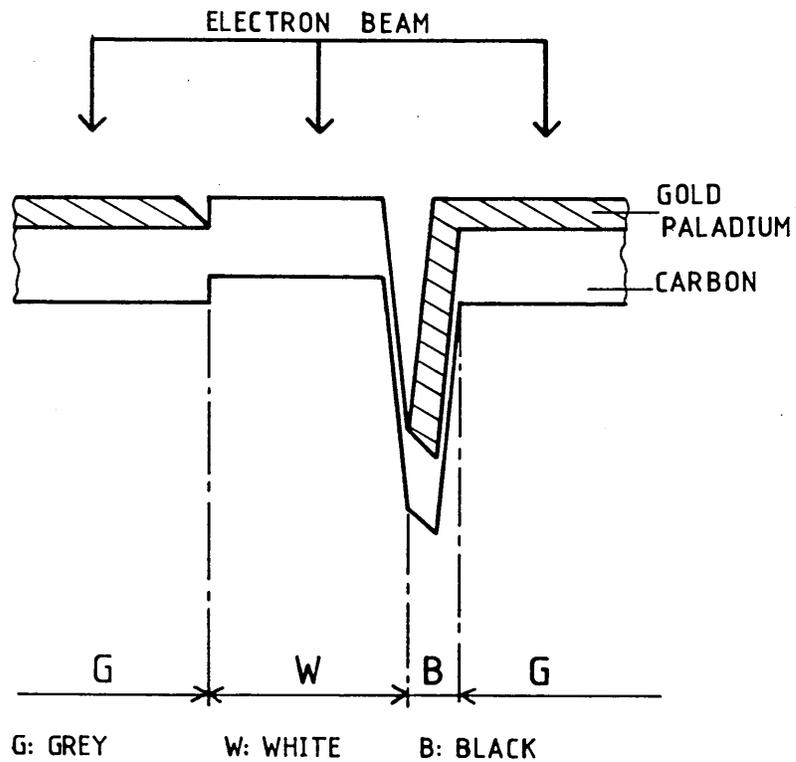
FIG. 55   MICROCRACK CONTRAST SEQUENCE
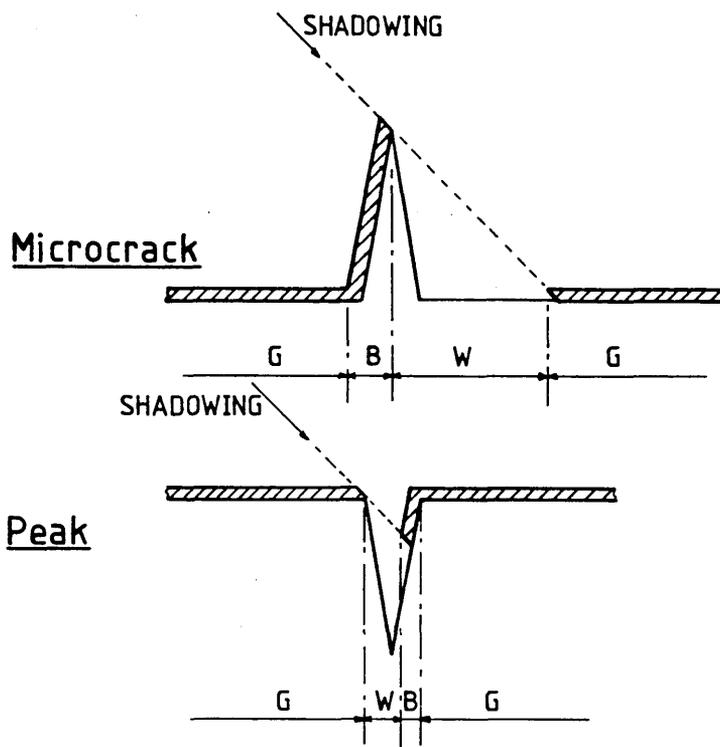
FIG. 56 COMPARISON BETWEEN A MICROCRACK
AND A PEAK SHADE SEQUENCES

G:GREY   B:BLACK   W: WHITE

(a)

(b)

(c)
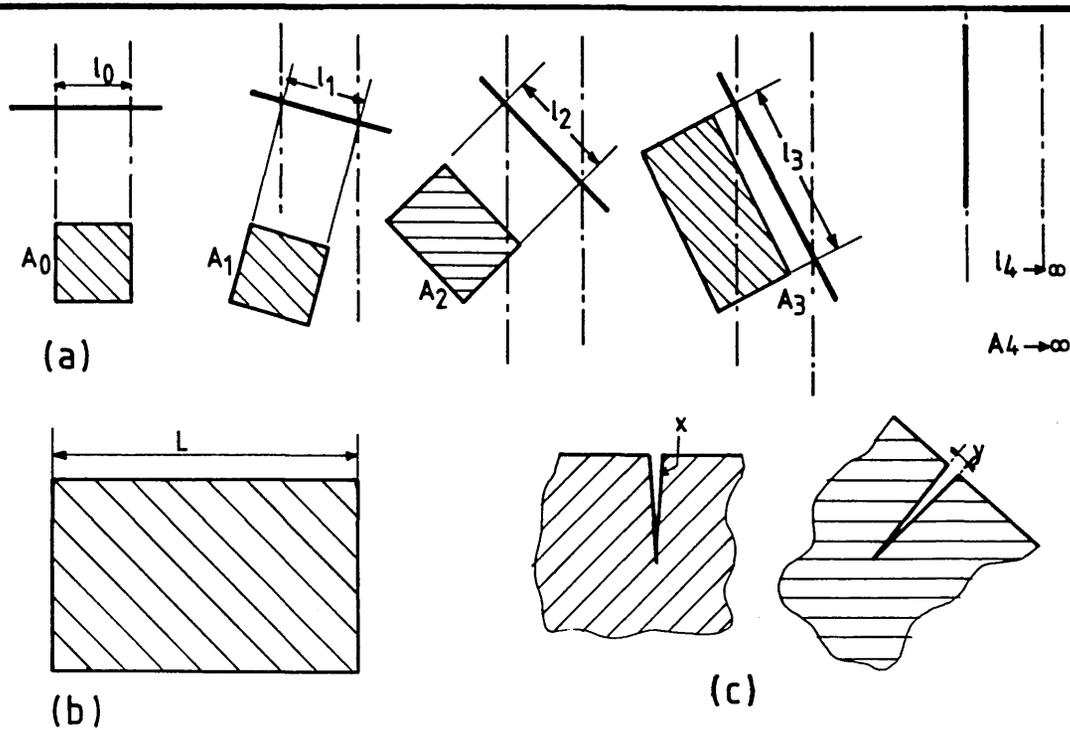
FIG. 57 <u>EFFECT OF SURFACE TILT ON MAGNIFICATION</u>
    a) Different values of tilt
    b) CRT scan area
    c) Surface microcracks

SHADOWING
DIRECTION
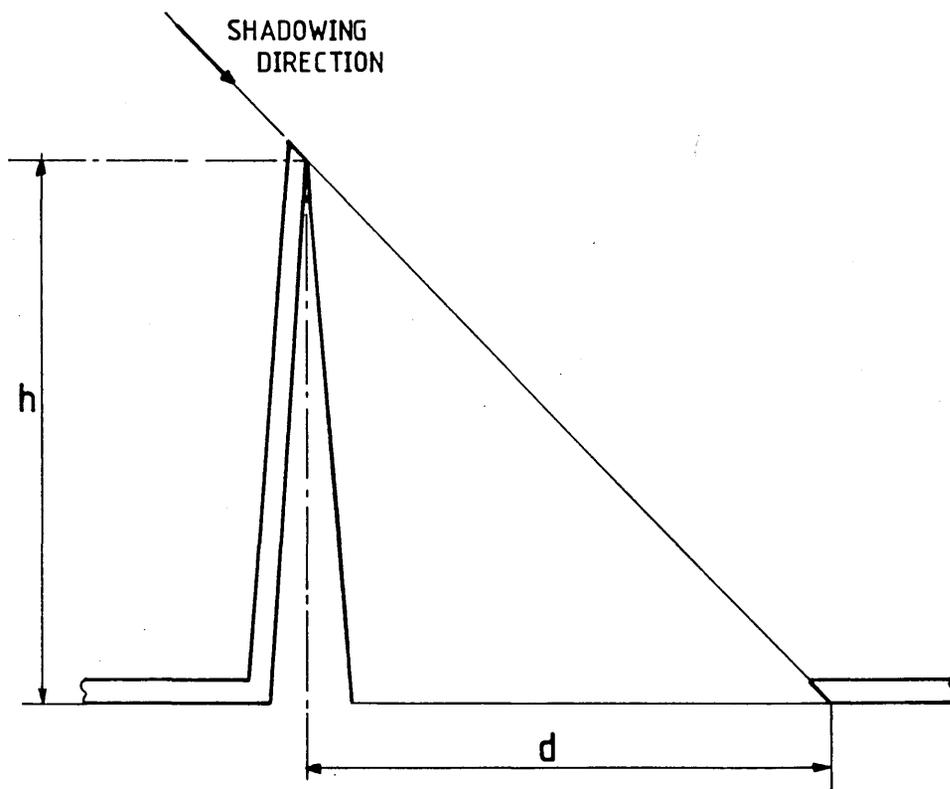
FIG. 58 <u>GEOMETRY OF SHADOWING EFFECT</u>
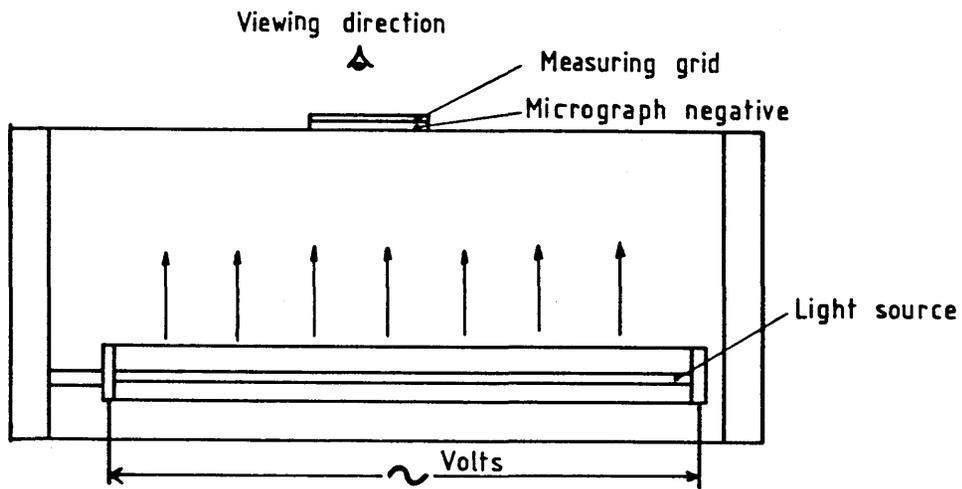
FIG. 59 SET-UP FOR MEASUREMENT OF SURFACE MICROCRACKING
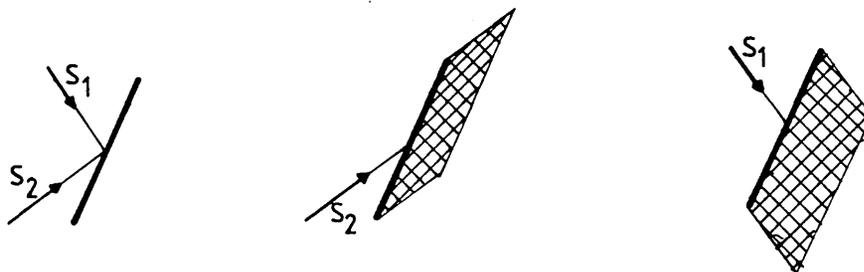
FIG. 60 LENGTH MEASUREMENT REPETITION
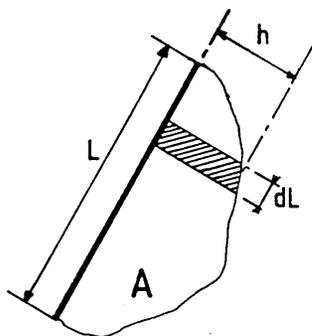
$$A = \int_{}^{L} h.dL$$

FIG. 61 RELATION BETWEEN AREA, DEPTH, AND LENGTH OF MICROCRACKS
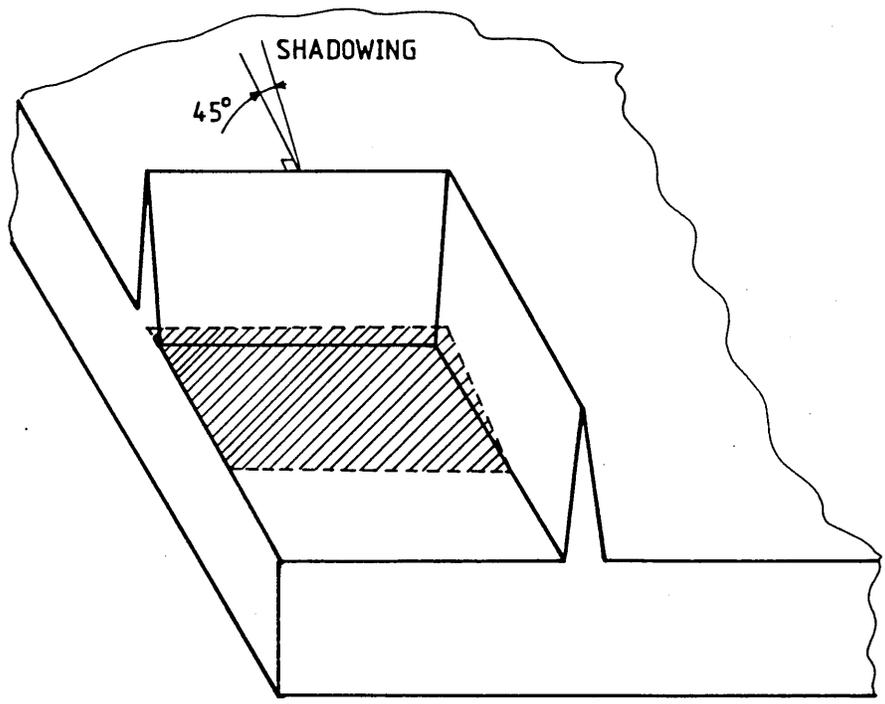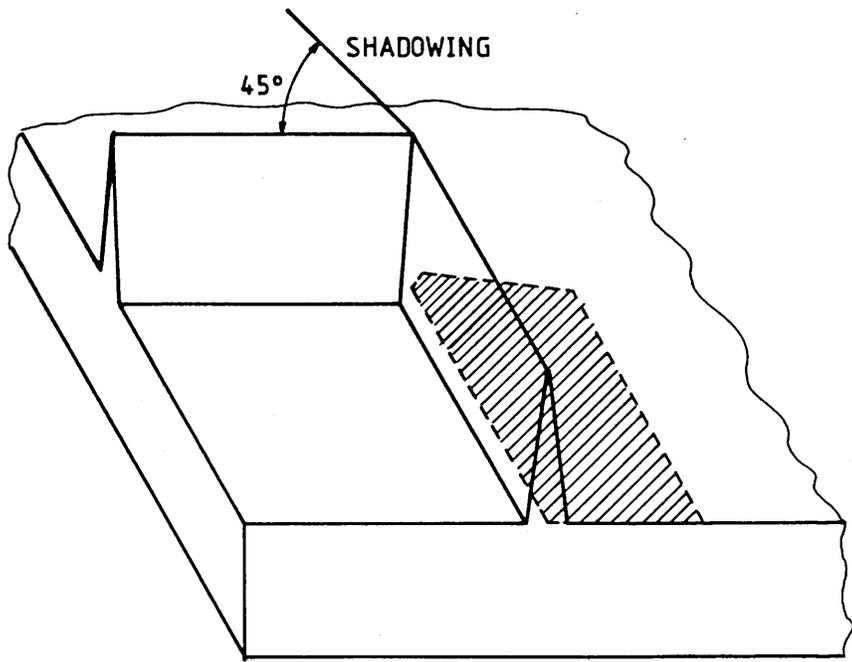
FIG. 62 EFFECT OF SHADOWING IN TWO
COMPLEMENTARY DIRECTIONS
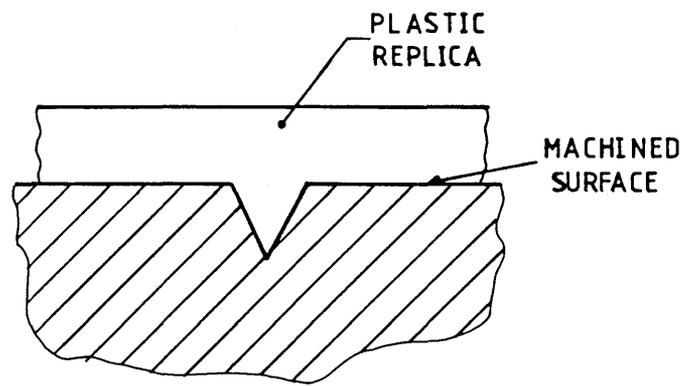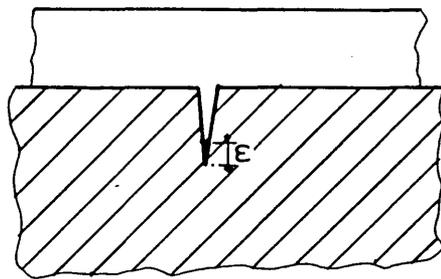
FIG. 63 PENETRATION OF REPLICATING MATERIAL INTO THE MICROCRACKS

(a) Shallow microcrack _ good penetration
(b) Steep microcrack _ incomplete penetration

(a)

(b)

(c) G=GREY   B=BLACK   W=WHITE
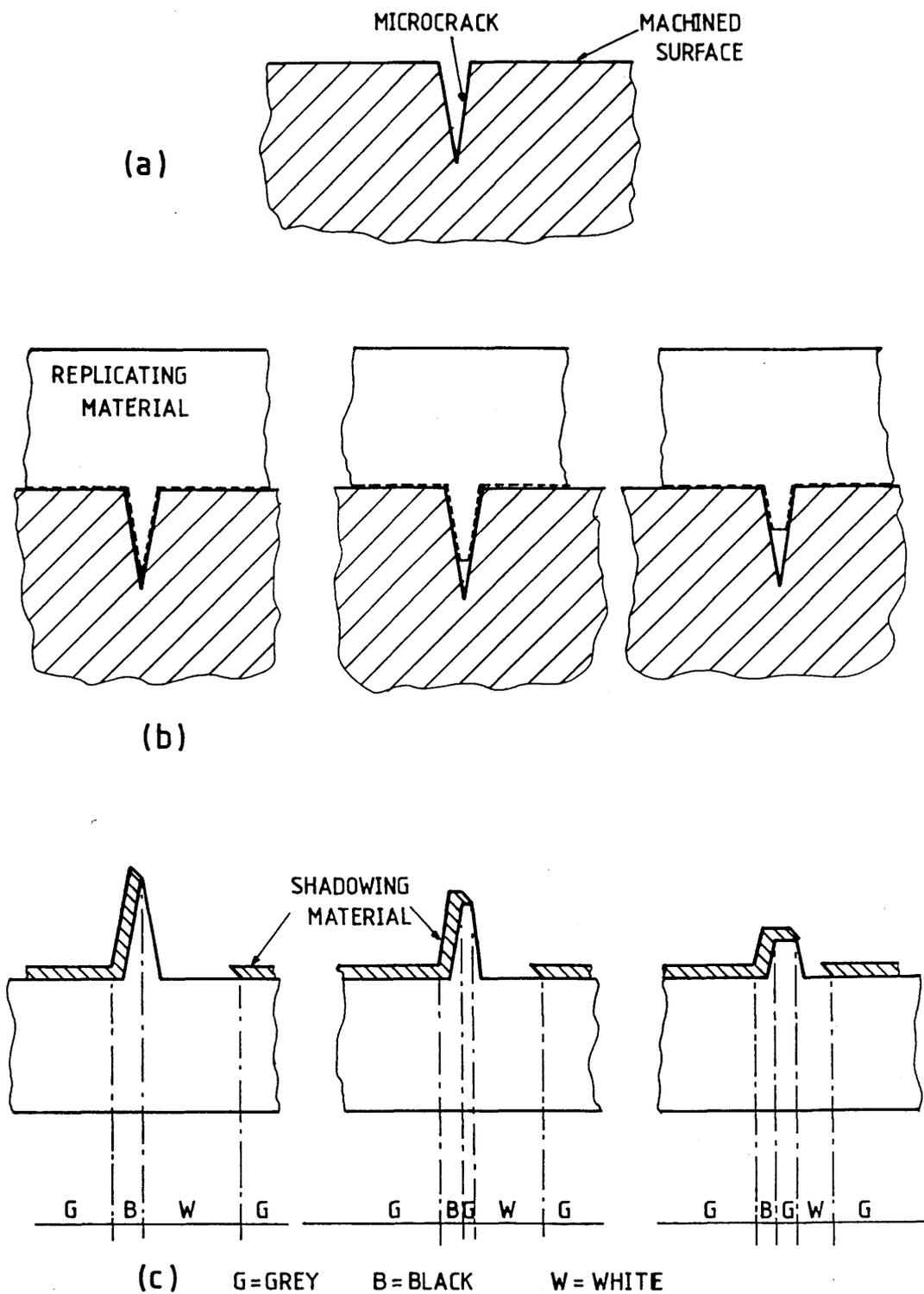
FIG. 64 EFFECT OF THE DEPTH OF PENETRATION OF REPLICATING MATERIAL ON THE FINAL CONTRAST SEQUENCE

(a) Microcrack

(b) Penetration of replicating material

(c) Shadowing and resulting contrast sequence
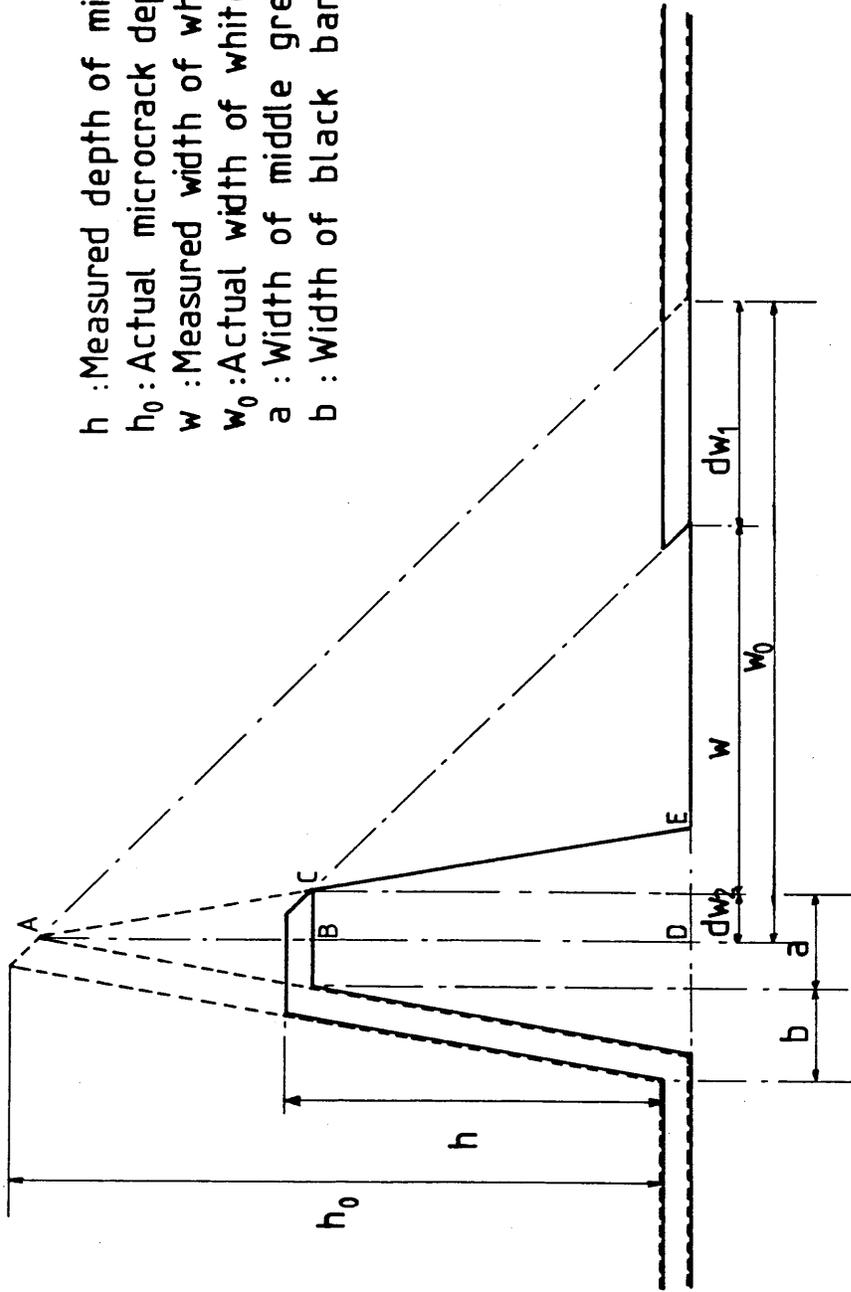
h : Measured depth of microcrack
h_0 : Actual microcrack depth
w : Measured width of white band
w_0 : Actual width of white band
a : Width of middle grey band
b : Width of black band

FIG. 65 GEOMETRY OF SHADOWING ILLUSTRATING THE EFFECT OF INCOMPLETE PENETRATION ON MICROCRACK MEASUREMENT

SHADOWING

45°

PLASTIC REPLICA

G   G   W   W   G   B   B   G   G
    G   W   G   B   B   G   G

G = GREY
B = BLACK
W = WHITE

FIG. 66 COLLAPSE OF THE PLASTIC REPLICA

SHADOWING
DIRECTION

45°

CARBON
COATING
DIRECTION

CARBON COATING
SHADOWING MATERIAL

G=GREY
B=BLACK
W=WHITE
D.G=DARK GREY
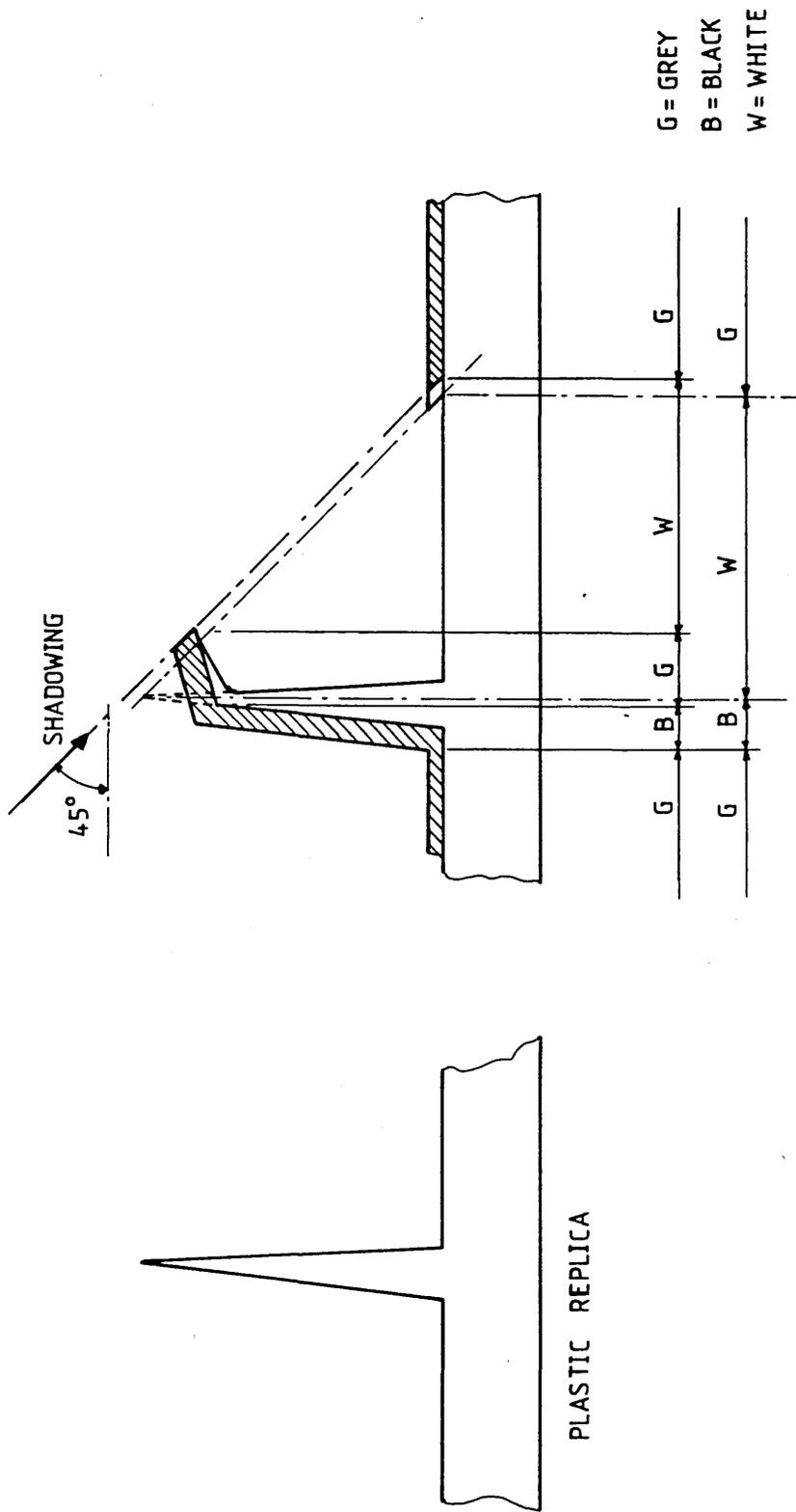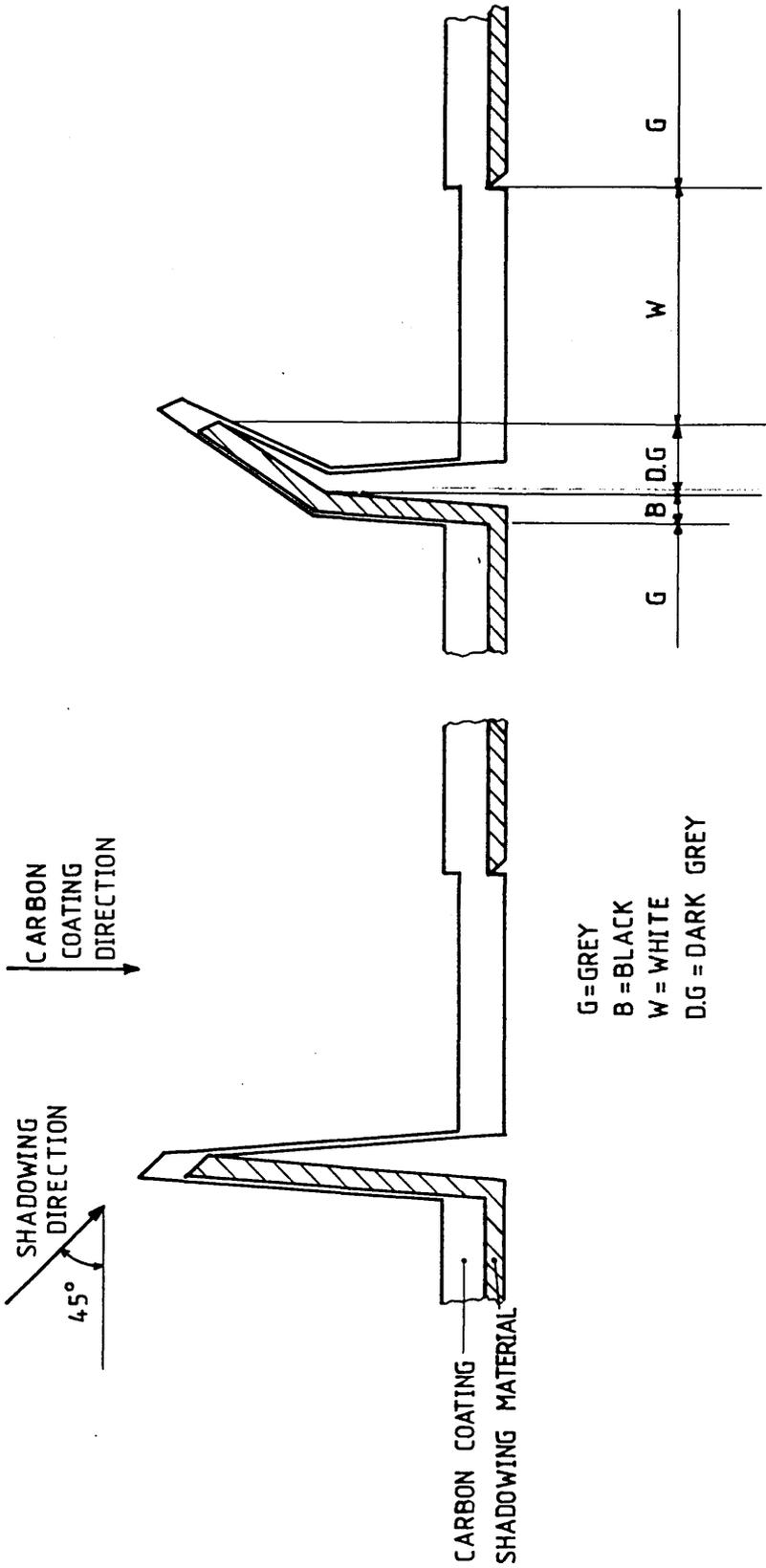
FIG. 67 COLLAPSE OF THE SHADOWING MATERIAL
AND CARBON COATING

WORKPIECE

FEED
DIRECTION
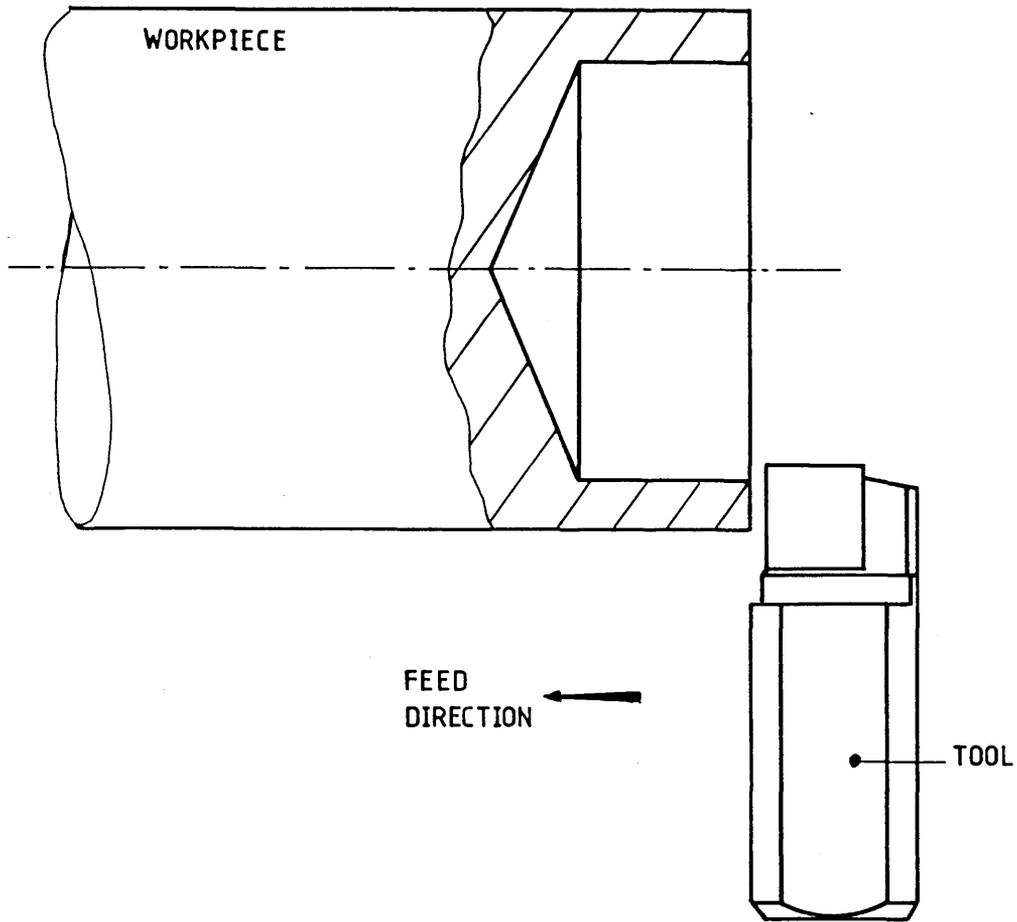
TOOL

FIG. 68 GEOMETRY OF CUTTING TESTS

STYLUS TRAVERSE

STYLUS

TOOL BIT
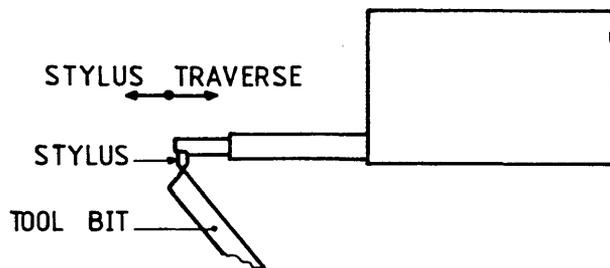
FIG. 69 TOOL SHARPNESS MEASUREMENT

CARBIDE TIP

TIP HOLDER
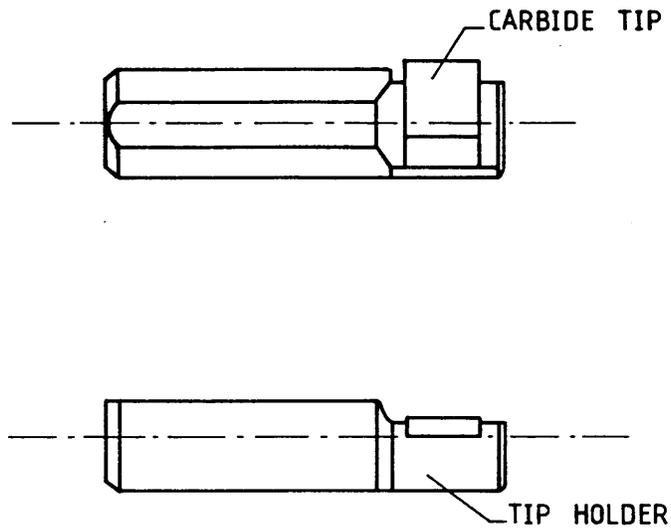
FIG. 70 CUTTING TOOL DESIGN

WORKPIECE

SURFACE TO
BE MACHINED

RECESS

TOOL

(b)
Alternative tooling

(a)

FIG. 71 WORKPIECE PREPARATION

(a)

(b)
PLASTIC (ACETATE) SHEET

(c)
PLASTIC

(d)
Shadowing
SHADOWING METAL
PLASTIC

(e)
Carbon Coating
CARBON
SHADOWING METAL
PLASTIC

(f)
CARBON
SHADOWING METAL
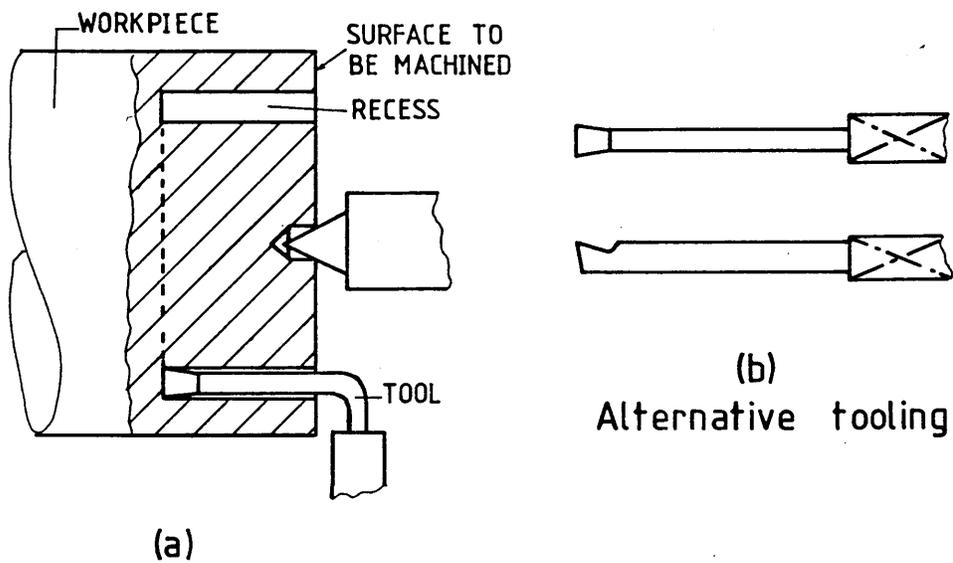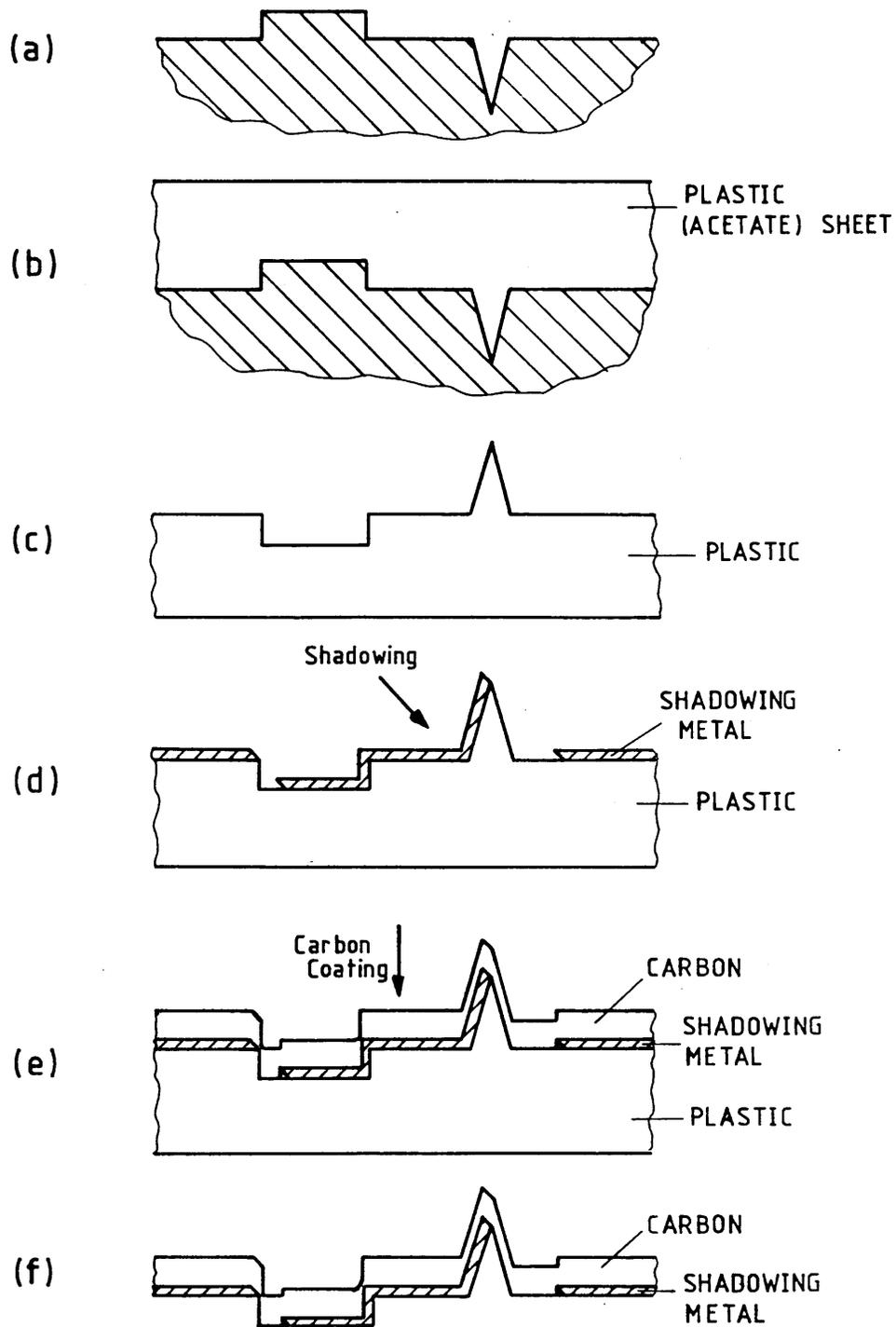
FIG. 72 TEM SPECIMEN PREPARATION PROCEDURES
(a) Selected and prepared surface
(b) Replication
(c) Plastic replica turned over
(d) Shadowing
(e) Carbon coating
(f) Final specimen (i.e. with plastic dissolved)

-241-
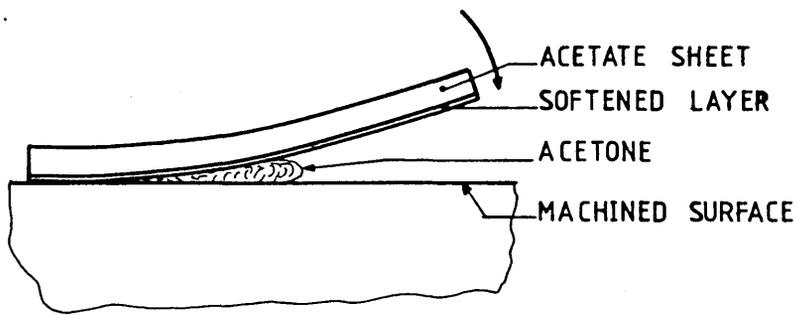
FIG.73   LAYING OF SOFTENED ACETATE SHEET
         DURING REPLICATION OF SURFACES
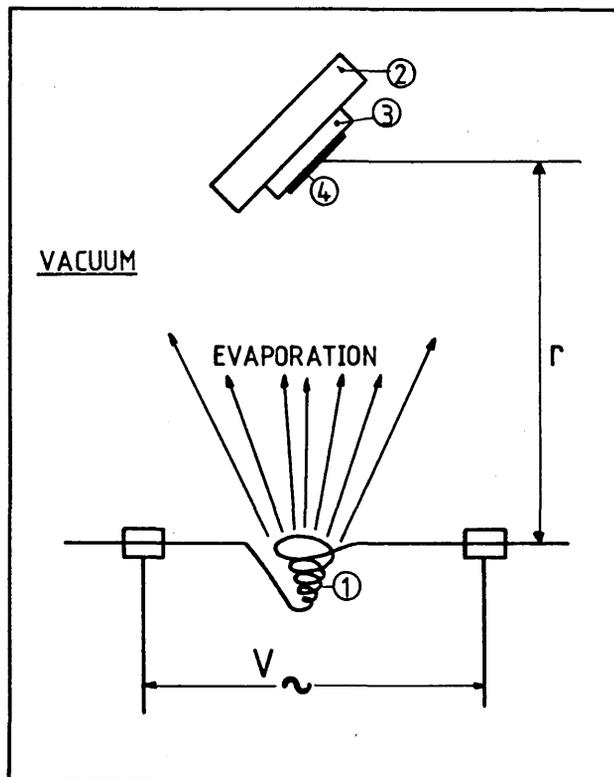
FIG.74   SCHEMATIC ILLUSTRATION OF THE SHADOWING

   ① Evaporating tungsten basket
   ② Glass slide holder
   ③ Glass slide carrying replicas
   ④ Replica
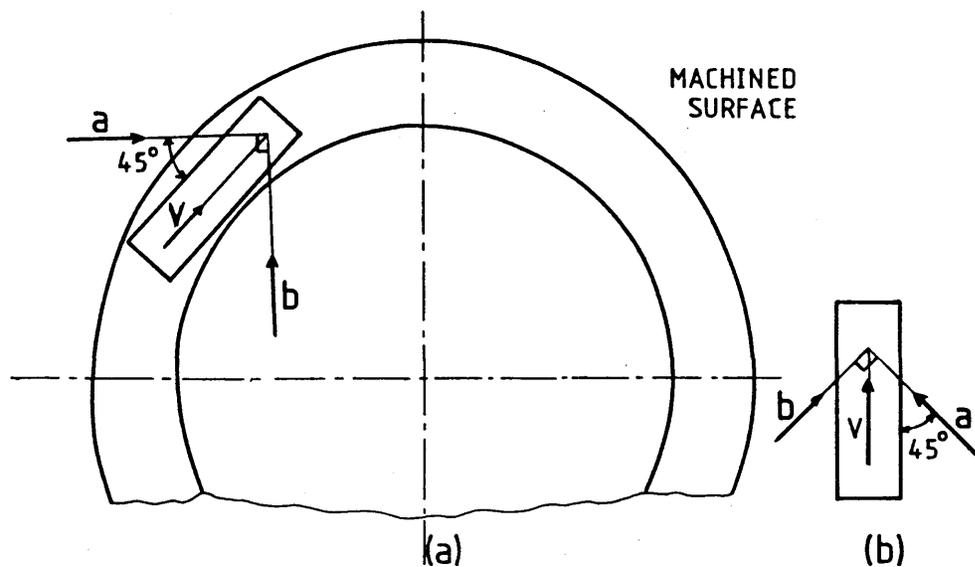
FIG. 75   IN-PLANE SHADOWING DIRECTIONS REFERRED
TO AS "a" AND "b" DIRECTIONS

   (a) Relative to machined surface
   (b) Relative to replica face (Replica turned over)
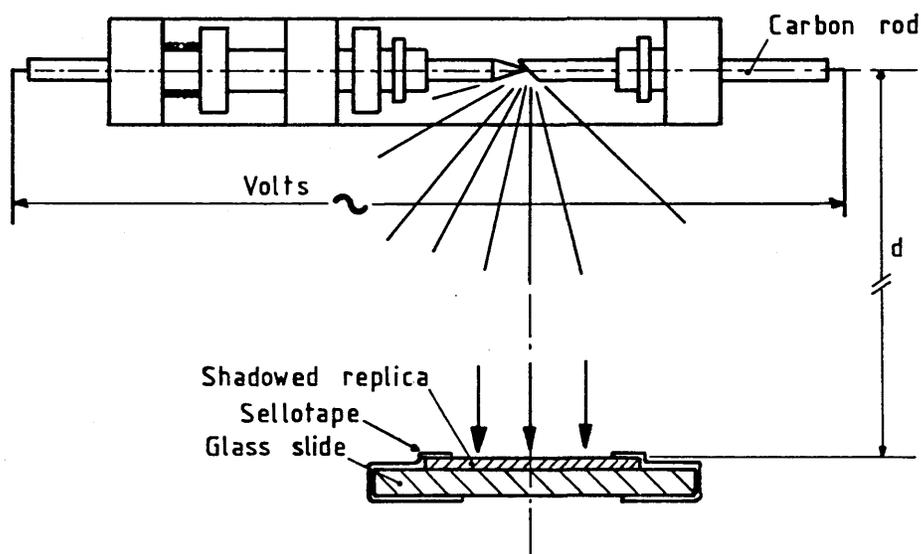
FIG. 76   CARBON COATING PROCESS

Support grids with specimens
Glass cover
Glass container
Copper gauze
Acetone
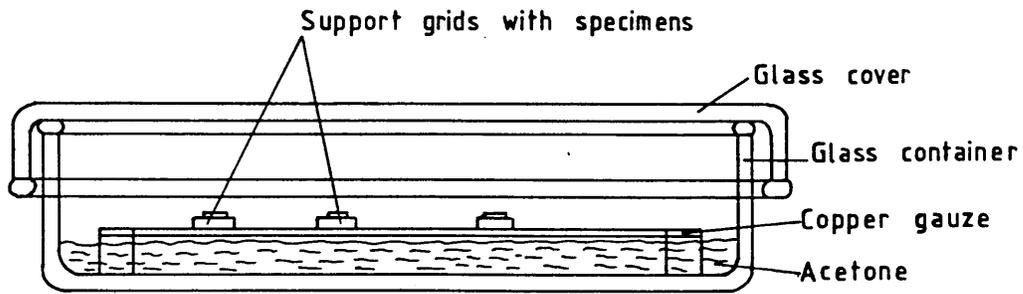
FIG.77 SOAKING OF SPECIMENS TO DISSOLVE
THE PLASTIC REPLICA
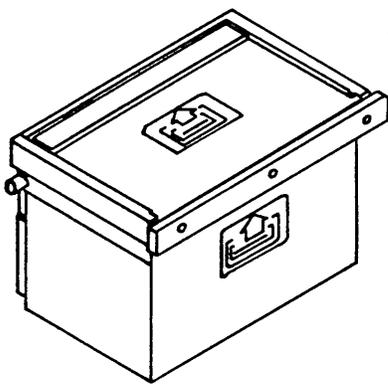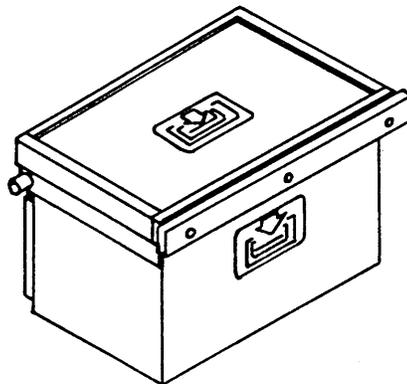
DISPENSING MAGAZINE   RECEIVING MAGAZINE

FIG.78 MAGAZINES FOR PHOTOGRAPHIC PLATES

Emulsion surface

Film

Cassette

Dispensing magazine

Bottom plate

Light-proof lid
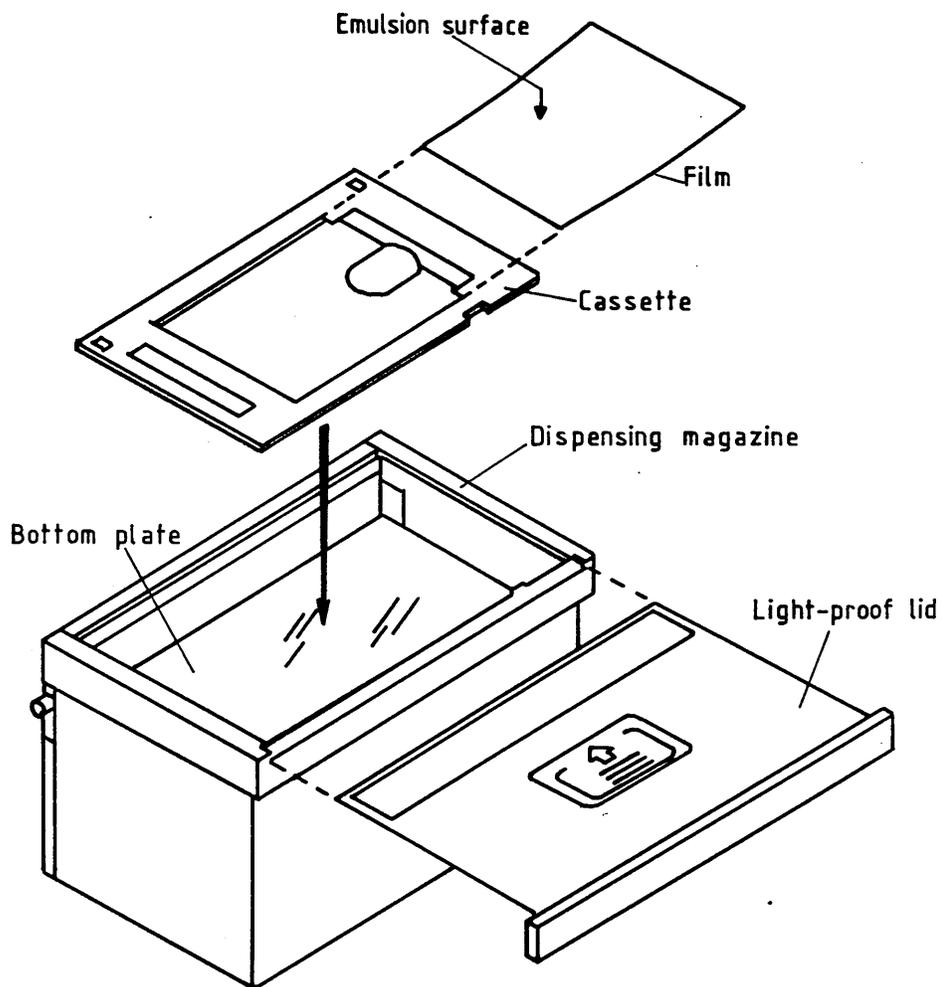
FIG.79 FILM AND CASSETTE

FIG. 80· EFFECT OF CUTTING SPEED ON THE MICROCRACK AREA RATIO

Regression line

$$M_d = 140 \cdot e^{-0.005\,V}$$

$$\underline{r = -0.938}$$

Mat: En 8
t = 0.244 mm
α = + 5°
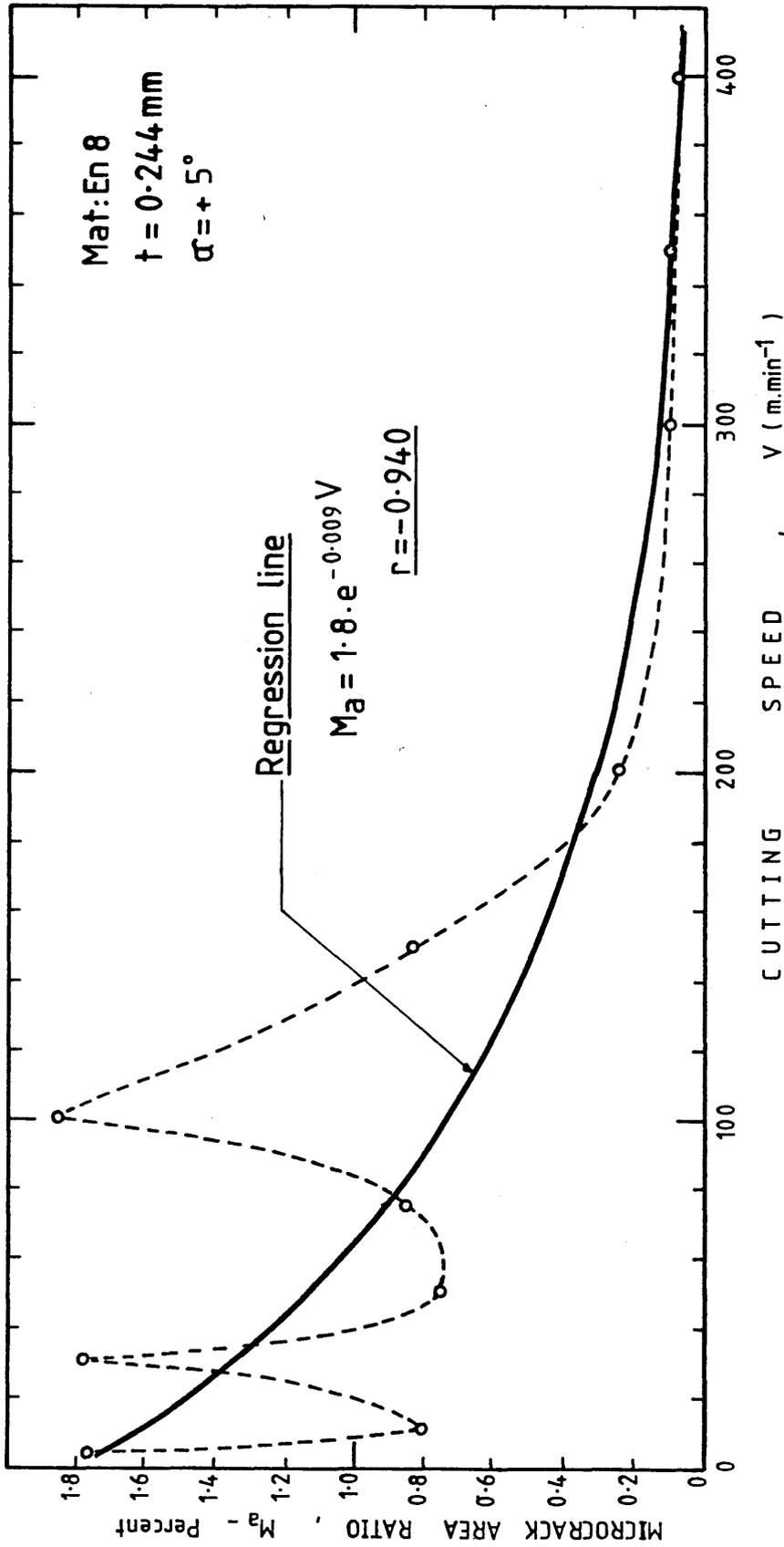
MICROCRACK DENSITY , M_d

CUTTING   SPEED ,   V (m.min^{-1})
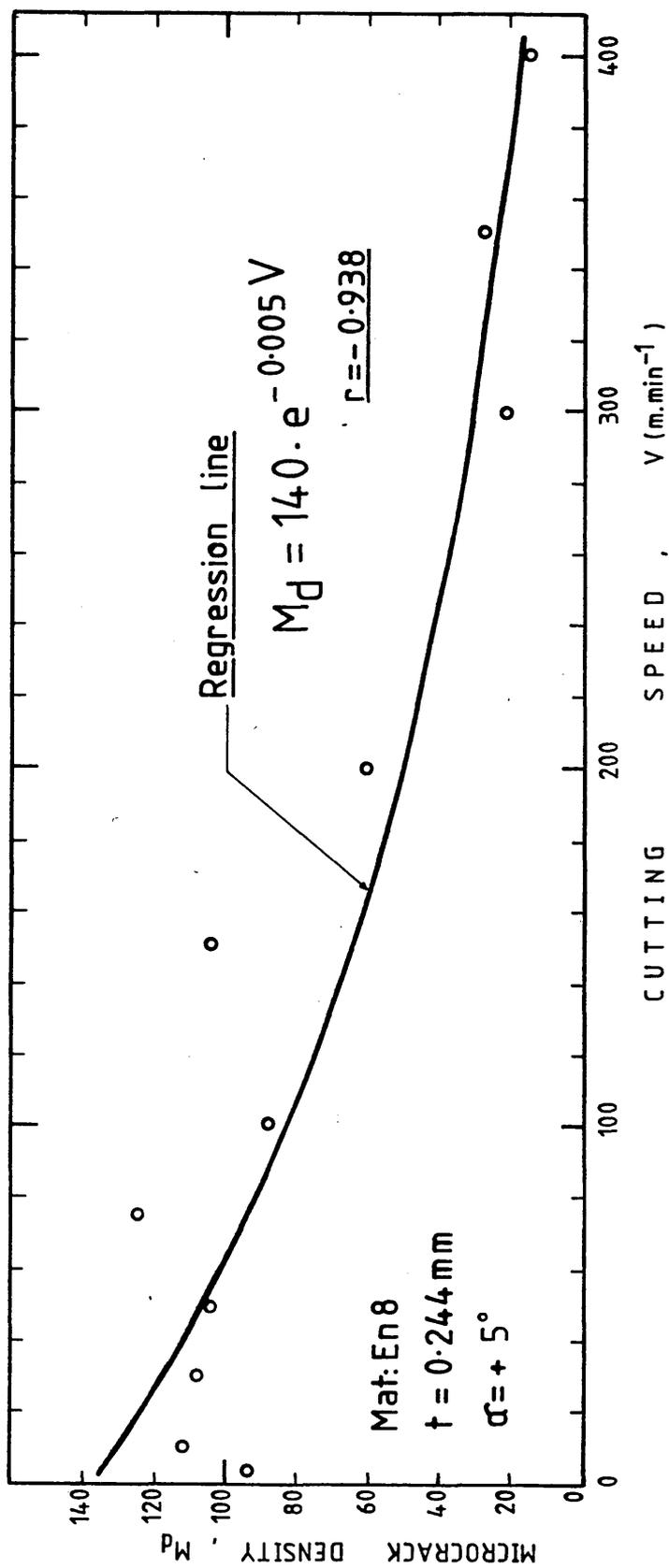
FIG. 81   EFFECT OF CUTTING SPEED ON MICROCRACK DENSITY

FIG. 82 EFFECT OF UNDEFORMED CHIP THICKNESS ON THE MICROCRACK AREA RATIO

The graph shows microcrack density M_d plotted against undeformed chip thickness t (mm).

Axis labels:
MICROCRACK DENSITY , M_d (vertical axis, values 10, 20, 30, 40, 50, 60, 70, 80, 90)

UNDEFORMED CHIP THICKNESS , t (mm) (horizontal axis, values 0, 0.1, 0.2, 0.3, 0.4)

Mat: En 8
$V = 200\,m.min^{-1}$
$\alpha = +5°$

Regression line

$$M_d = \frac{\text{Log } t}{-0.017 + 0.0054\,\text{Log } t}$$

$$r = -0.835$$
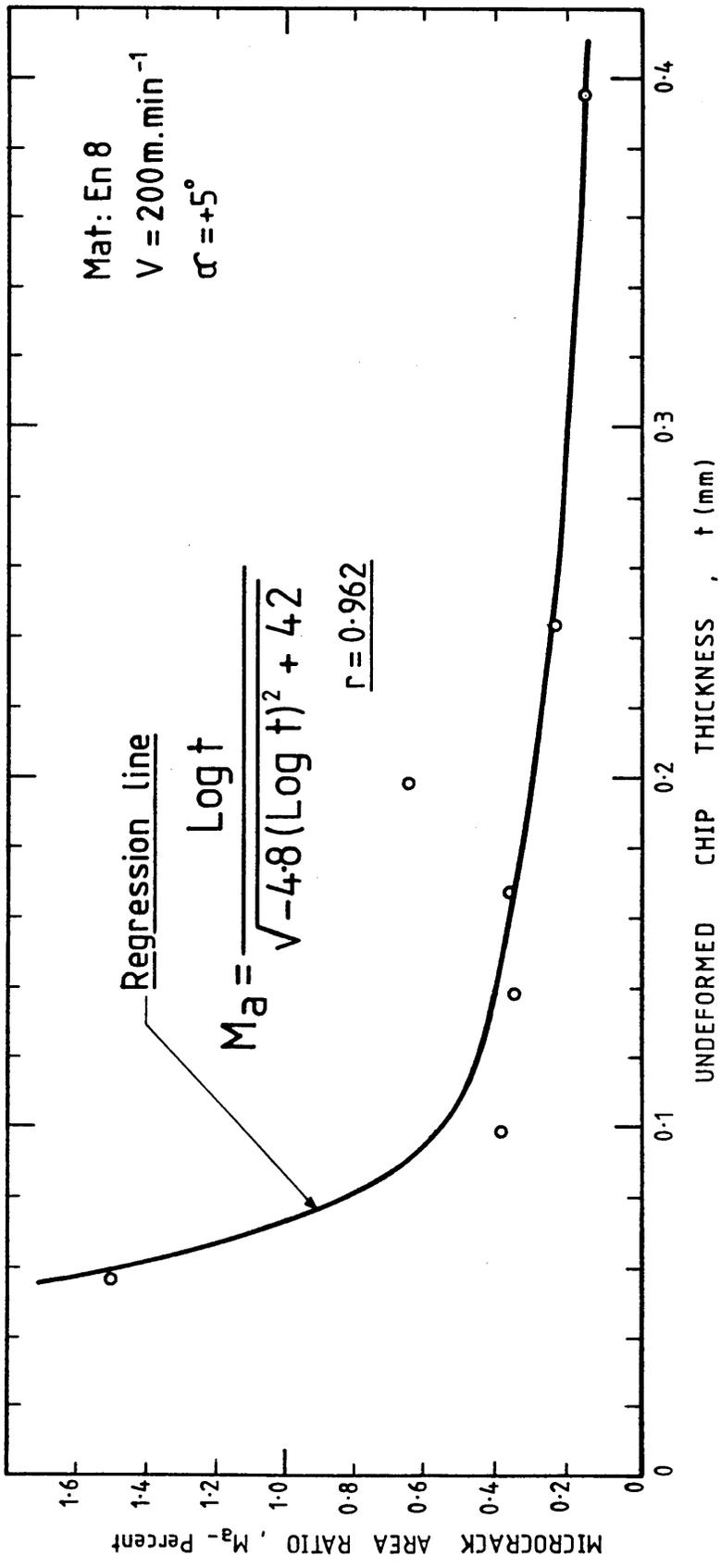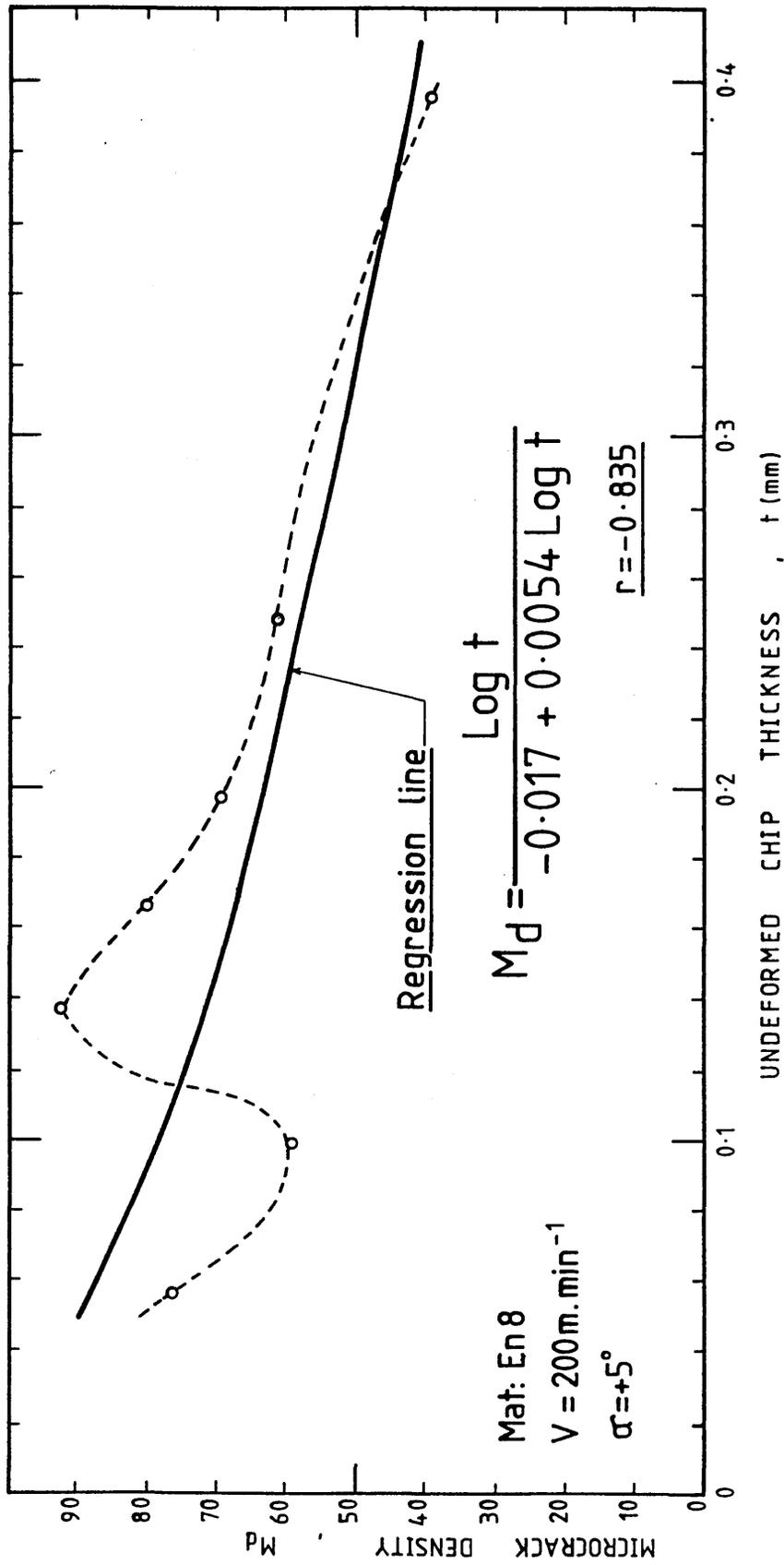
FIG. 83 EFFECT OF UNDEFORMED CHIP THICKNESS ON MICROCRACK DENSITY
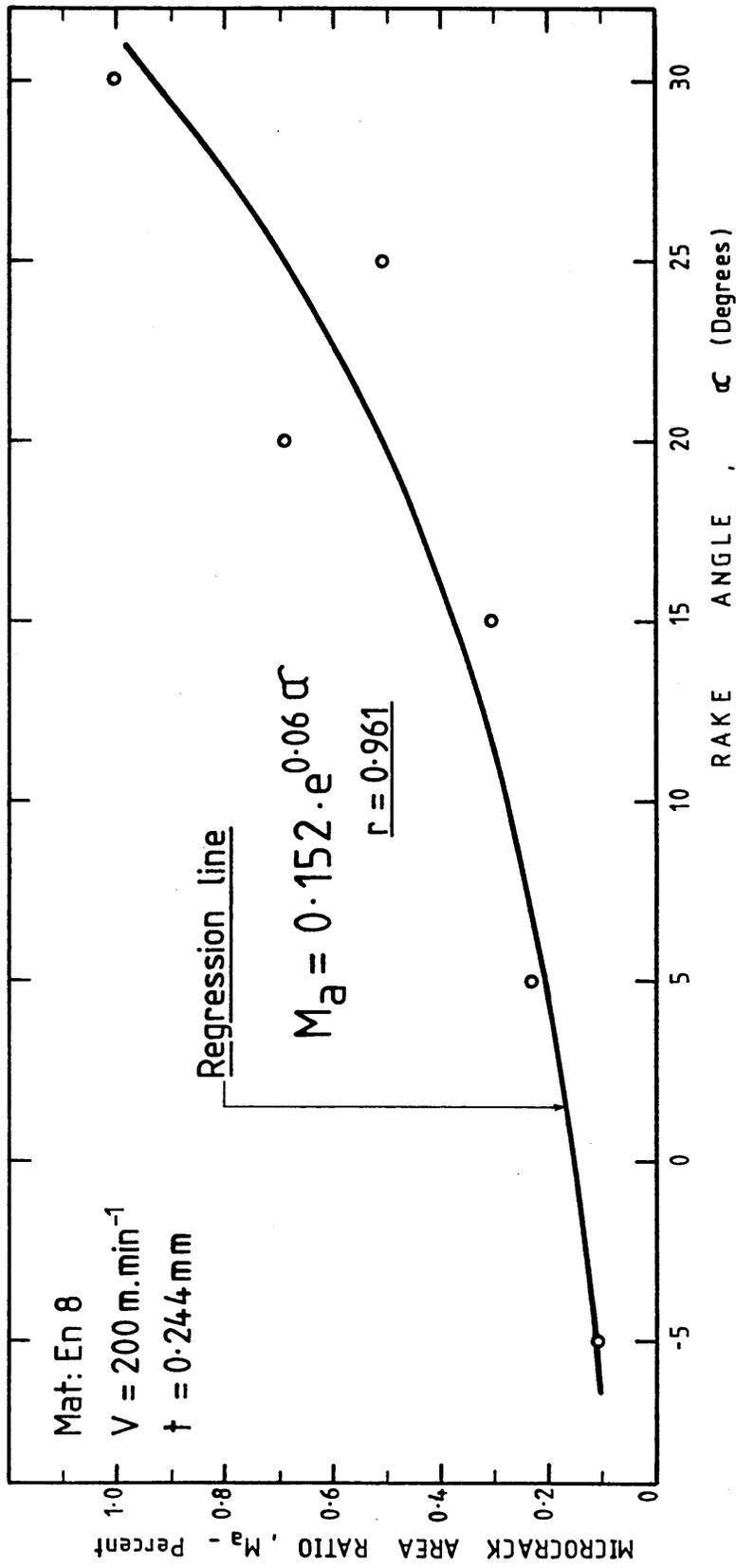
FIG. 84   EFFECT OF RAKE ANGLE ON THE MICROCRACK AREA RATIO
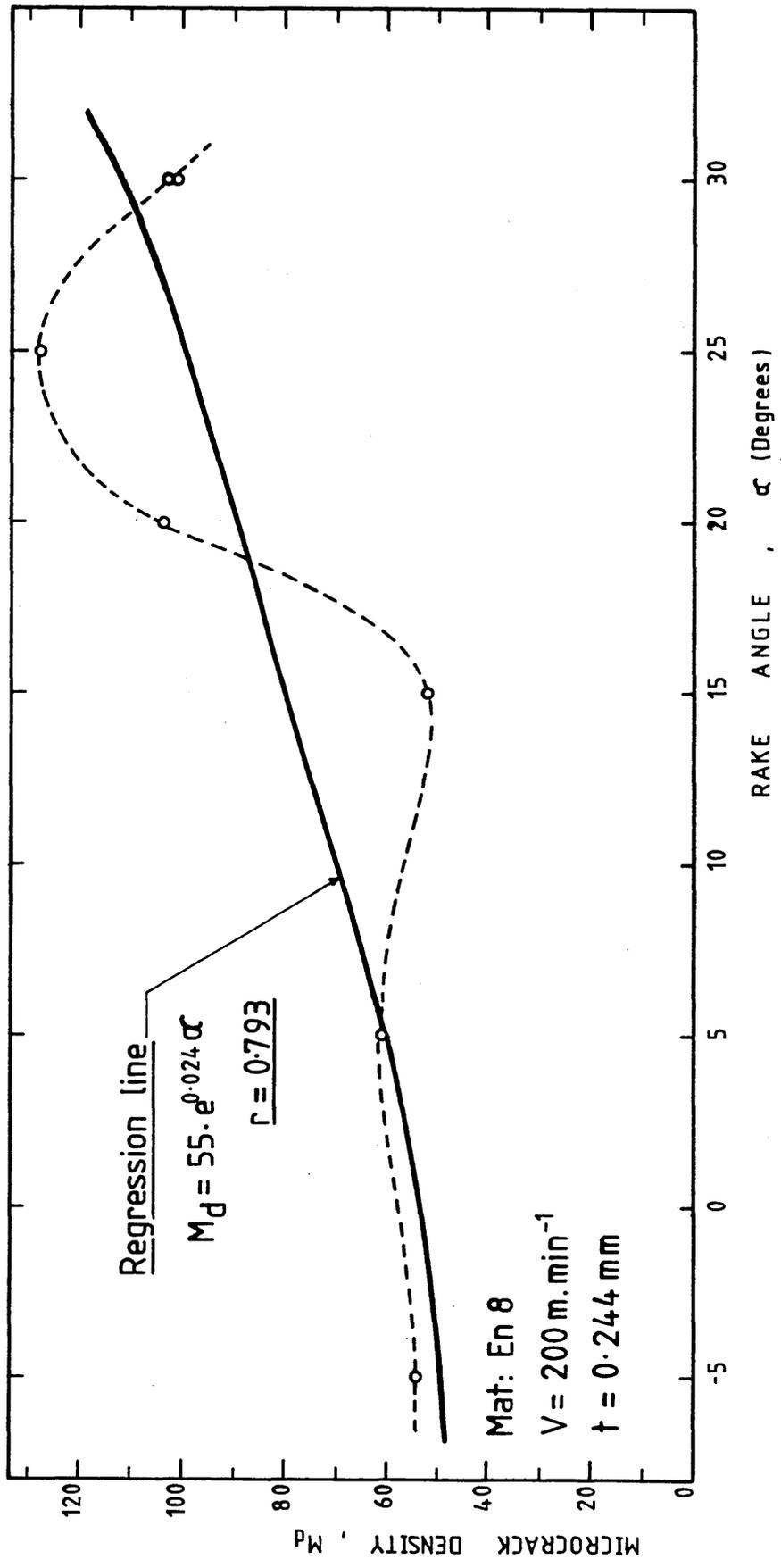
FIG. 85 EFFECT OF RAKE ANGLE ON MICROCRACK DENSITY
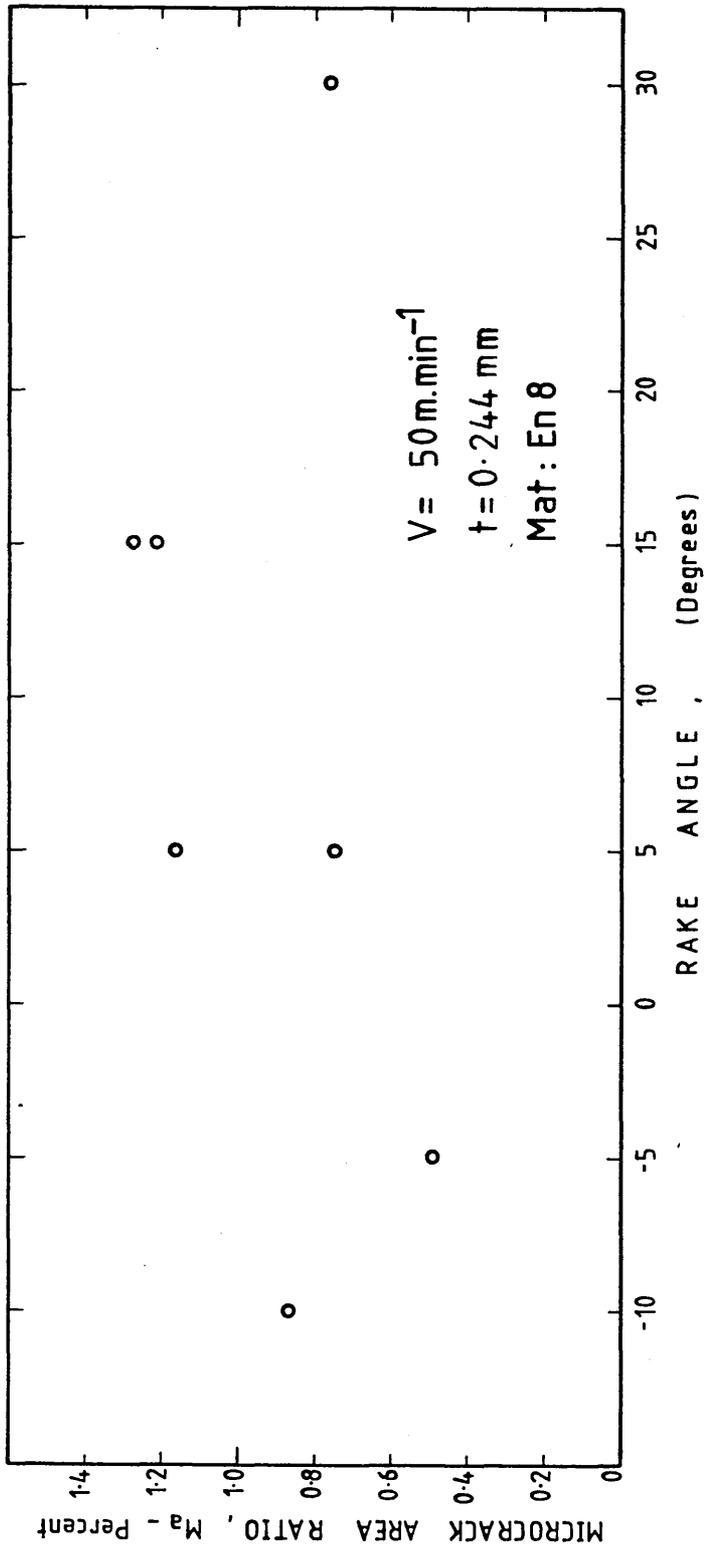
FIG. 86   EFFECT OF RAKE ANGLE ON THE MICROCRACK AREA
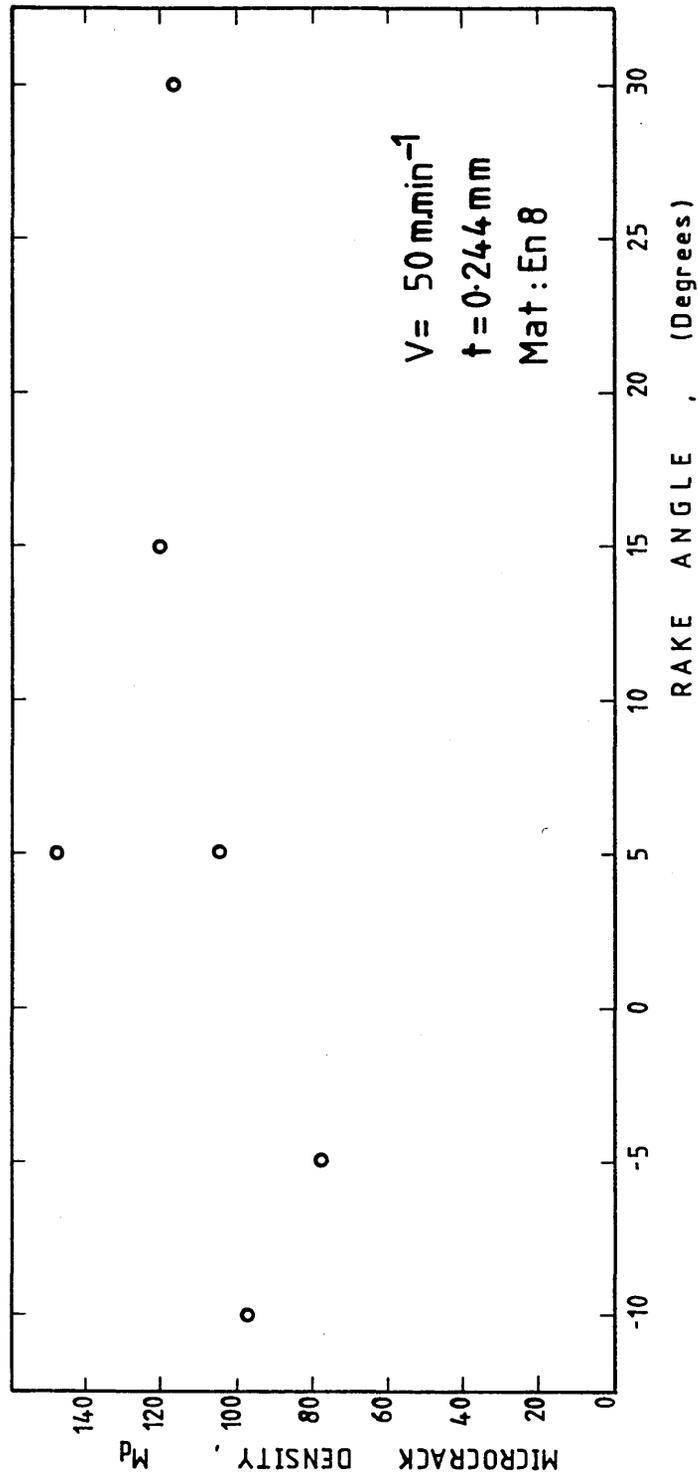
RATIO

FIG. 87 EFFECT OF RAKE ANGLE ON THE MICROCRACK DENSITY
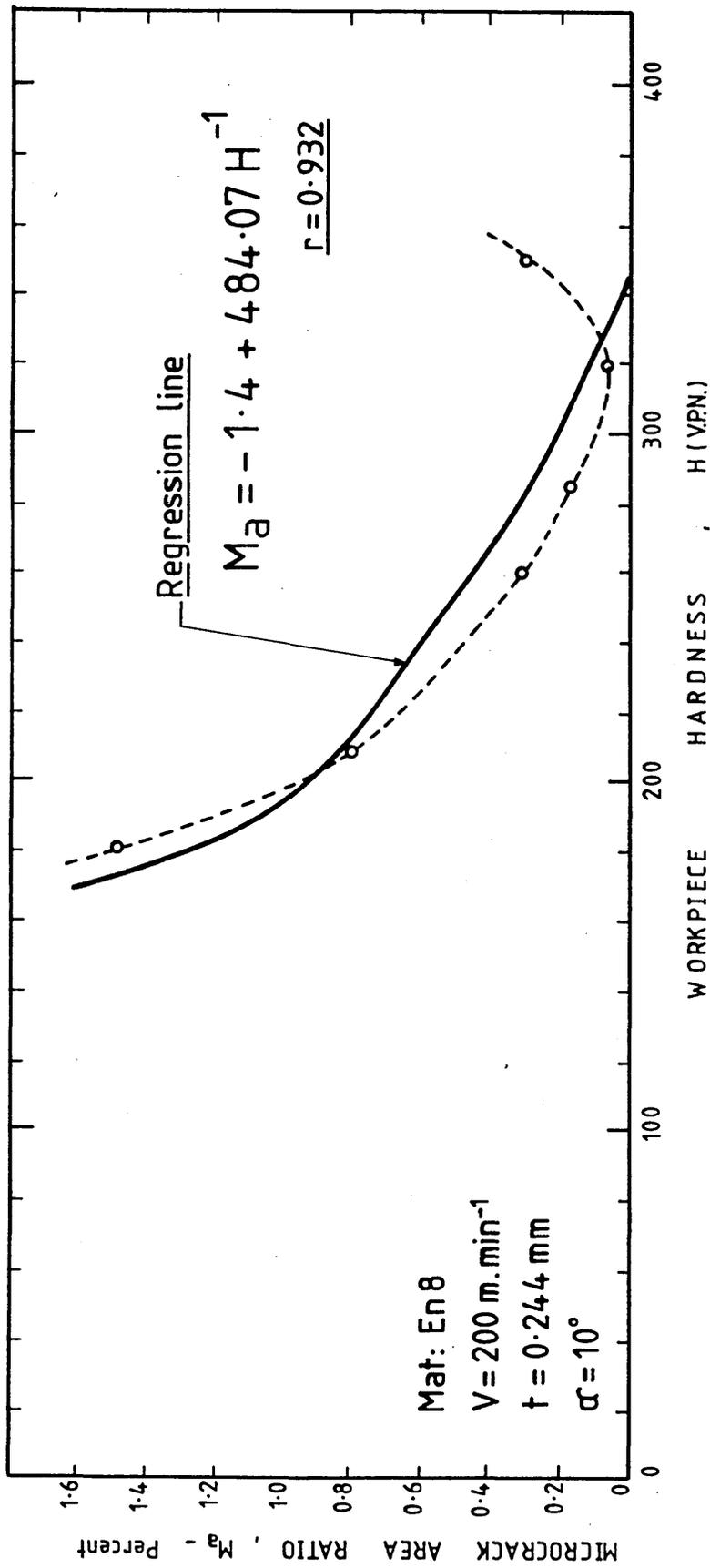
FIG. 88 EFFECT OF WORKPIECE HARDNESS ON THE MICROCRACK
AREA RATIO
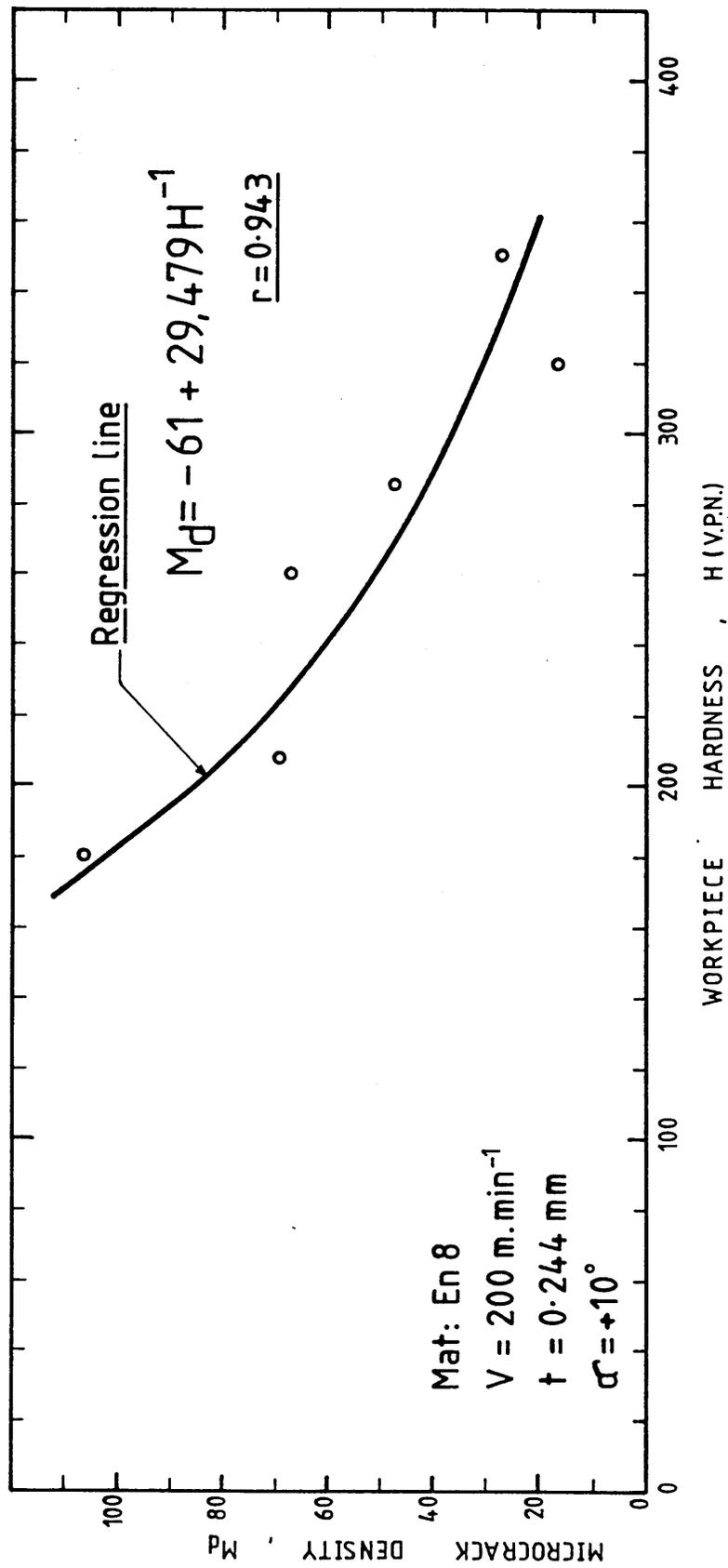
FIG. 89 EFFECT OF WORKPIECE HARDNESS ON MICROCRACK DENSITY
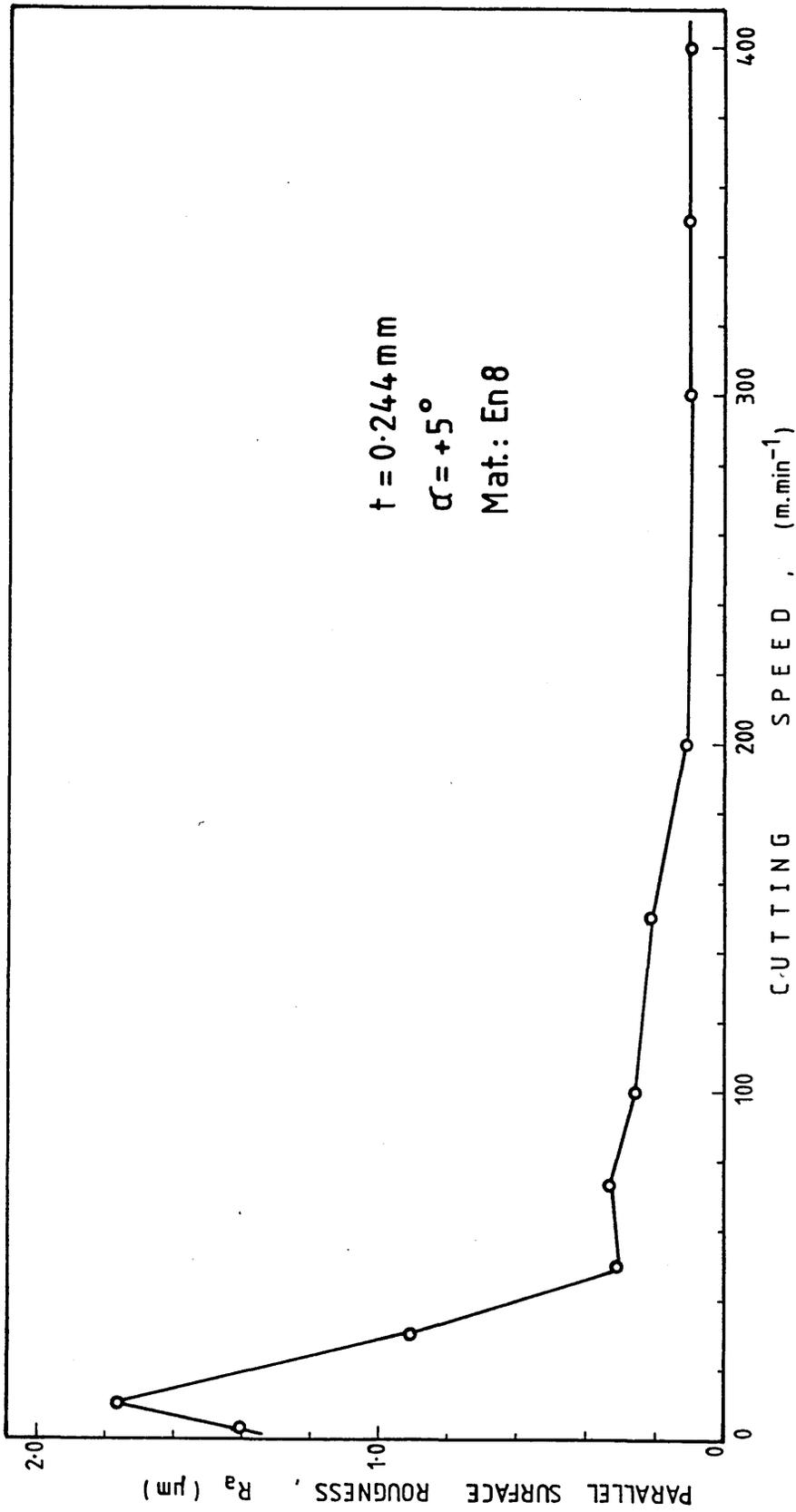
FIG. 90 VARIATION OF PARALLEL SURFACE ROUGHNESS WITH CHANGE IN CUTTING SPEED
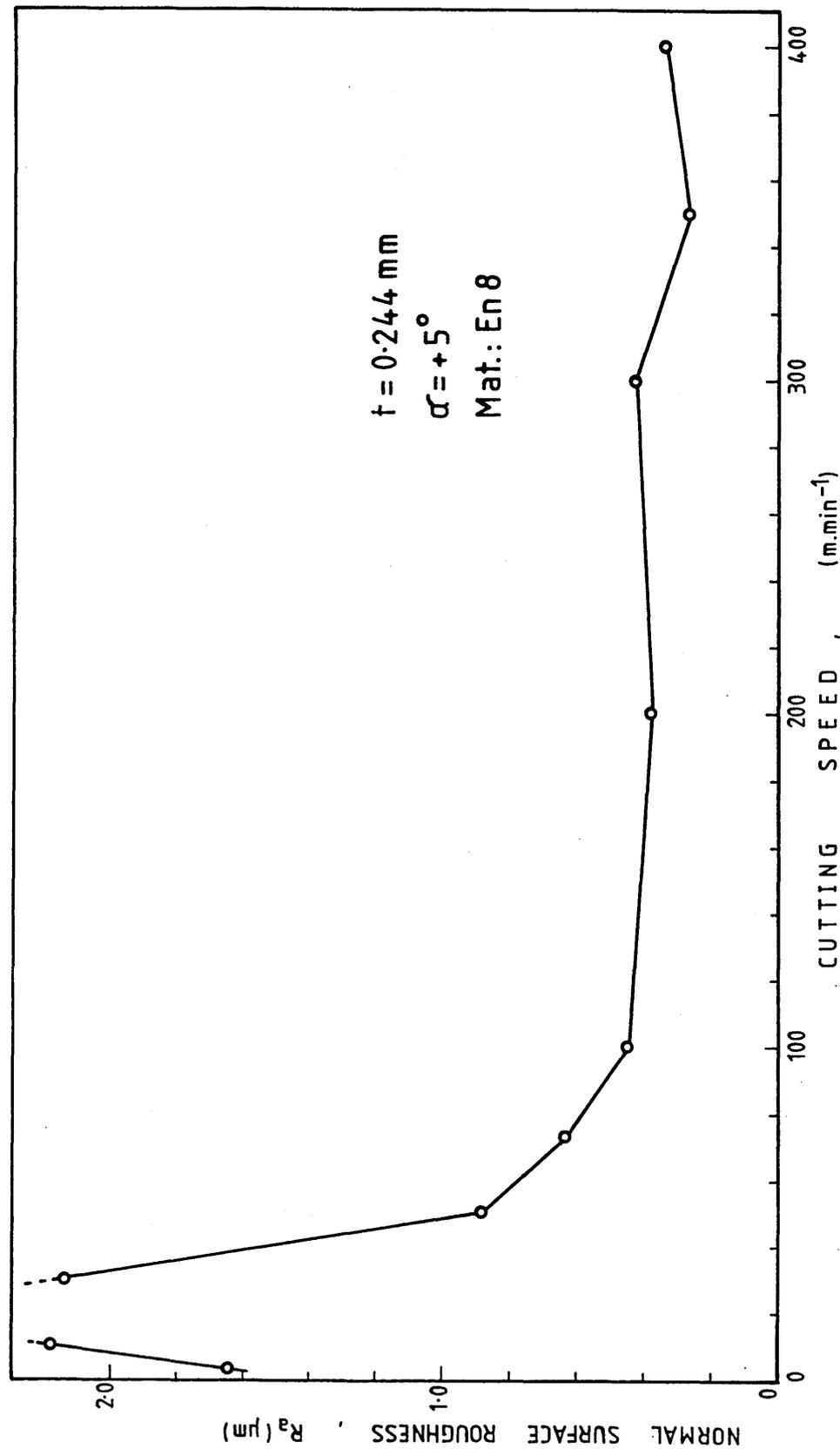
FIG. 91 VARIATION OF NORMAL SURFACE ROUGHNESS WITH CHANGE IN CUTTING SPEED
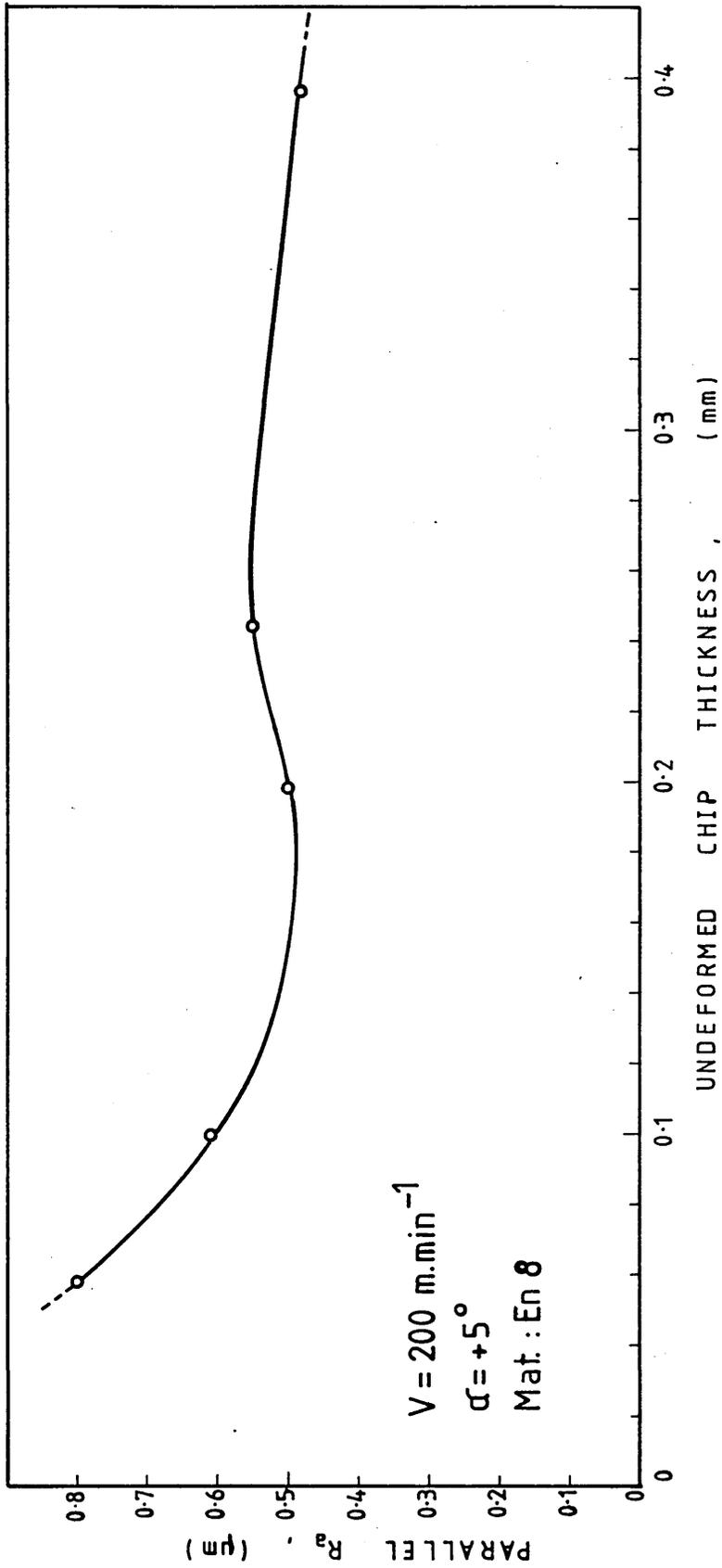
FIG. 92 VARIATION OF PARALLEL SURFACE ROUGHNESS WITH CHANGE IN UNDEFORMED CHIP THICKNESS
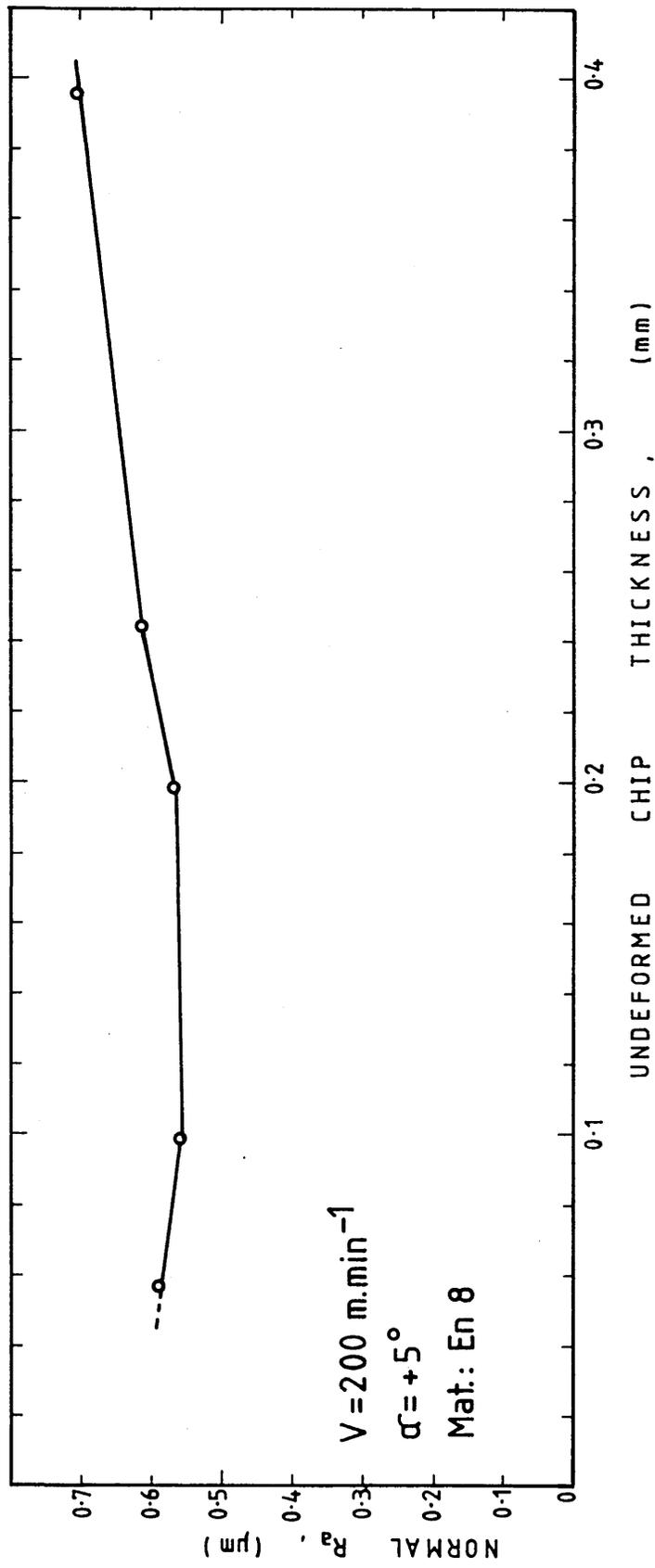
FIG. 93 VARIATION OF NORMAL SURFACE ROUGHNESS WITH CHANGE

IN UNDEFORMED CHIP THICKNESS
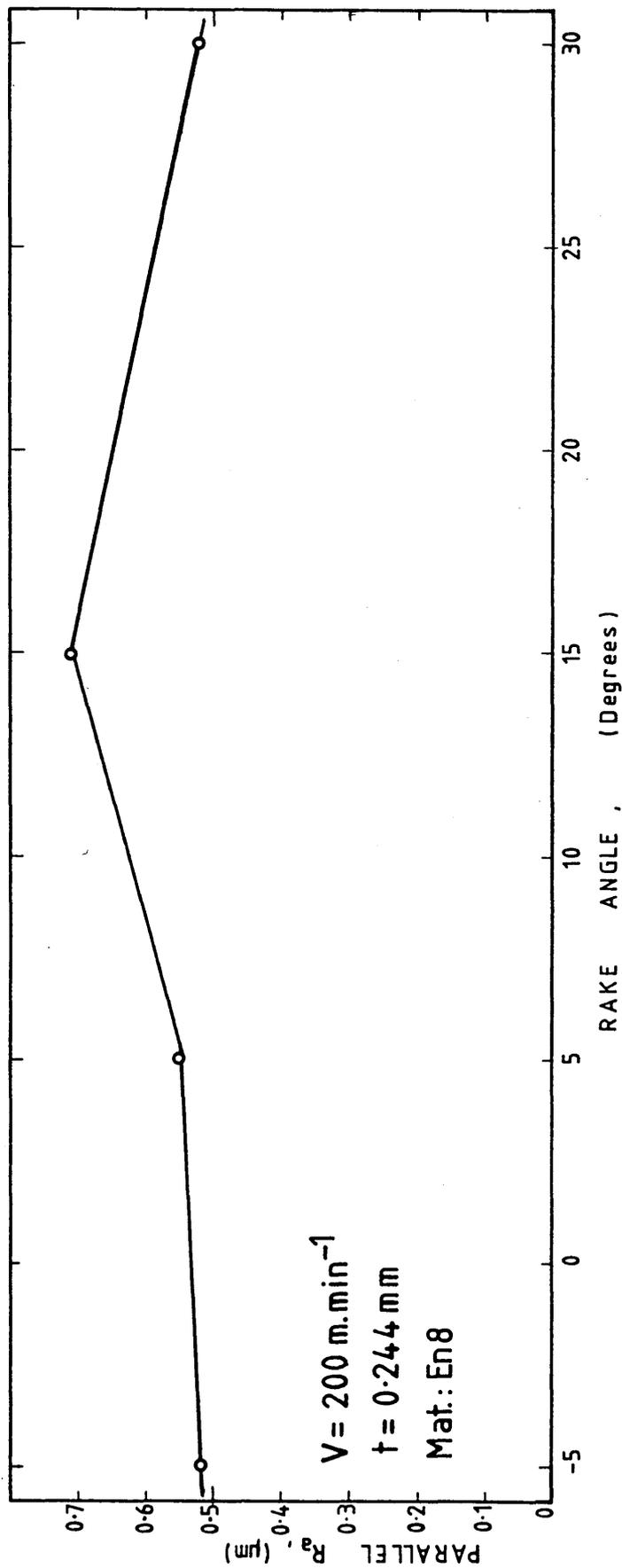
FIG. 94 VARIATION OF PARALLEL SURFACE ROUGHNESS WITH CHANGE IN RAKE ANGLE
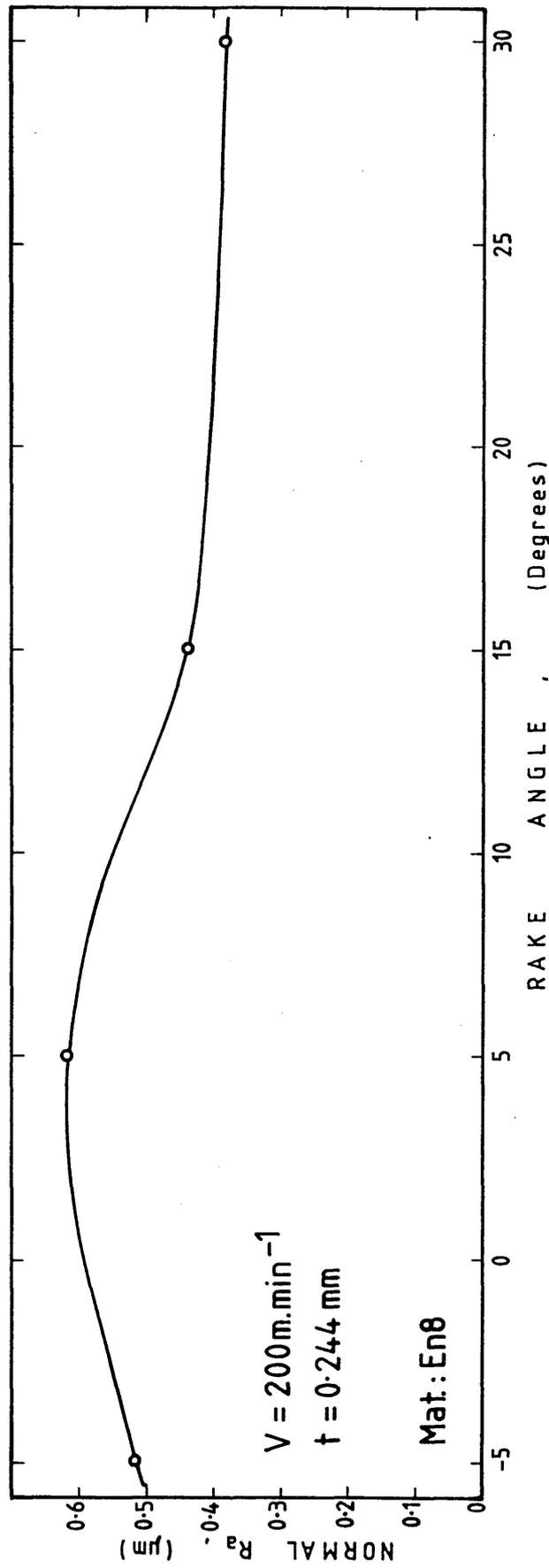
FIG. 95 VARIATION OF NORMAL SURFACE ROUGHNESS WITH CHANGE
IN RAKE ANGLE

-261-
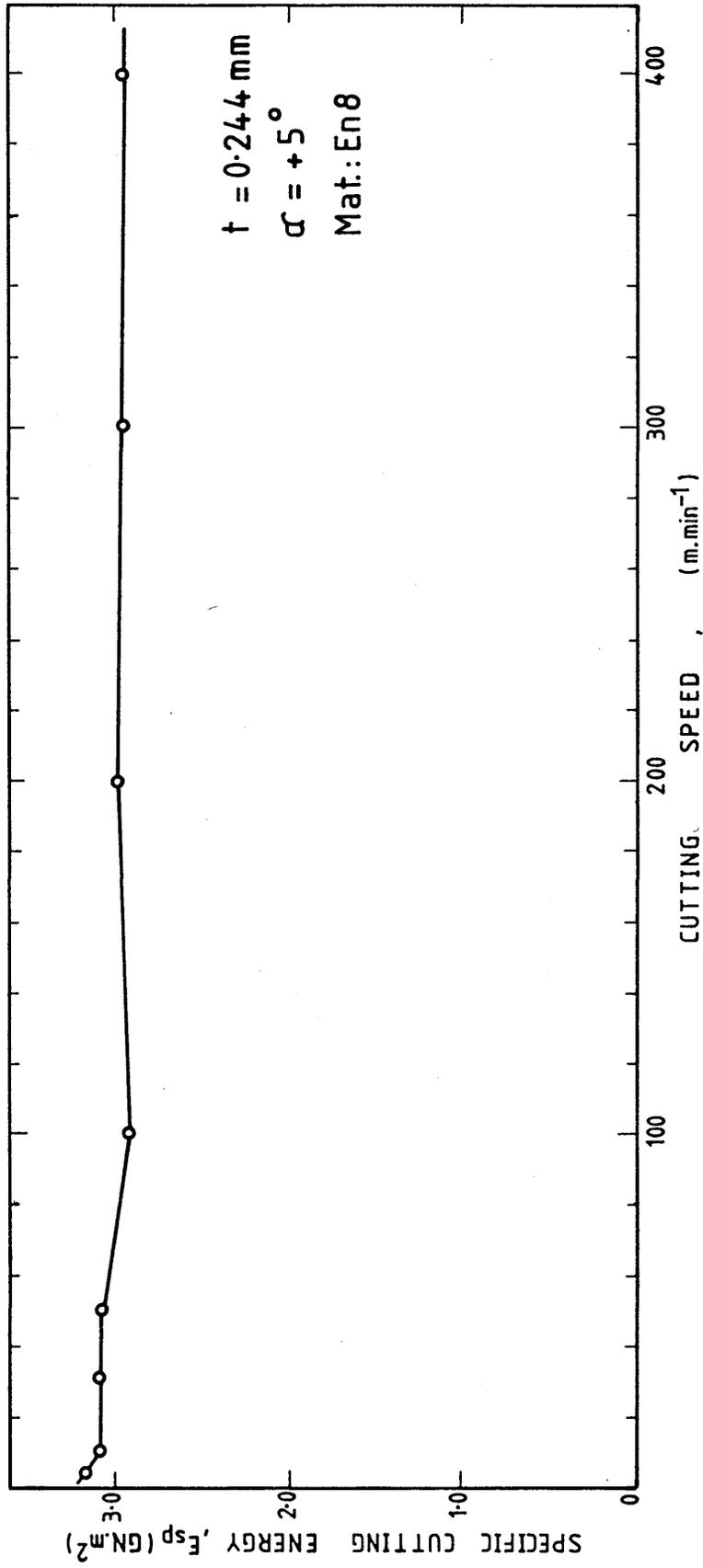
FIG.96 VARIATION OF SPECIFIC CUTTING ENERGY WITH CHANGE IN CUTTING SPEED
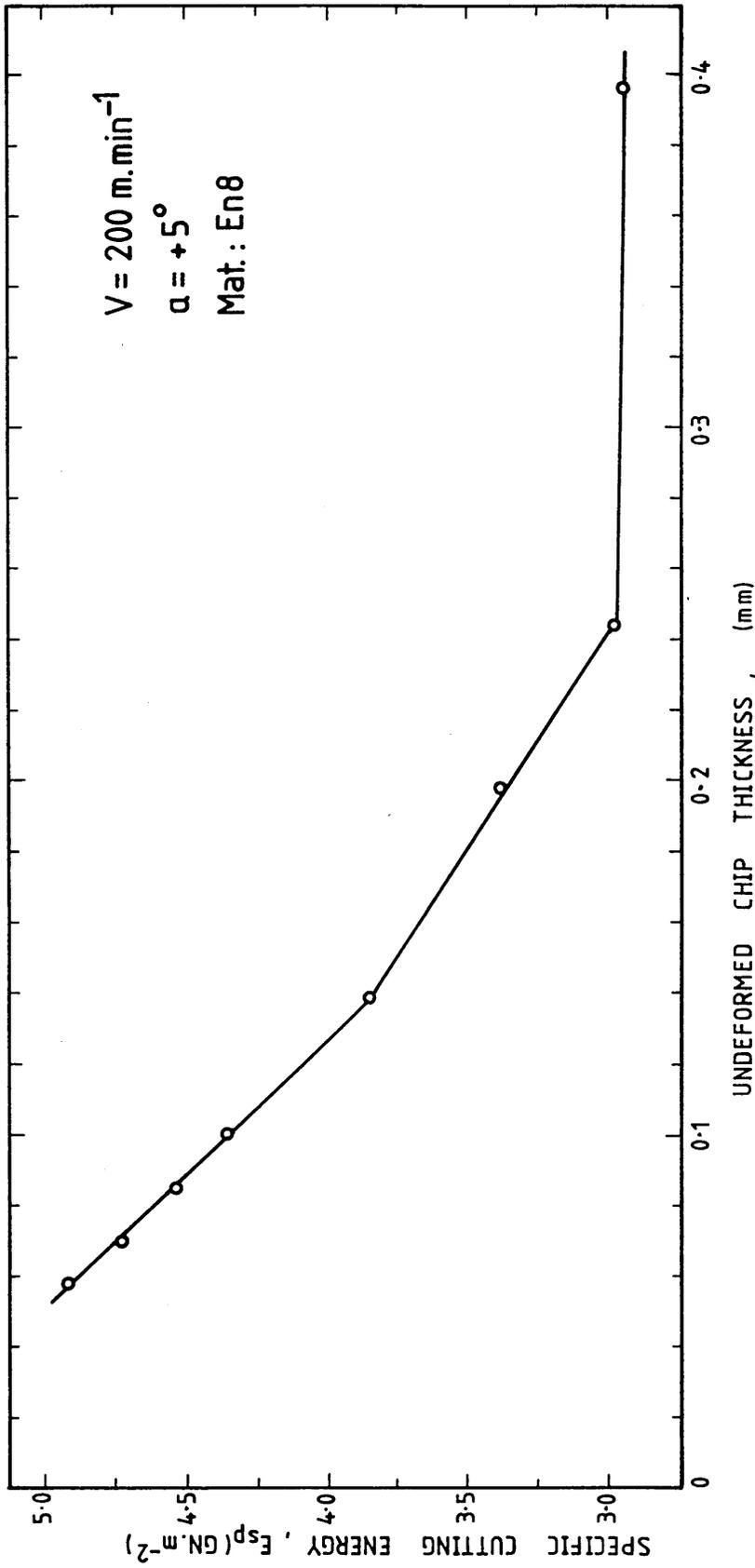
FIG. 97 VARIATION OF SPECIFIC CUTTING ENERGY WITH CHANGE IN UNDEFORMED CHIP THICKNESS
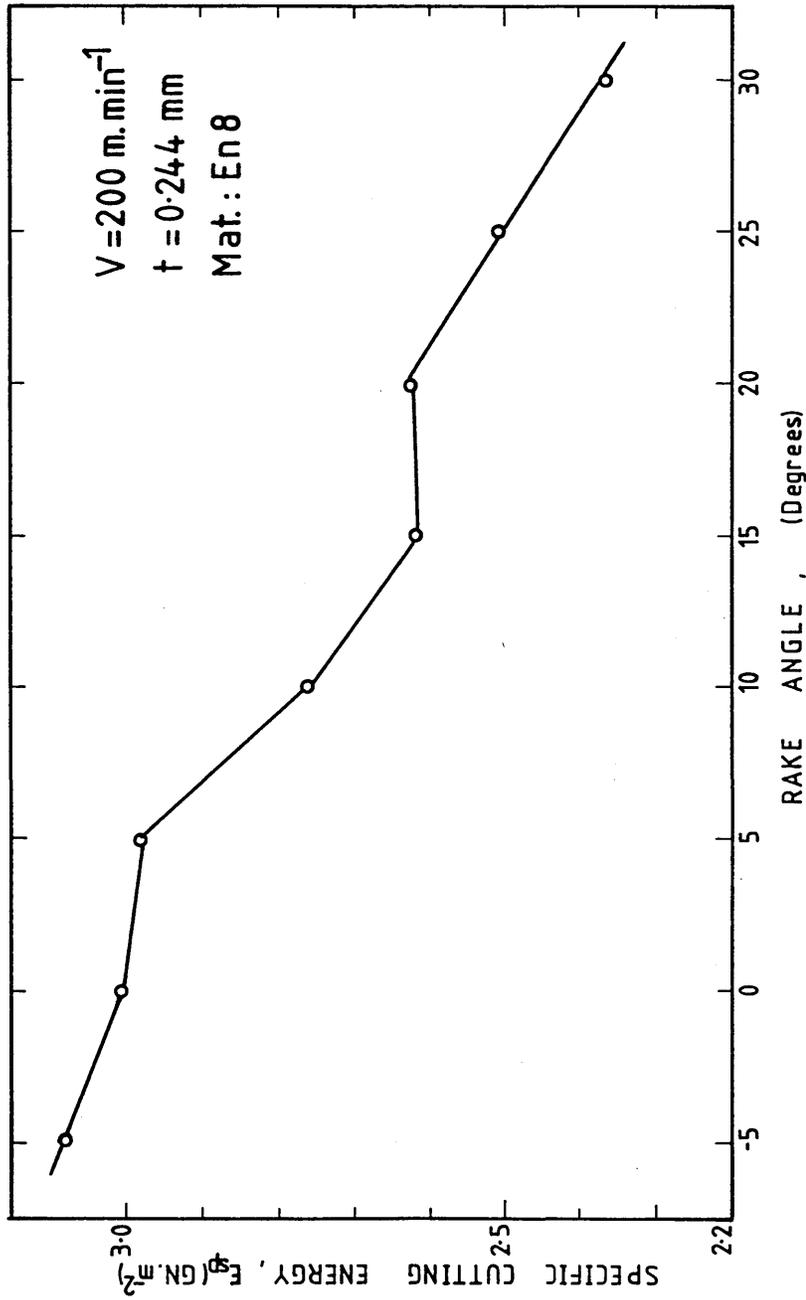
FIG. 98 VARIATION OF SPECIFIC CUTTING ENERGY WITH CHANGE
IN RAKE ANGLE

- 264 -
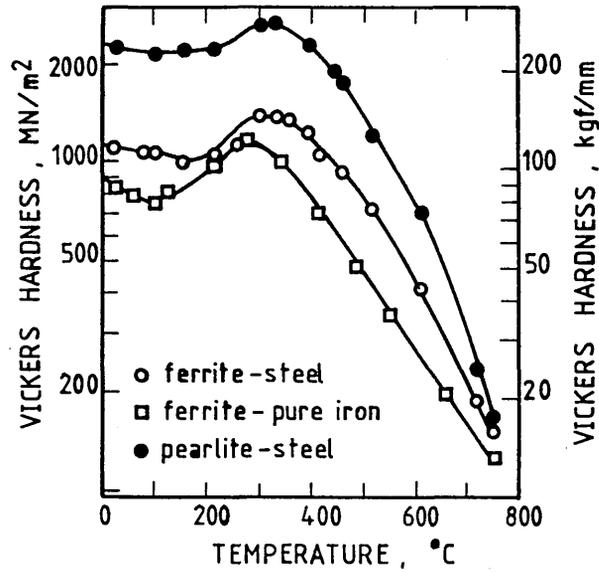
FIG.99 EFFECT OF TEMPERATURE ON THE FERRITE AND PEARLITE HARDNESS

(Ref. 143)
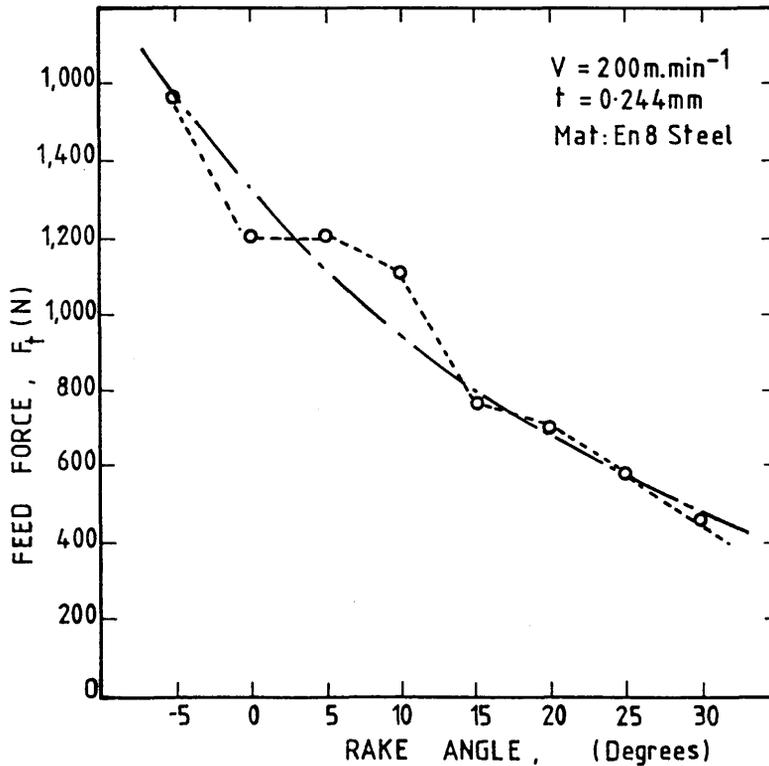
FIG.100 VARIATION OF FEED FORCE WITH CHANGE IN RAKE ANGLE

(a)

CHIP

BUILT-UP-EDGE

TOOL

MACHINED SURFACE

Length over which
shearing takes place

(b)

Built-up-edge

Shear stress

$\sigma_{tensile}$

Tool

Machined surface
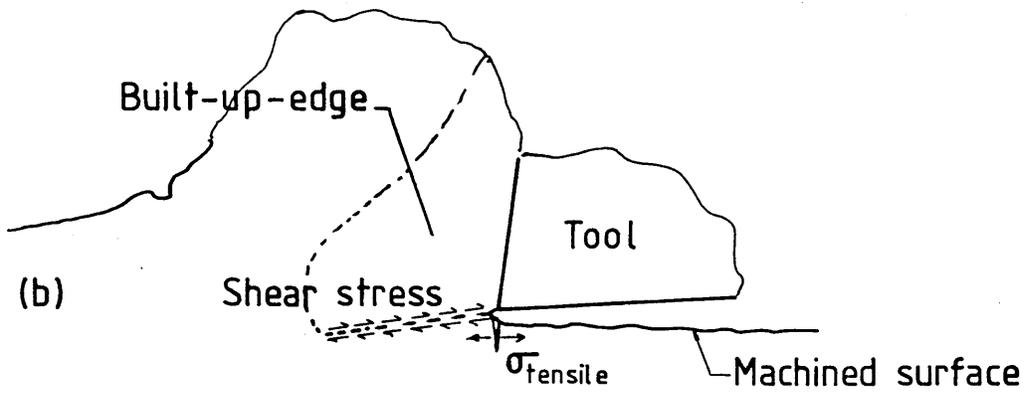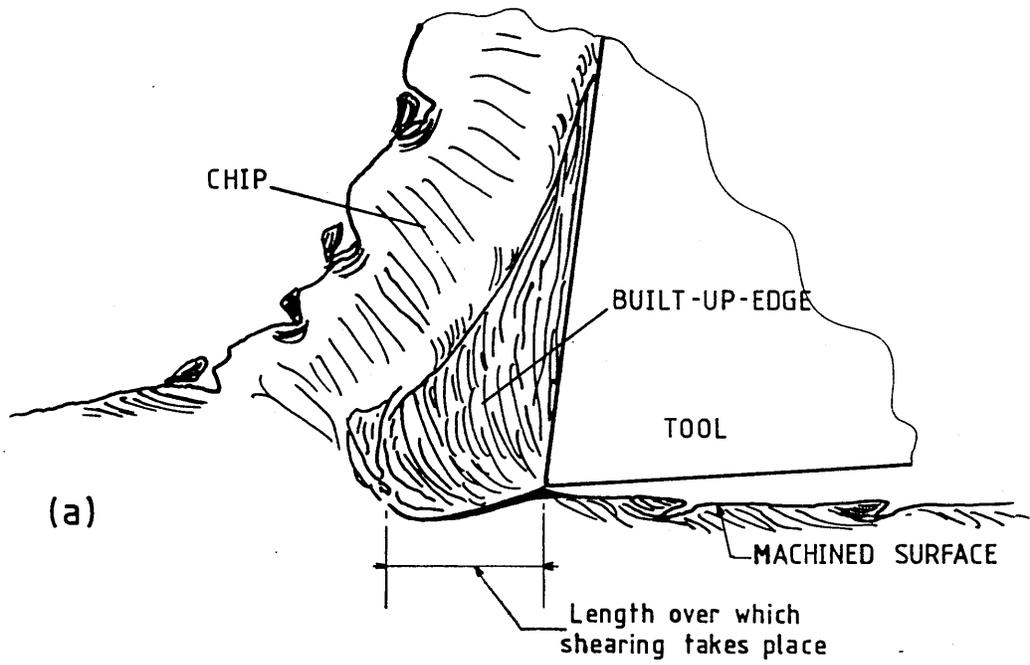
FIG.101   EFFECT OF BUILT-UP-EDGE ON THE
SHEARING OF SURFACE LAYER
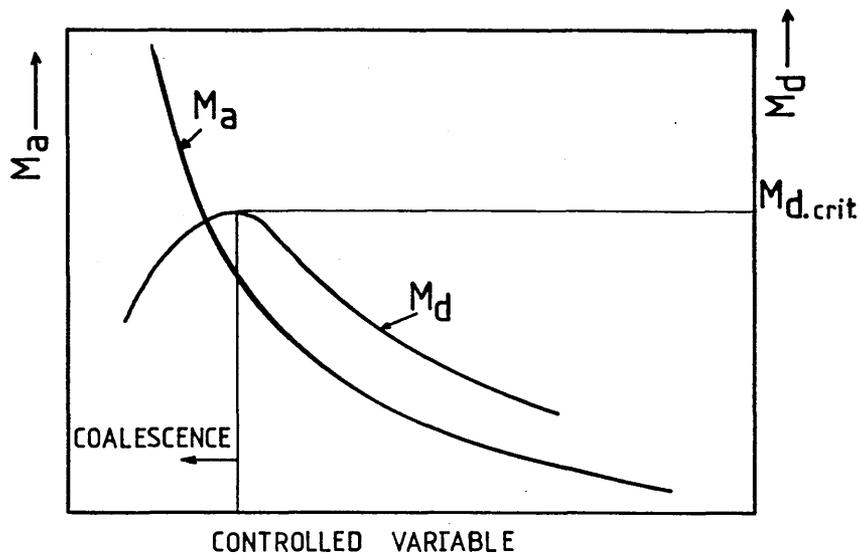
FIG.102 PROPOSED MODEL OF THE MICROCRACK
COALESCENCE PHENOMENON
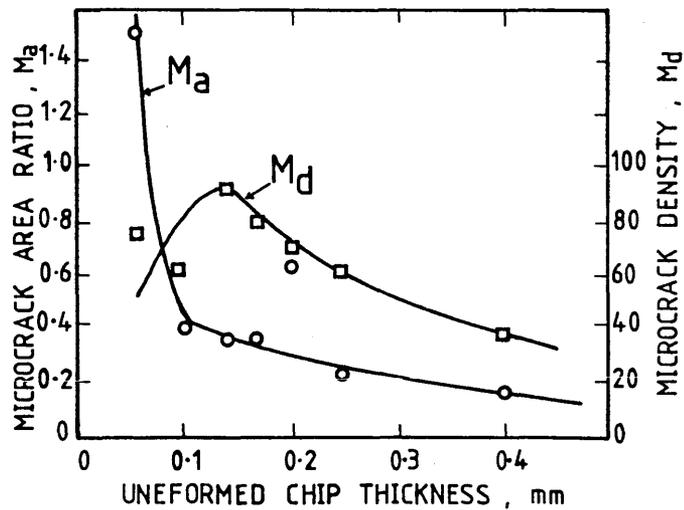
FIG.103 MICROCRACK COALESCENCE (EFFECT OF
UNEFORMED CHIP THICKNESS)
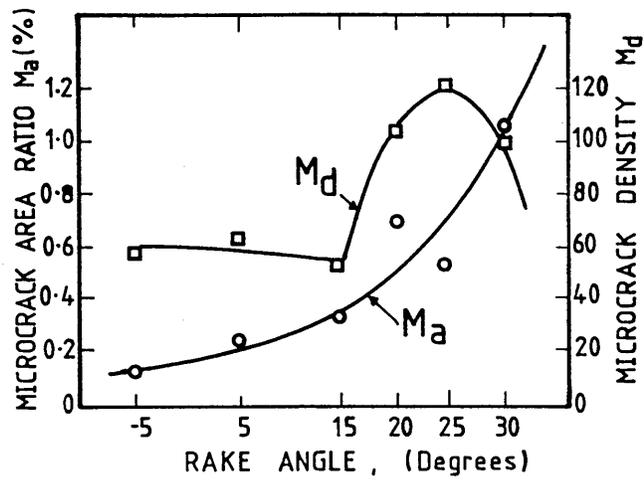
FIG.104 MICROCRACK COALESCENCE (EFFECT OF RAKE ANGLE)
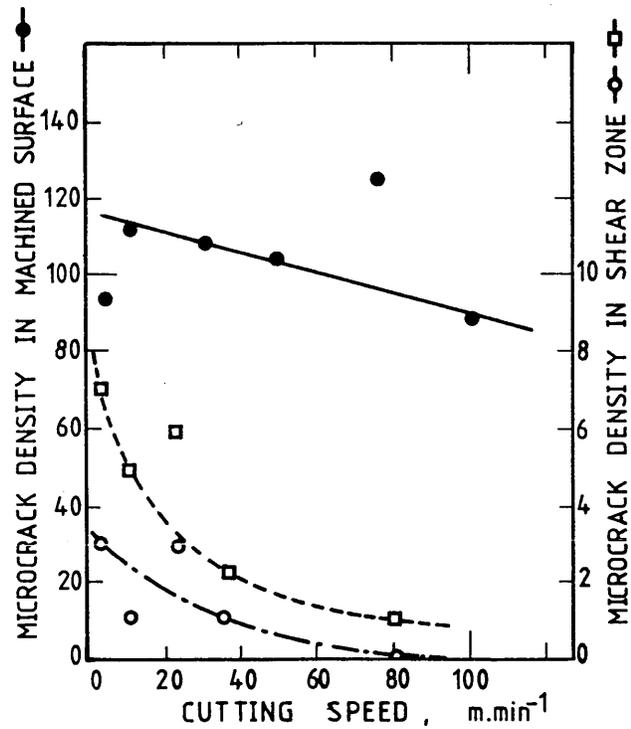
FIG.105 COMPARISON BETWEEN MICROCRACK DENSITY IN MACHINED SURFACE AND MICROCRACK DENSITY IN SHEAR ZONE
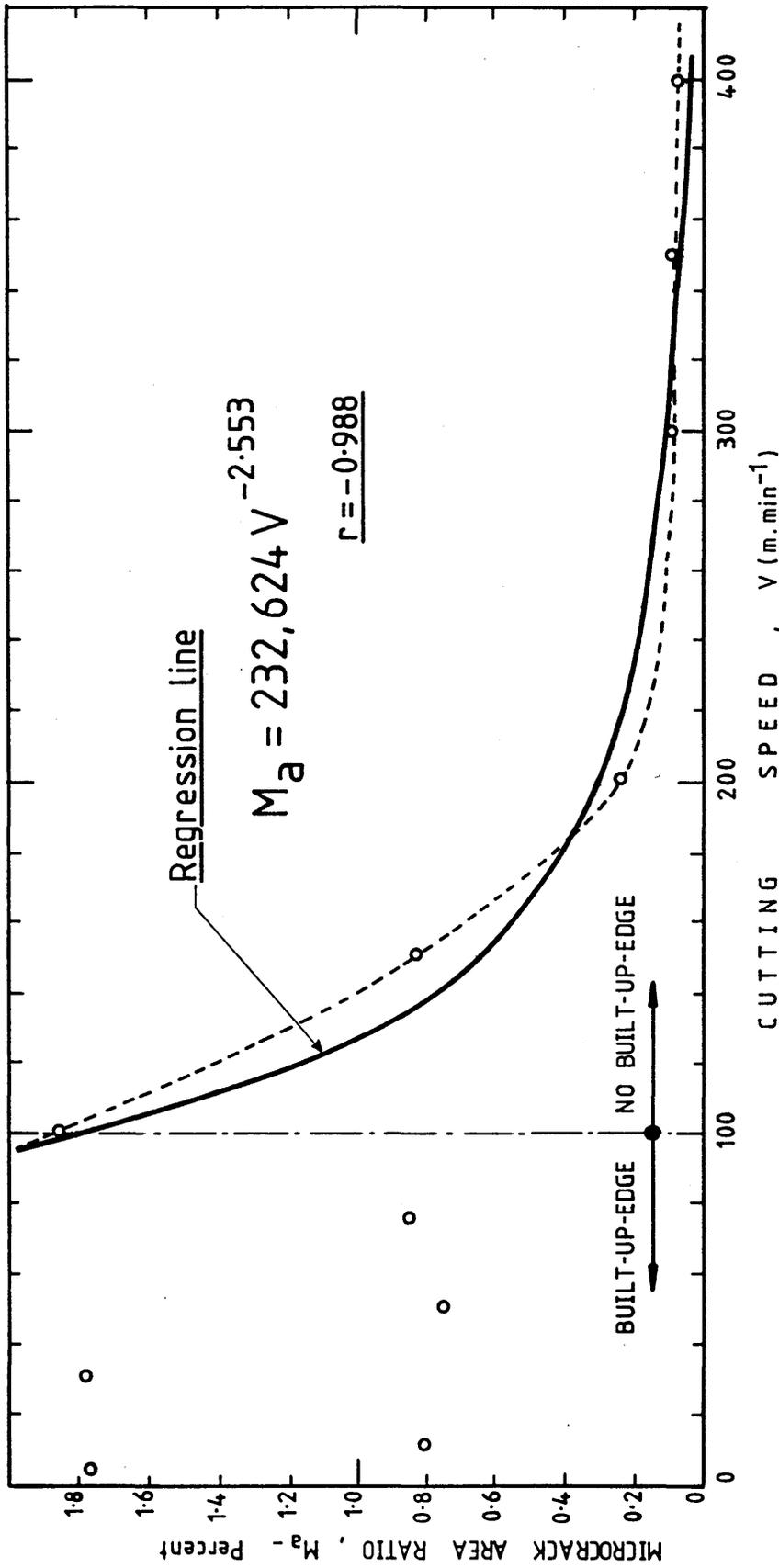
FIG. 106 VARIATION OF MICROCRACK AREA RATIO WITH CHANGE IN CUTTING SPEED FOR CONDITIONS OF NO BUILT-UP-EDGE
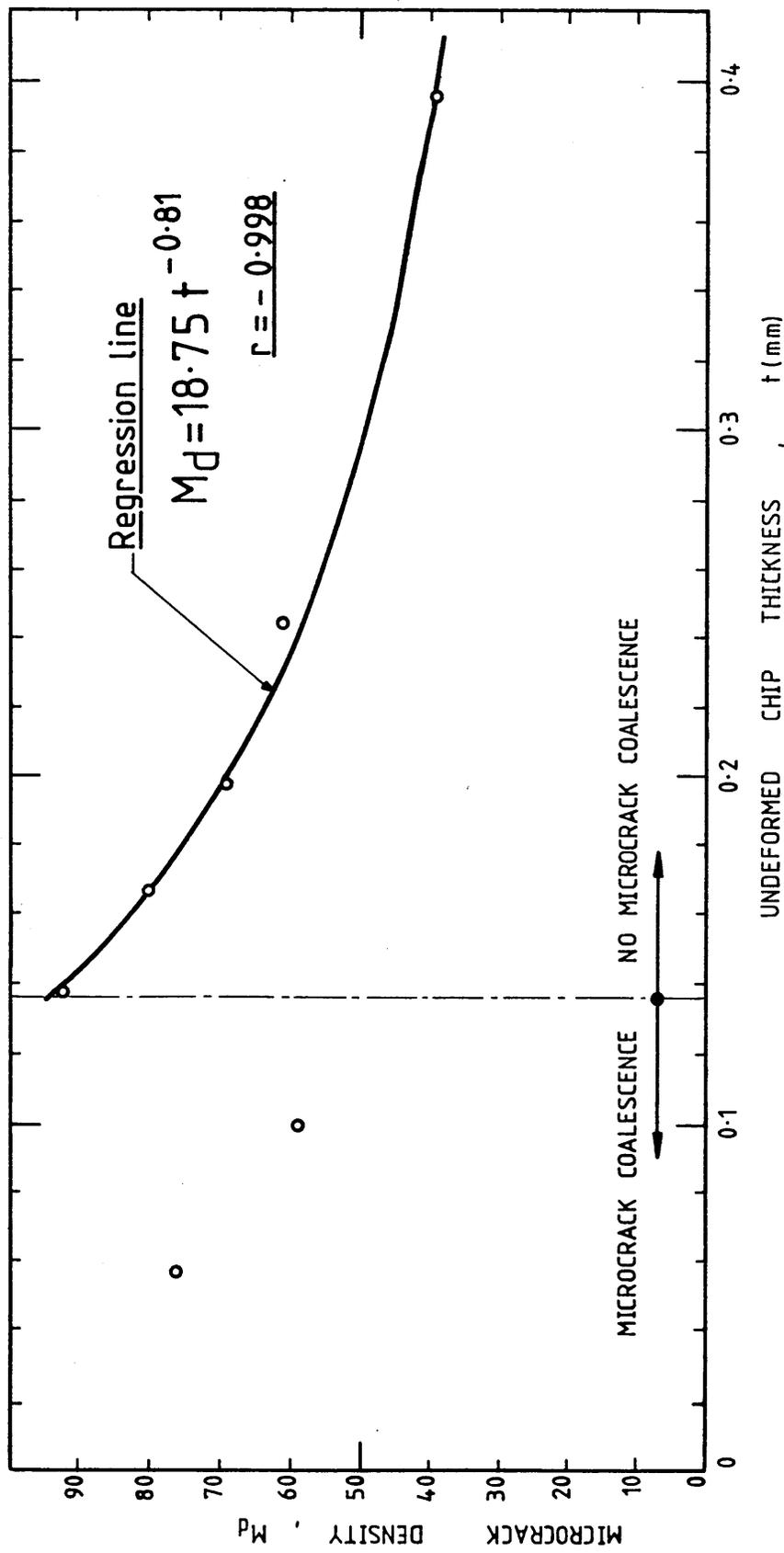
FIG.107 VARIATION OF MICROCRACK DENSITY WITH UNDEFORMED CHIP THICKNESS FOR CONDITIONS OF NO MICROCRACK COALESCENCE
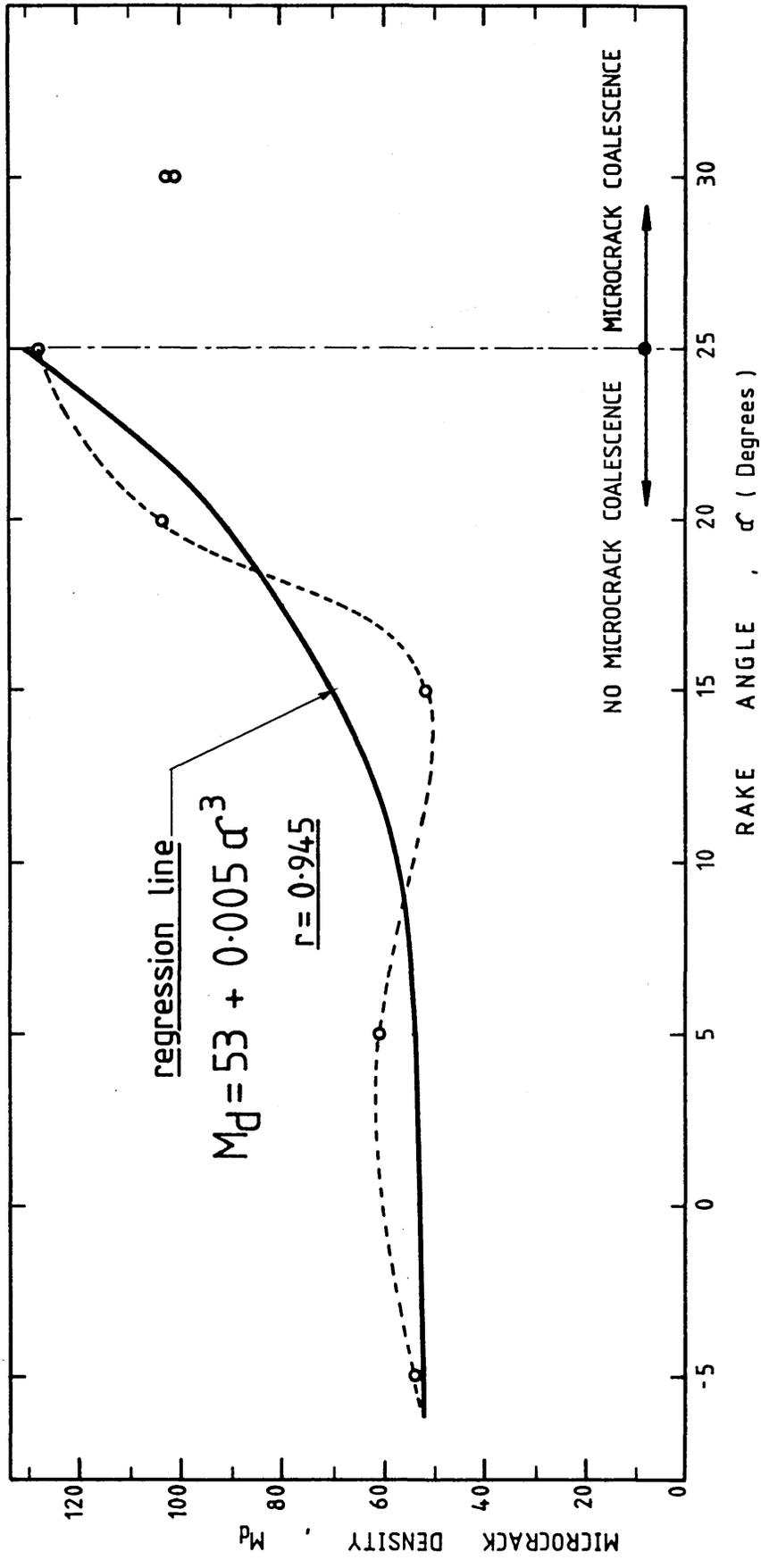
FIG.108 VARIATION OF MICROCRACK DENSITY WITH RAKE ANGLE FOR CONDITIONS OF NO MICROCRACK COALESCENCE
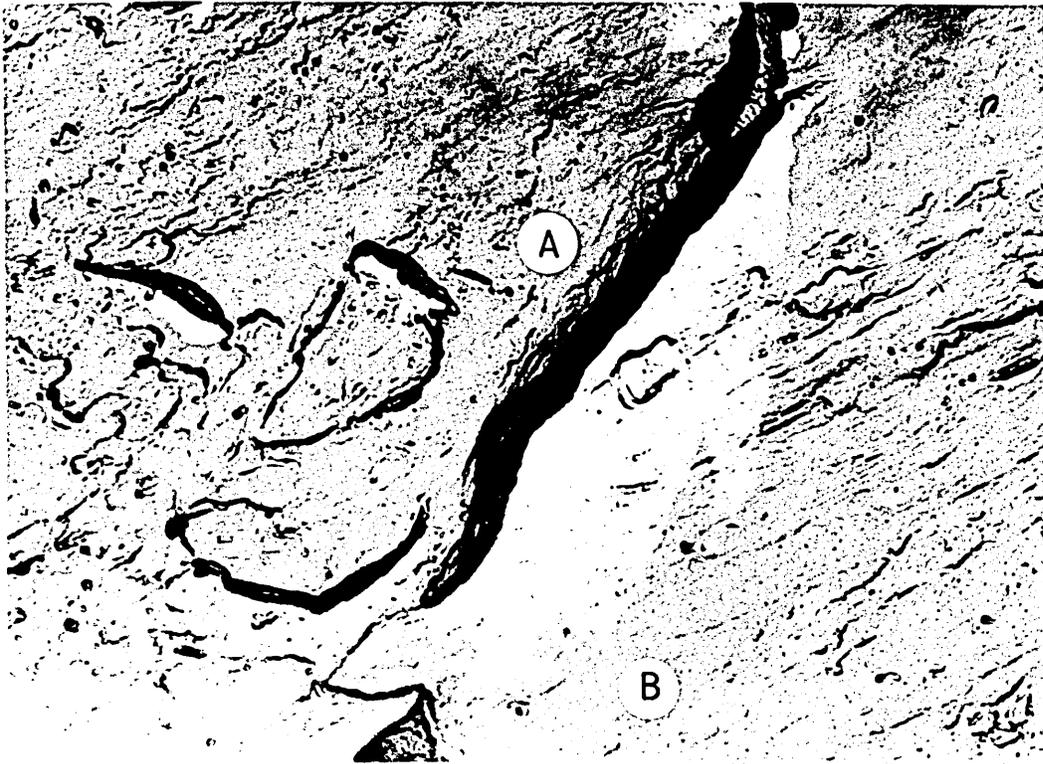
PLATE 1: EFFECT OF SHADOWING PROCESS ON MICROCRACK APPEARANCE
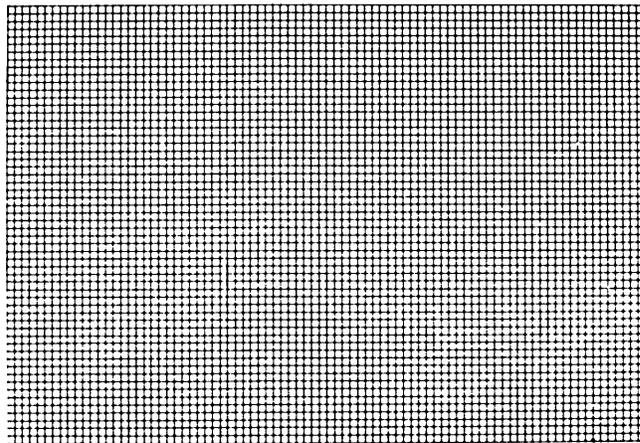
PLATE 2: STANDARD GRID PATTERN USED FOR MEASUREMENT OF SURFACE MICROCRACKING
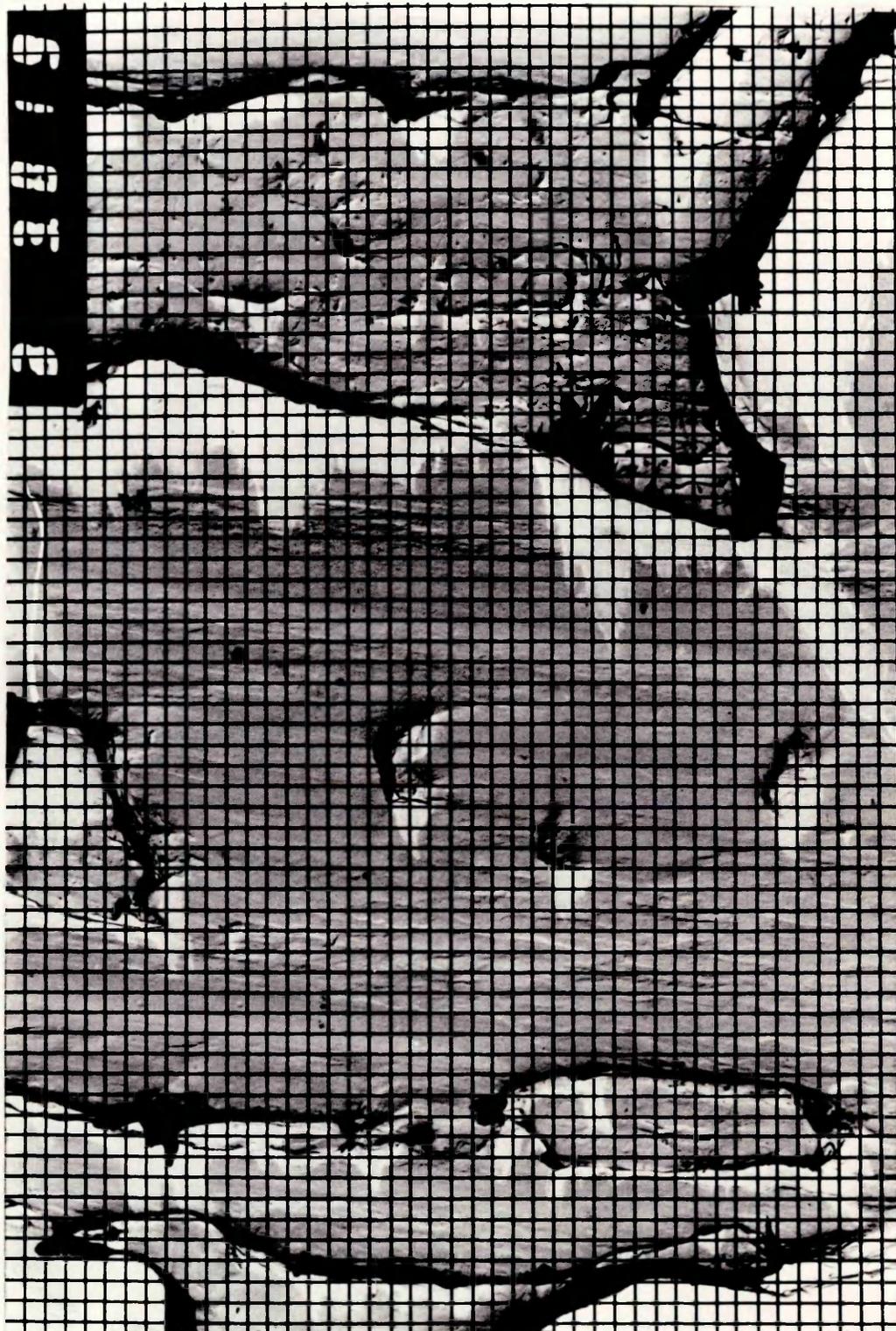
PLATE 3

MICROCRACK   MEASUREMENT

PLATE 4: MICROCRACK CONTRAST SEQUENCE SHOWING THE MIDDLE GREY BAND ASSOCIATED WITH POOR PENETRATION OF REPLICATING MATERIAL AND WITH THE COLLAPSE PHENOMENON
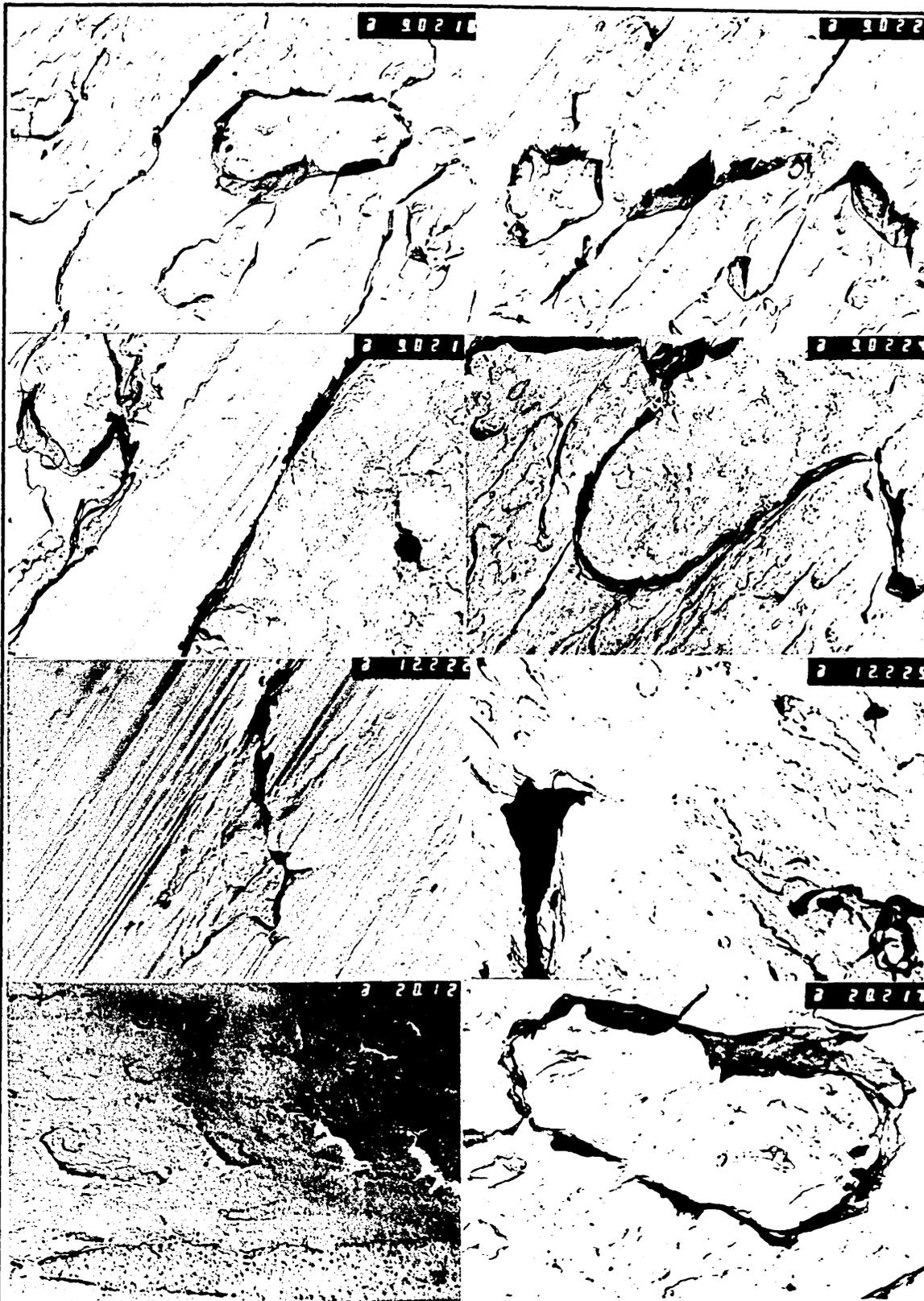
PLATE 5: TYPES OF MICROCRACKS IN THE MACHINED
SURFACE OF A RESULPHURIZED LOW CARBON STEEL

PLATE 6

MACHINED SURFACE
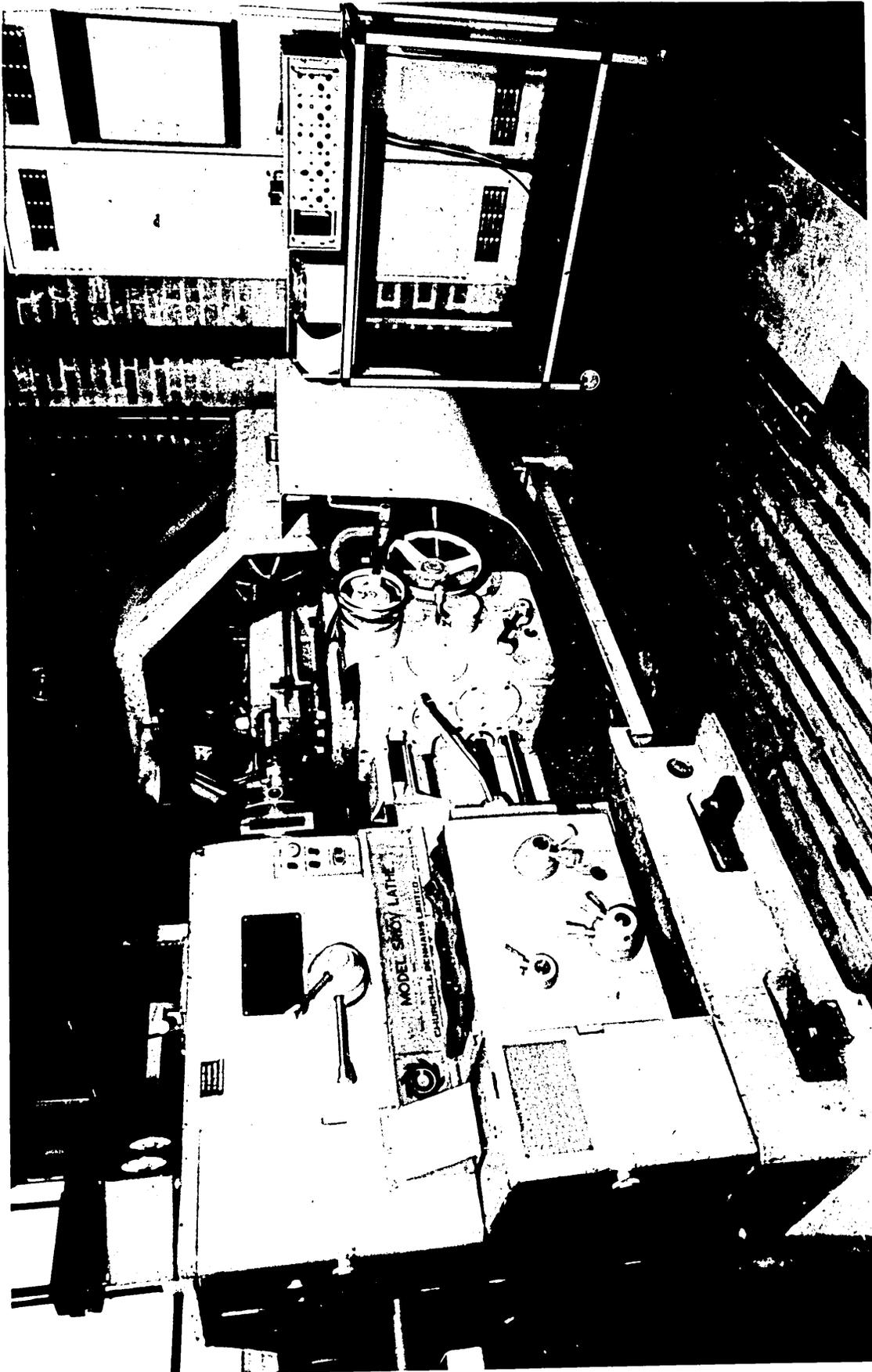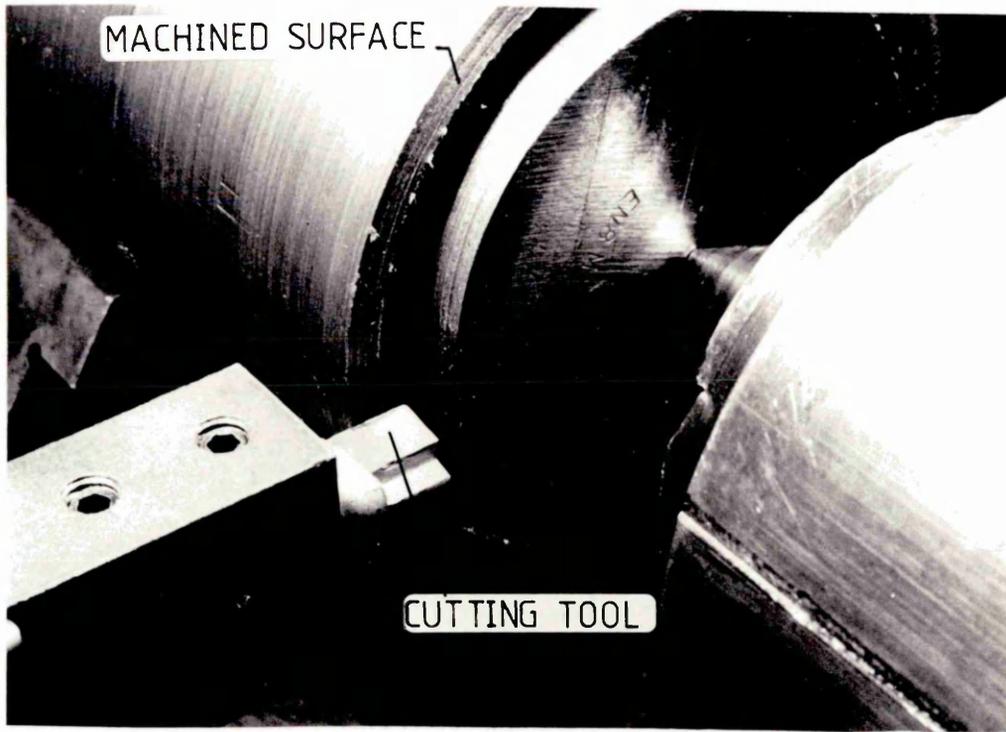
CUTTING TOOL

PLATE 7

EXPERIMENTAL SET UP FOR ORTHOGONAL
MACHINING

100X

100X
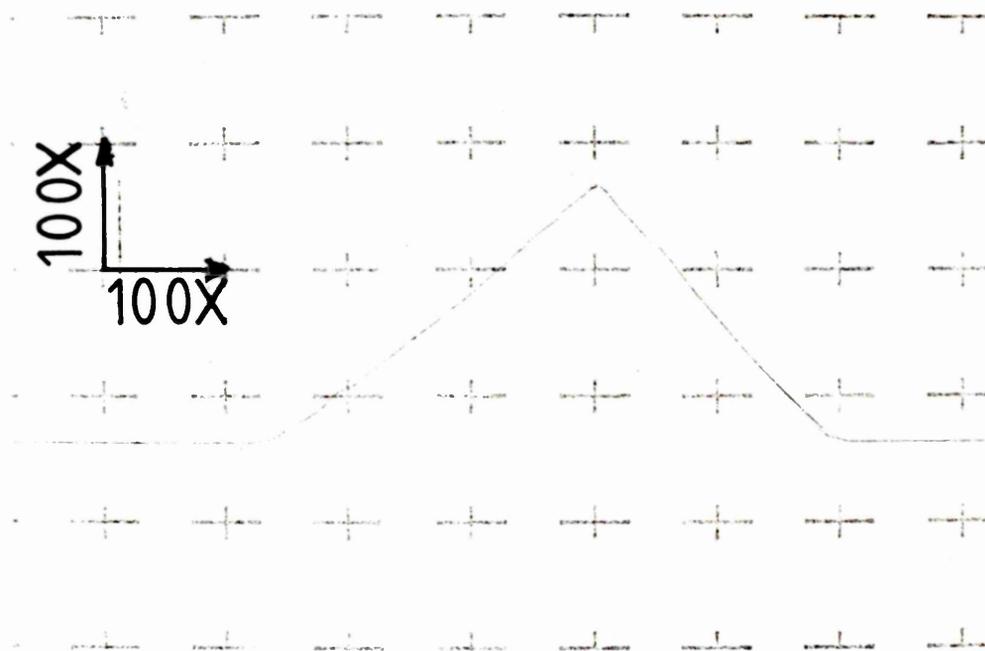
PLATE 8

STYLUS TRACE OF THE TOOL CUTTING EDGE
RADIUS
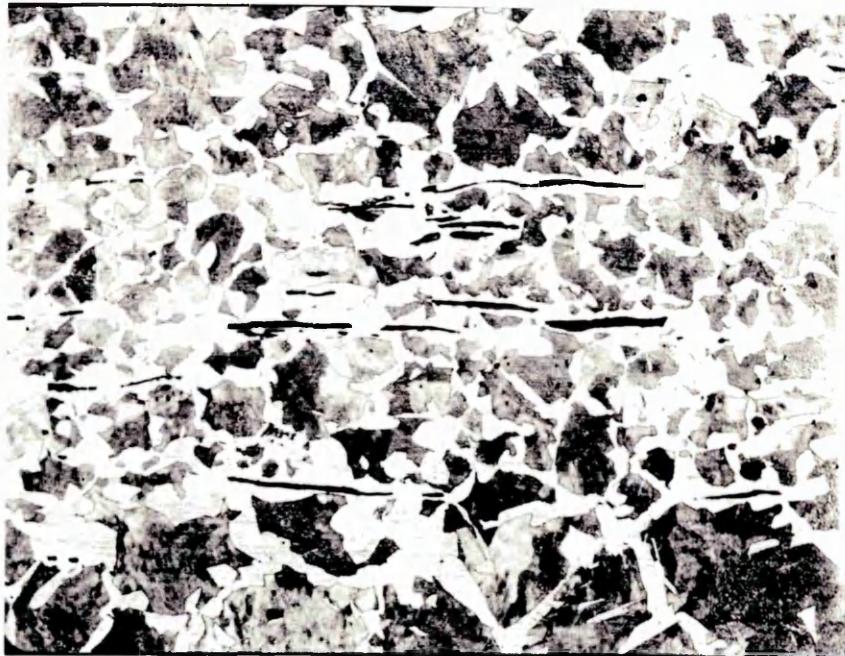
PLATE 9

MICROSTRUCTURE OF MEDIUM CARBON STEEL IN THE
AS-RECEIVED NORMALIZED CONDITION _ X-SECTION
NORMAL TO MACHINED SURFACE (X136)
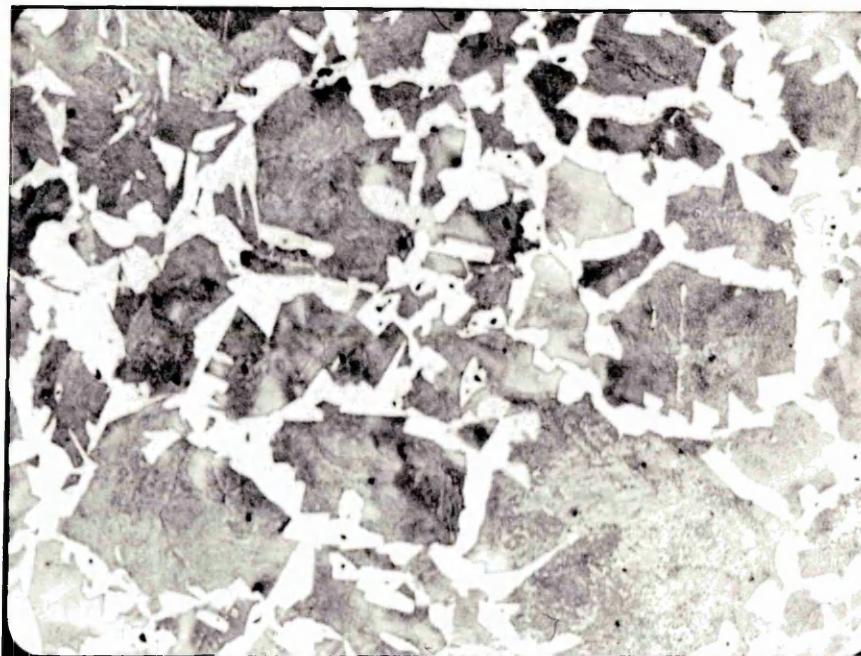
PLATE 10

MICROSTRUCTURE OF MEDIUM CARBON STEEL IN THE
AS-RECEIVED NORMALIZED CONDITION _ X-SECTION
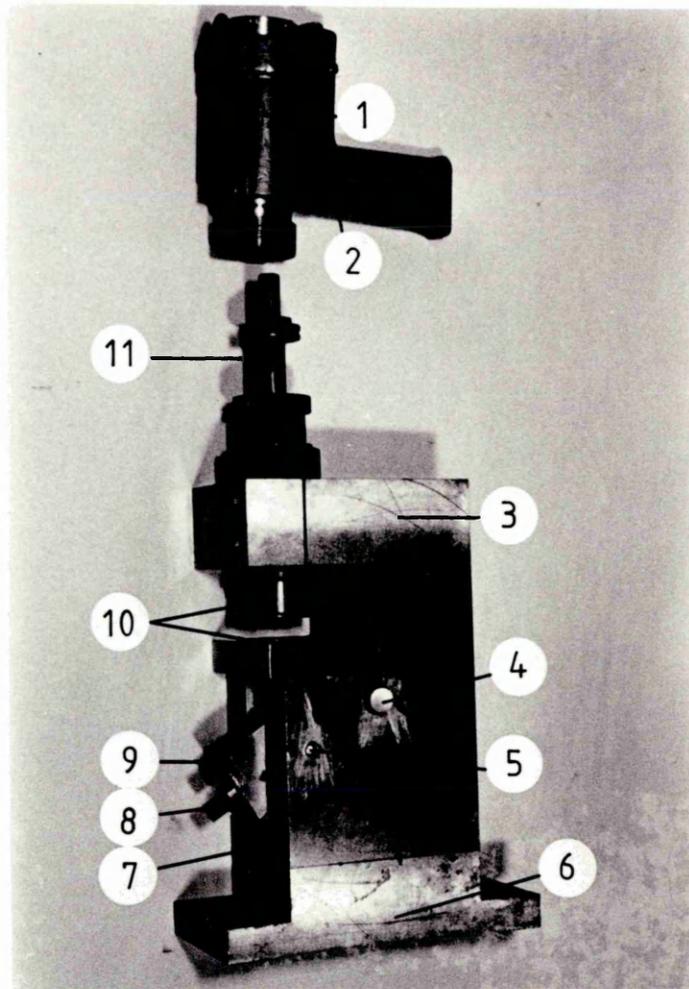PARALLEL TO MACHINED SURFACE (X136)

PLATE 11

QUICK STOP DEVICE

① HUMANE KILLER GUN ② TRIGGER
③ BODY OF QUICK STOP ④ PIVOT
⑤ SHEAR PIN HOLE ⑥ CLAMPING BASE
⑦ PLASTICINE ⑧ CUTTING TOOL
⑨ TOOL HOLDER ⑩ HAMMER GUIDES
⑪ HAMMER
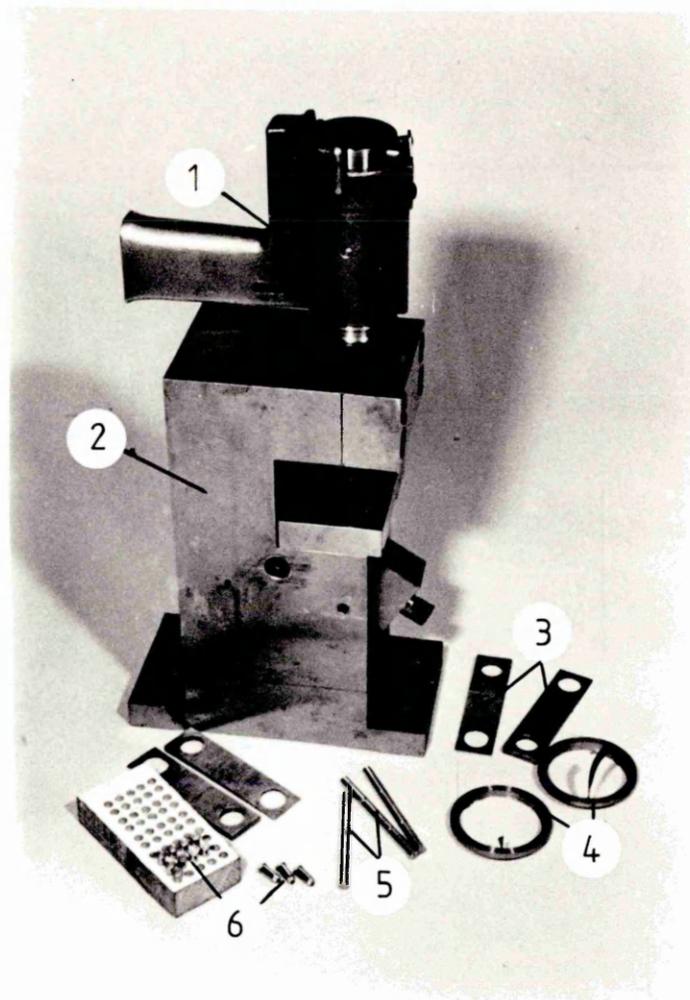
PLATE 12

QUICK STOP AND ACCESSORIES

① HUMANE KILLER GUN
② QUICK STOP
③ SLANTED SPACERS
④ MACHINED SURFACE AND CHIP ROOT
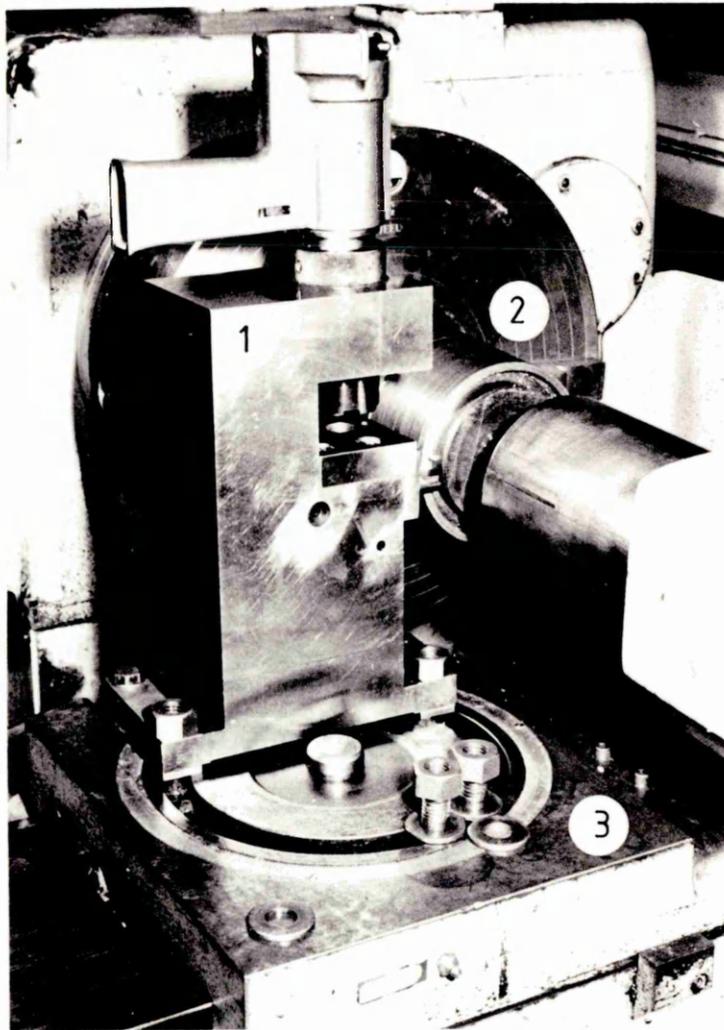⑤ SHEAR-PINS
⑥ BULLETS FOR HUMANE KILLER GUN

PLATE 13

QUICK STOP MOUTED ON CROSS-SLIDE OF LATHE

1. QUICK STOP DEVICE
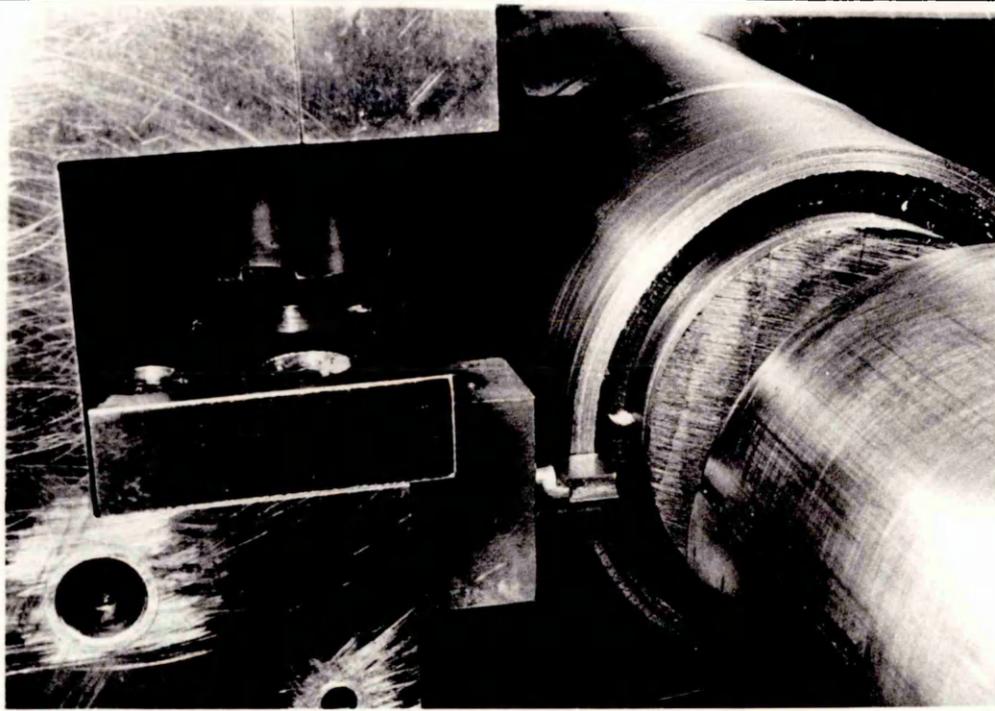2. WORKPIECE
3. CROSS-SLIDE OF LATHE

PLATE 14

QUICK-STOP DEVICE MOUNTED ON THE LATHE
(A CLOSE-UP VIEW)

TOOL HOLDER
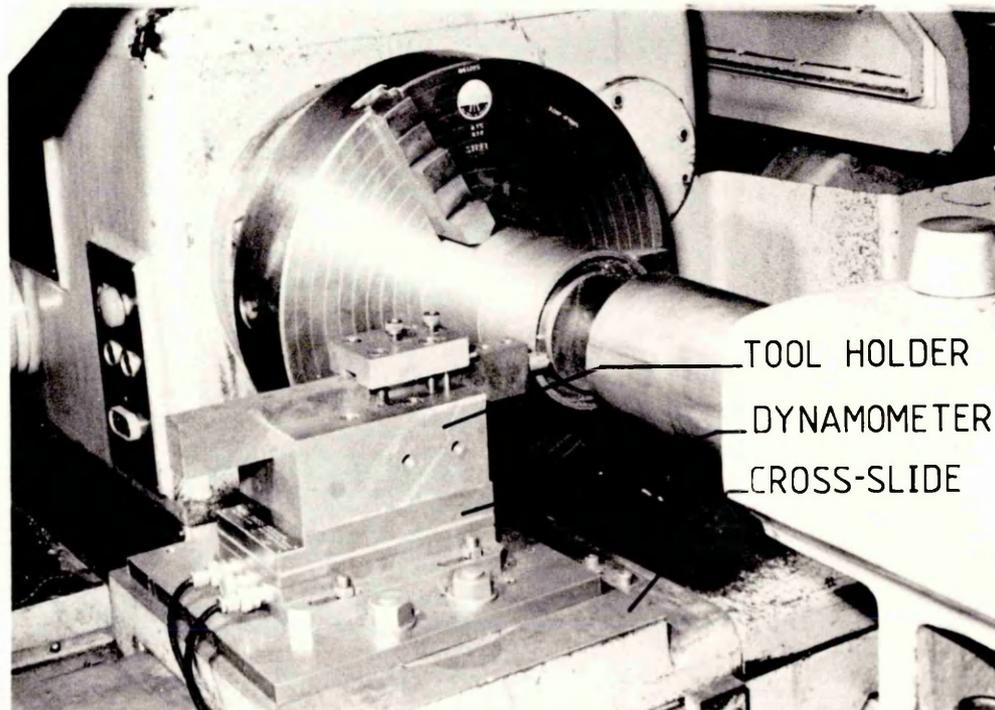DYNAMOMETER
CROSS-SLIDE

PLATE 15

DYNAMOMETER SET-UP FOR FORCE MEASUREMENT
DURING MACHINING
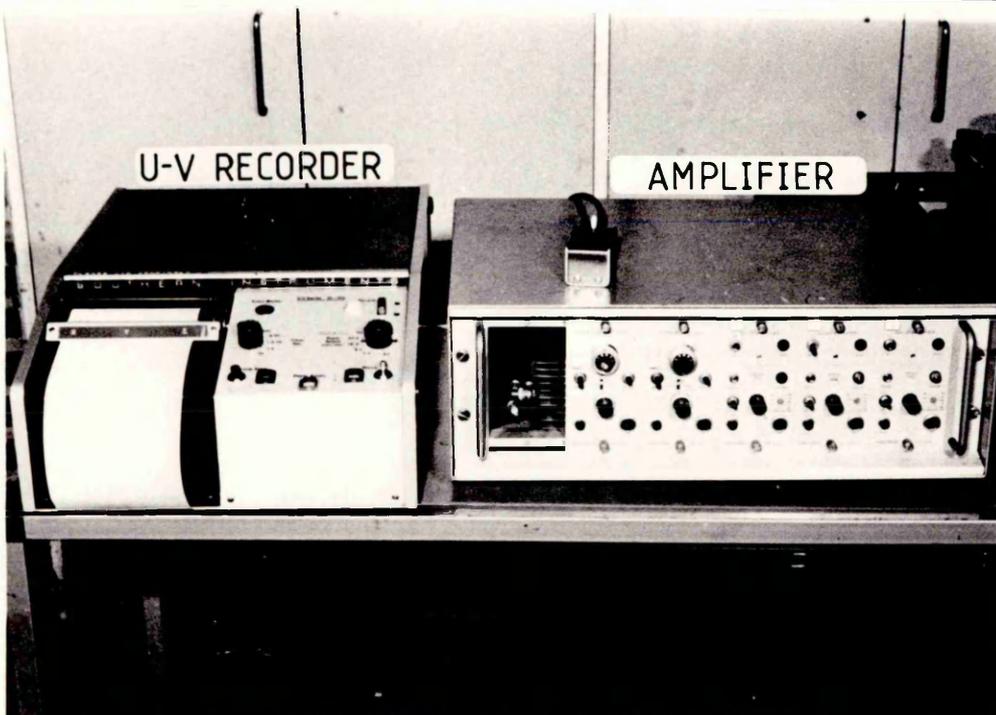
PLATE 16

AMPLIFIER AND U-V RECORDER USED WITH
DYNAMOMETER DURING FORCE MEASUREMENT
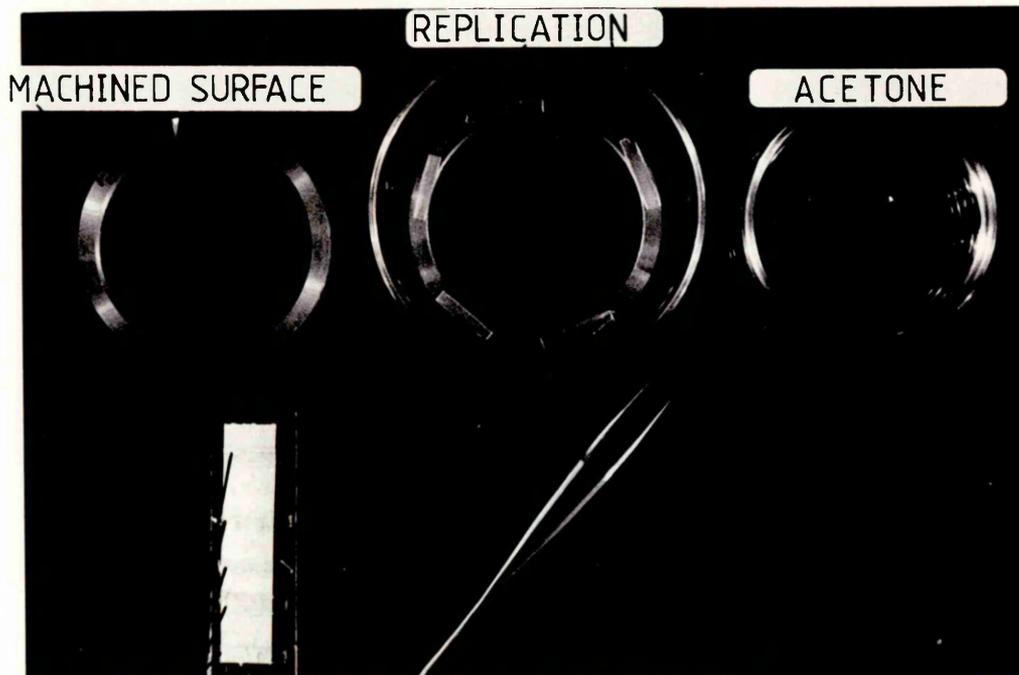
PLATE 17

SURFACE REPLICATION
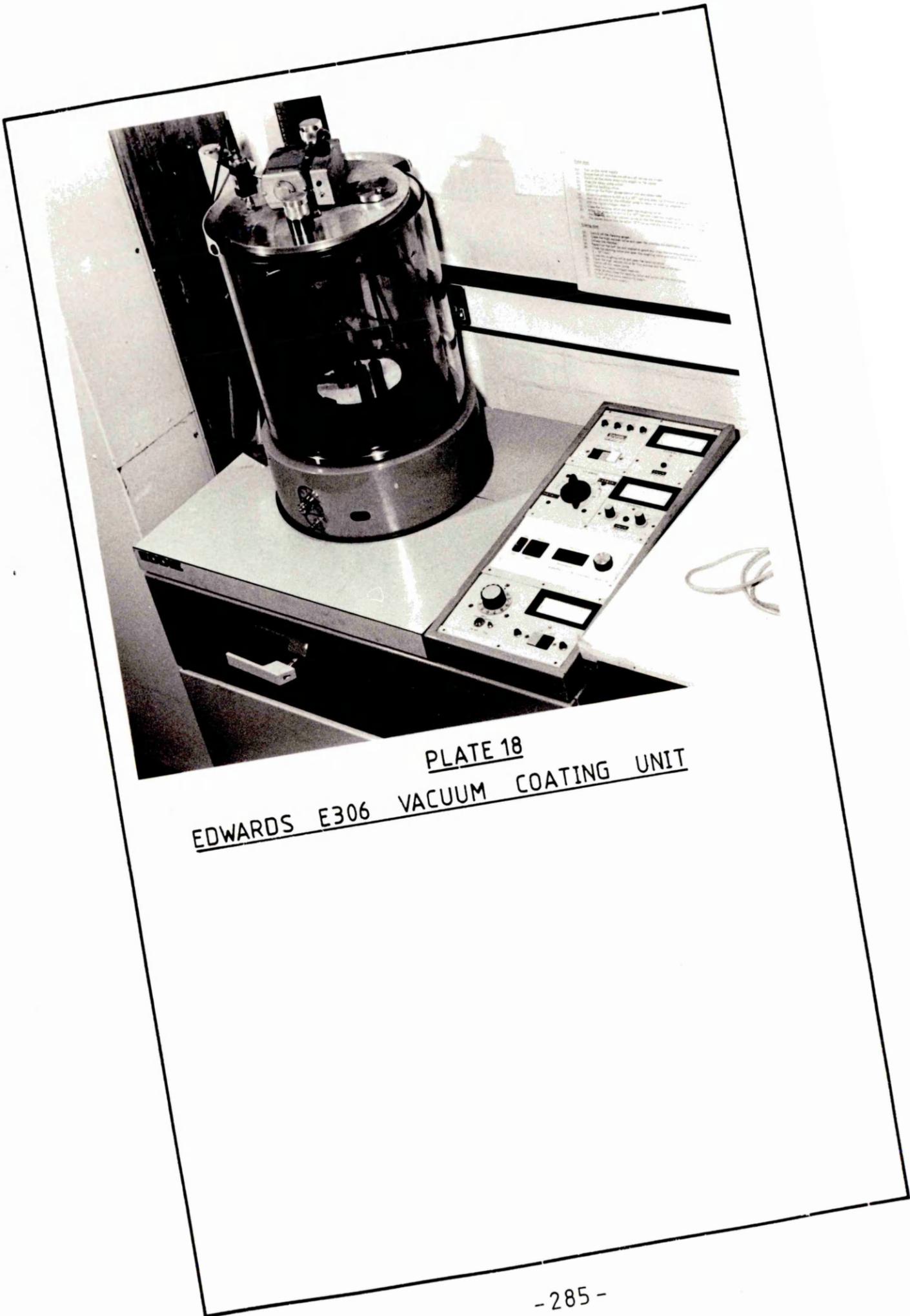
PLATE 18

EDWARDS E306 VACUUM COATING UNIT
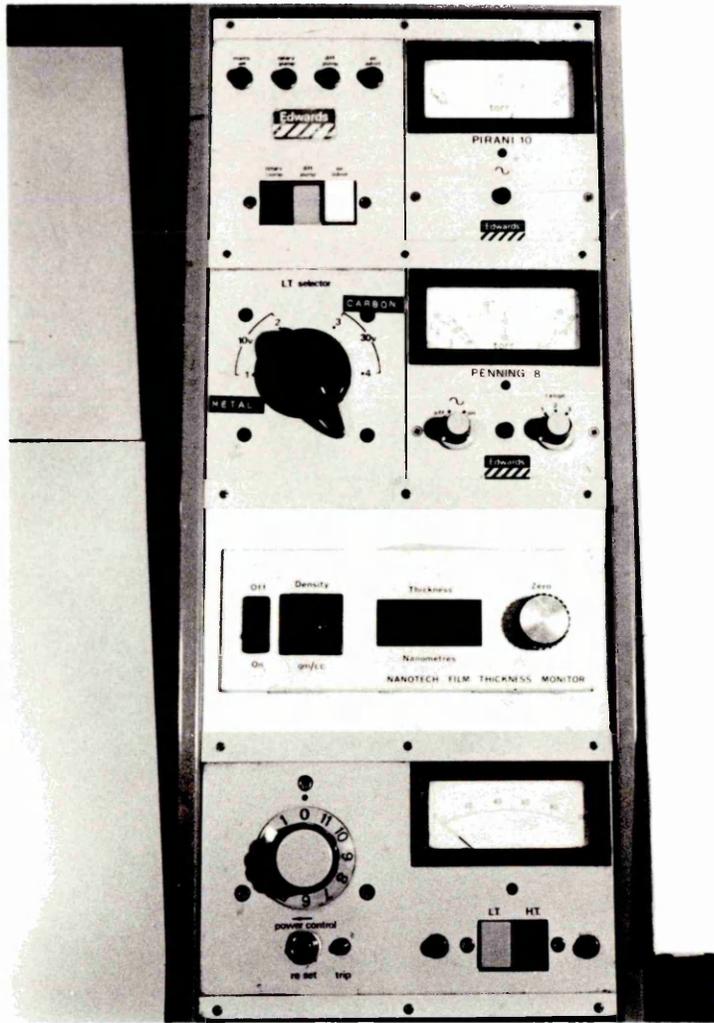
PLATE 19

CONTROL PANEL FOR VACUUM COATING UNIT
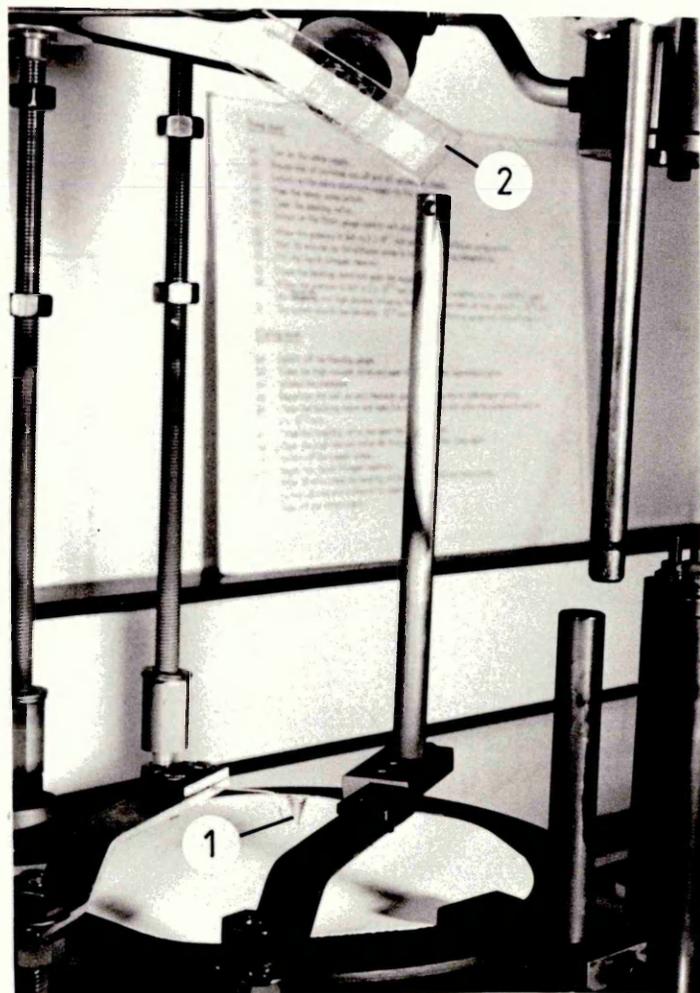
PLATE 20

VACUUM CHAMBER: SET-UP FOR SHADOWING PROCESS

① EVAPORATING TUNGSTEN BASKET

② REPLICAS TO BE SHADOWED ON GLASS SLIDE
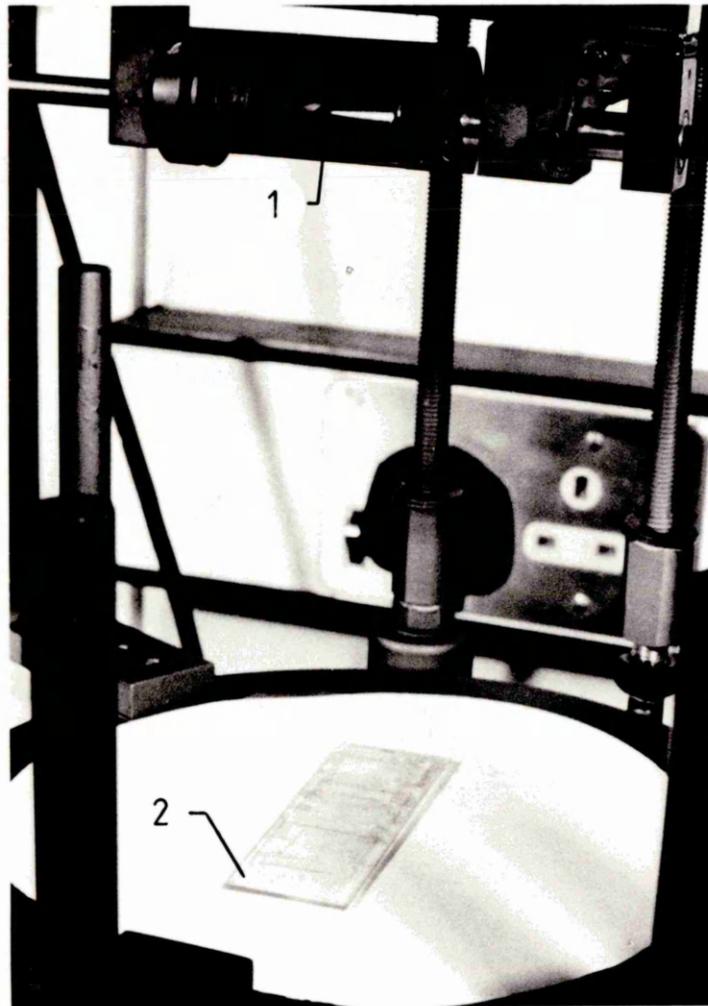
PLATE 21

VACUUM CHAMBER: SET-UP FOR CARBON COATING

① CARBON RODS

② SHADOWED REPLICAS ON GLASS SLIDE
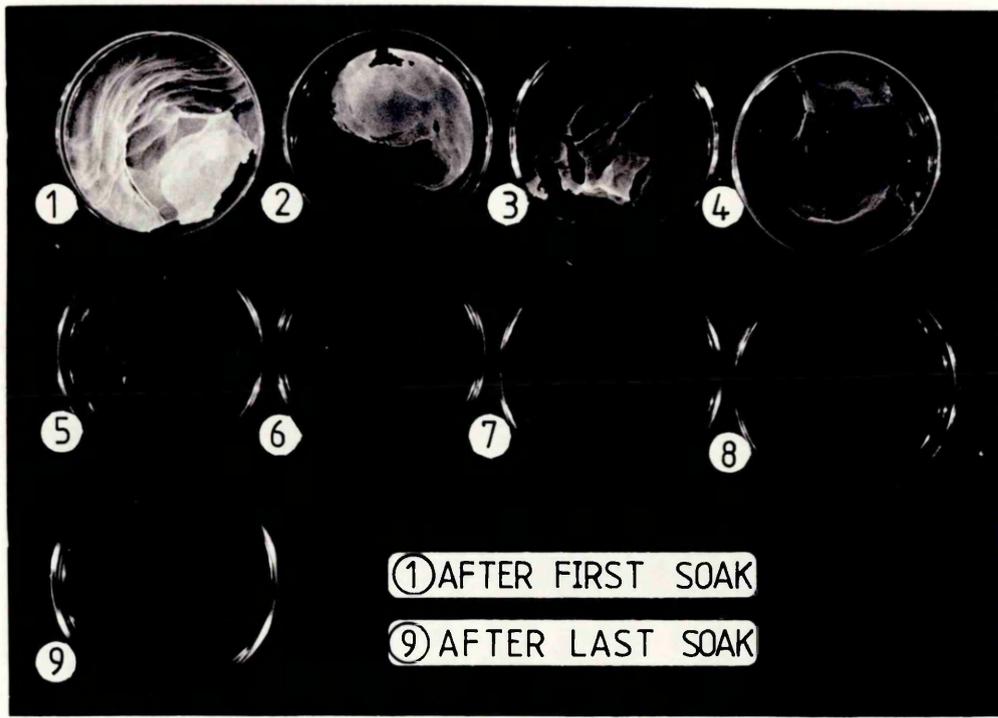
PLATE 22

PLASTIC RESIDUE INDICATING PROGRESSION
OF DISSOLVING PROCESS
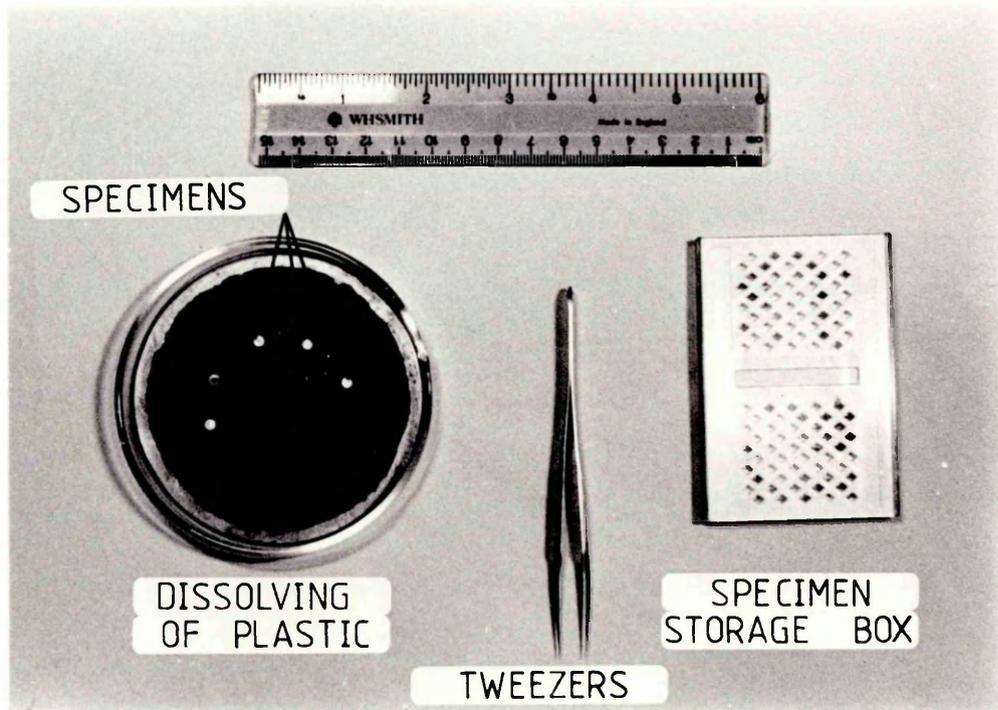
PLATE 23

DISSOLVING OF PLASTIC AND STORAGE BOX
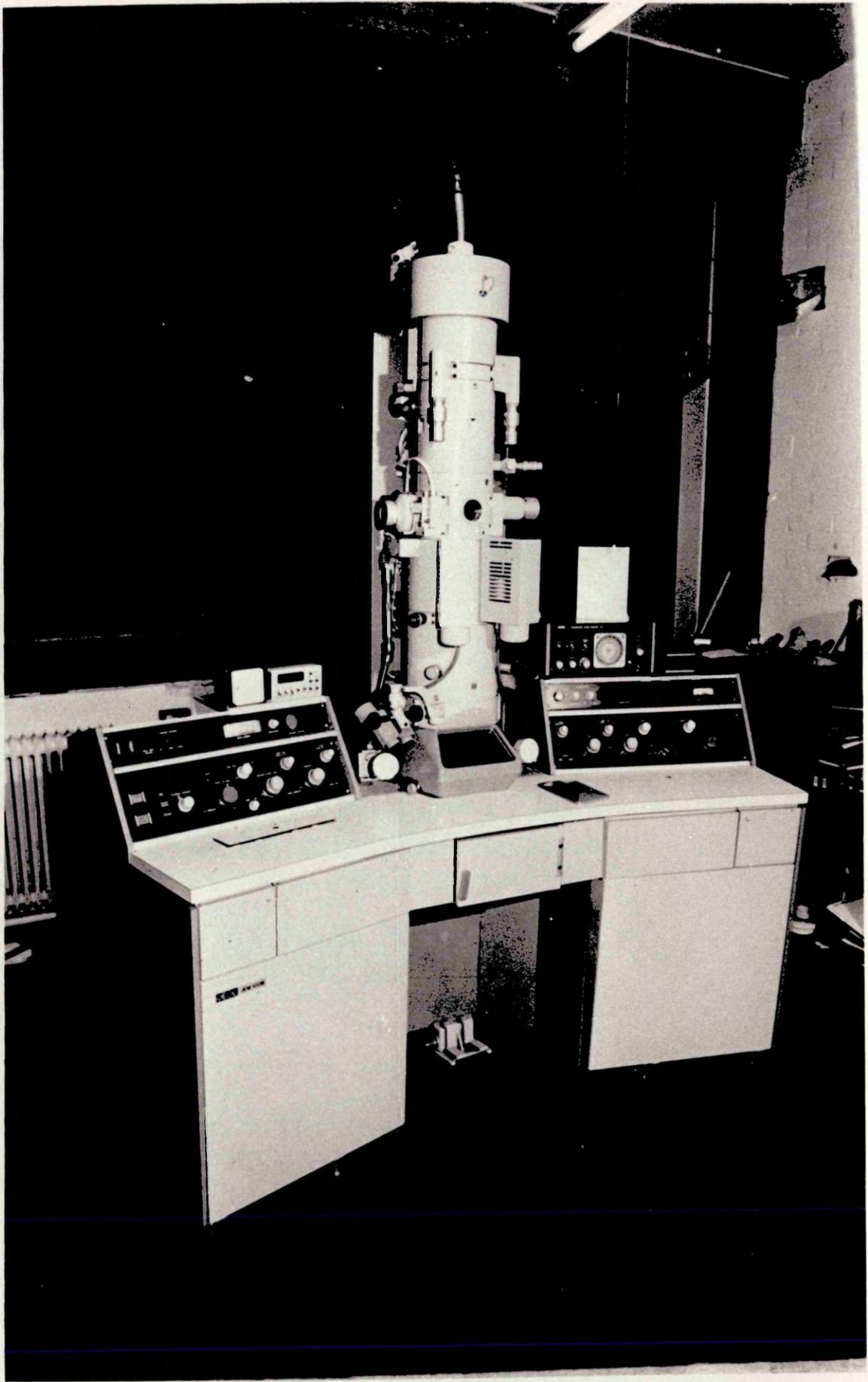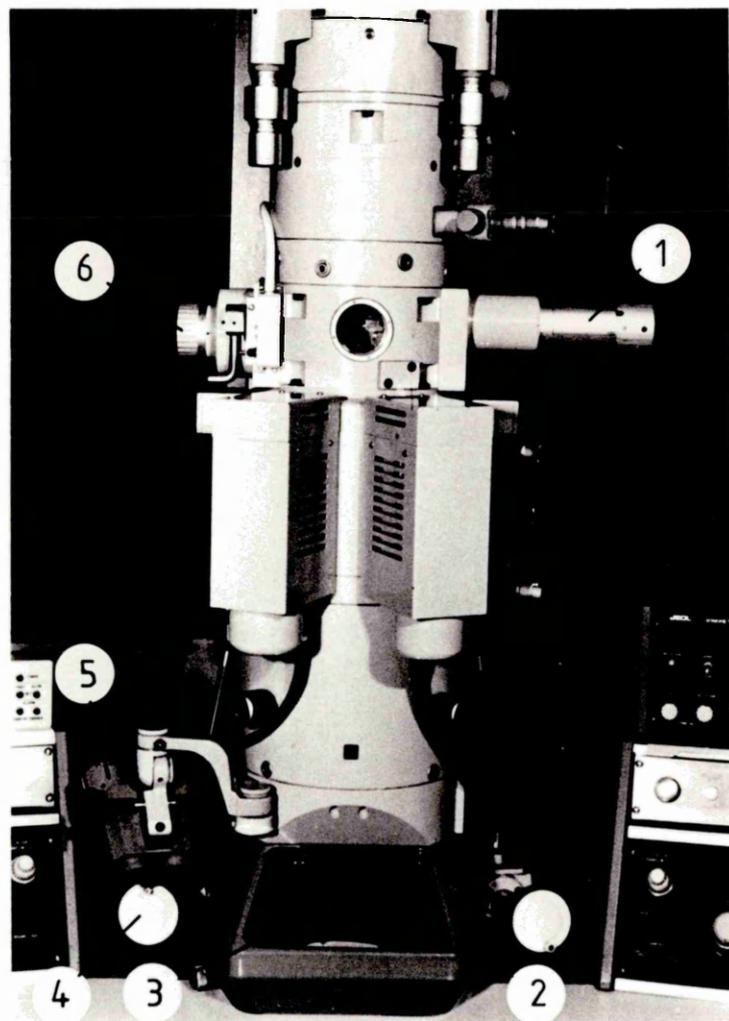
PLATE 24

PLATE 25

TRANSMISSION ELECTRON MICROSCOPE COLUMN

① SPECIMEN CARRIER
② SCREEN LEVER
③ VIEWING WINDOW
④ AREA SEARCH CONTROLS
⑤ BINOCULARS
⑥ SPECIMEN HOLDER MAGAZINE
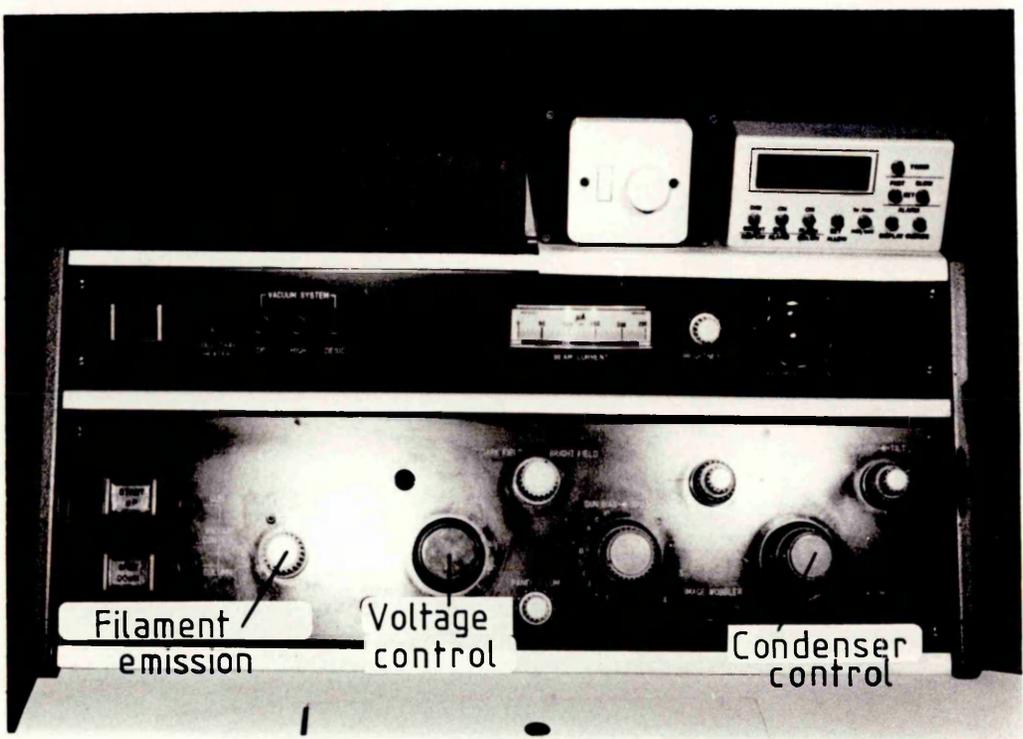
PLATE 26

TEM CONTROLS (LEFT-HAND SIDE)
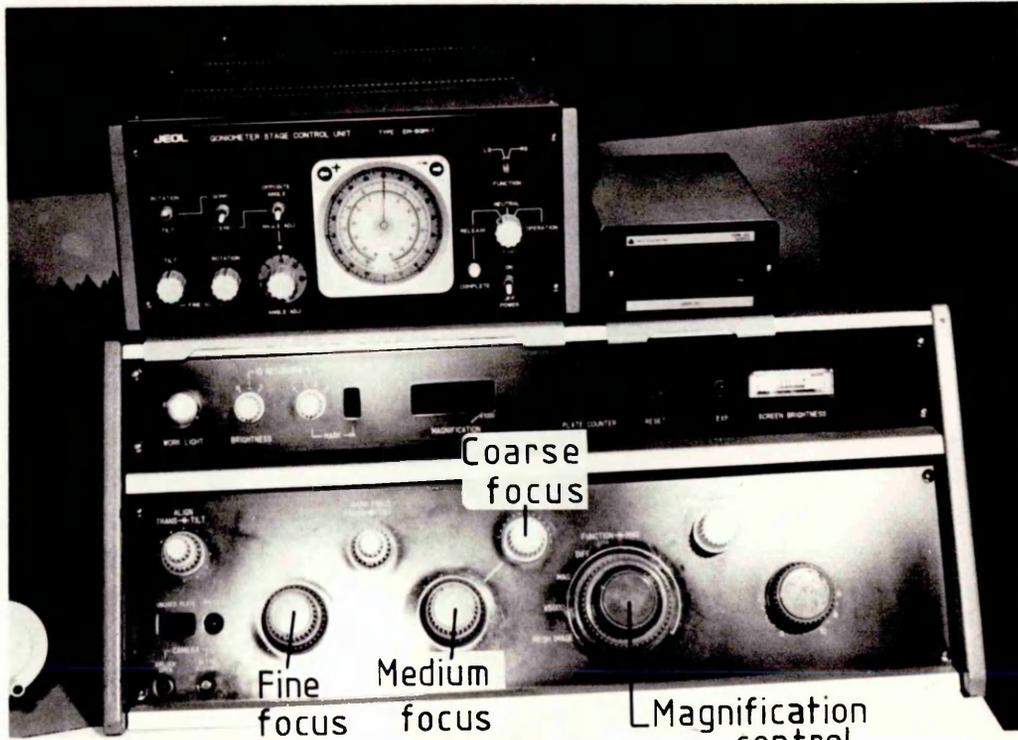
PLATE 27

TEM CONTROLS (RIGHT-HAND SIDE)

SPECIMENS ON GRIDS
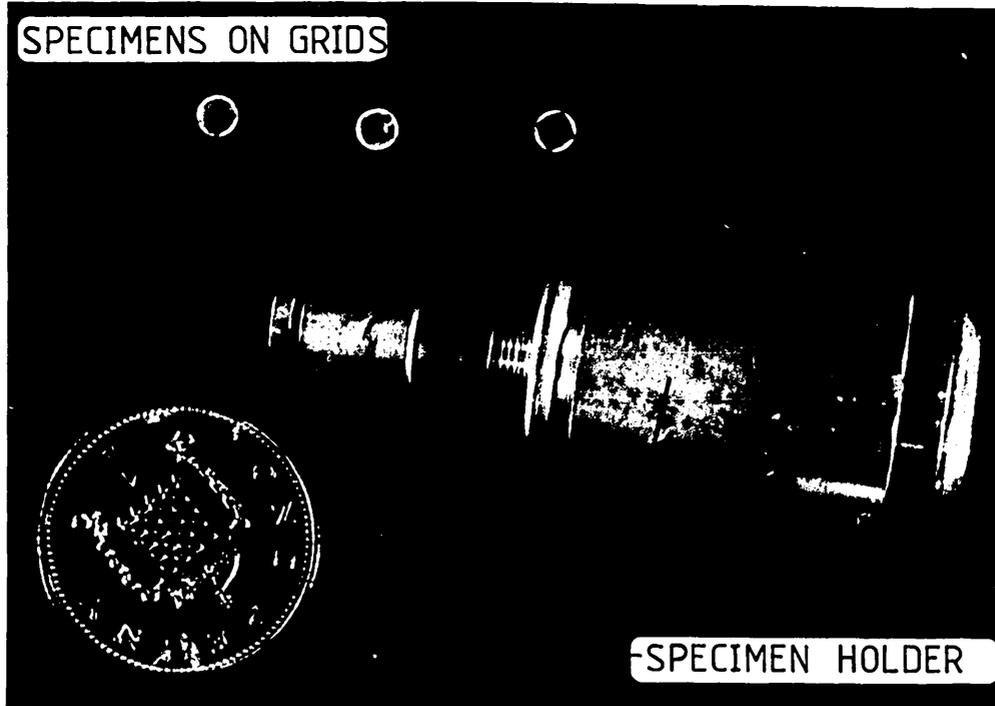
SPECIMEN HOLDER

PLATE 28

HIGH CONTRAST SPECIMEN HOLDER AND SPECIMENS
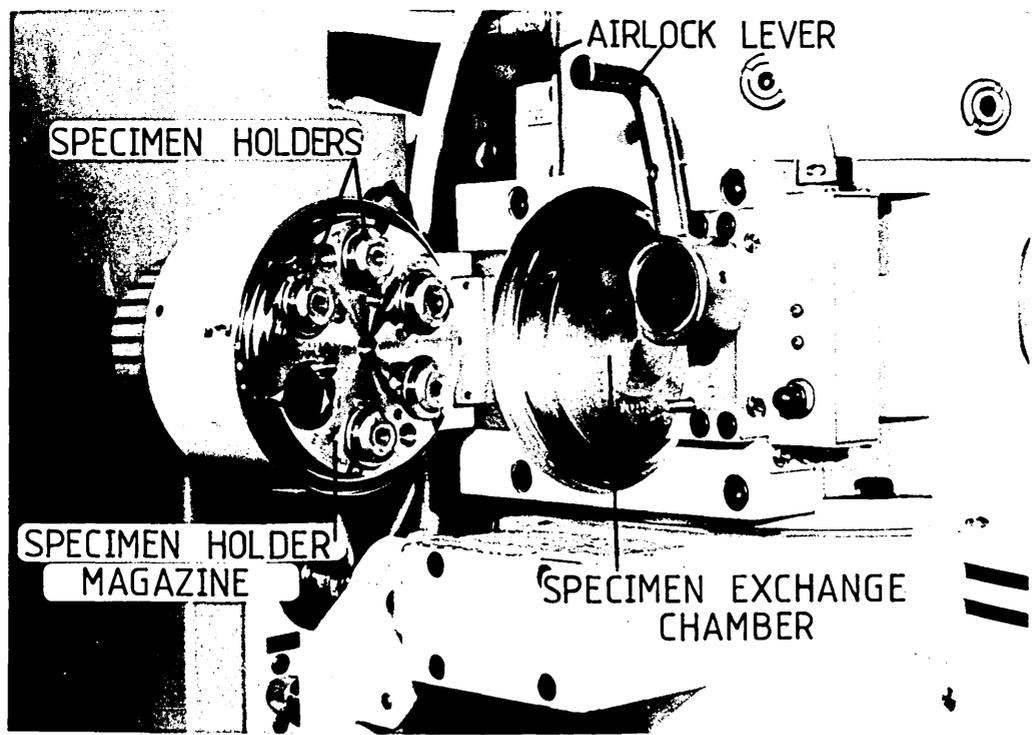
AIRLOCK LEVER

SPECIMEN HOLDERS

SPECIMEN HOLDER
MAGAZINE

SPECIMEN EXCHANGE
CHAMBER

PLATE 29

SPECIMEN HOLDER MAGAZINE
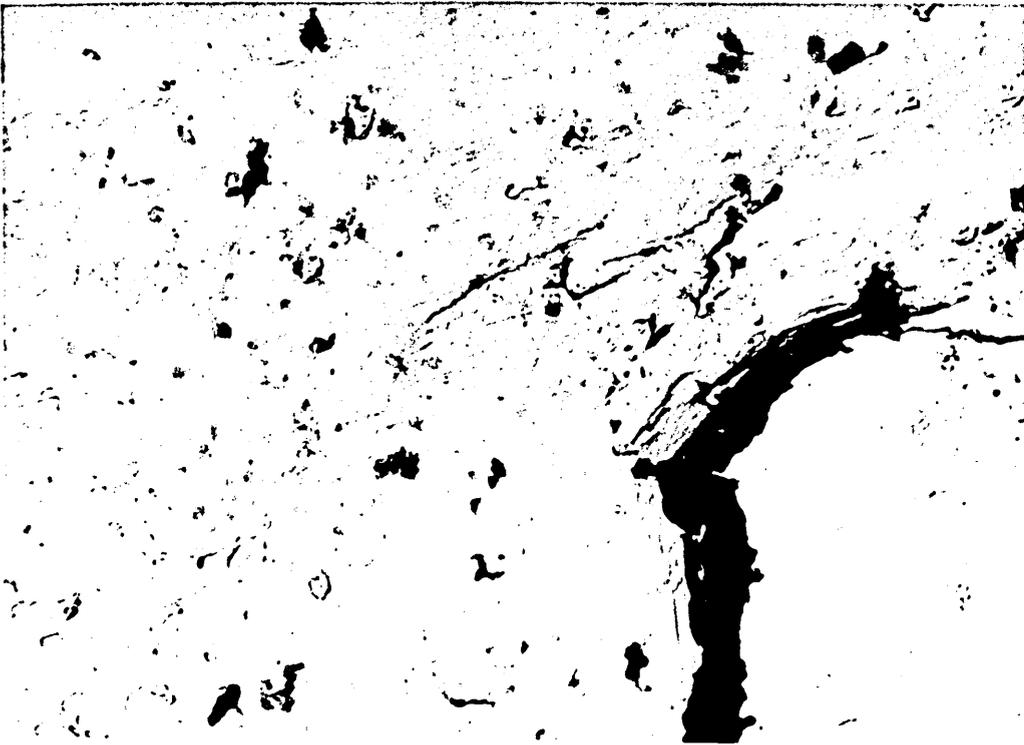
PLATE 30

TEM MICROGRAPH SHOWING THE MICROCRACKING IN A
SURFACE MACHINED AT $V=1000\,m.min^{-1}; t=0.244\,mm; \alpha=+5°$

PLATE 31

TEM MICROGRAPH SHOWING THE MICROCRACKING IN A
SURFACE MACHINED AT $V=400\,m.min^{-1}; t=0.244\,mm; \alpha=+5°$

PLATE 32

TEM MICROGRAPH SHOWING THE MICROCRACKING IN A
SURFACE MACHINED AT V=200m.min^{-1}; t=0·057mm; α=+5°

PLATE 33

TEM MICROGRAPH SHOWING THE MICROCRACKING IN A
SURFACE MACHINED AT V=200m.min^{-1}; t=0·396mm; α=+5°
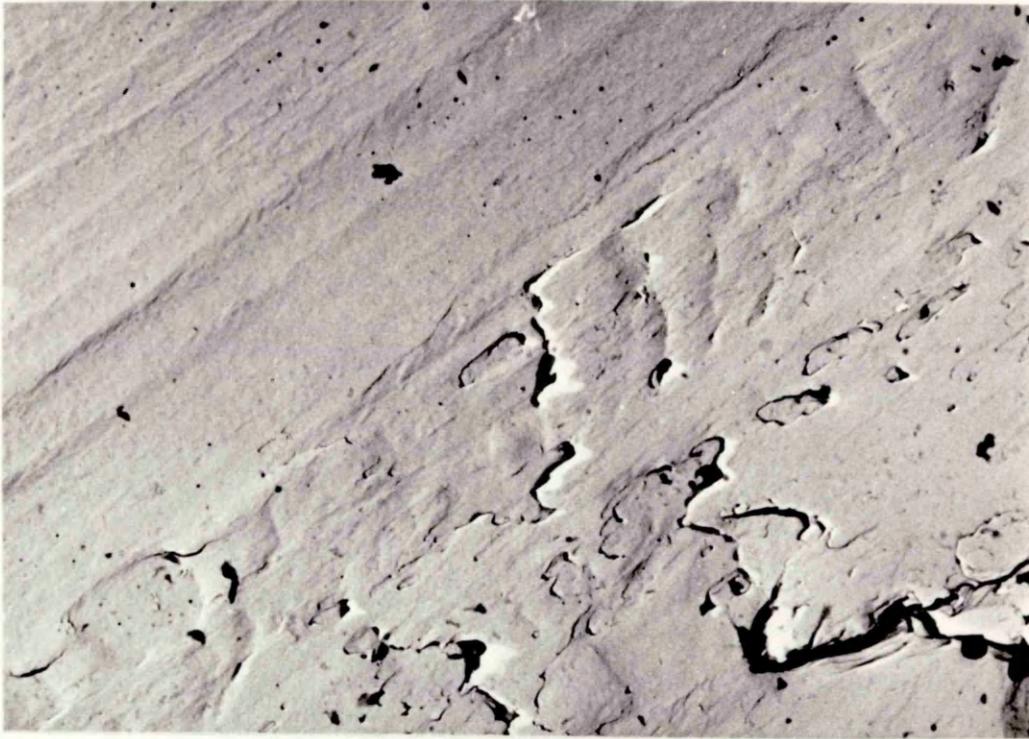
PLATE 34

TEM MICROGRAPH SHOWING THE MICROCRACKING IN A SURFACE MACHINED AT V=200m.min⁻¹; t=0·244mm ; $\alpha = -5°$
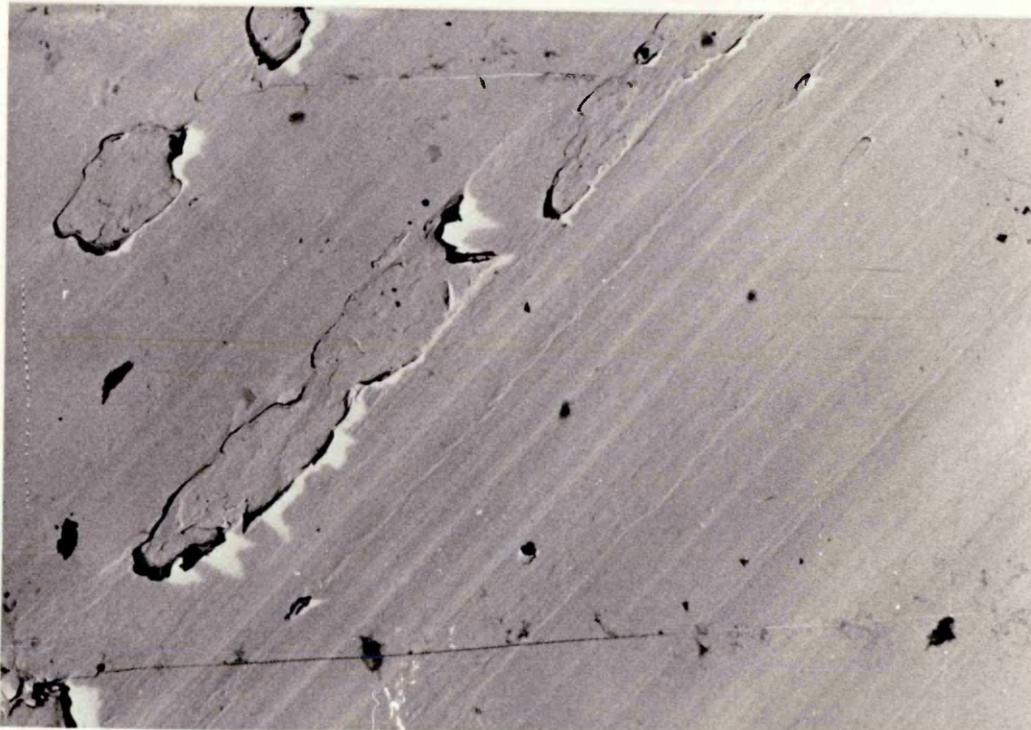
PLATE 35

TEM MICROGRAPH SHOWING THE MICROCRACKING IN A SURFACE MACHINED AT V 200m.min⁻¹; t=0·244mm ; $\alpha = +5°$
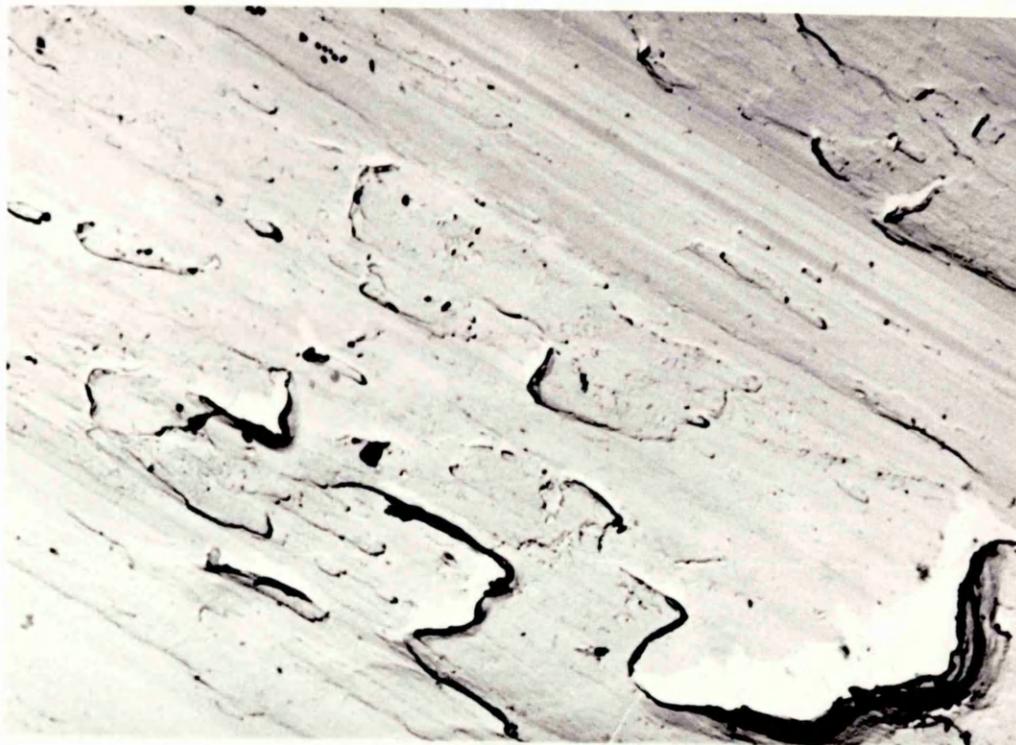
PLATE 36

TEM MICROGRAPH SHOWING THE MICROCRACKING IN A
SURFACE MACHINED AT $V=200 \text{m.min}^{-1}$; $t=0 \cdot 244 \text{mm}$; $\alpha=+30°$

PLATE 37

TEM MICROGRAPH OF FULLY-ANNEALED En8 STEEL(Hv:180)
SURFACE MACHINED AT $V=200 \text{m.min}^{-1}$; $t=0 \cdot 244 \text{mm}$; $\alpha=+10°$
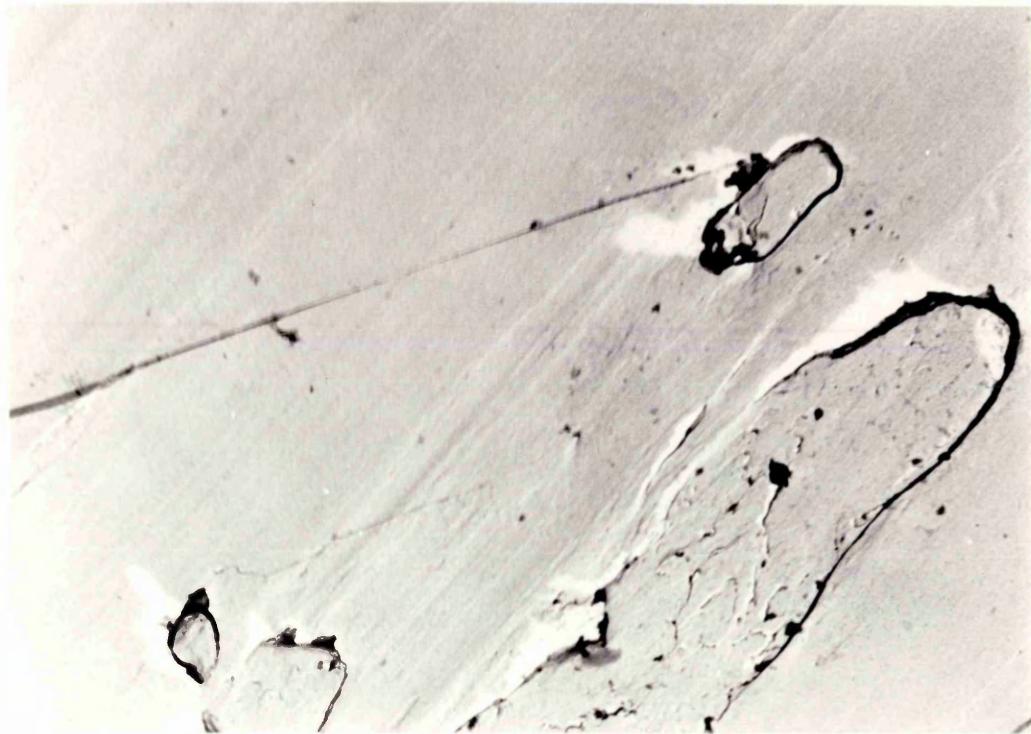
PLATE 38

TEM MICROGRAPH OF AS-RECEIVED (NORMALIZED) En8 STEEL
(Hv:208) SURFACE MACHINED AT $V=200\,m.min^{-1}$; $t=0.244\,mm$; $\alpha=+10°$

PLATE 39

TEM MICROGRAPH OF QUENCHED & TEMPERED En8 STEEL
(Hv:260) SURFACE MACHINED AT $V=200\,m.min^{-1}$; $t=0.244\,mm$; $\alpha=+10°$

-298-
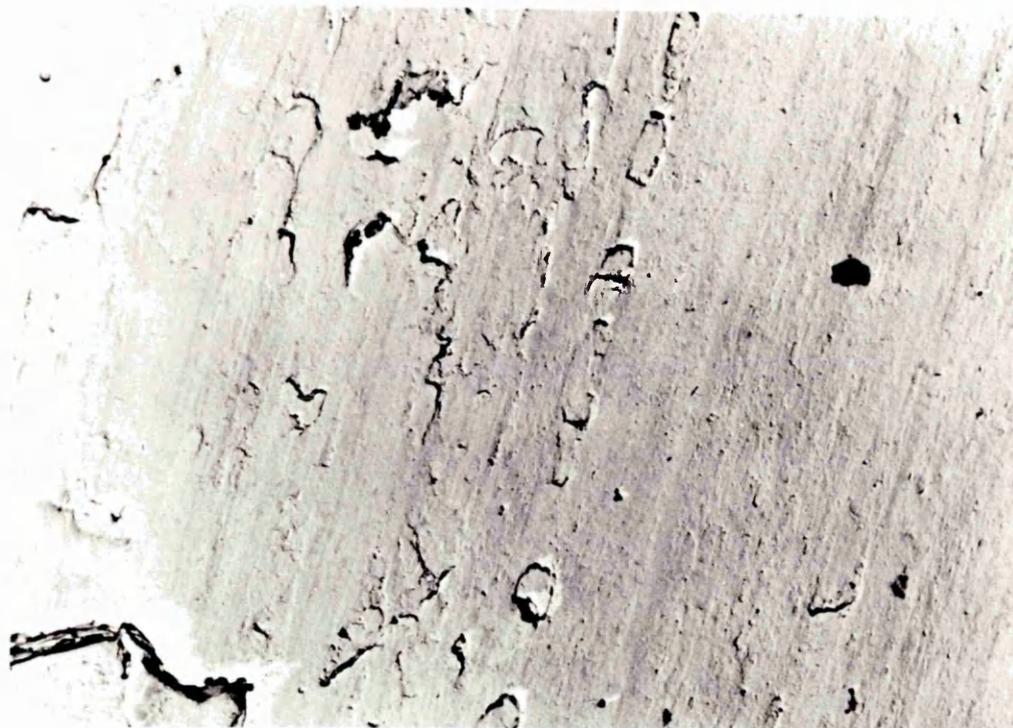
PLATE 42

TEM MICROGRAPH OIL-QUENCHED En8 STEEL (Hv:350)
SURFACE MACHINED AT V=200m.min^{-1}; t=0·244mm; a = +10°

a) Parallel to axis of bar   b) Normal to axis of bar

PLATE 43

MICROSTRUCTURE OF AS-RECEIVED (NORMALIZED) MEDIUM

CARBON STEEL (En 8) Hv = 208 V.P.N. ;   (X80)
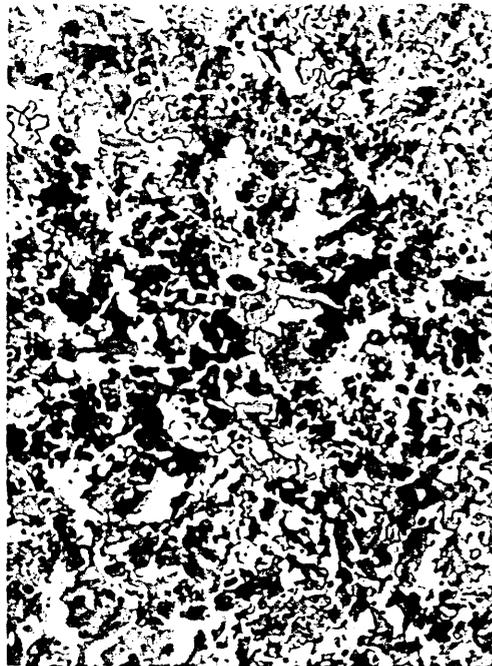
a) Parallel to axis of bar   b) Normal to axis of bar

PLATE 44

MICROSTRUCTURE OF FULLY ANNEALED En 8 STEEL

Hv = 180 VPN   (X80)

a) Parallel to axis of bar   b) Normal to axis of bar

PLATE 45

MICROSTRUCTURE OF En8 STEEL OIL-QUENCHED AND
TEMPERED TO Hv = 260 V.P.N.   (X 320)

a) Parallel to axis of bar   b) Normal to axis of bar

PLATE 46

MICROSTRUCTURE OF En8 STEEL OIL-QUENCHED AND
TEMPERED TO Hv = 285 V.P.N.   (X 320)
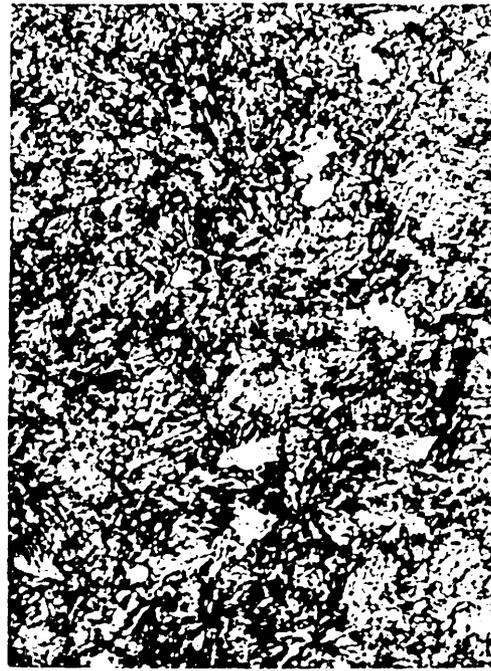
a) Parallel to axis of bar   b) Normal to axis of bar

PLATE 47

MICROSTRUCTURE OF En8 STEEL OIL-QUENCHED AND TEMPERED TO Hv = 320 V.P.N. (X320)
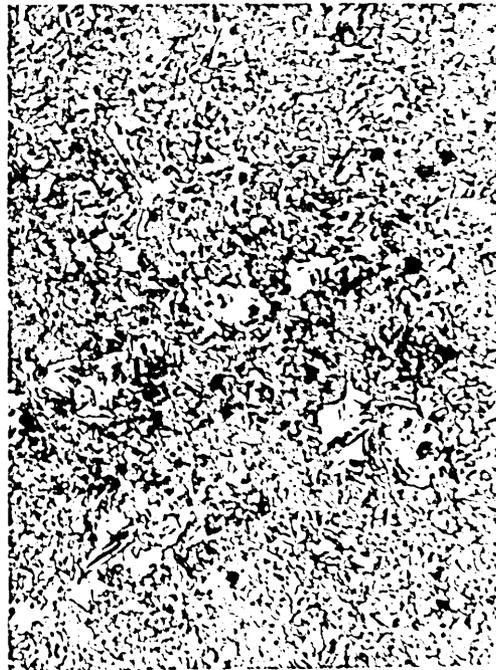
a) Parallel to axis of bar   b) Normal to axis of bar

PLATE 48

MICROSTRUCTURE OF OIL-QUENCHED En8 STEEL Hv = 350 V.P.N. (X320)

MINIMUM NUMBER OF MICROGRAPHS REQUIRED FOR THE MICROCRACK

MEASUREMENT TECHNIQUE AND REPEATABILITY OF MEASUREMENTS.

This appendix deals with the problem of consistency of the microcrack measurement technique in two sections. In section one, a convergence study is conducted to find the minimum number of micrographs required. In section two, statistical tests of significance are used to assess the repeatability of measurements based on the minimum number of micrographs determined in part one.

A1.1- Minimum Number Of Micrographs:

To determine the minimum number of micrographs required for the microcrack measurement technique, a number of micrographs were obtained for a surface of En8 steel machined at V=200m/min with a tool having a rake angle of 10 degrees and with an undeformed chip thickness of 0.244mm. The microcracking parameters "Ma" and "Md" were then determined using one micrograph, then two micrographs, then three and so on until all the micrographs had been used up. The results are shown in table A1. The convergence of "Ma" and "Md" with increase in the number of micrographs is illustrated in figure A1. It can be seen from this figure that "Ma" and "Md" converge to a constant value as the number of micrographs is increased. In the present study, using the convergence graph shown in figure A1, it was decided to standardize the micrograph measurement technique and base the measurements on 20 micrographs. The microcracking parameters were, therefore, determined from measurements on 10 micrographs for each shadowing direction, "Ma" being the average and "Md" the sum of the measurements corresponding to the two shadowing directions.

Table Al: Convergence of "Ma" and "Md" against
the number of micrographs used.

Micrograph Number (N)	Ma	Md	Micrograph Number (N)	Ma	Md
1	2.41	140	16	1.19	74
2	1.20	70	17	1.15	73
3	0.80	47	18	1.23	71
4	1.10	60	19	1.18	71
5	1.09	60	20	1.12	69
6	0.96	60	21	1.15	70
7	1.00	69	22	1.11	69
8	1.22	93	23	1.08	70
9	1.23	98	24	1.17	68
10	1.42	102	25	1.13	70
11	1.61	95	26	1.19	71
12	1.48	87	27	1.22	69
13	1.43	85	28	1.31	69
14	1.35	80	29	1.27	67
15	1.26	75	30	1.24	67

Al.2- Repeatability Of Measurements:

Al.2.1- F-Test:

The distribution of the ratio of two estimates of variance obtained for two independant sets of results is called the F-distribution. The distribution depends on the numbers of degrees of freedom f_1 and f_2 associated with the two estimates of variance.

The F-distribution is used to decide whether two independent estimates of variance can reasonably be accepted as being two estimates of the variance of the same universe of data. The probability that two such independent estimates of variance shall have any particular ratio can be calculated. F-test tables are available showing the ratio which will be equalled or exceeded by chance, with probabilities 0.1, 0.05 and 0.01 in relation to the number of degrees of freedom on which the two estimates are based.

Table A2 shows the samples of microcrack areas which are to be compared.

Table A2: Comparison of variances for two independent samples of microcrack area measurements having 1 and 9 degrees of freedom (F-test).

j	X_1	X_2	$(X_{1j}-\bar{X}_1)^2 + (X_{2j}-\bar{X}_2)^2$
1	117	86	2527.73
2	0	13	8179.13
3	0	20	7406.33
4	96	152	7187.93
5	51	19	3094.13
6	17	131	6199.73
7	59	87	330.13
8	134	186	17315.53
9	63	12	3597.73
10	151	11	10441.33
SUM	688	717	66279.70

$$\bar{X}_1 = 68.8 \ ; \ \bar{X}_2 = 71.7 \ ; \ M = 70.25$$

Let

$$Y_{i,j} = \underset{\substack{\uparrow \\ \text{overall} \\ \text{mean}}}{M} + \underset{\substack{\uparrow \\ \text{effect of ith} \\ \text{treatment}}}{T_i} + \underset{\substack{\uparrow \\ \text{random} \\ \text{error}}}{E_{i,j}} \qquad \begin{array}{l} i=1,2 \\ j=1,2,\ldots,10 \end{array}$$

where $\sum T_i = 0$ and $(E_{i,j})$'s are mutually independent with $\text{Var}(E_{i,j}) = S^2$.

It is required to test the null hypothesis H_0 = samples do not differ in their mean effect (i.e T_i's are zero) against the other alternative H_1 =some of the treatements differ in their mean effect (i.e some T_i's are different from zero).

The variance is estimated by:

$$S_1^2 = \frac{(X_i - M)^2}{(2-1)} \times 10 = 42.05 \quad \text{with one degree of freedom.}$$

- A4 -

It can also be estimated by:

$$S_2^2 = \sum_{j=1}^{10} \frac{(X_{1j} - X_1)^2 + (X_{2j} - X_2)^2}{2(10-1)} = 3682.2 \text{ with 18 deg of freedom.}$$

The F-ratio is given by the ratio of the two independent estimates of variance,

$$F(f_1, f_2) = \frac{S_1^2}{S_2^2} \quad \text{where } S_1^2 \text{ has } f_1 \text{ and } S_2^2 \text{ has } f_2 \text{ d.f.}$$

$$F_{1,18} = \frac{42.05}{3682.2} = 1.142 \times 10^{-2}$$

Entering F-tables at $f_1 = 1$ and $f_2 = 18$ gives:

$$F_{1,18,10\%} = 3.01.$$

Note that $F_{1,18}$ is very much smaller than $F_{1,18,10\%}$. Therefore the null hypothesis is strongly verified at the 10% significance level. In other words there is no significant difference between the two samples of results at the 10% level.

A1.2.2- T-test:

A check for variability in the microcrack measurement results at two different locations of the machined surface was made by treating two series of results as paired data and applying the "T-test". This test involves a comparison of the mean difference of the paired data with its standard error. The data to be compared is shown in table A3.

Let the individual results in the first sample be denoted by "X_1" and those in the second sample by "X_2". The difference between paired data is thus given by: $D = X_1 - X_2$

Table A3 : Comparison of means of two samples of microcrack
area measurements (T-test).

n	X_1	X_2	$D=X_1-X_2$	$D-\bar{D}$	$(D-\bar{D})^2$
1	117	86	31	33.9	1149.21
2	0	13	-13	-10.1	102.01
3	0	20	-20	-17.1	292.41
4	96	152	-56	-53.1	2819.61
5	51	19	32	34.9	1218.01
6	17	131	-114	-111.1	12343.21
7	59	87	-28	-25.1	630.01
8	134	186	-52	-49.1	2410.81
9	63	12	51	53.9	2905.21
10	151	11	140	142.9	20420.41
		SUM	-29		44290.9

$$\bar{D} = -2.9$$

The estimated standard deviation of the difference is given by:

$$S = \sqrt{\frac{(D-\bar{D})^2}{n-1}} = 70.15$$

The standard error of the mean is given by:

$$\bar{S} = \sqrt{\frac{S}{n}} = 22.18 \quad (n = \text{Number of observations} = 10)$$

The "t" value is given by:

$$t = \frac{\bar{D}}{\sqrt{\bar{S}}} = 0.138$$

Entering T-tables with degrees of freedom equal to 9, it is found that

the appropriate 10% significant point is:

$$t_{9,10\%} = 1.38$$

The value of t=0.138 is very small compared to $t_{9,10\%} = 1.38$.

Therefore it is not significant at the 10% level and so it is

concluded that there is no significant difference between the two sets

of data.

APPENDIX 2

EXPRESSION FOR THE INCERTITUDE IN MEASUREMENT OF

MICROCRACK AREA RATIO DUE TO POOR PENETRATION OF

REPLICATING MATERIAL INSIDE MICROCRACKS.

In this appendix an expression is derived which gives an estimate of the incertitude in the determination of the microcrack area ratio. The microcrack area ratio is given by:

$$Ma = (A/A_0) \times 100 \quad \text{-----------------------(A1)}$$

where "A" is the microcrack area measured using the standard measuring grid and "A_0" is the area of the measuring grid.

The incertitude in the measurement of Ma is given by:

$$dMa/Ma = (dA/A) + (dA_0/A_0) \quad \text{--------------(A2)}$$

But since A_0 is a constant standard value, then $dA_0/A_0 = 0$, hence,

$$dMa/Ma = dA/A \quad \text{----------------------------(A3)}$$

Now,
·

$$A = w.l \quad \text{------------------------------(A4)}$$

where "w" is the microcrack depth and "l" is the microcrack length.

The incertitude in "A" due to poor penetration of the replicating material inside the microcracks is given by:

$$dA/A = (dw/w) + (dl/l) \quad \text{------------------(A5)}$$

But the microcrack length is not affected by poor penetration, therefore $dl/l = 0$ and equation (A5) is reduced to:

$$dA/A = dw/w \quad \text{---------------------------(A6)}$$

From figure 65 the variation in the width "w" of the white band corresponding to variation "dw" of the microcrack depth is given by:

$$dw = dw_1 + dw_2$$

$$\text{but } dw_1 = h_0 - h \text{ and } dw_2 = a/2,$$

where "h_0" is the actual microcrack depth and "h" is the measured microcrack depth.

Equation (A6) can be re-written as:

$$dA/A = (dw_1 + dw_2)/w = (h_0 - h + a/2)/w \quad \text{-----(A7)}$$

From the similarity of triangles ABC and ADE (fig.65) the following relationship can be derived :

- A8 -

$$BC/DE = AB/AD$$

i.e. $(a/2)/[(a/2)+b] = (h_0-h)/h_0$

From the above equation "h_0" is found to be equal to:

$$h_0 = h[(a/2b)+1] \hspace{2cm} (A8)$$

Replacing equation (A8) into equation (A7) gives:

$$dA/A = (a/2)(1+h/b)/w$$

but h=w (shadowing carried out at 45 degrees) Hence,

$$dMa/Ma = dA/A = (a/2)[(1/b)+(1/w)] \hspace{1cm} (A9)$$

and the percentage error is given by:

$$dMa/Ma = 50a[(1/b)+(1/w)] \text{ percent} \hspace{1cm} (A10)$$

In terms of the contrast sequence obtained in the TEM micrographs of the machined surface, the significance of the above relationship is as follows:

"a" represents the width of the middle grey band,

"b" is the width of the black band,

"w" is the width of the white band.

APPENDIX 3

CALIBRATION OF TEM MAGNIFICATION FOR

HIGH CONTRAST SPECIMEN HOLDERS.

A magnification calibration was carried out on the high contrast specimen holders used during TEM examination. The procedures are described in this appendix.

First, micrographs of a standard calibration grid were taken at different magnifications. Magnifications of 5K, 9K, 17K, 25K, 40K, 60K, 90K, 120K, 200K and 300K (the "K" refers to X1,000). For the micrographs obtained:

$$Mtrue = F.Mcon$$

where "Mtrue" is the true magnification and "Mcon" is the console (or displayed) magnification and "F" is the calibration factor appropriate to the specimen holder and microscope stage used.

For each of the nine micrographs showing the cross-grating replica (plate A1), the line spacing "m" was measured as accurately as possible using a travelling vernier with eye-piece. Given that the calibration specimen has 2,160 lines per millimeter, the spacing "s" in the specimen could be calculated.

$$s = 1/2,160 = 0.00046 \text{ mm}$$

Hence the true magnification for each micrograph can be calculated by:

$$Mtrue = m/s \text{ ---------(A12)}$$

The value of "Mcon" for each micrograph was obtained from inscription on the print (e.g. "a 100 568" where the "100" indicates a console magnification of 100K).

The results for the nine micrographs are tabulated in table A4. From the graph of "Mtrue" against "Mcon" (figure A2), the slope determines the value of the magnification correction factor "F". In the TEM used there were three magnification ranges associated with lens changes at magnifications of 12K and 40K. This resulted in slight differences in the value of "F" for each range but an average value was determined. Calculation of the slope of the graph for each

magnification range (figure A2) gave an average value of "F" equal to
0.3 for the high contrast specimen holder used.

Table A4 : TEM Calibration Results.

Mcons (K)	Mtrue (K)
5	1.68
9	2.68
12	3.49
17	5.49
25	6.92
40	11.86
60	21.22
90	29.00
120	35.58
200	57.26
300	88.45

APPENDIX 4

STATISTICAL TECHNIQUES FOR ROUNDING UP VALUES OF

INTERCEPTS AND SLOPES IN THE REGRESSION EQUATIONS.

The values of Y, A and B in the regression equation (Y=A+BX) , are in fact estimates. Confidence limits for these estimates may be determined from the variance of the estimate.

The variance of Y estimated by the regression equation is given by:

$$S_y^2 = \frac{\sum E_i^2}{d.f.} \qquad \text{(A13)}$$

where $E_i = Y_i - (A+BX_i)$ and d.f.= degrees of freedom.

The regression line is subject to two constraints namely the centroidal $(\overline{X},\overline{Y})$ and either the slope or the intercept. The degrees of freedom will thus be the number of observations minus two.

The variance of the intercept A is given by:

$$S_a^2 = S_y^2 \left[\frac{1}{n} + \frac{\overline{X}^2}{\sum(X-\overline{X})^2}\right]$$

and the confidence limits are given by:

$$A \pm t.S_a \qquad \text{(A14)}$$

where "t" is the 'student' t value at the appropriate number of degrees of freedom and required level of significance. The level of significance equals the probability of our being wrong in saying A lies between the limits given by equation (A14). The 95% confidence limits are obtained by taking "t" at the 5% level. The 95% confidence limits for the slope "B" is given by $B \pm t.S_b$, where:

$$S_b^2 = \frac{S_y^2}{\sum(X-\overline{X})^2} \qquad \text{(A15)}$$

A4.2- Rounding Values Of Slope And Intercept:

    In order to test whether A and B are significantly different from rounded values A_0 and B_0 within the confidence limits, the required statistic is:

$$t_a = \frac{|A-A_0|}{S_a} \quad \text{and} \quad t_b = \frac{|B-B_0|}{S_b}$$

A4.3- Worked Example (Variation of microcrack area ratio with cutting speed):

    The regression equation which was found for the variation of the microcrack area ratio is given by:

$$Y = 0.56696 - 0.00863X \quad \text{-------(A16)}$$

where $Y = Log(Ma)$ and $X = V$.

In this case the number of observations is equal to 11. Therefore the number of degrees of freedom is equal to 9. The data for the statistical analysis is shown in table A5.

Table A5: Statistical Analysis Data

X	E_i^2	$(X-\bar{X})^2$
3	0.001	22092.656
10	0.345	20060.750
30	0.072	14795.312
50	0.196	10329.871
75	0.009	5873.074
100	0.830	2666.275
150	0.286	2.676
200	0.096	2339.076
300	0.110	22011.891
350	0.013	39348.293
400	0.021	61684.680
1668	1.98	201204.554

$$\overline{X} = 151.636$$

$$S_y = 0.469$$

$$S_a = 0.2124$$

$$S_b = 0.00105$$

(i)- To test whether A is significantly different from 0.6:

$$t_a = 0.155$$

at the 10% level t=1.833 for 9 degrees of freedom (from tables).

It can be seen that the value of "t_a" is very small compared to the tabulated value at the 10% level. It can therefore be concluded that the value of the intercept in the regression equation is not significantly different from 0.6.

(ii)- To test if B is significantly different from -0.009:

$$t_b = 0.3538$$

This value is smaller than the t value at the 10% level and so it is concluded that B is not significantly different from -0.009

Using the above rounded values for the slope and intercept, the regression equation (A16) can be simplified to:

$$Y = 0.6 - 0.009X \text{ ------------(A17)}$$

or in real terms, to:

$$Log(Ma) = 0.6 - 0.009V \text{ -------(A18)}$$

Equation (A18) can be re-written as:

$$Ma = 1.822188.exp(-0.009V) \text{ ---(A19)}$$

The value of C in the equation Y=C.exp(BV) in equation (A19) can be rounded to 1.82 which can be shown using statistical analysis.

Table A5-1: Effect of cutting speed on Ma & Md

V (m/min)	Ma	Md
3	1.760	94
10	0.899	112
30	1.779	108
50	0.735	104
75	0.839	124
100	1.850	88
150	0.825	104
200	0.230	61
300	0.095	22
350	0.0765	28
400	0.0645	15

Table A5-2: Effect of undeformed chip thickness on Ma & Md

t (mm.)	Ma	Md
0.057	1.4995	76
0.099	0.375	59
0.138	0.3455	92
0.167	0.361	80
0.198	0.643	69
0.244	0.230	61
0.396	0.148	39

Table A5-3: Effect of rake angle on Ma & Md

α (deg.)	at V=200m/min.		at V=50m/min.	
	Ma	Md	Ma	Md
-10	----	---	0.8575	97
- 5	0.108	54	0.477	77
+ 5	0.2315	61	0.735	104
+15	0.305	52	1.2125	120
+20	0.69	104	---	---
+25	0.51	128	---	---
+30	0.90	103	0.7525	116
+30	1.055	101	---	---

Table A5-4: Effect of material hardness on Ma & Md

H (VPN)	Ma	Md
180	1.48	106
208	0.84	69
260	0.295	67
285	0.171	45
320	0.0625	17
350	0.30	27

Table A5-5: Effect of cutting speed on cutting forces

V (m/min)	Fc (N)	Ft (N)	Esp= Fc/A
3	3870	1113	3172
10	3747	1113	3071
30	3775	1440	3094
50	3775	1508	3094
100	3565	1350	2922
200	3635	1238	2980
300	3582	1325	2936
400	3582	1458	2936

N.B: A is the x-section area of uncut chip

Table A5-6: Effect of rake angle on cutting forces

α (deg.)	Fc (N)	Ft (N)	Esp. (N/mm^2)
- 5	3755	1570	3078
0	3665	1200	3004
+ 5	3635	1200	2980
+10	3370	912	2762
+15	3195	764	2619
+20	3205	698	2627
+25	3060	582	2508
+30	2885	460	2365

Table A5-7: Effect of undeformed chip thickness on cutting forces

t (mm.)	Fc (N)	Ft (N)	Esp. (N/mm^2)
0.057	1400	876	4912
0.069	1630	960	4725
0.084	1905	1084	4536
0.099	2160	1120	4364
0.138	2660	1208	3855
0.198	3350	1166	3384
0.244	3635	1200	2980
0.396	5820	1470	2939

Table A5-8: Surface roughness versus cutting speed

V (m/min.)	Ra tangential (microns)	Ra radial (microns)
3	7.137	1.646
10	8.842	2.179
30	4.550	2.139
50	1.579	0.876
75	1.666	0.640
100	1.333	0.450
150	1.079	0.435
200	0.550	0.383
300	0.485	0.434
350	0.498	0.273
400	0.460	0.341

Table A5-9: Surface roughness versus undeformed chip thickness

t (mm)	Ra tangential (microns)	Ra radial (microns)
0.057	0.8014	0.586
0.099	0.6068	0.5618
0.198	0.4994	0.5726
0.244	0.5500	0.6170
0.396	0.4792	0.708

Table A5-10: Surface roughness versus rake angle

V = 200 m/min.

α (deg)	Ra tangential (microns)	Ra radial (microns)
- 5	0.515	0.515
+ 5	0.550	0.617
+15	0.709	0.436
+30	0.518	0.383

V = 50 m/min.

α (deg)	Ra tangential (microns)	Ra radial (microns)
-10	2.707	0.802
- 5	1.991	0.909
+ 5	2.028	1.286
+15	2.035	1.334
+30	2.926	1.286

Table A5-11: Surface Roughness versus material hardness

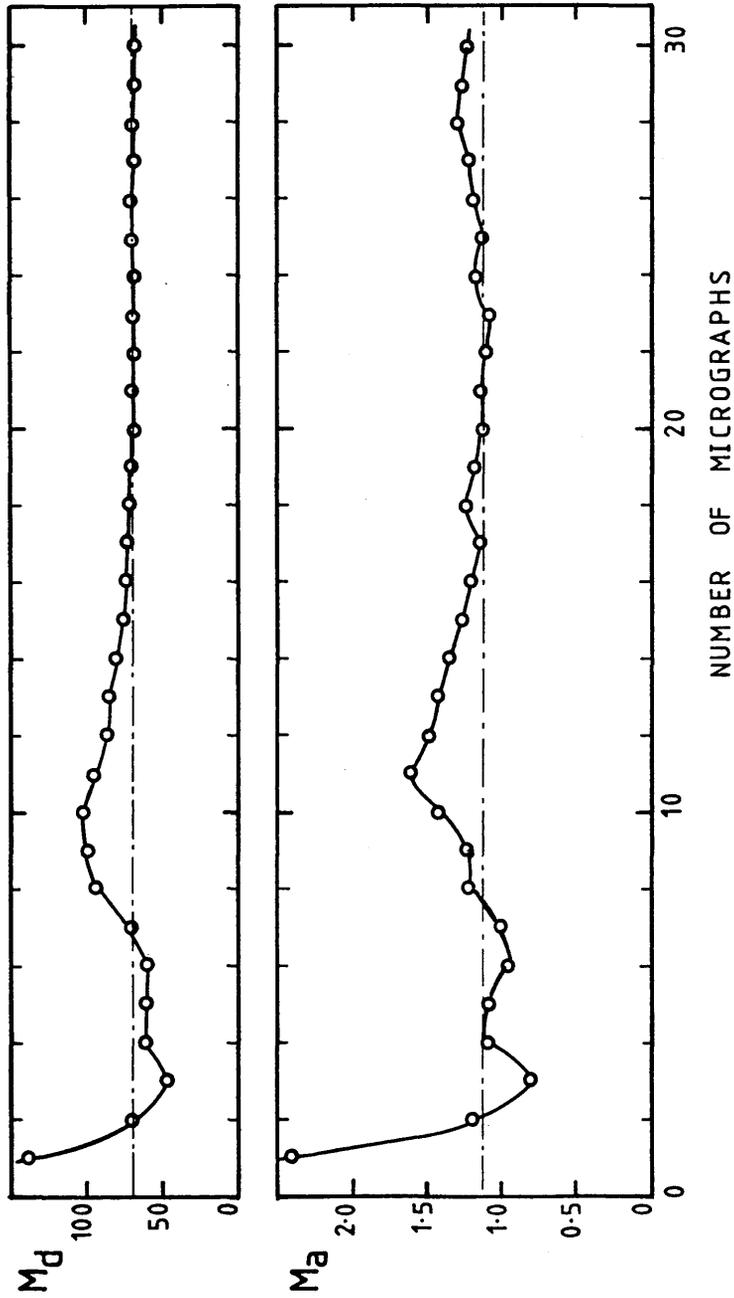| H (VPN)	Ra tangential (microns)	Ra radial (microns)
180	0.249	0.292
208	0.340	0.349
260	0.348	0.348
285	0.301	0.301
320	0.367	0.367
350	0.249	0.619

FIG.A1 <u>CONVERGENCE OF M_a & M_d WITH THE NUMBER OF</u>
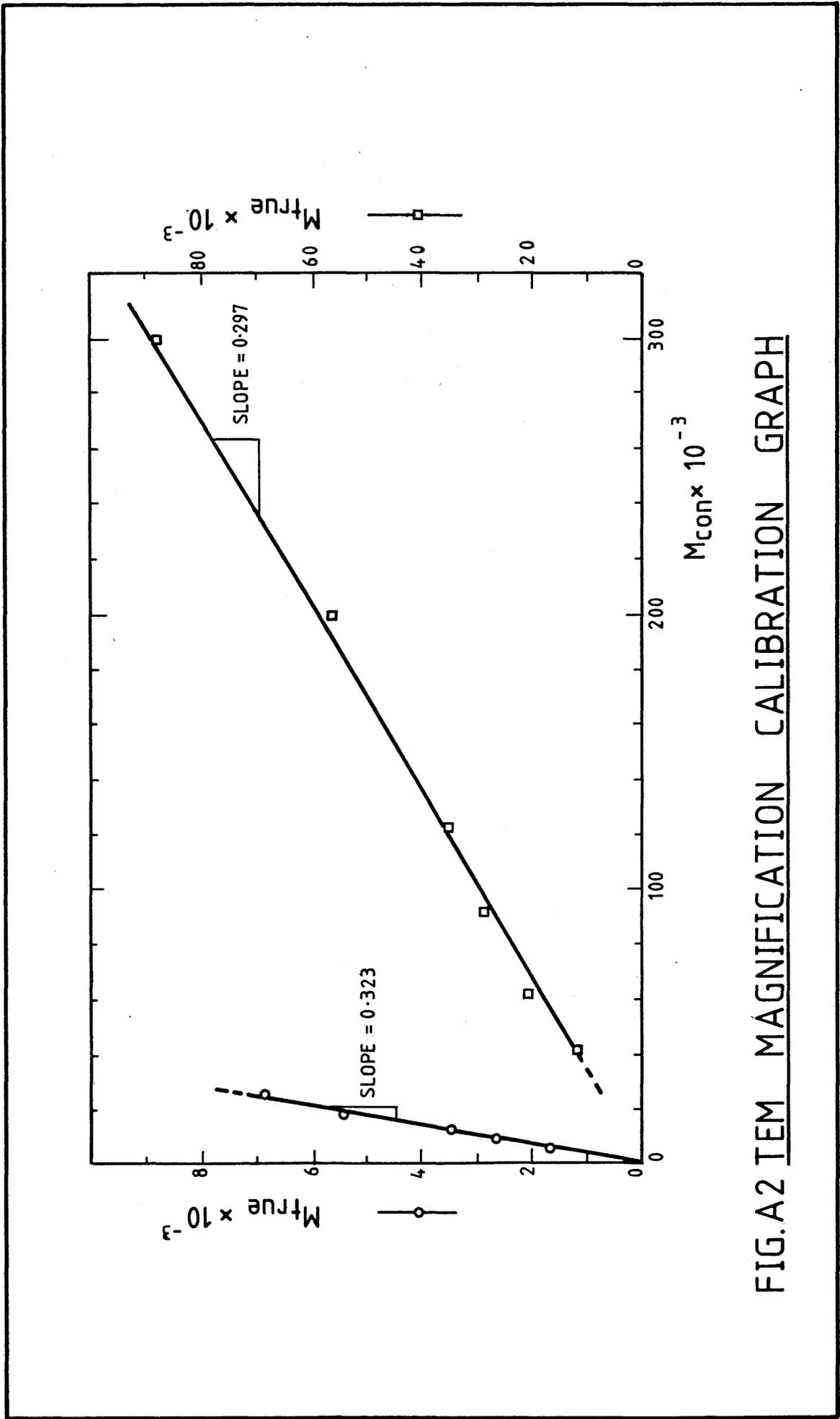
<u>MICROGRAPHS USED FOR THE MEASUREMENTS</u>

FIG.A2 TEM MAGNIFICATION CALIBRATION GRAPH

SLOPE = 0·297

SLOPE = 0·323

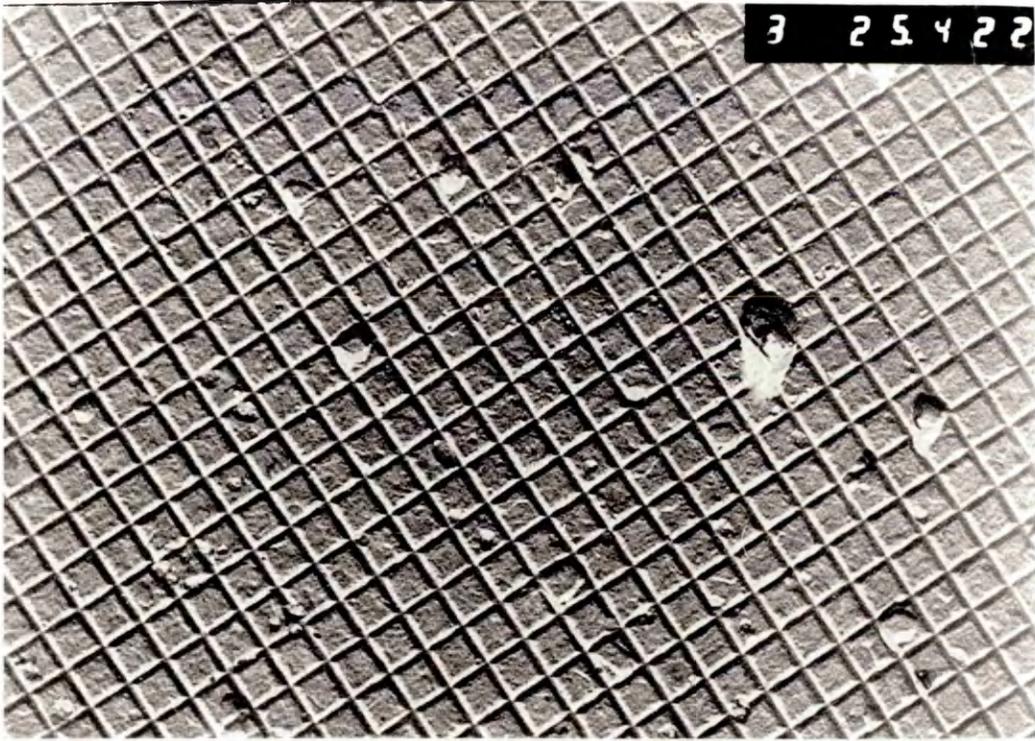$M_{con} \times 10^{-3}$

$M_{true} \times 10^{-3}$

$M_{true} \times 10^{-3}$

PLATE A1

MICROGRAPH OF STANDARD CALIBRATION GRID